PERFORMANCE ANALYSIS AND DESIGN OF FIBRE GRATINGS FOR SENSING APPLICATIONS

A THESIS

Submitted in fulfillment of the requirement for the award of degree of

DOCTOR OF PHILOSOPHY

IN

ELECTRONICS & COMMUNICATION ENGINEERING

By

NIDHI

Reg. No. 950906002

Supervisors

Dr. R.S. KALER & Dr. PAWAN KAPUR

DEPARTMENT OF ELECTRONICS & COMMUNICATION ENGINEERING

THAPAR UNIVERSITY

PATIALA-147001

October 2014

CERTIFICATE

I, Nidhi hereby certify that the work which is being presented in this thesis entitled "Performance Analysis and Design of Fibre Gratings for Sensing Applications" in fulfilment of requirements for the award of degree of Doctor of Philosophy in Electronics and Communication Engineering from Thapar University, Patiala is an authentic record of my own work carried under the supervision of Dr. R.S. Kaler and Dr. Pawan Kapur. The matter presented in this thesis has not been submitted to any other University/Institute for the award of any degree.

Nidhi

(Signature of the candidate) Date: 31/10/14

This is certified that above statement made by the candidate is correct to the best of my knowledge.

Supervisors:

(Dr. Pawan Kapur)
Director, PIT, Rajpura, Ex Director, CSIR-CSIO
Ex-Distinguish Emeritus Professor
AcSIR, New Delhi

Date: 31/10/14

(Dr. R. S. Kaler)
Senior Professor
ECED, Thapar University, Patiala

ACKNOWLEDGMENTS

First of all, I would like to pay my regards to The Almighty who has led me to the path of science and inspired to explore the exciting opportunities that come in the offering. All this would not have been possible without the constant support, encouragement and blessings of my beloved parents.

I would like to thank Dr. R.S. Kaler and Dr. Pawan Kapur, who have been positive all through the course of the project and lent full support and cooperation in every aspect possible.

Special thanks to Mr. N.S. Mehla who was always there to guide and give an insight into the technical aspects of Long Period Gratings and related fundamentals.

I would like to express my gratitude to Dr. G.S. Singh, Mr. S.C. Jain and Mr. Randhir Bhatnagar who helped me in building basic concepts in the subject and assisted wherever I got stuck.

I also take this opportunity to express my gratitude to Dr. Samir Mondal, Dr.Sudipta Sarkar, Dr. Bhargab Das, and Dr. Vinod Karar for the encouraging and inspiring sessions I had with them.

There were many others who were instrumental during the journey of this work. Sincere acknowledgements in this regard go to Dr. Akashdeep and Dr.Sunita Mishra

I offer immense thanks to my colleagues Asha Kumar, Deepa Srivastva, Madhu Mehta, Ravi Dhawan, Mansoor Khan and Nishtha Panwar.

I am deeply indebted to Dr. Umesh Tiwari and Dr. Vandana Mishra who always inspired me to think innovatively and gave their invaluable time to teach and enrich my knowledge in a plethora of subjects.

I wish to thank my close friends Divya Agrawal, Raj Kumar Pal and Samarpit Karar.

Most importantly, I would like to acknowledge the support of my mother Mrs. Neelam Chandel, my husband Ajay Singh, my sister Jyoti Singh and brother Gauarv Chandel. Their love and affection has helped me to overcome numerous hurdles on the road of life.

Last but not the least, my Reverend Father who did not live to see my work, but whose blessings have brought me to this platform- I thank him.

(NIDHI)

ABSTRACT

The role of optical technologies for non-contact type of measurements in the field of instrumentation and sensing is revolutionary. The exceptional sensitivity of fiber towards external perturbation has made research world extremely benefited. This property is explored to construct a large variety of instruments and sensors. This thesis also deals with the performance analysis and design of fiber gratings for sensing applications. Long Period Gratings (LPGs) are proposed as simple yet versatile optical fiber sensors. In case of LPG, periodic modulation of refractive index within core region is written in such a way that light propagating in the core can interact with cladding and outside thereby yielding an output spectrum that includes changes due to all external parameters to which the fiber may be subjected to. The phase matching condition causes light from the fundamental mode to couple with discrete forward-propagating cladding modes. These cladding modes attenuate rapidly on propagation and result in loss bands at discrete wavelengths in the grating transmission spectrum. One of the aims of this work has been to develop an analytical model to predict the location of resonance bands as function of grating periods as well as core and cladding refractive indices. The transmission characteristics of uniform LPGs are simulated theoretically by using coupled-mode theory.

Studies undertaken in the thesis include review of number of LPG fabrication methods and understanding the mechanism of photosensitivity in germanosilicate fibers using different reported models. The fabrication of these gratings has been done using TeraXian grating writing station. In this work, uniform LPGs are

fabricated by using a line-narrowed KrF excimer laser adopting point by point method. The fibers used in experiments are photosensitive optical fibers (Boron co-doped) and gratings can be written directly into these fibers without hydrogenation.

In the thesis it is experimentally demonstrated that the high refractive index overlay increases the refractive index sensitivity of LPG refractive index sensor. The utilization of Indium Tin Oxide (ITO) as coating material enhances refractive index sensitivity of LPG due to the phenomena of rearrangement of cladding modes.

This thesis gives an insight about the scope of LPG for relative humidity (RH) measurement applications. For realization of LPG based humidity sensors, unique feature of LPG i.e. its susceptibility to perturbations in the surrounding medium is investigated. It has been previously reported that coating the cladding of LPGs with thin layer of specific coating materials brings about sensing capability for certain target application. Taking account of this finding, LPG has been coated with a hygroscopic mixture of Cobalt chloride doped Gelatine by dip coating technique. Refractive index measurements and thin film characterisation have been performed by Refractometry, FE-SEM and NSOM imaging respectively. The coated LPG has been experimentally tested for its response to relative humidity levels varying from 35% to 90%. The designed sensor gives an output response of 0.18 nm/%RH. The ITO and $CoCl_2$/gelatine coated LPG as humidity sensor is also demonstrated very first time. The sensor measured RH variation efficiently in the range of 40 % to 95 %RH with sensitivity of 0.12 nm/%RH.

The thesis also highlights the investigative study of Fiber Bragg Grating (FBG) written in multi-mode fibers (MMF). The fabrication is done by phase mask

technique using the static mode of grating writing station. The gratings are characterized by taking different concentration of glycerol solutions. The effect of temperature and strain is studied theoretically using software Optigrating 4.2.2. Also, FBG as a current sensor is demonstrated successfully by using two configurations: with housing and without housing. The minimum and maximum values of measured current are 0.05 Amp and 1 Amp for without housing and it is 1 Amp and 4 Amp with housing setup. The designed sensor has accuracy 0.05 Amp and repeatability 95%. This sensor is different from available current sensors in terms of its new and simple design, low cost and ability to withstand harsh environment.

Thus research work presented in this thesis combines refractive index sensitivity enhancement of LPG by using simple dip coated Indium tin Oxide overlay on it. Further sensor/coating attachment method to develop an RH sensor for informative evaluation of the humidity effect using gelatin and cobalt chloride combination on LPG surface.All the issues addressed in the work contribute to implement a simple and economical index of refraction and moisture measurement system. These sensors offer numerous advantages in corrosion monitoring, chemical & food processing and biochemical sensing. The investigative study of FBG in MMF is very useful for developing low cost sensing systems. Most of the research findings of the thesis have been published in various international referred journals as per list at pages (207-208).

TABLE OF CONTENTS

LIST OF FIGURES

LIST OF TABLES

LIST OF SYMBOLS

n	Refractive index
Δn	Index modulation
κ	Coupling coefficient
Γ or δ	Detuning parameter
β, β_1, β_2	Propagation constants
K	Wave number
Λ	Grating period
k_0	Wave vector
λ_0	Free space wavelength
λ_{res}	Resonant wavelength
λ_B	Bragg wavelength
n_{eff}	Effective modal index/effective refractive index
β_{co}, β_{cl}	Core/Cladding propagation constant
n_{eff_co}	Core effective refractive index
n_{eff_cl}	Cladding effective refractive index
n_1, n_2, n_s	Core, cladding, surrounding refractive index
A_m	Mode field amplitude of m^{th} order

Ψ_m	Transverse filed profile of m^{th} order
$\overline{\Delta n}$	Average index modulation
ε_r	Relative permittivity
ε_0	Permittivity
μ_0	Magnetic permeability
ω	Angular frequency
E	Electric field
$\varphi_i(x,y)$	Modal filed profile
R_f	Refractivity
V	Volume
P_i, P	Volume percent/Hydrostatic pressure
T_g	Transition temperature
α	Thermal expansion coefficient
ϱ	Specific gravity
r,a	Radius
d_p	Penetration depth
t	Time
η	Viscosity
l, L	Length

ε_z	Applied strain
p_e	Effective photo-elastic coefficient
p_{ij}	Strain-optic tensor
ζ	Thermo-optic coefficient
v	Poisson's ratio
H	Heat
I	Current
R_{coil}	Resistance of coil

LIST OF ACRONYMS

TIR	Total Internal Reflection
FOS	Fiber Optic Sensor
FPI	Fabry-Perot Interferometer
EFPI	Extrinsic Fabry-Perot Interferometer
FFPI	Fiber Fabry–Perot interferometer
FBG	Fiber Bragg Grating
LPG	Long Period Grating
CRC	Canadian Communications Research Centre
RI	Refractive Index
RH	Relative Humidity
CMT	Coupled Mode Theory
SHM	Structural Health Monitoring
PEO	Polyethylene Oxide
PVA	Polyvinyl Alcohol
PCF	Photonic Crystal Fiber
POF	Plastic Optical Fiber
OTDR	Optical Time-Domain Reflectometer

HPC	Hydroxypropylcellulose
HEC	Hydroxyethylcellulose
PMMA	Poly-Methyl-Methacrylate
CMC	Carboxymethylcellulose
ITO	Indium Tin Oxide
PI	Polyimide
SMF	Single Mode Fiber
MMF	Multi-Mode Fiber
LED	Light Emitting Diode
ASE	Amplified Spontaneous Emission
LP	Linearly Polarized
OSA	Optical Spectrum Analyzer
UV	Ultra Violet
SRM	Stress-Relief Model
CDM	Compaction-Densification Model
CW	Continuous Wave
EW	Evanescent Wave
PBS	Polarizing Beam Splitter
BS	Beam Tap

BA	Beam Analyzer
BD	Beam Dump
OS	Optical Shutter
PCU	Power Control Unit
FM	Flipper Mirror
PM	Phase Mask
SRI	Surrounding Refractive Index
FESEM	Field Scanning Electron Microscope
FTIR	Fourier Transform Infra-red spectroscopy
IR	Infrared
ISMA	Ionic Self-Assembled Multilayer
NSOM	Near-Field Surface Optical Microscopy
DI	De-ionized
ESA	Electrostatic Self Assembly
NA	Numerical Aperture
EMI	Electromagnetic Interference
AC	Alternating Current
DC	Direct Current
EDF	Erbium Doped Fiber

CHAPTER 1. INTRODUCTION

1.1 Introduction and Overview

Optical fibers are the true representative of remarkable advancements, speed of adoption and commercialization of technology in recent decades. An optical fiber consists of a core (usually doped silica), cladding, and a buffer (a protective outer coating), in which cladding guides light along the core by using the Total Internal Reflection (TIR) phenomena. Incidentally silica, being the primary constituent of sand, is found abundantly on earth. Optical fiber that acts as transmission channel carrying light beam loaded with any kind of information. Undoubtedly fiber is the most important component of light wave communication system. The key element in fiber optics revolution has been the dramatic improvement in transmission characteristics of optical fibers. In the year 1970, Corning Glass works, US developed low loss fiber with 20 dB loss per kilometer at 633 nm wavelength. If we talk about the commercial availability, fibers with loss of 0.2 dB/km at 1550 nm, capable of transmission at 2-10 Gb/s are also present in the market [1]. Fibers used in variety of applications due to much lower attenuation and interference. Optical fiber offers larger advantages over existing copper wire in long-distance and high-demand applications [2]. However, in early stage the infrastructure development within cities was relatively difficult and time-consuming. The fiber-optic systems were relatively complex and expensive to install and operate. Due to these difficulties, primarily fiber-optic communication systems have been installed in long-distance applications, where they can be used to their full transmission capacity, offsetting the increased cost. Since 1990, when optical-amplification systems became commercially available, the telecommunications industry laid a vast network of intercity and transoceanic fiber communication lines. The prices for fiber-optic communications have dropped considerably. But nowadays rolling out fiber to each home has certainly become more cost-effective

than that of rolling out a copper based network. Over past 30 years two major product revolutions have taken place due to growth of fiber optic communications industries and optoelectronics. The optoelectronics industry has brought about such successful products as laser pointers, bar code scanners, laser printers and compact disc players. The fiber optic communications industry has revolutionized telecommunications industry with decreased bandwidth cost, but higher performance and more reliable telecommunication links. This revolution is bringing about the benefits of high-volume production to component users and a true information glass superhighway. In parallel with these developments, a major user technology zone is also associated with the optoelectronic and fiber optic communications industries i.e. fiber optic sensor technology. Many of the components associated with these industries were often developed for fiber optic sensor applications [3]. Fiber optic sensor technology, in turn, has often been driven by the development and subsequent mass production of components to support these industries.

1.2 Optical Fiber Sensing Technology

The scope of optical technique in the area of instrumentation and sensing has made a quantum jump with the readily availability of low loss optical fiber and associated photonics and optoelectronic components as described earlier. As quality improvements have been made and component prices have fallen, the ability of fiber optic sensors to replace traditional sensors for acceleration, rotation, electric and magnetic field measurement, pressure, linear and angular position, acoustics, temperature, vibration, humidity, viscosity, strain, chemical and biochemical measurements, and a host of other sensing applications has been enhanced. In early days, sensor technology associated with optical fibers was squarely targeted at markets most, where existing sensor technology was either marginal or nonexistent. The inherent advantages of fiber optic sensors, which include lightweight, small size, passive, low power, and resistant to electromagnetic interference, high sensitivity,

bandwidth and environmental ruggedness, were heavily used to offset their major disadvantages of high cost and end-user unfamiliarity.

A generic optic sensing system consists of a light source, a detector, optical fiber, a transducer or sensing element. A simple fiber sensor module is shown in the Figure 1.1. An applied perturbation modulates the properties of transmitted light and produces a change at the detection end. The desired characteristics of an ideal sensor include high resolving power, low insertion loss, wide dynamic range, ease of fabrication, simple signal processing, multiplexing features and multi measured capabilities [4, 5].

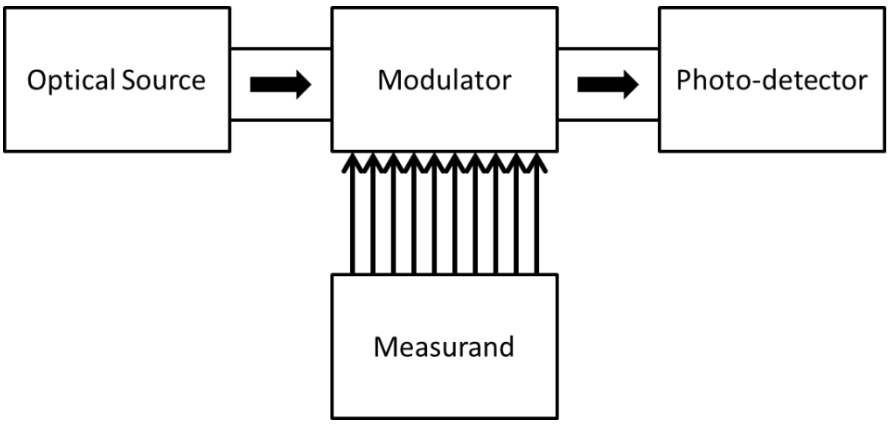

Figure 1.1 A simple fiber sensor module

The Fiber Optic Sensors (FOS) can be either Intrinsic or Extrinsic depending on whether modulation takes place directly in the fiber or is performed by some external transducer.

Table 1.1 Comparison of the two types of optical sensors

	Extrinsic	**Intrinsic**
Application	Temperature, Pressure, Liquid level and Flow	Rotation, Acceleration, Strain, Acoustic pressure and Vibration
Sensitivity	less	More
Multiplexed	Easily	Tougher to multiplex

Connection problems	Ingress/ egress	reduces
Cost	Less expensive	More expensive
Flexibility	Easier to use	More elaborate signal demodulation

They may broadly be classified as phase-based or intensity-based depending on parameter of propagating light that is modulated by the external perturbation. One or more characteristics of a propagating light is altered and correlated to an externally-induced physical or chemical parameter. Phase based or interferometric sensors [6] are highly sensitive and have been demonstrated as excellent short gage-length, strain and temperature transducers. Intensity based sensors have simple signal processing techniques and provide absolute, real-time information about the measurand [4]. The types of fiber optic sensor are classified here according to altered characteristics as follows:

1.2.1 Intensity based sensors

The basic concept of intensity based sensors is very simple, either reflected or transmitted intensity of light is modulated by the measurand. Any intensity fluctuations in the output not associated with measurand produce erroneous result [7].

1.2.2 Spectrally based fiber optic sensors

Spectrally based fiber optic sensors depend on a light beam modulated in wavelength by an environmental effect. Examples of these types of fiber sensors include those based on absorption, etalons, fluorescence, blackbody radiation and dispersive gratings [8-10]. Grating based sensors falls in the category of spectrally based sensors. Grating can be divided into two types: Fiber Bragg Grating (FBG) and Long-Period Fiber Grating (LPFG or LPG). The FBG relies on detection of the shift in a reflected wavelength and relating it to the applied measured. The technique is limited because the forward- and reverse-propagating light remains confined to the fiber core and so the cladding has to be modified to gain local access to this light.

Further, it is difficult to isolate strain effects from temperature effects. LPG first proposed by Vengsarkar *et al* [11, 12] are fast gaining popularity as simple yet versatile component for a multitude of applications in optical engineering. LPG is formed by inducing a spatial refractive index modulation in the core of germanosilicate or photosensitive fibers with periodicity typically ranging in hundreds of micrometres [11]. The phase matching condition between the guided and cladding mode causes the propagation light to couple out of the core at discrete wavelengths. Light launched in a guided core mode interacts within the grating and is converted into a number of cladding modes. These modes transmit over short distances in the cladding before being attenuated by the lossy jacket and bends in the fiber.

One important property of these modes is that their propagation characteristics are strong functions of the refractive index of the medium surrounding the cladding. Hence, LPG can be used to sense a variety of measurement without resorting to chemical etching. The environmental sensitivities of LPG can be controlled by varying the refractive index profile of the optical fiber, significantly reducing the cross-sensitivity problems inherent in fiber Bragg grating sensors. LPG holds much promise for the future of fiber optic sensing. As the demand for multiplexed measurements increases, long-period gratings will be the sensor platform of choice for a wide range of industrial applications. Since present, various ideas have been proposed and various techniques have been developed for various measurands and applications. The continuous rapid progress in grating based work has hastened the quest of researchers and scientists to develop devices that serve to overcome the existing limitations and perform the task of precursors for the future advancements in the sensing technology. A lot of work needs to be done to promote and develop these sensors in advanced applications. Novel optical fiber sensors that offer excellent performance characteristics would ease the transition of laboratory research to commercial products that offer a viable alternative to electronic and

mechanical transducers. The most prominent reason for the successful incorporation of LPGs in communication systems is the fact that they provide a mechanism for producing wavelength-dependent attenuation in the transmission. However they are very sensitive to external effects (especially temperature, axial strain, fiber bends and ambient refractive index), which could adversely affect the transmission spectrum.

1.2.3 Interferometric fiber optic sensors

One of the areas of greatest interest has been the development of high-performance interferometric fiber optic sensors. Substantial efforts have been undertaken on Sagnac interferometers [13], ring resonators [14], Mach–Zehnder [15] and Michelson interferometers [16], as well as dual-mode, polarimetric, grating, and etalon-based interferometers. All-fiber interferometers, such as Mach–Zehnder and Michelson interferometers in particular, possess one of the greatest advantages of extremely flexible geometries and a high sensitivity that allow the possibility of a wide variety of high-performance elements and arrays. One of the basic issues with the Mach–Zehnder interferometer is that the sensitivity varies as a function of the relative phase of the light beams in the two arms of the interferometer. One way to solve the signal fading problem is to introduce a piezoelectric fiber stretcher into one of the legs and adjust the relative path length of the two legs for optimum sensitivity. The Michelson interferometer is in many respects similar to the Mach–Zehnder. The major difference is the placement of mirrors on the ends of the interferometer legs. This results in very high levels of back reflection into the light source, degrading massively the performance of early systems. In combination with the recent introduction of phase conjugate mirrors to eliminate polarization fading, the Michelson is becoming a good alternative for systems that can tolerate the relatively high present cost of these components. In order to successfully implement an effective Mach–Zehnder or Michelson-based fiber sensor, construction of an appropriate transducer is necessary. This can involve a fiber coating which could be further optimized for acoustic, electric, or magnetic field response. In many cases the

mechanical details of the transducer design are critical for good performance. Generally, the Mach–Zehnder and Michelson interferometers can be configured with sensitivities that are better than 10^{-6} radians per square root hertz. For the optical receivers, the noise level decreases as a function of frequency. This results in specifications in radians per square root hertz [17].

The Fabry–Perot Interferometer (FPI) sometimes called the Fabry Perot etalon belongs to the general class of interferometric sensors. It consists of two mirrors of reflectance R_1 and R_2 separated by a cavity of length L. Interference occurs due to the multiple superpositions of both reflected and transmitted beams at two parallel surfaces. FPI sensors can be largely classified into two categories: one is extrinsic and the other is intrinsic [18, 19] as shown in the Figure 1.2 (a) and (b). The Extrinsic FPI (EFPI) sensor uses the reflections from an external cavity formed out of the interesting fiber. The reflection or transmission spectrum of an FPI can be described as the wavelength dependent intensity modulation of the input light spectrum, which is mainly originated by the optical phase difference between two reflected or transmitted beams. Fiber FPI are extremely sensitive to the perturbations that affect the optical path length between the two reflecting mirrors. The sensing region can be very compact—equivalent to a point transducer in some applications. Unlike other fiber interferometers (Mach–Zehnder, Michelson, Sagnac) used for sensing application, the Fabry–Perot includes no fiber couplers—components that can makes matter worse for the sensors deployment and the interpretation of data. The fiber FPI comes out to be an ideal transducer for many smart structure sensing applications. Since the light in the EFPI cavity is not confined, optical loss in the interferometer due to diffraction effectively limits the practical length of the optical cavity to a few hundred microns for most applications.

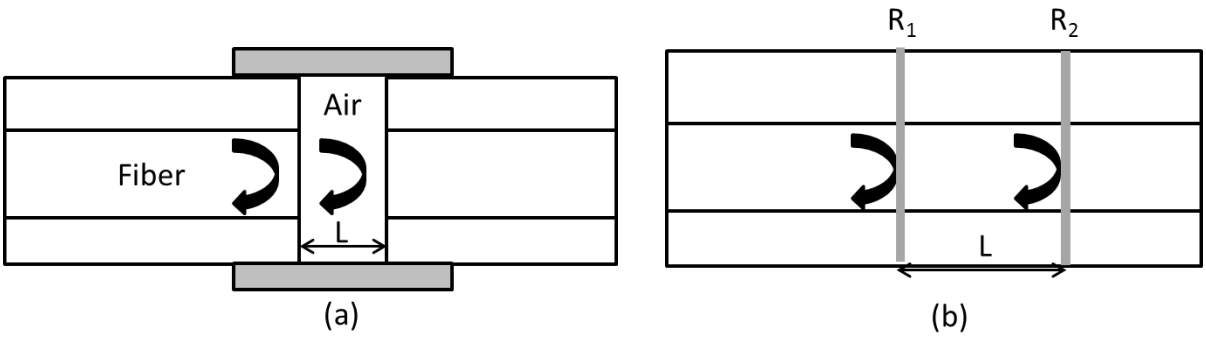

Figure 1.2 (a) Extrinsic FPI sensor made by forming an external air cavity and (b) intrinsic FPI sensor formed by two reflecting components, R1 and R2, along a fiber [17]

1.2.4 Polarimetric optical fiber sensors

In a typical fiber polarimetric sensor, linearly polarized light is launched at an angle of 45° to the principal axes of a birefringent fiber such that both Eigen modes are equally excited [20]. The polarization state at the output is converted to intensity using a polarizer analyzer oriented at 90° to the input polarization state.

Since the determination of the polarization rotation is essentially reduced to a measurement of intensity of the optical transmission, the arrangement thus described is vulnerable to errors associated with variations in the source output or within the fiber sensor input leads.

This problem can be overcome by using a Wollaston prism and two detectors. Using the Wollaston prism, the signals at the detectors are equivalent to those produced by polarizing analyzers oriented at +45° and –45° to the fiber's birefringent axes. Processing results in a signal independent of the optical power. This advantage comes, however, with the additional difficulty of correctly aligning the Wollaston prism and the two detectors with respect to the fiber birefringent axes.

As we know, Refractive Index (RI) is a fundamental physical property of any substance and its measurement has promising potential in the field of chemistry, biochemistry, process control, pharmaceuticals and biology. The potential of FBG

and LPG as refractive index sensor have been explored by various research groups worldwide [21-25]. The RI sensitivity enhancement is always a major concern for researcher without importing any physical changes in its structure. Similarly, Relative Humidity (RH) monitoring has a significant impact in various application fields, such as industrial process control, pharmaceutical, farming, goods preservation, storage, medical facilities. Nowadays, compact, sensitive, hand held RI and RH sensors are highly in demand [26, 27]. In the next section, the concepts along with various conventional and optical techniques for humidity sensing are discussed.

1.3 Humidity Sensing

Humidity is the amount of water vapour per unit volume of the total moist air. A common way to relate the amount of water vapour present in the environment is to take the ratio of the actual water vapour pressure (P_w) and the saturation water vapour pressure (P_{ws}) at a specific temperature. The resultant term, known as the relative humidity (RH), simply represents the ratio of the amount of water vapour present in the atmosphere to the maximum amount the atmosphere can hold and is often expressed as a percentage using Equation 1.1 [28].

$$RH = \frac{P_w}{P_{ws}} * 100\% \quad (1.1)$$

The significant role of humidity in a diverse range of applications makes its measurement all the more expedient. Figure 1.3 is a pictorial retranslation of some of the areas where humidity level monitoring plays a critical role in proper functioning of control processes.

Much research has been gone into development and performance based humidity sensing devices and making them bring to the shelf. It all started with analog mechanical based hygrometers to sophisticated electronic ones.

Figure 1.3 Applications of humidity sensing

There has been much attention paid to the development of fiber optic based humidity sensors in the last decade. A brief review of all the prototypes developed have been presented in the sections that follow [29].

1.3.1 Conventional Techniques for Humidity Sensing

1.3.1.1 Mechanical hygrometer

A typical mechanical hygrometer is based on one of the oldest practice that relies on the use of materials which expand and contract in proportion to the humidity change [30]. Common materials used include synthetic fibres and human hair. The hair hygrometer uses the characteristic of the hair that its length expands or shrinks in response to the relative humidity. The dimensions of various organic materials vary with their moisture content. The length of human hair from which liquid are removed increases by 2 to 2.5% when relative humidity changes by 0 to 100%. Different types of human hair show different changes in length. However, there is still a relationship between the length of hair and relative humidity. In addition, calibration is essential to relate the displacement with different relative humidity levels. Although this type of method is inexpensive and easy to implement but it is slow and has inherent non-linearity and hysteresis issues which need to be

compensated during implementation. Thus, for rapidly changing environment it is certainly unsuitable choice.

1.3.1.2 Chilled mirror hygrometer

The chilled mirror hygrometer, also known as the optical condensation hygrometer, is a device based on an optical technique for the determination of the dew point temperature. It is known to be the technique which provides the most accurate and reliable measurements, and is often used for measurements setting a calibration standard. In operation, a conventional chilled mirror hygrometer contains a temperature-controlled reflective condensation mirror and an optoelectronic module which monitors the optical signal reflected from the surface of the mirror. In the 'dry' condition, where the mirror temperature is higher than the dew point, the maximum signal is reflected into the detector of the optoelectronic module. When the temperature drops below the dew point, the signal intensity is reduced due to the scattering of light as a result of water droplets forming on the mirror surface [31]. This method is expensive and requires regular maintenance due to its susceptibility to surface contamination.

1.3.1.3 Wet and dry bulb psychrometer

A simple and relativity low cost method which has been popular for humidity measurements is the wet and dry bulb psychrometer. It consists of two thermometers (e.g., electric or glass), one of which is covered with a damp wick to determine the wet bulb temperature and the other to measure the temperature of the sampled gas (dry bulb temperature). The dry bulb temperature is simply the temperature of the air, whereas the wet bulb temperature is the temperature achieved as a result of water evaporation and latent heat transfer [28].

This measurement device is relatively inexpensive, yet can also be used to provide a calibration standard. However, it is not suitable for operation in small enclosed areas (where the moisture from the wet bulb significantly changes the water vapour

content in the environment) and precautions are necessary to minimize measurement errors caused by contamination on the wick covering the thermometer, inconsistency in the wetting of the wick and the inaccuracy of the thermometers used.

1.3.1.4 Infrared (IR) optical absorption hygrometer

One of the less common methods, however, because of its inherent advantages bears further consideration. This is the absorption spectra method. Fundamentally this is an optical method based on the absorption affected by water vapor in certain spectral regions. Basically the absorption spectra instrument comprises a beam of energy and some scheme for measuring the attenuation of this beam due to the presence of water vapor. The absorption spectra instrument has several advantages not found in other hygrometers. First, as to the matter of sampling, it is possible to sample instantaneously any desired path length of atmosphere from a few inches to thousands of feet, and in doing so arrive at an integrated value of the absolute humidity in the path in question. Surprisingly enough, the absorption function results in an increase of sensitivity of the measuring equipment as the humidity concentration decreases. In contrast, the psychrometer, hair hygrometer, electrical hygrometer, and even the dew point apparatus all become less sensitive or more difficult to operate as the temperature falls and the humidity becomes less. Third, the speed of response is limited only by the speed of the indicator or recorder. This makes the method ideal for use in measuring humidity from an airplane or under any circumstance where rapid changes of humidity can occur. Finally, the method in no way alters the sample concentration by either adding or subtracting water or changing the state of any part of the sample as occurs in the psychrometric or dew point methods [32].

1.3.1.5 Electronic sensors

Electronic hygrometers detect the change in the electrostatic capacity or electric resistance of a sensor when it absorbs moisture [33, 34]. The electrical capacitive

hygrometer uses a dielectric material made of high polymer membrane, as a sensor. Development of miniaturized electronic humidity sensors have been driven by the demand for low cost, reliable and compact sensors. For meteorological purposes, the sensor is put in a ventilation shelter to protect the sensor from precipitation and sunlight with the aspiration speed of 2 to 4 m/s around the sensor. The time constant with the shelter from the saturation to the room humidity is about 20 minutes, which is longer than that without the shelter, because of the shelter's large thermal capacity. The electronic capacitive hygrometer can be used in any environment where human can live. However, do not use the hygrometer in the atmosphere containing oil mist, flammable gas, dust, organic solvents, acid, alkaline or ammonia. Using the hygrometer in the atmosphere may cause its sensor electrodes to corrode, thus the sensor life is shortened. Generally, both sensor types, which are classified as secondary measurement devices, are inexpensive and have low power consumption, covering a wide humidity range with good repeatability but suffer from temperature dependency and cross-sensitivities to some chemical species.

1.3.2 Fiber-Optic Techniques for Humidity Detection

With the advent of optical fibre technology, a considerable level of research has been focused on fibre-optic-based techniques for humidity sensing. In a similar way to their electronic or mechanical counterparts, fibre-optic humidity sensors are secondary devices but show additional features like small size, immunity to electromagnetic interference, multiplexing and remote sensing capabilities, of which the counterpart electronic sensors lack. However, the limitations of the operating and accuracy of the fibre-optic-based humidity sensors are some of the drawbacks which researchers are striving to continue to address. Nevertheless, these sensors have found useful applications in various areas where electronic sensors were found to be inappropriate, thereby showing the real potential of fibre-optic-based sensors. Generally, fiber-optic based humidity sensing techniques include direct

spectroscopic, evanescent wave, in-fibre grating and interferometric methods, as discussed in sections below.

1.3.2.1 Direct spectroscopic-based sensors

This method examines the optical signal obtained and relates absorption or fluorescence based measurements to the concentration of the target analyte.

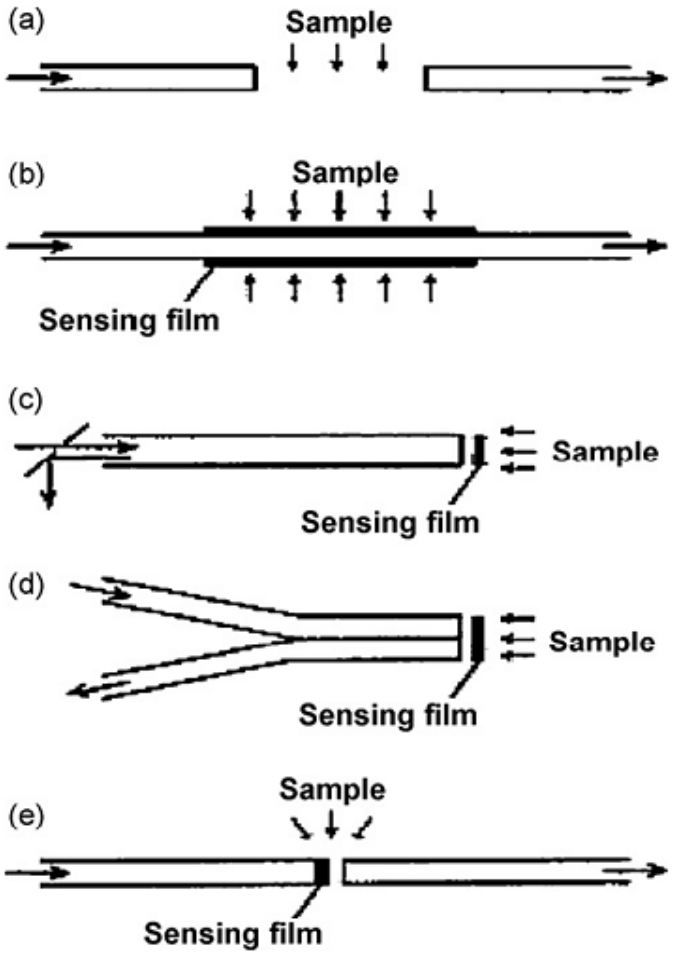

Figure 1.4 Various configurations for spectroscopic fibre-optic sensors[35]

Generally, as shown in Figure 1.4, the design of the sensors can simply comprise optical fibres with a sample cell for direct spectroscopic measurements or be configured as fibre optrodes, where a chemical selective layer, comprising chemical reagents in suitable immobilizing matrices, is deposited onto the optical fibre [36, 37].

Most spectroscopic-based configurations for humidity sensing are based on the optrode design where moisture sensitive reagents are attached to the tip of the sensing fibre, usually with the aid of a polymeric material to form the supporting matrix.

1.3.2.2 Evanescent wave sensors

Since 1985 onwards several evanescent wave (EW) based humidity sensors have been reported. This sensing method allows the optical fiber to be used as an intrinsic sensor where the EW field generated at the fiber interface interacts with the humidity sensing material surrounding the fiber which in turn allows for the detection of the attenuation/insertion loss or the resonant wavelength shift of the fiber structure due to the change in refractive index, optical absorption, or scattering of the sensing material with respect to the ambient RH [38, 39] . In fiber at each point of TIR, the interference between the incident and reflected signals at the core/cladding interface generates a standing wave which extends beyond the core of the optical fibre and penetrates into the cladding region. This creates an evanescent field, as shown in Figure 1.5.

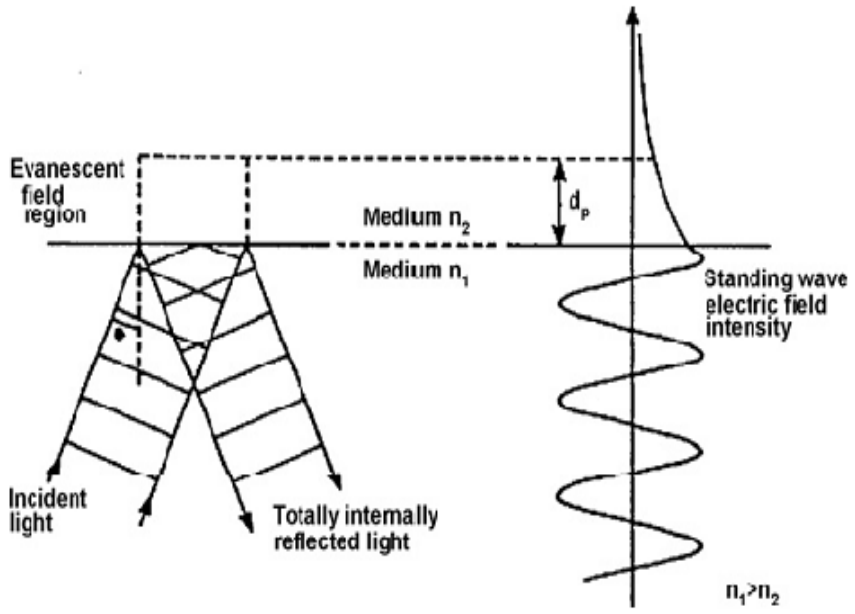

Figure 1.5 Evanescent field generated at the interface of two optically transparent media [5]

The amplitude of such wave decays exponentially with distance away from the core/cladding interface and follows the form [38] :

$$E(z) = E_0 e^{\left(\frac{z}{d_p}\right)} \tag{1.2}$$

where the penetration depth (d_p) is defined as the depth at which the amplitude of the evanescent field, E, has decayed to 1/e of the initial value E_0 at the core/cladding interface. The evanescent wave sensing method allows the optical fibre to be used as an intrinsic sensor where the field generated at the interface interacts with the target analyte surrounding the fibre, thus giving information as a result of optical absorption, refractive index change or scattering.

One of the earliest evanescent wave absorption-based humidity sensor was demonstrated by Russell and Fletcher [40] in 1985 using a 600 nm optical fibre with 12 cm of $CoCl_2$/gelatine sensing film. In such sensors, the general operating range was limited and they could only respond to a humidity level higher than 50%RH. Using the same chemical reagent and organic film combination ($CoCl_2$/gelatine), Kharaz and Jones [41] later demonstrated a quasi-distributed FO humidity sensing network consisting of 4 sensors using a 200 m hard clad silica fibre with each sensing point positioned about 20 m apart.

From the studies performed using films of a similar reagent/immobilizing material ratio, gelatine film was found to be insensitive below 40% RH, whereas HEC was able to respond to the 30–96% RH range, hence clearly showing the influence of the film constituent on the operating range of the sensor. This observation was substantiated by the work discussed by Jindal *et al* [42]. In their research, a U-bent humidity sensor, shown in Figure 1.6 using $CoCl_2$/polyvinyl alcohol (PVA) film was reported to be sensitive to a humidity range from 3 to 90% RH.

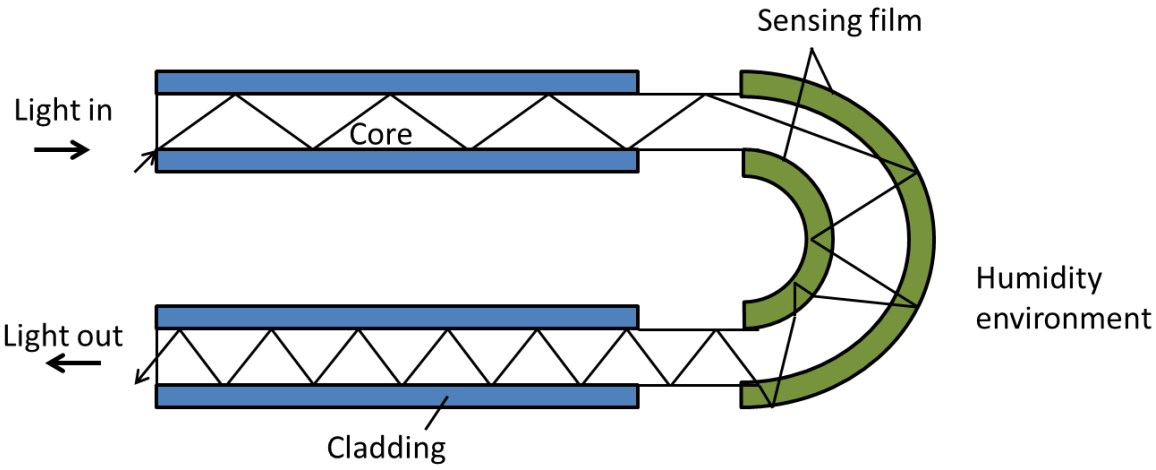

Figure 1.6 U-bent evanescent wave sensor configuration using cladding as the active sensing region [43]

Further detailed work to optimize the performance of the $CoCl_2$/PVA sensor was then undertaken by Khijwania et al. [44], in which the effects of film thickness, bend radius and fibre core diameter were investigated.

1.3.2.3 In-fiber grating sensors

The in-fiber gratings are created by inducing periodic refractive index modulation of the fiber core. Depending on the grating period they can be classified as fiber Bragg grating (FBG) or long period grating (LPG) sensors. An FBG based RH sensor commonly uses a sensing material that will expand and induce strain on the FBG with respect to RH. LPG based RH sensors are realized by coating the fiber with hygroscopic materials whose refractive index change with respect to RH.

The concept of in-fibre grating devices for humidity sensing is still fairly new. To date, there have only been a few literature reports on the subject, the earliest of which dates back to the year 2001. Humidity sensing using a FBG was first reported by researchers from EPFL, Switzerland [45, 46] where studies were carried out to investigate the influence of humidity on commercial polyimide-recoated FBGs. The findings from the investigations concluded that an FBG with polyimide coating was able to respond linearly over a wide humidity range. The sensor was reported to respond well to a humidity range of 10–90% RH and display good repeatability. Due

to its inherent sensitivity to temperature, a compensation scheme was required to extract humidity measurements from the sensor readings. The same sensing scheme proposed for humidity sensing was further explored by various groups and has been demonstrated in several interesting applications which include soil moisture monitoring [47, 48] and moisture detection in concrete [49].

The use of LPGs for humidity sensing was first reported by Luo *et al* [50] from Luna Innovations, USA. In the sensor design discussed and shown in Figure 1.7, carboxy methylcellulose (CMC) hydrogel was covalently attached to cladding of a LPG to form the humidity sensor.

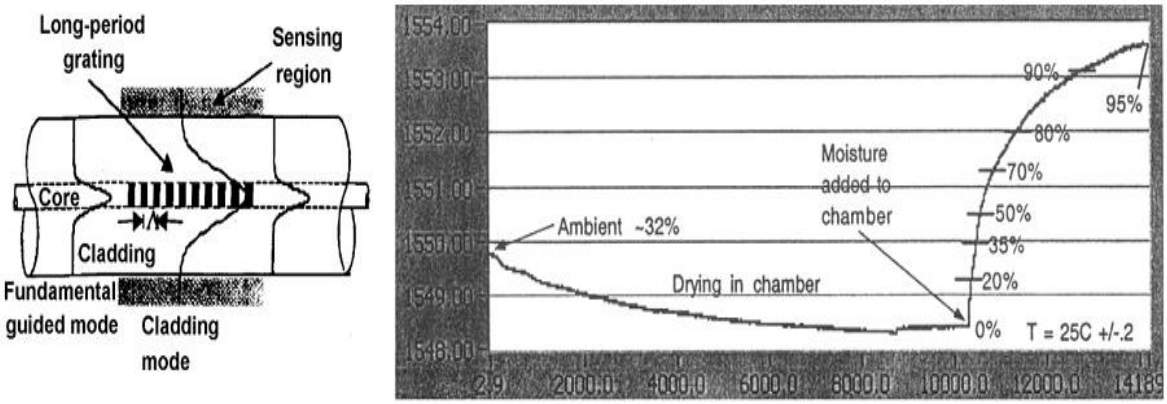

Figure 1.7 Schematic and sensing characteristics of a CMC-coated LPG humidity sensor [50]

The sensor demonstrated was found to operate well over a humidity range from 0 to 95%, with a non-linear response dependency with humidity change. A similar LPG-based humidity sensing scheme was demonstrated by Tan et al. [51] using a gelatine-coated LPG and Konstantaki *et al* [52] proposed a LPG humidity sensor utilizing polyethylene oxide (PEO)/$CoCl_2$ hybrid overlay as the moisture sensitive coating. Recent studies by Venugopalan *et al* [53] have shown the use of polyvinyl alcohol (PVA) film as a sensing material for LPG-based humidity detection.

1.3.2.4 Interferometric sensors

Optical sensing mechanism of an interferometric type fiber optic RH sensor relies on the perturbation of the phase properties of the light signal travelling in an optical

fiber introduced by the humidity change. The detection of the phase change is realised by mixing the signal of interest with a reference signal, consequently converting the phase difference between the two signals into an optical intensity change or wavelength shift [54, 55]. The different type of fiber interferometers used for RH sensing are Fabry-Perot interferometer, Michelson interferometer, modal interferometer, micro-ring interferometer, and Sagnac interferometer configurations. Interferometry is a powerful and versatile tool that has been applied in optical fibre sensing to yield high performance fiber optic sensors.

One of the earliest FO interferometric humidity sensors was demonstrated by Mitschke [56]. The proposed sensor design consists of a thin film Fabry–Perot interferometer formed at the tip of the fiber. As shown in Figure 1.8, the Fabry–Perot cavity in the proposed design was created by a layer of TiO_2 sandwiched in between two partially reflecting mirrors, with the thickness of the cavity optimized to match the operation at the wavelength of the input diode laser source. As the refractive index of the cavity material has a dependence on humidity, the resonance was therefore shifted in response to humidity change and can be conveniently detected by performing intensity measurement at a fixed wavelength.

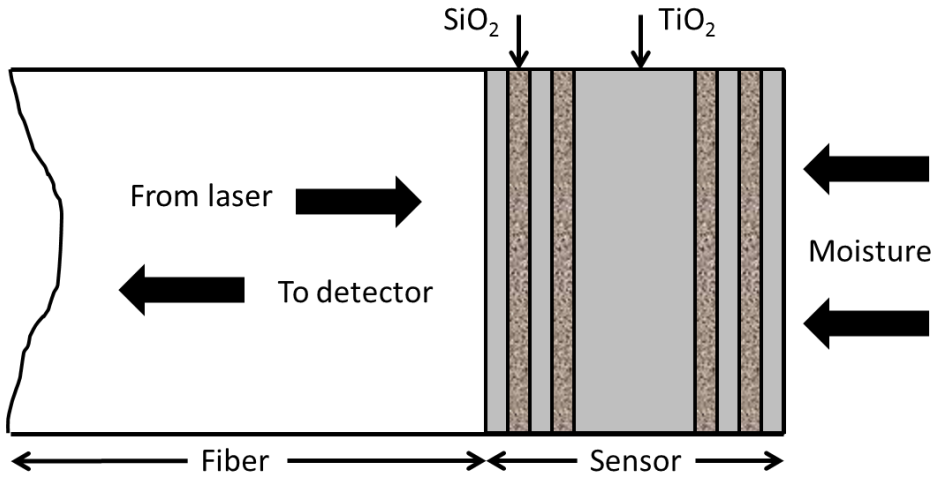

Figure 1.8 Fiber Optic Fabry–Perot interferometric humidity sensor [56]

Similar Fabry–Perot interferometric humidity sensors with a submicron cavity length were reported by Arregui *et al* [7] and Yu *et al* [8]. A typical multilayer thin-

film interferometric cavity was formed by stacking bilayers of alternating cationic and anionic polymers at the fibre tip. This was achieved by using the ionic self-assembled multilayer (ISAM) technique which gives good control over the cavity length as well as the material composition of each coating layer. Sensors with a cavity length (or the number of bilayers) optimized at a specific operating wavelength were shown to be able to operate over a wide humidity range.

As reported in literature, LPG based humidity sensors have been designed by synthesizing coatings of hygrosensitive materials on the cladding surface. Previously reported configurations have confirmed the feasibility of LPG based humidity sensors using gelatine, PVA, and other polymers as outcladding overlays. As far as performance aspect of sensor is concerned, trade-offs between sensor accuracy and bandwidth (the range of RH levels that the sensor can correctly read) have been witnessed [51-53]. Efforts are on-going for increasing the accuracy and range of LPG-based RH sensor by experimental investigation of certain materials or combinations of such materials that may render the sensor more sensitive and reliable.

1.4 Advantages of grating based sensing

As stated earlier, the fiber sensors should ideally possess a number of desired characteristics. This section will give the advantages and reasons for focusing on grating based sensing. Most intensity-based and interferometric sensors satisfy a majority of these features but are ultimately limited by one or more drawbacks. For example, interferometric sensors offer a very high degree of sensitivity but suffer from the requirement of expensive demodulation schemes, such as fringe counters. Additionally, the basic forms of such sensors suffers from directional ambiguity at certain points of the transfer function curve [6].

Phase–based sensors that operate over the linear region of the sinusoidal output curve are highly susceptible to drifts in source central wavelengths and minute ambient temperature fluctuations. Intensity based sensors offer unambiguous,

absolute output but require calibration that might be a function of the optical source characteristics and physical deformation along the fiber length. Moreover, such sensors provide limited sensitivities and might be difficult to multiplex.

Even the elegant Bragg grating based sensors have a few limitations that prevented their utilization in certain specific applications. Bragg grating sensors suffer from a number of frailties that include the requirement of a highly stable fabrication system [57]. Moreover, in order to implement sensors with higher sensitivities, uneconomical interferometric demodulation techniques have to be employed [58] and optical isolators might be required to prevent back-reflection induced source oscillations.

Additionally, existing fiber optic sensors of refraction are either too complex for feasible implementation or have limited sensitivities. For example Bragg grating based refractive index sensors require cladding etching within few microns of the core to gain access to the evanescent field of guided mode [5]. The etching process reduces the strength and integrity of the sensor and degrades the sensors performance in harsh environmental conditions. Surface Plasmon sensors have also been proposed as attractive refractive index sensors, but these types of sensors require polishing the cladding of the fiber for interaction of the induced Plasmon with evanescent field of propagating mode [59]. Though such sensors are highly sensitive to the small changes in the ambient index of refraction, they suffer from polarization sensitivity and are difficult to fabricate [60].

The cross sensitivity to the thermal changes can result in erroneous measurement in a sensor that has been calibrated to measure a perturbation other than temperature [61, 62]. Although temperature compensation and stabilization methods can be employed to overcome the thermal cross sensitivity, such schemes either complicate the signal processing or result in increased system cost. Any approach that preserves the mechanical strength of the LPG and results in sensitive index of refraction sensor

is always an open area of research. A LPG RH sensor with reasonably good sensitivity and wide RH range is again an area need to be explored.

The most influential development in LPGs is perhaps the demonstration of efficient coupling between the guided mode and the cladding modes of a single-mode fiber by using an LPG. Because cladding-mode LPGs do not need any special means to separate the coupling modes, their deployment for various applications is quite simple. The availability of a large number of cladding modes also offers flexibility in sensing applications. It should be mentioned that LPGs have also found many applications in optical sensing. The transmission characteristics of an LPG, whether formed in a single-mode fiber or waveguide, can be analyzed by the coupled-mode theory [11, 63, 64]. There exists a specific wavelength (resonance wavelength), at which the coupling between the guided mode and a specific cladding mode is strongest. The transmission spectrum of an LPG usually consists of a number of rejection bands centered at resonance wavelengths that correspond to different cladding modes. The center wavelength of a rejection band is in general sensitive to a number of physical parameters (temperature, strain, external refractive index index, fiber/waveguide dimensions, grating pitch, etc.).This property of the LPG has been explored for the realization of tunable devices and sensors. LPG has been considered as a distinct field of study (like fiber Bragg grating) only for the past ten years, i.e., since the cladding-mode LPG was proposed, regardless of the fact that many LPGs in different forms had been studied much earlier. In terms of application, the cladding-mode LPG has two distinct advantages, compared with other types of LPGs (e.g. polarization converters, acousto-optic filters, few-mode fiber gratings). First, it does not require any other component like polarizer or mode converter to separate the coupling modes. It can just be used as it is and thus simplifies its deployment, especially in systems where many gratings are needed. Second, the light that is coupled to the cladding of the fiber is no longer shielded from the fiber and becomes sensitive to any changes in the surrounding medium.

This property opens up many new possibilities for various applications (e.g., fiber-to-fiber coupling, add/drop multiplexing). The potential for the development of new devices through the manipulation of the cladding modes is large. It is envisaged that the activities in the development of LPG-based sensing devices to provide new functions will continue to grow. The following points highlight the various advantages of LPG.

- High sensitivity for multiple quantities (temperature, strain, Refractive index)
- Possibility of measuring at multiple points with one optical fiber
- Insensitive to corrosion
- Ideally suited to be embedded in composite structures
- Does not affect the mechanical properties of the material in which they are embedded
- Withstand high temperatures
- Very small and light
- Can have a sensor function and be signal carrier (optical transmission) at the same time
- Insensitive to electromagnetic interference
- Multi parameter sensing

1.5 Mode Theory of Fiber Grating

The section includes the discussion on Coupled Mode Theory (CMT), the formulae derivation for the resonant wavelengths of FBG and LPG and the differences between the two types of gratings. Wave propagation in optical fibers is analyzed by solving Maxwell's equations with appropriate boundary conditions. The problem of finding solutions to the wave-propagation equations is simplified by assuming weak guidance, which allows the decomposition of the modes into an orthogonal set of transversely polarized modes. The solutions provide the basic field distributions of the bound and radiation modes of the waveguide. These modes propagate without

coupling in the absence of any perturbation (e.g., bend). In literature, widely used methods mentioned are coupled mode theory, matrix method for complex structures, Bloch theory approach to find exact Eigen mode solutions of periodic structures and effective medium approach for short period gratings [65-69]. We have used coupled mode theory to analyze the grating structures.

Coupling of specific propagating modes can occur if the waveguide has a phase and/or amplitude perturbation that is periodic with a perturbation "phase/amplitude-constant" close to the sum or difference between the propagation constants of the modes. The technique normally applied for solving this type of a problem is coupled-mode theory. The basic principle is that energy can be transferred from one propagating mode to another as long as certain boundary conditions are satisfied. An index grating is one type of passive waveguide structure that is commonly used to achieve mode coupling. Index gratings, which consist of periodic variations in the refractive index of a waveguide, induce wavelength dependent mode coupling. The method assumes that the mode fields of the unperturbed waveguide remain unchanged in the presence of weak perturbation.

1.5.1 Coupled mode theory

Here, wave-propagation in optical fiber is introduced, followed by the theory of mode coupling. The coupling will occur in co-propagating or counter propagating modes. Let us consider an optical fiber with a refractive index profile $n^2(x,y)$ in which there is a periodic z-dependent perturbation given by Δn^2(x,y,z) this perturbation could correspond to periodic index variation as in FBG. The general forms of the coupled mode equations [70, 71] for two modes, A and B, are

$$\frac{dA}{dz} = \kappa_{12} B e^{i\Gamma z} \tag{1.3}$$

$$\frac{dB}{dz} = -\kappa_{21} A e^{-i\Gamma z} \tag{1.4}$$

where κ is the coupling coefficient, A and B are the amplitudes of the propagating waves and Γ is the detuning parameter [72, 73].

For each additional mode considered, another differential equation can be added, but here, the discussion will be limited to two modes for simplicity and clarity. Coupling takes place primarily between modes whose phases are matched. The detuning parameter Γ or δ is used to determine the phase matching condition and is defined as:

$$\Gamma = \Delta\beta - \mathrm{K} = (\beta_1 - \beta_2) - \frac{2\pi}{\Lambda} \tag{1.5}$$

where β_1 and β_2 are the propagation constants K=2π/Λ is the wave number defined by the grating period Λ. The propagation constant of each mode can be further defined by:

$$\beta = \mathrm{k_0} * \mathrm{n_{eff}}, \text{ where } \mathrm{k_0} = \frac{2\pi}{\lambda_0} \tag{1.6}$$

where λ_0 is the free space wavelength, and $\mathrm{n_{eff}}$ is the effective refractive index carry by mode as it propagates through the fiber and $\mathrm{k_0}$ is the wave vector.

When the two modes are perfectly phased matched (i.e.$(\beta_1 - \beta_2) - \frac{2\pi}{\Lambda}$), the detuning parameter goes to zero, and the exponential term in the coupled mode equations is maximized. In theory, the detuning parameter can go to zero, but in practice, it is usually a very small finite value when the phases of the two modes are closely matched. When the detuning parameter is not equal to zero, coupling still occurs, but the exponential term is not maximized. In many cases, the core mode will couple energy to several different modes, each of which have its own propagation constant and require an additional differential equation. The coupling coefficient κ, the phase relation of the two modes and the length of interaction will determine how much energy will be transferred from one mode to the other.

As there are two main types of index gratings in fiber optics – FBG and LPG. Structurally, both types of gratings are identical except that the periods of Bragg gratings are two orders of magnitude smaller than those of LPGs (~10^{-6} meters) versus ~10^{-4} meters, respectively. FBGs induce contra directional coupling. Light energy from forward propagating modes is transferred to modes traveling in the opposite direction. FBGs are often referred to as reflection gratings because of this effect. LPGs, on the other hand, couple energy co-directionally. Energy from the forward propagating incident modes is transferred to either forward propagating cladding or radiation modes depending on the structure of the waveguide.

1.5.2 Fiber Bragg Grating

If β_+ is the propagation constant for the core mode traveling in the +z direction and β_- is the propagation constant for the core or cladding mode traveling in the –z direction as shown in the Figure 1.9.

Then the phase matching condition in case of FBG is re written as [1, 74-77]:

$$(\beta_+) - (-\beta_-) - \frac{2\pi}{\Lambda} = (\beta_+) + (\beta_-) = \frac{2\pi}{\lambda_0}\left(n_{eff+} - n_{eff-}\right) - \frac{2\pi}{\Lambda} = 0 \qquad (1.7)$$

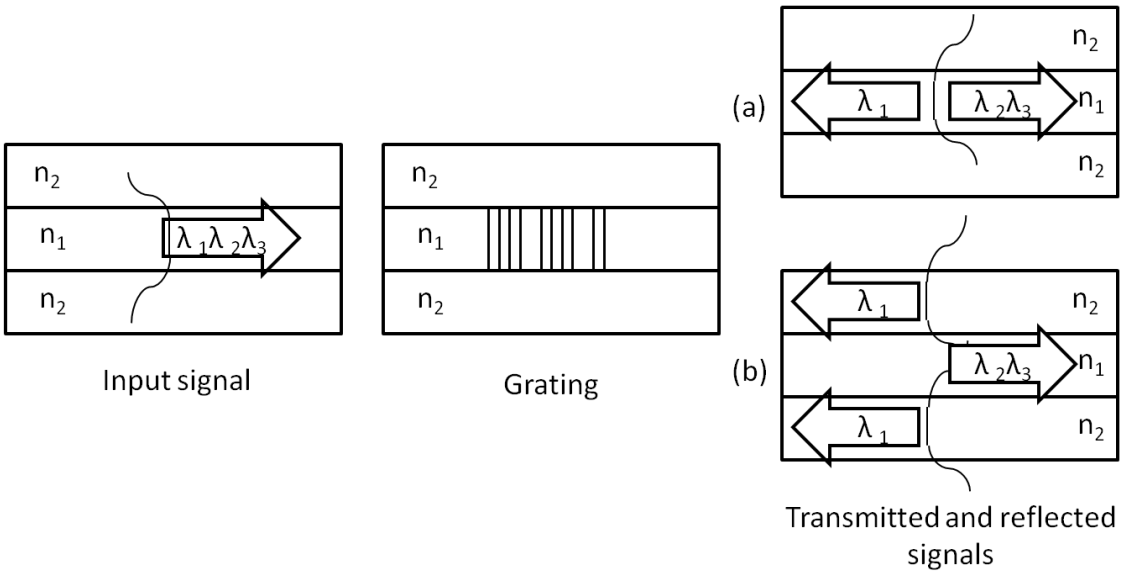

Figure 1.9 Contra directional coupling in a single mode fiber for a) core mode/core mode coupling b) core mode/cladding mode coupling [78]

The resonant wavelength is found from the phase matching condition solving for λ, i.e.

$$\lambda = (n_{eff+} + n_{eff-}) * \Lambda \quad (1.8)$$

Since a single mode fiber only has one propagating core mode in each direction, the propagation constants of these two core modes are equal in value but have opposite signs (i.e. $\beta+ = -(-\beta-)$). As a result, contra directional core mode/core mode coupling in a single mode fiber is a special case, and the resonant wavelength called Bragg wavelength can be written as:

$$\lambda_B = 2 * n_{eff} * \Lambda \quad (1.9)$$

where the Bragg grating wavelength, λ_B is the free-space center wavelength of the input light that will be back reflected from the Bragg grating, n_{eff} is the effective refractive index of the fiber core at the free-space-center wavelength and Λ is the grating period. In general form, the Bragg wavelength is reflected at the output as shown in the Figure 1.9 (a). The Figure 1.9 (b) is typical case of fiber Bragg grating, here the coupling between the core mode and contra-propagating cladding modes takes place, when some tilt angle or tapering in the grating structure is introduced. These cladding modes attenuate rapidly along the propagation axis.

1.5.3 Long period grating

Unlike FBGs, LPGs induce co directional coupling. Energy transfer occurs between core and cladding modes traveling in the +z direction. However, in single mode fibers, energy cannot be transferred to another mode within the core. Therefore, energy can only be coupled to cladding modes illustrated in the Figure 1.10.

As before, only two forward propagating modes will be considered and each will have their own unique propagation constant. β_{co} is the propagation constant for the incident core mode and β_{cl} is the propagation constant for the interacting cladding mode.

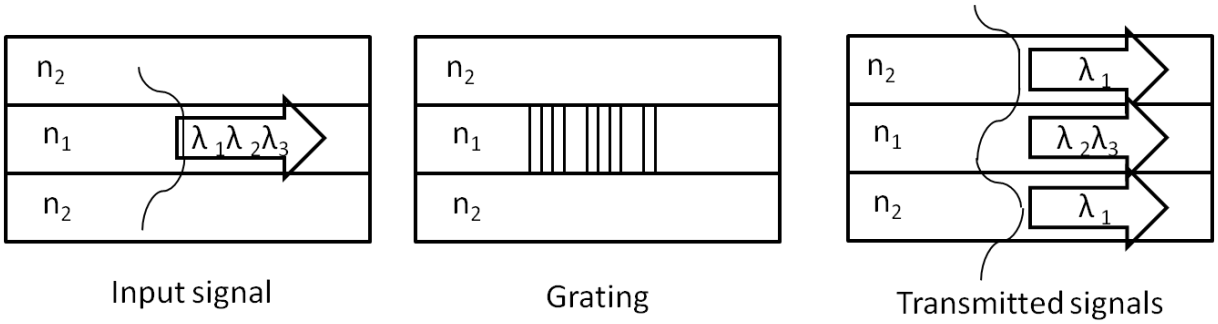

Figure 1.10 Co-directional coupling in a single mode fiber (core mode/cladding mode) [78]

The phase matching condition is written as:

$$(\beta_{co}) - (\beta_{cl}) - \frac{2\pi}{\Lambda} = (\beta_{co}) - (\beta_{cl}) = \frac{2\pi}{\lambda_0}\left(n_{eff\_co} - n_{eff\_cl}\right) - \frac{2\pi}{\Lambda} = 0 \quad (1.10)$$

Therefore resonant wavelength of LPG in single mode fiber is given by:

$$\lambda = \left(n_{eff\_co} - n_{eff\_cl}\right) * \Lambda \quad (1.11)$$

As with the FBGs, LPGs are often fabricated to filter wavelengths around 1550 nm. If $\left(n_{eff\_co} - n_{eff\_cl}\right)$ is on the order of 10^{-2} to 10^{-3}, the required grating period would be on the order of 10^{-3} to 10^{-4} meters, which is three orders of magnitude greater than the grating period required to filter 1550 nm with a FBG. Thus, LPGs are so named because their grating periods are two to three orders of magnitude greater than the wavelengths of light that they couple out of the incident signal.

1.6 Applications

FBGs have proven attractive in a wide variety of optical fiber applications, such as multiplexers, narrowband and broadband tunable filters, Gain equalization, Wavelength selective filters, Optical fiber mode converters and add/drop Mach-Zehnders, long-distance dispersion compensation in telecommunication networks, and improved pump efficiency in erbium-doped fiber amplifiers (EDFA), Optical strain gauges in bridges, Spectrum analyzers, Specialized narrowband lasers, elevators, building structures, structural heath monitoring, bone decalcification sensors in medical field applications, current sensors, soil moisture detecting sensors, smart structures, reactors, composites and mines [79-86]. Similarly

interesting diversity in LPG applications has been achieved as shown in the Table 1.2.

From Table 1.1, a picture of local access in optical network can be depicted as figure, in which the long-period gratings are liberally applied to very possible field ranging from central office to the subscriber's premises.

Table 1.2 Applications of LPG in various fields

Applications	**References**
Band rejection filters	[11, 87-91]
Band pass Filters	[71, 77, 92-94]
DWDM isolation filters	[93]
DWDM add/drop multiplexers	[95-102]
EDFA gain flattening and equalizers (1530-1560 nm)	[88, 103]
Laser fine tuning, modulation and wavelength stabilization	[98, 99]
Optical bend sensors	[100, 101]
Optical coupling schemes	[92, 104, 105]
Optical signal processing	[95, 96]
Optical fiber mode, spatial and polarization converters	[71, 77]
Refractive index sensors	[97, 106, 107]
Strain sensors	[22, 89]
Temperature sensors	[108, 109]
Wavelength selective devices	[90, 91]

1.7 Summary

The chapter outlines the overview of optical fiber sensing technology. Different types of Fiber Optic sensors like intensity based, spectrally based, Interferometric based, polarization based, Fabry-perot interferometer and grating based sensors are

discussed. Fundamental concepts of Mode theory for both LPG and FBG are covered. It is observed that LPG and FBG plays very successful role as sensor in various application fields.

CHAPTER 2. LITERATURE SURVEY

2.1 Introduction

At first, the observation of photo-induced refractivity in fibers was only a scientific curiosity, but over time it has become the basis for a technology that now has a broad and important role in optical communications and sensor systems. Research into the underlying mechanisms of fiber photosensitivity and its uses is on-going in many universities and industrial laboratories in North and South America, Asia, Europe and Australia. Several hundred photosensitivity and fiber grating related articles have appeared in the scientific literature and in the proceedings of topical conferences, workshops, and symposia. The formation of permanent gratings in an optical fiber was first demonstrated by Hill *et al*. [110] in the year 1978 at the Canadian Communications Research Centre (CRC), Ottawa, Ont., Canada. They launched intense Argon-ion laser radiation into a Germania-doped fiber and observed that after several minutes an increase in the reflected light intensity occurred which grew until almost all the light was reflected from the fiber. Spectral measurements, done indirectly by strain and temperature tuning of the fiber grating, confirmed that a very narrowband Bragg grating filter had been formed over the entire 1-m length of fiber. This achievement, subsequently called Hill gratings, was an outgrowth of research on the nonlinear properties of Germania-doped silica fiber. This established an unknown photosensitivity of Germania fiber, which prompted other associated inquires. Several years later, into the cause of the fiber photo-induced refractivity and its dependence on the wavelength of the light, which was used to the form the gratings. Similarly a number of novel and interesting techniques have been reported for the fabrication of LPG since the first was realized by Vengsarkar *et al*. [11] using the amplitude-mask writing method. Through this technique, hydrogen loaded germanosilicate fibers were exposed to a KrF laser (λ=248nm) through an amplitude mask made of chrome-plated silica. The optical

threshold level for mask damage was ≈ 100 mJ/cm^2 per pulse. Each grating imprint on the mask was one inch long, the duty cycle of the modulation structure was 50% and the grating periodicities ranged from 60 μm to 1 mm. Typical exposure condition of energy 25 mJ/pulse, pulse repetition frequency 20 Hz and beam area 2.6x1.1 cm^2 were used. The transmission spectrum of the grating was actively monitored as the grating being written. The fabrication times were in the 5-10 min ranges for fibers with 2-3% H_2/D_2. The amplitude-mask writing method is the most widely used due to its fundamental reliability and an amplitude-mask permit the repeated use to produce multiple LPG with little requirements for precision during the writing. The weakness of this technique is that change of grating periodicities could be realized only by using different periodicities of amplitude-mask which makes it expensive.

As discussed in the Chapter 1, FBG and LPG have very vast field of sensing applications. But when we talk about chemical or bio sensing, it is little difficult to obtain the sensors that can detect the presence of chemicals and radiation by using fiber Bragg gratings, because the light passing through the core of the optical fiber is isolated from the chemicals by the cladding of the optical fiber, and the core of the optical fiber is typically unaffected by radiation. In applications such as environmental monitoring, food quality and safety, refractometric sensors based on LPGs have shown very promising results.

On the same node, humidity sensing has become equally important in the industry through a wide spectrum of applications such as Structural Health Monitoring (SHM), food processing and storage, medicine, ecology, agriculture, mineral processing, fuel quality control, aerospace and other applications supporting human comfort. There is a lot of scope to explore new methods, design or configurations to enhance refractive index sensitivity and increase RH sensing range and demonstrate more accurate and reliable sensor.

2.2 LPG Theoretical Analysis

This section will cover the work reported on the theoretical aspects of LPG modeling, experimental verifications, higher refractive index coating concepts and different approaches to achieve highest enhancement factor in refractive index sensitivity.

Erdogan [77] reported experimentally and theoretically the transmission of a mode guided by the core of an optical fiber through an ultraviolet-induced fiber grating when substantial coupling to cladding modes occurs. A straightforward theory was presented that is based on the calculation of the modes of three-layer step-index fiber geometry and on multimode coupled-mode theory that accurately models the measured transmission in gratings that support both counter propagating (short-period) and co-propagating (long-period) interactions.

Vikram Bhatia *et al* [22, 111] presented photo induced LPG as versatile sensors for temperature, axial strain and index of refraction measurements. The principle of operation of such devices was discussed and the application to simultaneous temperature and strain was demonstrated. A grating fabricated in a conventional optical fiber was demonstrated for concurrent measurements of strain over a range of 2100 μ∈ and temperature over a range of 125°C, with maximum errors of 58 μ∈ and 1°C, respectively.

Yahei Koyamada *et al* [112] described first time the analysis of core-mode to radiation-mode coupling in LPGs that was surrounded with dielectric material whose refractive index is higher than that of the cladding. They calculated core-mode transmission spectra through LPGs by integrating numerically the coupled-mode equations between the core mode and a continuum of radiation modes. Also shown that the calculated core-mode transmission spectra that exhibit such loss band continuums as have already been observed experimentally but not yet theoretically estimated.

R. Hou *et al* [113] highlighted a new mathematical model, that can be used to explore the response of a long-period fiber grating to changes in ambient refractive indices of values both greater and less than that of the cladding. A numerical method was also presented to calculate the HE core and cladding modes. The result obtained suggested that LPGs coated with a material of higher refractive index than the cladding may be used as index sensors.

Xuewen Shu *et al* [114] explained the possibilities for ultrasensitive sensors by performing detailed investigation into the sensitivity of long-period fiber gratings (LPFGs) as a function of surrounding refractive index, strain, and temperature with specific attention given to the higher order cladding modes. The analysis revealed the existence of turning points in the mode dispersion characteristics at which ultrasensitive operation may be obtained. By performing wide range of coordinated experiments, they verified the theoretical predictions with close agreement and provided demonstrations of the device behavior close to those turning points.

J Besley *et al* [115] demonstrated a simple method of characterizing the sensitivities of the cladding modes of an optical fiber to environmental conditions through the analysis of a single device. The group designed and fabricated LPGs to couple with selected cladding modes and measure the sensitivities of these devices directly and good agreement was found between the directly measured and inferred sensitivities.

Kun-Wook Chung *et al* [116] presented tunable long-period grating in single-mode fiber analyzed by use of an ultrathin cladding layer and higher-order cladding mode coupling. The numerical simulation showed that a 225-nm tuning range in the newly designed ultrathin long-period grating (cladding thickness, 35 μm) with third-order cladding mode coupling can be obtained. The analyzed tuning range was seven times wider than those of the other known long-period gratings.

Xavier Daxhelet *et al* [117] reported very interesting study on LPG losses showed there is an optimal loss value that provides side lobe-free, 100% power transfer from

the core to the cladding mode for a uniform LPG. New approaches to LPG design in a fiber as well as in waveguide platforms for fiber-optic communication and sensor applications were proposed. A simple equation was revealed that relates this optimum lose value to the LPG length and the cross-coupling coefficient.

Rashmi Singh *et al* [118] reported a complete three-layer analysis of LPG giving design calculations corresponding to actual applications of long-period gratings as sensors and gain equalization filters for EDFA.

Imran M. Ishaqa *et al* [119] described that cladding was modified by a thin film of thickness of order 100 nm on it. This made LPG sensitive to surrounding refractive indices greater than that of silica and exhibited an enhanced sensitivity to external refractive indices lower than that of silica.

Ignacio Del Villar *et al* [72] demonstrated that the sensitivity to ambient refractive index changes in a great manner when deposited by an overlay of higher refractive index than the cladding in a Long Period Fiber Grating. The concepts of rearrangement of cladding modes and reasons related to fast shifts of the resonance wavelength of the attenuations bands in the transmission spectrum were explained. The experimental results were verified with numerical model.

Zhiyong Wang *et al* [120] presented theoretically and experimentally that only a nm-thick thin-film with a refractive index higher than that of the glass cladding can shift resonant wavelength of LPG in a great manner. The resonant wavelength shift was related with the variation of the thickness of the film and/or the variation of its refractive index.

Ignacio Del Villar *et al* [121] reported the detail analysis of cladding modes variations in effective index, mode profile, cross-coupling coefficient with the core mode, and self-coupling coefficient. The key parameters: thickness and the refractive index of the overlay, and the ambient refractive index were studied in detail. The work also

presented additional phenomenon of vanishing of the attenuation bands in the transmission spectrum if refractive index of the overlay was complex.

C. Qin *et al* [122] presented tuning characteristics of electrically tunable long-period gratings. A precise four-layer model was presented to quantitatively analyze the tuning potential of the gratings, and experimental data was provided to support the analysis. The reorganization effect was reported due to presence of inner electrode layer, made of high refractive index ITO, that landed to a significant increase (ten plus fold) in the tuning range of LPG tunable filters.

Jian Yang *et al* [123] described the dependency of the cladding-mode effective index on the parameters of the structure-modified LPG, such as the overlay refractive index (RI), the overlay thickness, the cladding-layer radius, and the ambient RI, as well as the order of cladding mode in detail.

Hannes Hochreiner *et al* [124] demonstrated the transmittance spectra of a long-period fiber grating element immersed in different mixtures of water and di-methyl sulfoxide. The obtained data was compared with a theoretical model based upon coupled mode theory and shown excellent agreement over a wide wavelength range.

Edward Davies *et al* [125] reported the method to increase the LPG sensitivity by sol gel coating. It was revealed that the RI sensitivity of an LPG was affected by both the thickness and the index value of the sol–gel derived titanium and silicon oxide higher index coatings.

Jianwei Mu *et al* [126] presented a simple analytical expressions for guided power transmission through a periodic long-period grating with consideration of the significant radiation loss derived from the complex coupled- mode theory. Further the effect of the radiation field on the guided mode was presented and explained by a decay factor for the envelope of the power profile along the waveguide.

2.3 LPG RH Sensor

In Phase 2, the reported work on the measurement of humidity is covered. The work includes RH sensors based upon evanescent wave, absorption and fiber gratings. The main focus reflects the material used, RH sensitivity reported and the range covered in the published work.

D.C. Bownass *et al* [127] reported the RH sensing based on humidity-induced refractive index change in an organic film coated onto the cladding of a bent fiber. The sensor was exposed to respond at relative humidity > 62% and > 80% using gelatin and polyethylene oxide films respectively.

Candido Bariain *et al* [128] presented an optical fiber humidity sensor fabricated using a hydrophilic gel agarose deposited on the thinner zone of a biconically tapered single-mode optical fiber. The sensor showed transmitted optical power variation of up to 6.5 dB with relative humidity RH changes between 30% and 80%.

Pascal Kronenberg *et al* [46] demonstrated a novel intrinsic relative humidity sensor that used polyimide-recoated fiber Bragg gratings. Strain induced Bragg wavelength measurement was the sensing method. The sensor showed linear, reversible, and accurate response behavior at 10–90% RH and at temperature varied from 13–60°C. The RH and temperature sensitivities were measured as a function of coating thickness.

Khay Ming Tan *et al* [51] reported gelatin coated long-period grating relative humidity sensor. The sensor showed a sensitivity of 0.833 %RH/dB with an accuracy of ±0.25 %RH, and a resolution of ±0.00833 %RH. The LPG RH sensor also reported repeatability, hysteresis and stability errors of less than ±0.877, ±0.203 and ±0.04 %RH respectively.

Maria Konstantaki *et al* [52] demonstrated a Poly(ethylene oxide)/cobalt chloride (PEO/$CoCl_2$) coated LPFG humidity sensor. The sensor was analyzed for RH range

from 50% to 95% with a resolution better than 0.2% and the response time constant of the sensor in order of a few hundred milliseconds.

T. Venugopalan *et al* [129] reported Polyvinyl Alcohol (PVA) coated LPG humidity sensor. The humidity range covered was 33- 97 %RH, sensitivity 5.68 nm/%RH (For 75-97 %RH) and response time < 1 min.

F. Ding [130] presented experimental studies on humidity measurements by using a FBG with multi-layer polyimide coating. The RH range covered was 30-80 %RH with sensitivity 2 pm/%RH.

R. Aneesh *et al* [131] reported an optical fiber humidity sensor based on TiO_2-nanoparticle doped nano structured thin film as the fiber sensing cladding and evanescent wave absorption was reported. The work showed a sensitivity of 27.1 mV/%RH with a throughout-linear sensor response over a dynamic range 24% to 95 %RH with an average response time of 0.01 s for humidification and 0.06 s for desiccation.

D. Viegas *et al* [132] reported a novel configuration able to measure relative humidity and temperature simultaneously. The sensing head was based on LPG coated with silica nanospheres in-line with a FBG. The sensor showed the sensitivity of 63.33 pm/%RH for humidity range of 20 to 50 %RH and 451.78 pm/%RH for 50 to 80 %RH respectively with response time of less than 1 sec.

Ming–Yue-Fu *et al* [133] presented a novel high-sensitivity fiber-optic humidity sensor based on a calcium chloride thin film to be coated on an air-gap LPG by combining the fiber side-polishing and fiber etching method. The humidity range covered was 55–95 %RH with reported sensitivity of 1.36 nm/%RH.

W. Zhang *et al* [134] investigated the response time of humidity sensors based on polymer optical fiber Bragg gratings. The humidity range covered was 30-90 %RH with sensitivity 3.6 pm/%RH and response time 7 mins.

Shijie Zheng *et al* [135] developed a Photonic Crystal Fiber (PCF) LPG humidity sensor high sensitivity and selectivity for nondestructive detection of moisture ingression into structures. The experimental results revealed that when compared to conventional fiber LPG, both, the exterior nano film-coated PCF-LPG and the interior nanofilm-coated PCF-LPG humidity sensors have the most sensitive resonance intensity change of $0.00022\%/10^{-3}$ dBm for relative humidity (RH) of 38% to 39% and average wavelength shift of 0.0007%/pm for a relative humidity variation from 22% to 29%.

Lourdes Alwis *et al* [136] very recently demonstrated LPG-based relative humidity sensor by using a tailored layered polyimide coating on the grating region at the distal end of the fiber probe. The range covered was from 20% to 80% RH. The sensitivity of the sensor was estimated to be 0.10 nm/%RH with negligible hysteresis (<1% RH).

Table 2.1 Work reported on RH sensing using Evanescent wave and Absorption Measurement

RH Sensing using Evanescent Wave and Absorption Measurement [29]			
%RH Range	**Sensing Method**	**Sensing Material**	**Reference**
50–80	Absorption measurement using straight and U-bent fiber	$CoCl_2$ doped gelatin film	[137]
25–95	Attenuation measurement using Optical Time-domain Reflectometer (OTDR) technique	Porous SiO_2 optical fiber Cladding	[138]
20-50	Direct in-line absorption	Etched borosilicate optical fiber segment doped with$CoCl_2$	[139]
20–80	Absorption measurement using OTDR technique	$CoCl_2$ doped gelatin film	[140]
0-95	Absorption measurement	Rhodamine B doped Hydroxy propyl cellulose	[35]

	using U-bent fiber	(HPC)Film	
30-96 for HEC 40-90for gelatine	Absorption measurement using U-bent fiber	$CoCl_2$ doped Hydroxyethyl cellulose (HEC) and gelatin films	[43]
30-80	Attenuation measurement using tapered fiber	Agarose gel	[128]
20-80	Absorption measurement using U-bent fiber	Phenol red doped Poly-Methyl-Methacrylate (PMMA) Film	[141]
>78 U bend 3-90	Absorption measurement using straight and U-bent fiber	$CoCl_2$ doped PVA film	[142]
20-80	Attenuation measurement using PMMA plastic optical fiber	HEC/PVDF film	[143]
50-90	Attenuation measurement using side-polished fiber	PVA film	[144]
0-80	Wavelength resonance shift using side-polished fiber	TiO_2 overlay	[145]
3-90	Attenuation measurement	Porous sol–gel cladding	[26]
75-100	Attenuation measurement using tapered fiber	Nanostructured sensing overlay using ISAM technique	[146]
9-94	Output power measurement of a diameter tapered MMF	Gelatin	[147]
20–34,35-80,80-92	Measurement of optical power loss of a U-bend cladding stripped (Plastic optical fiber) POF	Co/Polyiniline	[148]
5–50,50-90	Power loss measurement of a SMF connected to a coated U-bend glass rod	ZnO	[149]
5–95	Absorption measurement of U-bend cladding removed POF (MMF)	Ag-Polyaniline	[150]

50-89	Wavelength measurement in a SMF-MMF-SMF sensor structure	PVA	[151]
10–95	Transmission loss measurement in straight hydrothermally thinned silica fiber	ZnO Nano rods grown on fiber	[152]
40-90	Transmission power loss measurement of a hetero-core SMF	Hydrogel	[153]
2-10	Direct in-line absorption	Porous sol–gel fiber segment doped with $CoCl_2$	[154]
20–80	Wavelength measurement using SPR	ITO	[155]
10-70	Measurement of reflected optical power	Xerogel	[156]
20-80	Absorbance spectra measurement using SPR	Polymeric film with Agnano-particles	[157]
0-90	Absorption power measurement of a hollow core photonic bandgap Filter	No coating	[158]

In particular, Table 2.2 gives us an overview of some recent work reported by many research groups in between year 2008-2013[159]. The work tabulated here is RH sensing based on LPG and FBG, which is already described in the previous section.

Table 2.2 RH Sensing reported using LPG and FBG in the year (2008 to 2013)

Sensing method	**Sensing material**	**Range**	**(%RH) Sensitivity & response time**
Strain induced Bragg wavelength measurement	Polyimide(PI)	22-97	4.5 pm/%RH ~25 min
LPG resonance band wavelength shift measurement	PVA	33–97	~5.68 nm/%RH (for 75–97 %RH)

			<1 min
Intensity variation measurement following external RI change of a tilted FBG	PVA	20–74 74–98	2.52 dB m/%RH 14.9 dB m/%RH <2 s
LPG resonance band wavelength shift measurement	Poly(ethylene oxide)/$CoCl_2$	50–77 77–95	0.23 nm/%RH 0.33 nm/%RH <10 s
Strain induced Bragg wavelength measurement	PI	30–80	~2 pm/%RH
Strain induced Bragg wavelength measurement	PI	0–75	2.1 pm/%RH
Resonance-band wavelength measurement of an Air-Gap LPG	CaCl2	55–95	1.36 nm/%RH
Wavelength measurement of a LPG and a FBG configured in series (FBG for temperature calibration)	SiO2 nano-sphere film	20–50 50–80	63.33 pm/%RH 451.78 pm/%RH
Strain induced Bragg wavelength measurement	Silica/di-ureasil	5–95	22.2 pm/%RH
Strain induced Bragg wavelength measurement of etched POF	No coating (PMMA polymer cladding)	30–90	33.6 pm/%RH 7 min
Intensity and wavelength measurement of a LPG written in a PCF	$Al_2O_3^+$ +/PSS^- nano-film	22–29 38–39	0.0007%/pm 0.00022%/10^{-3}dBm

2.4 Investigation of FBG in MMF

FBGs have been recognized as important fiber-optic devices used for spectral filtering, dispersion compensation, wavelength tuning, and sensing in optical

communication and optoelectronics. We also want to explore the application of FBG in multimode fibers. As single mode fiber (SMF) has a small core diameter, the insertion loss is undeniably high when it couples light with non-single-mode-based optical devices. As Multi-mode fiber (MMF) has a large core diameter of typically 50 or 62.5 μm, it is easy to couple with other lasers or optical sources. The reported work on investigation of FBG in MMF is as follows:

Wanser *et al* [160] reported first the calculation of the theoretical spectrum of a Bragg grating in MMF, showing multiple peaks, and proposed its applications as bending sensors.

Mizumami *et al* [161] experimentally investigated the spectral characteristics of Bragg gratings in graded-index MMF and an analysis of grating behavior including excitation condition of propagating modes, temperature, and polarization characteristics. An advantage of Bragg gratings in multimode fiber and the applications was also discussed.

Zhao *et al* [162] demonstrated fabrication of a Bragg grating in a multimode fiber by phase mask technique, whose spectrum was similar to that of Bragg gratings in single-mode fibers, and its temperature and strain responses were analyzed.

Szkopek *et al* [163] proposed a novel multimode fiber structure with modal propagation characteristics and tailored it to facilitate the creation of narrowband high reflectivity Bragg gratings, and later demonstrated gratings with reflectivity of >98% and bandwidths of <0.5 nm at ~1550 nm in this fiber [164].

Tongyu Liu *et al* [165] reported a low-cost fiber optic sensor system based on multimode fiber and an Light emitting diode (LED) light source. A multimode fiber Bragg grating element was used as a strain sensor.

Changgui Lu *et al* [166] investigated theoretically Bragg gratings in optical fibers in multimode propagation by using the coupled-mode theory and considering two

modes coupling. It was reported that Bragg gratings in multimode fibers showed multiple reflection peaks due to the coupling between all bounded modes.

Lim *et al* [167] presented the fabrication of two Bragg grating sensors in 62/125 μm graded-index multimode fiber by the holographic method and phase mask technique respectively for application in a power-by-light hydraulic valve monitoring system.

Xinzhu Sang *et al* [168-170] analyzed the formation characteristics of Bragg gratings in single mode and MMFs and found that different kinds of grating can be achieved with different irradiation pulses. A chemical sensor based on a Bragg grating in the multimode fiber was demonstrated experimentally. The sensor has been used to measure the concentrations of propylene glycol solutions and sugar solutions, which could detected 0.05% and 0.04% concentration change for them with the wavelength interrogation module of 1-pm resolution.

2.5 Gaps Identified in Present Study

As stated in the introduction, the common limitations encountered while dealing with optical fiber sensing systems, the importance of these drawbacks and elucidate the reasons for attempts to arrive at solutions to these problems.

Grating-based sensors are commonly used in chemical sensing. The LPG can be employed as a general refractive index sensor and used in conjunction with chemical selective materials to create a species-specific chemical sensor. This thus forms a very attractive refractive index based chemical sensing mechanism which has been employed in the detection of a variety of chemical species. As mentioned in Literature survey; Table 2.2 described the RH sensing reported using LPG and FBG in the year (2008 to 2013). The use of LPGs for humidity sensing was first reported by Luo *et al*. [50] from Luna Innovations, USA. With Carboxy methylcellulose (CMC) hydrogel, that was covalently attached to cladding of a LPG to form the humidity

sensor. The sensor demonstrated was found to operate well over a humidity range from 0 to 95%, with a non-linear response dependency with humidity change. The sensor was observed to be unstable when it was fully saturated at conditions approaching 100%RH and temperature compensation was also required to obtain accurate humidity measurements.

A similar LPG-based humidity sensing scheme was demonstrated by Tan *et al* [51] using a gelatine-coated LPG and Konstantaki *et al* [52] proposed a LPG humidity sensor utilizing polyethylene oxide (PEO)/CoCl2 hybrid overlay as the moisture sensitive coating. In both sensors, however, the operating humidity range was found to be limited.

Venugopalan *et al* [53] have shown the use of polyvinyl alcohol (PVA) film as a sensing material for LPG-based humidity detection. Using a similar approach to the examples discussed in Table 2.1, PVA overlay of ~4 μm was coated onto the optical fiber in which an LPG with a period of 300μm was inscribed. The sensor was evaluated over a relative humidity range from 33 to 97% using the resonance loss band at 1500 nm where the change in transmission dip was monitored and calibrated against humidity change, but the response time of sensor was 80 sec.

On critically analyzing the findings reported by various research groups, there is a tradeoff between sensitivity, RH range and response time. Therefore to design a sensor that is capable to cover wide RH range with acceptable sensitivity and response time is always open area of research.

Whilst FBG sensors are advantageous in many aspects over their electronic counterparts, the relatively high cost of the optical signal interrogators present a major limitation in many applications, even though it's per sensor cost could be competitive in a large capacity multiplexing system. This is particularly the case where the number of sensors required is not very large. For example, in a temperature monitoring system for an electrical transformer, it normally requires

only a few sensors to monitor the temperature of the winding coil and the oil. It will be difficult to justify the cost associated with the implementation of a tunable laser based sensor system as the large multiplexing capacity provided by such system is excessive for such application. A solid state laser is difficult to couple with SMF, and therefore it can be a candidate to be tuned with a Bragg grating in MMF.

2.6 Problem Formulation

The large scale commercialisation of optical fiber sensors has, to a certain sense, been restricted by one or more limitations. One of the most significant issues is the cost of the sensor and the signal–processing equipment. Thus, the optical fiber sensor market would benefit tremendously from a sensing scheme that is simple cost effective and easy to implement.

In most of the refractive index sensors that are based on optical fiber as the primary waveguide require a mechanism with which the access to the fundamental core mode to detect fluctuation in the ambient chemical environment becomes possible. This interaction with the core mode can be achieved directly by chemical etching or indirectly by coupling to a cladding mode which can then interact with the medium surrounding the cladding material.

Existing FBG refractive index sensors are based on the interactions between the evanescent field of the fundamental core mode and the surrounding materials. Because a normal FBG is intrinsically insensitive to the ambient refractive index, the fiber cladding should be removed by chemically etching the cladding around the grating to within a few microns of the core. This process is time consuming, requires a high degree of control and, most importantly, reduces the mechanical strength and integrity of the fiber, another disadvantage is the FBGs cross-sensitivity. Thus the mechanical strength and the durability of such kinds of sensors will be inevitably reduced greatly and the costs will increase due to the use of special kind of fibers. These disadvantages limit the possible applications of FBG index of refraction sensor

enormously. No doubt the tilted FBG has the potential to provide highly sensitive optical platform for RI sensing [171]. LPG sensors couple the guided core mode to co propagating cladding mode, thus causing the attenuation peaks in transmission spectrum. LPG has a higher sensitivity to the refractive index of the ambient media without diminishing the mechanical strength of the fiber grating, because the stronger dependences of its cladding modes on the ambient refractive index. A sensitive refractive index and humidity sensors are highly attractive choice. As we all know, RH monitoring has a significant impact in various application fields. Various sensing schemes based on fiber optics have been studied to develop all-optical RH sensors. Several LPG based humidity sensors using different overlay materials and distinct sensitivities have been reported as discussed in the Literature survey. Previous work includes geometrical modification of fiber leading to fiber losses and limited robustness of the sensor. Therefore it was chosen to explore the scope of LPG particularly in refractive index and relative humidity sensing fields.

MMF offer more flexibility in grating design and performance characteristics as compared to single-mode fiber, since the spectral response may be tuned by core size, numerical aperture, and mode coupling characteristics of the gratings.

MMFs have the merit of easy coupling with inexpensive light sources and other optical components due to their large core, and so gratings in multimode are preferred to yield lower cost systems. Therefore, Bragg gratings in MMFs have also received attention in recent years.

A low-cost fiber optic sensor system based on multimode fiber and an LED light source can be very useful. The high cost normally associated with wavelength interrogators for single mode fiber FBG sensors can be overcome by the utilization of a low cost multimode fiber pigtailed LED light source.

The MMFBG sensing schemes could be used for short distance, high sensitivity, high speed, strain, temperature and acoustic sensing applications.

Furthermore in many industrial monitoring and control applications the distance between the sensors and the interrogator is not very long which does not require the high optical power level from tunable laser or the Amplified Spontaneous Emission (ASE) source. Therefore it is of great importance to develop low cost, high performance OFS solutions for the small sensor count, short distance applications in order to make the FBG sensor systems more competitive to conventional technologies both in the industrial and the domestic applications [165].

Optical sensors are often interrogated using broad-band light sources and such sources of high output are generally pigtailed using MMF. Thus, it is application advantageous and cost effective if sensors can be made in MMF. Therefore it is required to investigate FBG in multimode fibers.

2.7 Objectives

- To model and characterize the Long Period Gratings by using appropriate simulation tools
- To fabricate and validate LPG sensors for sensing application
- To investigate and analyze FBG sensors in multimode fibers

2.8 Major Contribution of Thesis

The research work presented in this thesis combines refractive index sensitivity enhancement of LPG by using simple dip coated Indium tin Oxide (ITO) overlay on it. Further sensor/coating attachment method to develop an RH sensor for informative evaluation of the humidity effect. Here for the first time, a sensor probe based on LPG coated with gelatin-Cobalt Chloride ($CoCl_2$) is proposed and experimentally demonstrated. However the same combination was reported by Russell and Fletcher [137] on plastic cladding silica fiber 12cm long with 0.6mm silica core and bent in the middle into a 5-mm diameter to form U-shape. The work reported described an optical sensor with a bonded reagent on its surface which

changes color when exposed to gaseous moisture. Optical fiber resulted in sensors for humidity over a range of about 40-80% RH by observing the absorption spectrums. It was concluded in the work that spectrum of cobalt chloride on the fiber was similar to a transmission spectrum rather than an attenuated total reflection spectrum .Therefore, spectrum was found less sensitive to measurements near the critical angle, and to refractive index changes than was the case with an attenuated total reflection spectrum. However, this sensor device was limited to the determination of the relative humidity above 40%. In the year 1988, Quan Zhou *et.al* [139] utilized $CoCl_2$, in conjunction with a porous optical-fiber matrix to develop a new humidity sensor with enhanced sensitivity capable of detecting the relative humidity down to 0.5% at 25 ^{O}C. The high surface area and direct absorption of light passing through the porous glass sensor segment resulted in a device with the demonstrated capability to measure relative humidity levels below **1%** at room temperature. The above mentioned work of 80's signaled the utility of gelatin and cobalt chloride combination for humidity measurements and opened the possibility of utilizing same combination for different fiber structures. All the issued addressed in the work contribute to implement a simple and economical index of refraction and moisture measurement system. Other than humidity, this LPG based RH sensors offer numerous advantages in corrosion monitoring, chemical and food processing. Similarly LPG-based refractive index sensor has wide application in biochemical sensing. The investigative study of FBG in MMF is very useful for developing low cost sensing systems.

2.9 Outline of Thesis

The thesis has been organized into eight chapters. Contents of each chapter are briefly described as under:

Chapter 1 introduces the overview of Optical fiber sensing technology and different types of Fiber Optic sensors like intensity based, spectrally based, Interferometric

based, polarizations based, Fabry–perot interferometer and grating based. Fundamental concepts of the operating principle of long-period gratings with short-period fiber Bragg gratings using Mode theory of grating are discussed.

Chapter 2 provides the comprehensive literature review, gaps in present study, problem formulation and objectives.

Chapter 3 describes the mathematical model used to analyze the LPG. Chapter highlights coupled mode theory and the solutions obtained for the coupled mode equations. Analysis of transmission spectra obtained for LPGs in single mode fiber using Matlab and software package Optigrating 4.2.2 is covered. The chapter also includes the experimental validation of theoretical observations.

Chapter 4 introduces the phenomenon of photosensitivity in optical fibers and the techniques for improving photosensitivity. It also covers the techniques of fabrication for long-period gratings like Excimer laser and point by point method. The process of fabrication of LPG using Teraxian grating writing is discussed in length. Various optical and non-optical components along with the different modes of grating writing are highlighted. Experiments conducted for the characterization of fabricated uniform LPG are also included.

Chapter 5 describes the theoretical and experimental analysis of metal oxide coated LPG refractive index sensor. The coating structure and its properties have been investigated using SEM, FTIR and Raman spectroscopy analysis. The RI sensitivities of the uncoated as well as ITO coated LPG is monitored with glycerol solutions of different concentrations. A comparison of both demonstrated that the sensitivity is enhanced by 2-3 times because of coating in our case.

Chapter 6 outlines the significance of moisture measurement and the existing technologies; both electronic and optical are highlighted. Also describes the experimental demonstration of gelatin/$CoCl_2$ coated LPG as Relative humidity

sensor at length. The LPG coated with mixture demonstrated a sensitivity response of 0.18 nm/%RH with an error of ±1.45%. The design offers minimal hysteresis loss of ±0.18% and a stability error of 0.056% and repeatability of 99.7%. In addition to this, the effect of grating period on the performance of sensor has also been studied. It is seen that LPGs with a lower grating period have higher sensitivity of RH level changes. The ITO and $CoCl_2$/gelatine coated LPG as humidity sensor is also included in the chapter. The sensor measures RH variation efficiently in the range of 40% to 95% RH with sensitivity of 0.12 nm/%RH, accuracy of 98.45%, stability error 0.031%, hysteresis error of ±0.12% RH and repeatability of 98.7%.

Chapter 7 deals with the analysis of FBG written in MMF, the scope of FBG as current sensor is covered in detail. The chapter highlights the fabrication and characterization of FBG in MMF. The effect of temperature and strain on FBG in MMF is also studied theoretically using software package Optigrating 4.2.2. FBG as a current sensor is demonstrated successfully using two configurations: Without housing and with housing. The designed sensor shows resolution 0.05 Amp, accuracy 95%, and repeatability 5 pm.

Finally, Chapter 8 covers conclusions, recommendations of the thesis and provides the future scope of the work.

CHAPTER 3. MODELING OF LONG PERIOD GRATING

3.1 Modeling of Long Period Grating

This chapter describes a mathematical model for the analysis of LPG. As described in chapter 1 that LPG enables coupling from core mode to co-propagating modes i.e. higher order core modes or cladding modes for the wavelengths which satisfy the phase matching condition. Coupled mode theory (CMT) is the most widely used technique to analyze such waveguides with periodic perturbation [65, 66]. This method assumes that the modal fields of the waveguide remain unchanged in the presence of weak perturbation. A set of first order differential equations giving the change in the modal field amplitudes along the perturbed waveguide region is obtained which have analytical solutions for uniform periodic perturbation. Another widely used method is matrix method [66, 67] which provides clear solutions for more complex structures. This assumes slow variation in the nature of perturbation such that complex grating may be considered as a concatenation of several uniform gratings. Bloch theory approach [68] has also been used to analyze grating structures which results in exact Eigen mode solutions of periodic structures. Another interesting method which is used to analyze wave propagation in periodic structures, applied mainly to short period gratings is the effective medium approach [69]. Recently graphical solution method and new transfer matrix method have been reported to analyze LPG [172, 173].

Throughout this thesis coupled mode theory is used to analyze the grating structures. In this chapter, the results of coupled mode theory analysis used to compute the transmission spectra of LPG are reviewed. A brief introduction about mode theory is included in the chapter 1; the following section gives detail explanation about CMT.

3.2 Coupled Mode Theory

Coupled-mode theory gives only approximate solutions of Maxwell's equations in layered media still it is straightforward and intuitive. The solutions obtained give the optical properties of most fiber gratings of interest. We consider an optical fiber with axis along the z-direction. In the absence of any perturbation, the total field propagating in the fiber can be expressed as a linear combination of normal modes as [70]

$$E(x,y,z,t) = \sum_m A_m \Psi_m(x,y) e^{-i(\omega t - \beta_m z)} \quad (3.1)$$

where A_m is the constant amplitudes and Ψ_m (x,y) represents the transverse field profile of the m^{th} mode with a propagation constant β_m, when a field of frequency ω is excited into the fiber if there is a sinusoidal perturbation of period Λ along the fiber axis in the core, the perturbed refractive index in the core is then given by:

$$n_{pt} = n_1 + \delta n(z) \quad (3.2)$$

$$\text{where } n_z = \overline{\Delta n} + \Delta n \sin\left(2\pi z/\Lambda\right) \quad (3.3)$$

In above equation n_1 is the refractive index in the unperturbed core, $\overline{\Delta n}$ is the increased average index in the core, Δn is the peak modulation in the refractive index and Λ is the period of perturbation. The perturbed relative permittivity can now be written as:

$$\varepsilon_r + \Delta\varepsilon_r = (n_1 + \delta n(z))^2 \quad (3.4)$$

where the relative permittivity of the unperturbed medium $\varepsilon_r = n_1^2$ and assuming the perturbation to be only a small fraction of the refractive index it follows that:

$$\varepsilon_r \cong 2n_1 \delta n(z) \quad (3.5)$$

Now the total induced polarization can be defined as:

$$P = \varepsilon_0(\varepsilon_r - 1 + \Delta\varepsilon_r(z))E$$

$$= \varepsilon_0 \chi E + \varepsilon_0 \Delta\varepsilon_r(z) E \quad (3.6)$$

$$= P_{unpert} + P_{grating}$$

We have wave equation [1]:

$$\nabla^2 E = \mu_0 \varepsilon_0 \frac{\partial^2 E}{\partial t^2} - \mu_0 \frac{\partial^2 P}{\partial t^2} \quad (3.7)$$

Substituting Equation (3.6) in Wave Equation, we get

$$\nabla^2 E = \mu_0 \varepsilon_0 \frac{\partial^2 E}{\partial t^2} - \mu_0 \frac{\partial^2 P_{grating}}{\partial t^2} \quad (3.8)$$

Now considering the total field as the combination of fields due to only 2 modes (co-propagating) having maximum interaction due to perturbation, Equation (3.1) becomes [71]:

$$E(x, y, z, t) = A_1(z)\Psi_1(x, y)e^{-i(\omega t - \beta_1 z)} + A_2(z)\Psi_2(x, y)e^{-i(\omega t - \beta_2 z)} \quad (3.9)$$

where β_1 and β_2 are the propagation constants of the modes calculated in the absence of perturbation in the fiber, $A_1(z)$ and $A_2(z)$ are their corresponding amplitudes, ψ_1 and ψ_2 represent the normalized field profiles. Substituting Equation (3.9) in Equation (3.8) and considering that in the presence of weak perturbation, the variation in mode amplitude is slow (slowly varying envelope approximation (SVEA) satisfying [1, 77] :

$$\left|\frac{\partial^2 A_k}{\partial z^2}\right| \ll \left|\beta_k \frac{\partial A_K}{\partial z}\right| \quad (3.10)$$

where the subscript k denotes the mode number, we get:

$$-2i\beta_1 \frac{\partial A_1}{\partial z}\psi_1 e^{i(\omega t - \beta_1 z)} - 2i\beta_2 \frac{\partial A_2}{\partial z}\psi_2 e^{i(\omega t - \beta_2 z)} = \mu_0 \frac{\partial^2 P_{grating}}{\partial t^2} \quad (3.11)$$

Multiplying both sides of Equation (3.8) by ψ_1* and integrating over the whole grating cross section and by considering the orthogonality relation between modes given by:

$$\int_{-\infty}^{\infty} 1 \int_{\infty}^{\infty} \Psi_1 \Psi_m^* \, dx \, dy = 0 \tag{3.12}$$

We get

$$-2i\beta_1 \frac{\partial A_1}{\partial z} \psi_1 e^{i(\omega t - \beta_1 z)} = \int_{-\infty}^{\infty} 1 \int_{\infty}^{\infty} \mu_0 \frac{\partial^2 P_{grating}}{\partial t^2} \Psi_1^* \, dx \, dy \tag{3.13}$$

Substituting for $P_{grating}$ from Equation (3.6) in Equation (3.13) and choosing the appropriate synchronous terms we get,

$$\frac{\partial A_1}{\partial z} = -i\kappa_{11} A_1 - i\kappa_{12} A_2 e^{i(\beta_1 - \beta_2 - K)z} \tag{3.14}$$

where $K=2\pi/\Lambda$ represents the grating vector. Similarly by multiplying both sides of Equation (3.11) by Ψ_2^* and repeating the steps as described above we get,

$$\frac{\partial A_2}{\partial z} = -i\kappa_{22} A_1 - i\kappa_{21} A_1 e^{i(\beta_1 - \beta_2 - K)z} \tag{3.15}$$

where $\kappa_{11}$and κ_{22} represent dc coupling coefficients andκ_{12} and $\kappa_{21}$are cross coupling terms. The κ values can be computed analytically or numerically knowing the field expressions. We can substitute $\kappa = \sqrt{\kappa_{12}\,\kappa_{21}}$ leading to coupled mode equations as follows:

$$\frac{\partial A_1}{\partial z} = -i\kappa A_2 e^{i(\beta_1 - \beta_2 - K)z} \text{ and } \frac{\partial A_2}{\partial z} = -i\kappa A_1 e^{-i(\beta_1 - \beta_2 - K)z} \tag{3.16}$$

Now making a variable transformation, we get:

$$A_1 = R\, e^{i(\beta_1 - \beta_2 - K)z} \tag{3.17}$$

$$A_2 = S\, e^{-i(\beta_1 - \beta_2 - K)z} \tag{3.18}$$

The CM Equations can be rewritten as [174]:

$$\frac{dR}{dz} = -i\kappa S - i\delta R \tag{3.19}$$

$$\frac{dS}{dz} = -i\kappa R + i\delta S \tag{3.20}$$

where $\delta = (\beta_1-\beta_2-K)/2$, represents the detuning factor, as mentioned in Chapter 1. Coupling between the two modes is maximum, for frequency satisfying zero detuning condition, i.e. $\delta=0$; given by:

$$\beta_1 - \beta_2 = {}^{2\pi}/_{\Lambda} \tag{3.21}$$

where Λ is the grating period. The Equation (3.21) represents the phase matching condition between two modes.

3.3 Solution of Coupled Mode Equations

Imposing the boundary condition (that all the power is launched into the core mode at the input to the grating, which is the usual case), i.e.

$$R(z = 0, \delta) = 1 \tag{3.22}$$

$$S(z = 0, \delta) = 0 \tag{3.23}$$

The solutions to the coupled mode equations given in Equations (3.19)-(3.20) can be obtained. The transmission coefficient of the grating of length L would be given by R (L,δ). Closed form solutions of the coupled mode equations can be obtained for uniform gratings [174].

In uniform gratings the grating length and period is uniform throughout the length of the grating in which the CM equations can be solved analytically. Differentiating Equation (3.19)-(3.20) and substituting for the first order derivatives from the original Equation (3.19)-(3.20), the resulting set of equations can be solved by applying the boundary conditions given by Equation (3.22) and (3.23). The general solutions obtained are given by:

$$R(z = L, \delta) = \cos(\gamma L) - i\frac{\delta}{\gamma}\sin(\gamma L) \quad (3.24)$$

$$S(z = L, \delta) = -i\frac{\kappa}{\gamma}\sin(\gamma L) \quad (3.25)$$

where $\gamma = \sqrt{\kappa^2 + \delta^2}$ (3.26)

The transmitted power corresponding to the two interacting modes at the end of the grating of length L are given by $|R(z = L, \delta)|^2$ and$|S(z = L, \delta)|^2$. The core mode transmitted power:

$$|R(z, \delta)|^2 = 1 - \frac{\kappa^2}{\gamma^2}(Sin(\gamma z))^2 \quad (3.27)$$

For a wavelength corresponding to zero detuning, i.e. $\delta = 0$, $\gamma == \kappa$, the transmitted power in the core would be simply $(cos(\gamma z))^2$, and for a given grating strength the power output at the core varies as a cosine function with increasing grating length. It is clear from Equation (3.22) that total power associated with the two modes is conserved i.e.

$$|R|^2 + |S|^2 = 1 \quad (3.28)$$

Thus if an output power of unity is launched into the fundamental mode of the fiber containing a grating of length L, the frequency dependent transmitted field amplitude at the end of the grating would be:

$$R(z = L, \delta) = Cos(\gamma L) - i\frac{\delta}{\gamma}\sin(\gamma L) \quad (3.29)$$

This is the LPG transmission coefficient. The LPG coupling efficiency is the power lost to the cladding mode from the core mode i.e.

$$\eta = 1 - |R(z, \delta)|^2 = \frac{\kappa^2}{\gamma^2}(Sin(\gamma z))^2 \quad (3.30)$$

3.4 LPG in Standard Fiber: Analysis

The core-cladding mode interaction in a fiber grating can be explained by treating the coupling among the core mode and the multiple cladding modes simultaneously at a particular wavelength, using coupled mode theory [77]. However in most cases individual resonances are sufficiently narrow and spectrally separated that coupling between core mode and a single cladding mode well describes the transmission. In such cases simple two mode coupled theory can be used as done in this thesis. The coupled mode theory and the results discussed in section 3.2 are general and can be applied to any fiber provided the propagation constants of the interacting modes and the coupling coefficients for interaction between any two modes is calculated numerically, which would depend on the fiber geometry. Erdogan [77] used linearly polarized approximation to describe core guided modes while the cladding modes fields have been obtained using exact vector field treatment since the interface between the cladding and its surrounding might have large index difference. In our case also linearly polarized (LP) approximation is used to calculate both core and cladding fields. The difference in the result due to use of scalar approximation would be shift in peak position of the resonances. However, to design gratings for any practical application, scalar approximation would be sufficient since the behavior of the transmission spectra can be well described by this approximation. The peak position of resonance, obtained experimentally, would be sensitive to index fluctuation or radius fluctuation in the fiber spool and exact match in peak position is not expected even if vector calculation of the fields is performed.

3.4.1 Core mode analysis

Core modes are supported by the total internal reflection at the core cladding boundary and have a propagation constant β such that, $n_2^2k_0^2 < \beta^2 < n_1^2k_0^2$ where k_0 the wave vector in vacuum [175]. We consider simple 3-layer step index fiber geometry with core radius a_1, refractive index n_1, cladding radius a_2 and refractive index n_2 and surrounding medium of refractive index n_3. The transverse modal fields are

oscillatory in the core and decay outside it. The transverse dependence of the core modal field is given by [1, 175, 176]:

$$\Psi(r,\phi) = A_{co}\,\frac{J_l\,(Ur/a_1)}{J_l\,(U)}\begin{bmatrix}\cos(l\phi)\\ \sin(l\phi)\end{bmatrix} \qquad r < a_1 \tag{3.31}$$

$$= A_{co}\,\frac{K_l(Wr/a_1)}{K_l(W)}\begin{bmatrix}cos(l\phi)\\ \sin(l\phi)\end{bmatrix} \qquad r > a_1 \tag{3.32}$$

where $\mathrm{U} = a_1\sqrt[2]{(\mathrm{k}_0^2 n_1^2 - \beta^2)}$, $W = a_2\sqrt[2]{(\beta^2 - n_1^2\mathrm{k}_0^2)}$ and normalized waveguide parameter V, is key parameter in determining what modes propagate in a fiber and is defined as:

$$V = \sqrt{(U^2 + W^2)} = k_0 r\sqrt[2]{(n_1^2 - n_2^2)} \tag{3.33}$$

Here J_l is a Bessel function of the first kind, K_l is a modified Bessel function of the second kind. The continuity of ψ is assumed at r = a_1. The interface at r = a_2 is neglected since the decaying field has negligible strength at this point. Therefore continuity of $\frac{\partial\psi}{\partial r}$ at r = a_1 leads to:

$$U\,\frac{J_l'(U)}{J_l(U)} = W\,\frac{K_l'}{K_l} \tag{3.34}$$

With respect to the cladding modes, their derivation is more complicated, since the waveguide geometry includes two boundaries. By using recursion formulas we get:

$$U\,\frac{J_{l+i}'(U)}{J_l(U)} = W\,\frac{K_{l+i}'}{K_l} \tag{3.35}$$

We will use above equation to study the guided modes in step index fiber. For *l*=0 we get:

$$U\frac{J_l(U)}{J_0(U)} = W\,\frac{K_l\,(U)}{K_0(W)} \tag{3.36}$$

Here the boundary conditions used in deriving the Eigen value equation are consistent with the approximation involved in scalar value wave equation. To solve

the above equation it is convenient to define the normalized propagation constant, which is given by:

$$b = \frac{\frac{\beta^2}{k_0^2} - n_2^2}{n_1^2 - n_2^2} = \frac{W^2}{U^2} \tag{3.37}$$

Thus, $W = V\sqrt{b}$ and $U = \sqrt{(V^2 - W^2)} = V\sqrt{1-b}$.

For guided modes: $n_2^2k_0^2 < \beta^2 < n_1^2k_0^2$ i.e $0 < b < 1$ and for $l = 0$ the equation can be re written as:

$$V\sqrt{1-b}\frac{J_1(V\sqrt{1-b})}{J_0(V\sqrt{1-b})} = V\sqrt{b}\frac{K_1(V\sqrt{b})}{k_0(V\sqrt{b})} \tag{3.38}$$

The solution of the above equation will give us universal curves describing the dependence of b on V. The effective refractive index of the mode which is given by:

$$n_{eff}^{co} = \frac{\beta}{k_0} = \sqrt{n_2^2 + b(n_1^2 - n_2^2)} \tag{3.39}$$

Solving this numerically one gets the allowed values corresponding to different guided modes supported by core. For example we consider a fiber of n_1 = 1.4573, n_2= 1.45, n_3= 1.0, a_1 = 2.5μm and a_2 = 62.5μm at λ= 1.55 μm, this fiber supports only one core mode whose propagation constant can be obtained by solving Equation (3.34) as core n_{eff}= 1.45160, β (LP_{01}) =5.88432μm^{-1}. The parameters mentioned above are same as taken by Erdogan [71, 77]. The same value for LP_{01} for core n_{eff} =1.4516052 is obtained correctly up to 7th decimal point using software Optigrating 4.2.2 as shown in the Table 3.1.

Table 3.1 Calculated values of n_{eff} for fundamental mode

Mode	**Core n_{eff} (Optigrating 4.2.2)**	**Core n_{eff} (Reported model [176])**
LP_{01}	1.4516052	1.45160

The Figure 3.1 shows the 3D preview of the field, where maximum light is carried by the fundamental mode LP_{01} with component $E_{y,}$ taking mesh X=40 and Y=40 by using same above said parameters.

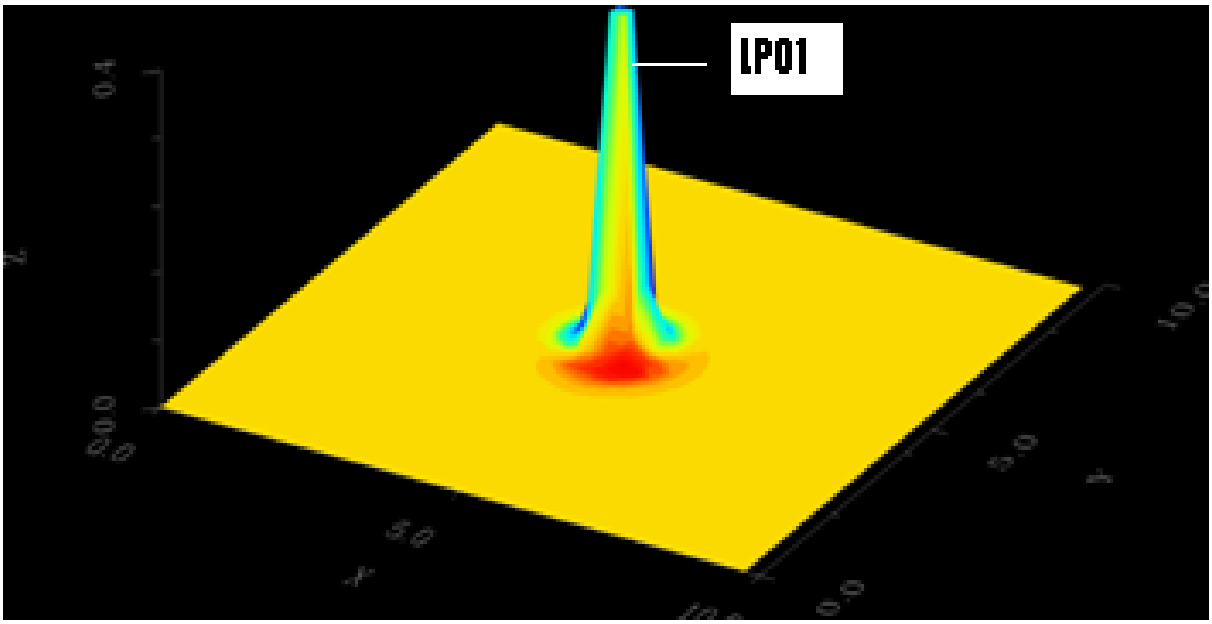

Figure 3.1 3D preview of the field for fundamental mode

3.4.2 Cladding modes

Cladding modes are those modes which are propagated by total internal reflection at the cladding air interface. They have propagation constant β such that $n_3^2\kappa_0^2<\beta^2 < n_2^2\kappa_0^2$ the transverse field is oscillatory in both core and cladding and decays outside the cladding. Calculation of cladding modes uses the approximation that the fiber can be considered as a multimode step index structure ignoring the presence of core, an approach that has commonly been used to simplify cladding mode analysis.

3.4.2.1 Two Layer Model

The two-layer model basically treats the cladding and core as one multimode fiber and the surrounding environment as the new cladding only in the LPG region. In the two-layer approximation used by various authors, the refractive index profile used to evaluate the propagation characteristics of core and cladding modes is given by [118]:

$$n = n_1 \qquad r < a_1$$

$$= n_2 \qquad a_1 < r < a_2$$

$$= n_{air} \qquad r > a_2 \tag{3.40}$$

where a_1, a_2 are the core and cladding radii n_1, n_2, and n_{air} are the refractive indices of core, cladding and air respectively.

3.4.2.2 Three Layer Model

To calculate $n_{eff,cl}$ the three layer model is used to overcome the design inaccuracies of two layer model. In three layer model the variation of effective refractive index can be calculated correctly up to fourth decimal point whereas this is not possible in two layer model. The three layer model takes more data points between the two values of effective indices therefore it is more accurate. Figure 3.2 shows the representation of three layer model.

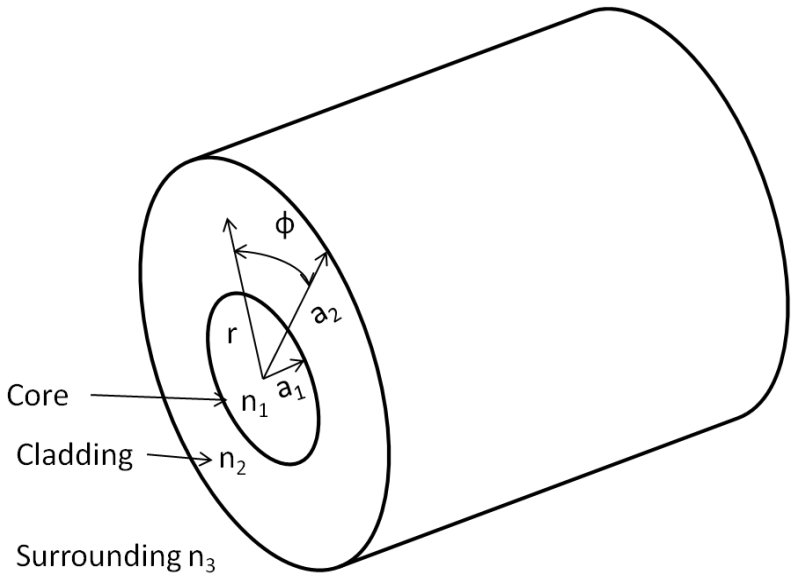

Figure 3.2 Representation of Three layer model

The transverse dependence of cladding mode is given by [176]:

$$\Psi(r, \phi) = AJ_l(U_1 r/a_1)\begin{bmatrix}\cos(l\phi) \\ \sin(l\phi)\end{bmatrix} \qquad r < a_1 \tag{3.41}$$

$$= BJ_l(U_2\, r/a_2) + CY_l(U_2\, r/a_2)\begin{bmatrix}\cos(l\phi)\\ \sin(l\phi)\end{bmatrix} \qquad a_1 < r < a_2 \tag{3.42}$$

$$= DK_l(W_3\, r/a_2)\begin{bmatrix}\cos(l\phi)\\ \sin(l\phi)\end{bmatrix} \qquad r > a_2 \tag{3.43}$$

where $U_1 = a_1\sqrt[2]{(\mathrm{k}_0^2 n_1^2 - \beta^2)}$, $W_1 = a_2\sqrt[2]{(\mathrm{k}_0^2 n_2^2 - \beta^2)}$, $W_3 = a_2\sqrt[2]{(\beta^2 - \mathrm{k}_0^2 n_3^2)}$

Continuity of the field and derivative of the fields at the boundaries $r = a_1 \& r = a_2$ leads to following equations:

$$AJ_l(U_1) = BJ_l(U_2\, a_1/a_2) + CY_l(U_2\, a_1/a_2) \tag{3.44}$$

$$A\frac{U_1}{a_1}J_l(U_1) = B\frac{U_2}{a_2}J_l(U_2\, a_1/a_2) + CY_l(U_2\, a_1/a_2) \tag{3.45}$$

$$BJ_l(U_2) + CY_l(U_2) = DK_l(W_3) \tag{3.46}$$

$$B\frac{U_2}{a_2}J_l(U_2) + C\frac{U_2}{a_2}Y_l(U_2) = D\frac{W_3}{a_2}K_l(W_3) \tag{3.47}$$

Here Y_l is a modified Bessel function of the first kind. If the modes are normalized to carry unit power then under the weakly guiding approximation, we may write [77]:

$$\frac{\beta}{2\omega\mu_0}\int_0^{2\pi}\int_0^{\infty}\Psi^2(r)cos^2(l\phi)rdrd\phi = 1 \tag{3.48}$$

For a frequency component ω and free space permeability μ_0, the four equations (3.44-3.47) form a set of coupled equations. For a given $a_1, a_2, n_1, n_2, n_3\ and\ \lambda$ we can find β such that the determinant formed by coefficients of A, B, C, D from the four equations is zero. Figure 3.3 shows propagation characteristics of the cladding modes obtained by the three-layer approximation. In Table 3.2, we consider a fiber of parameters n_1 = 1.4573, n_2= 1.45, n_3= 1.0, a_1 = 2.5 μm and a_2 = 62.5 μm to calculate n_{eff} using both three layer model and optigrating 4.2.2. At λ= 1.55 μm, the β values of seven lowest order modes given by LP_{02} = 5.8775 μm^{-1}, LP_{03} = 5.8768 μm^{-1}, LP_{04} = 5.8755 μm^{-1}, LP_{05} = 5.8738 μm^{-1}, LP_{06} = 5.8723 μm^{-1}, LP_{07} = 5.8699 μm^{-1} and LP_{08}= 5.8674 μm^{-1}

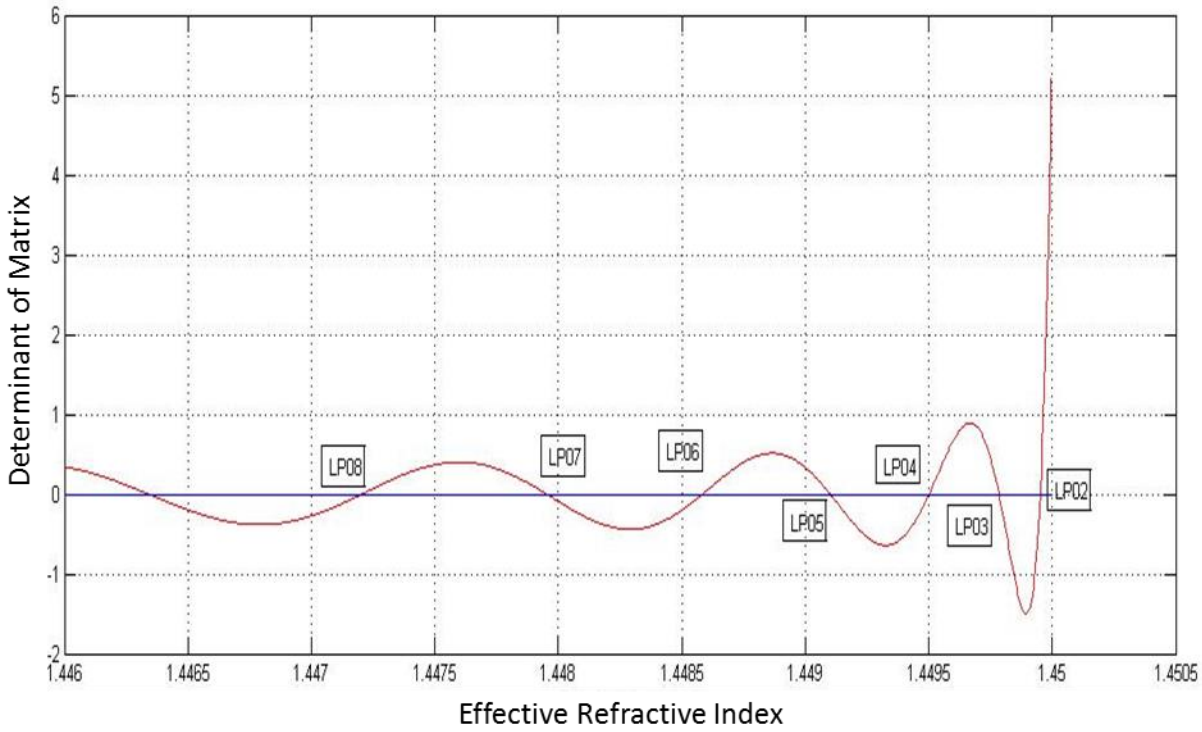

Figure 3.3 Calculation of effective refractive index of cladding modes using three layer model

Here, it is evident from the Table 3.2, that the values obtained by Optigrating 4.2.2. are in accordance with the values obtained by three layer model.

Table 3.2 Values of n_{eff} cladding modes calculated by Optigrating 4.2.2 and three layer model

Mode	**n_{eff}(Optigrating 4.2.2)**	**n_{eff} (Three layer model)**
LP_{02}	1.4499502	1.4499
LP_{03}	1.4497850	1.4498
LP_{04}	1.4495086	1.4495
LP_{05}	1.4491241	1.4491
LP_{06}	1.4486341	1.4485

LP_{07}	1.4480403	1.4480
LP_{08}	1.4473437	1.4472

Figure 3.4 shows the 3D preview of the field profile calculated by software Optigrating 4.2.2, for all cladding modes LP_{01} to LP_{05} with component $E_{y,}$ taking mesh X=40 and Y=40 using same above said parameters.

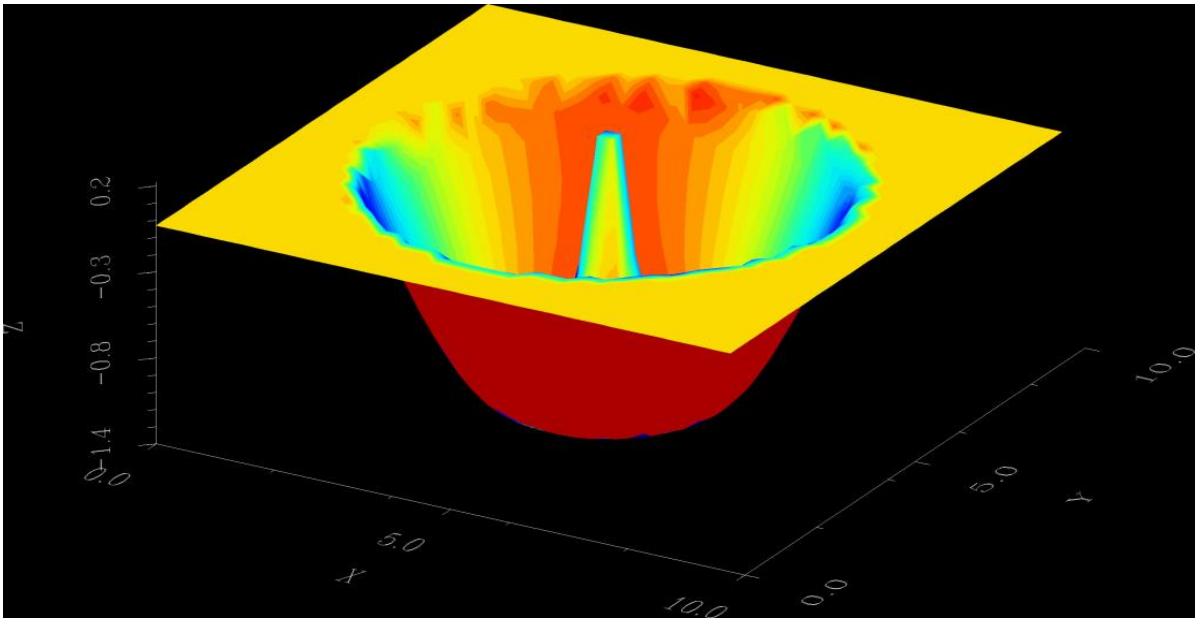

Figure 3.4 3D preview of filed profile for cladding modes LP_{01} to LP_{05}

A typical transmission spectrum for a grating length 2cm, period=539 μm and center wavelength=1585 nm with index modulation 0.0003 on a fiber chosen in the example shown in the Figure 3.5 . This period enables coupling from LP_{01} (core mode) to LP_{06} (5^{th} cladding mode) with resonance peak at 1585 nm. The 3D preview of the field profile is generated by software Optigrating 4.2.2, for coupled mode between LP_{01} to LP_{06} with component $E_{y,}$ taking mesh X=40 and Y=40 is shown in Figure 3.6. Simulation results also suggest that, the central wavelength is a function of grating period. For the same resonant wavelength, the fundamental mode can be coupled to LP_{04} mode with period 783 μm,LP_{05} mode with period 653 μm and LP_{07} with period 445 μm keeping rest of the parameters same.

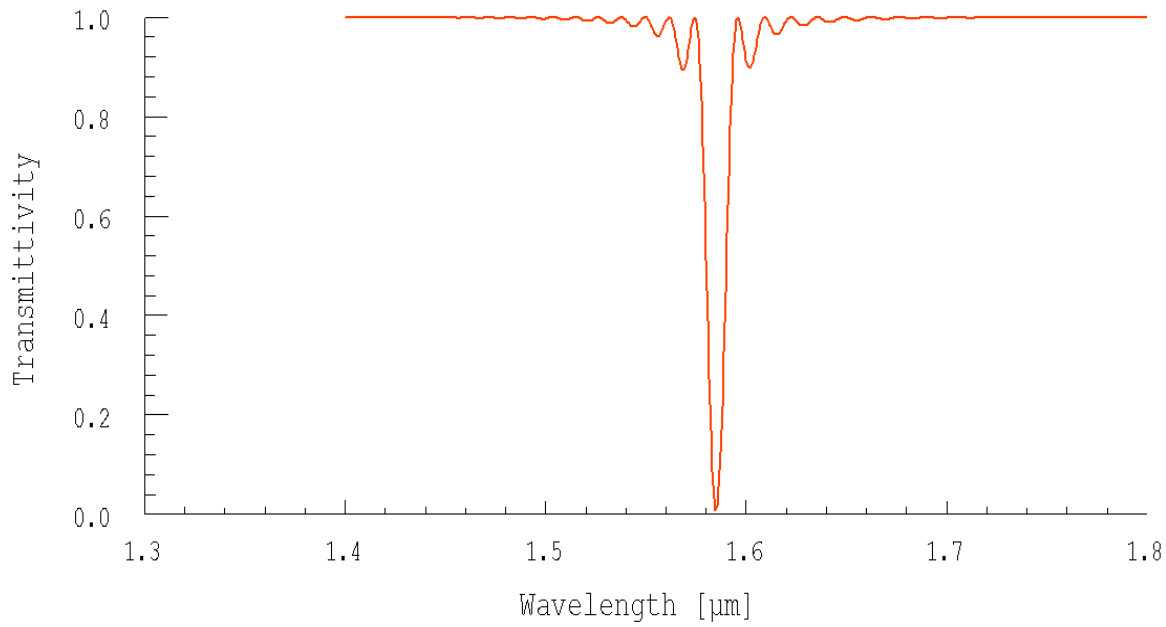

Figure 3.5 Transmission spectrum of LPG with period 539 µm, index modulation 0.0003 enabling coupling of 5th cladding mode at 1585 nm

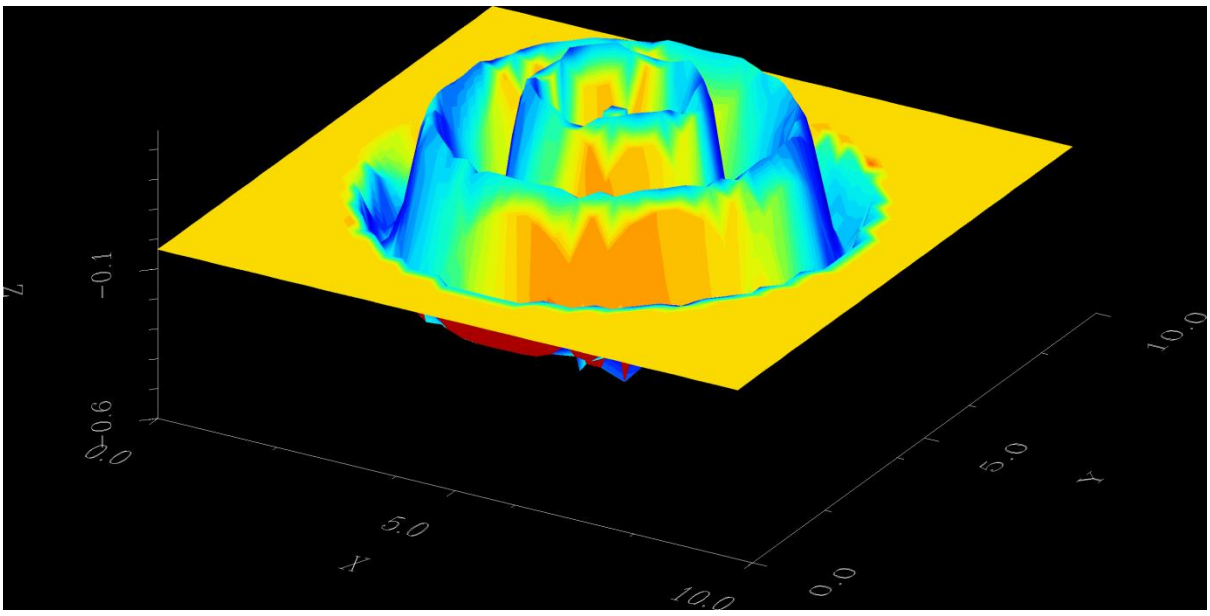

Figure 3.6 3D preview of field profile for LPG with period 539 µm, index modulation 0.0003 enabling coupling of 5th cladding mode at 1585 nm

Similarly, the values of n_{eff} for cladding modes are also calculated by software Optigrating 4.2.2 for LP_{01} to LP_{05} by taking core & cladding refractive indices and radii values 1.458, 1.45, 2.5, 62.5 respectively. The resonant wavelength is taken 1450 nm. The results are compared with existing two and three layer values. As shown in Table 3.3, we observed that Optigrating 4.2.2 calculated values more accurately up to

seventh decimal point. Additionally, values are also in accordance with the one obtained by three layer model.

Table 3.3 Comparison of n_{eff} core & cladding modes values calculated by Optigrating 4.2.2 with reported values [118]

Mode	n_{eff}(Optigrating 4.2.2)	n_{eff} (Three layer model)	n_{eff} (Two layer model)
LP_{01}	1.4523316	1.45233	1.45233
LP_{02}	1.4499581	1.44995	1.4498
LP_{03}	1.4498174	1.44980	1.4496
LP_{04}	1.4495803	1.44954	1.4493
LP_{05}	1.4492489	1.44918	1.4489

3.5 Experimental Validation

Using this simulation work, LPG is fabricated in boron co-doped fiber with core radius a_1 = 2.5 μm and cladding radius a_2 = 62.5 μm, center wavelength=1585 nm and period 539 μm, couple modes between LP_{01} to LP_{06}. The simulated spectrum of LPG is shown in Figure 3.5. The experiment was performed with different standard refractive index liquids and the transmission spectrum was monitored on an optical spectrum analyzer to verify the theoretical response. The schematic of the experimental setup is shown in Figure 3.7.

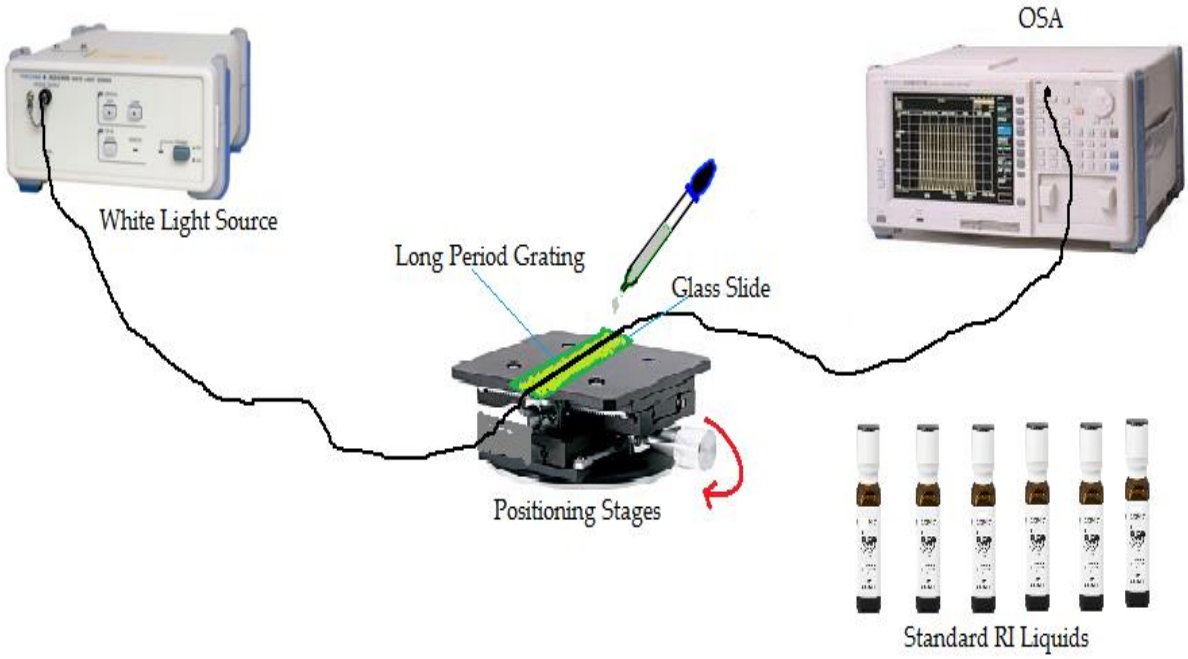

Figure 3.7 Schematic of experimental setup

The portion of the fiber with grating inscribed in it is fixed at both ends. Micro-positioning stages with a glass slide attached on its surface are placed beneath the grating. The stages can be positioned in such a way that the LPG gets submerged completely with the standard RI liquid (Cargille Labs), which have a quoted accuracy of ± 0.0002 .To avoid any bending fiber is held straight by use of two fiber holding stages. Extra attention is given to observe the spectrum on highly sensitive Optical spectrum Analyser (OSA).

As the wavelength based measurement has been chosen over intensity based, which is more reliable particularly in sensing applications. Prior to the next RI liquid, the previous liquid is rinsed off the slide, the slide is cleaned and the LPG is washed thoroughly with isopropyl alcohol several times so that the LPG spectrum returns to its original position. Similar steps are followed for subsequent RI liquids. The spectrum is shown in Figure 3.8, when LPG is subjected to three different RI values.

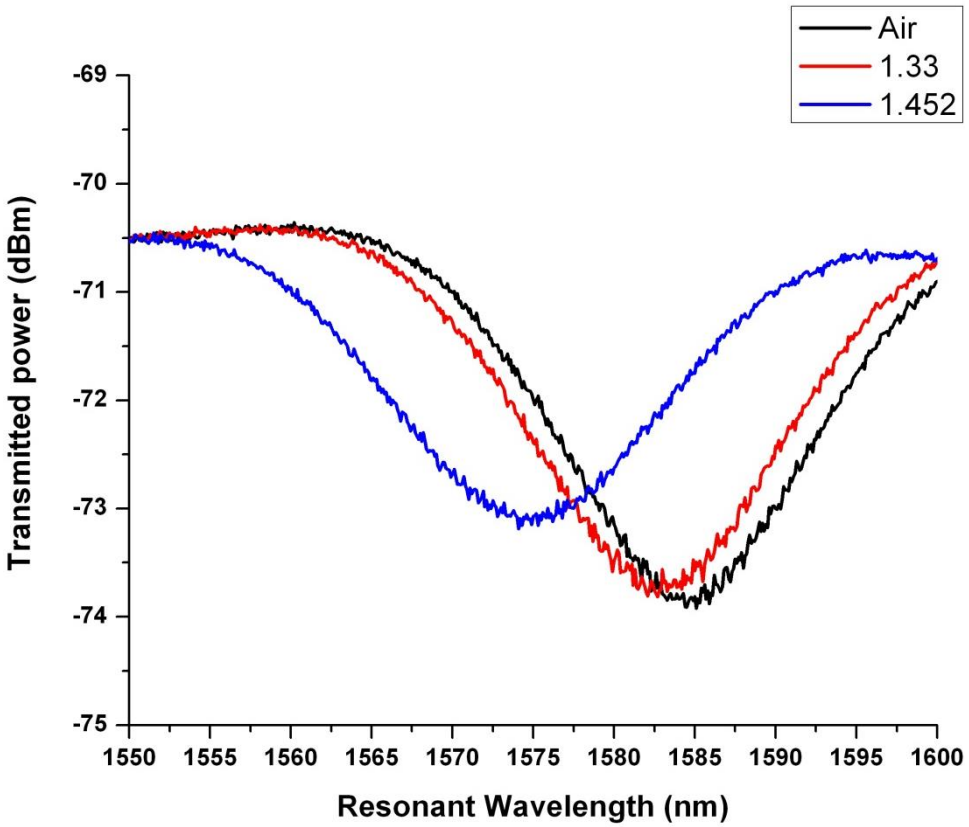

Figure 3.8 Spectral signature of LPG subjected to different RI values

Whole experiment is performed at room temp i.e. 25^0C. Unlike Fiber Bragg grating, the temperature effect on sensor can be taken care of by using temperature compensation techniques. While performing the experiment no effect of ambient light is observed as chemical etching of cladding is not performed to make it more sensitive towards ambient RI change. Then the response with standard liquids of refractive indices 1.4-1.45, 1.452, 1.454 & 1.458 is monitored and matched with the simulated response within the same range.

The theoretical and experimental results are compared with graphs shown in Figure 3.9.The simulated result depicts the shift in wavelength of LPG for its coupling mode LP_{06}, when subjected to standard RI solutions ranging from 1.4 to 1.458. It starts with the reference point and then RI varies up to 1.458. It is scrutinized that shift is highest between RI value 1.45 to 1.458. Whereas, experimental results validates this variation within the same range and reflects that the experimental results are in accordance with the simulated results.

The wavelength shift at resonance is 11nm for simulations and 19 nm for experiment, the difference between these could be due to the difference in core RI; in the theoretical analysis a core RI of ~1.45 was used. Fiber parameters used for simulations are not exactly the same. The grating used in this experiment is written on SMF28 after hydrogen loading, therefore it is difficult to perfectly estimate fiber parameters in simulating the results.

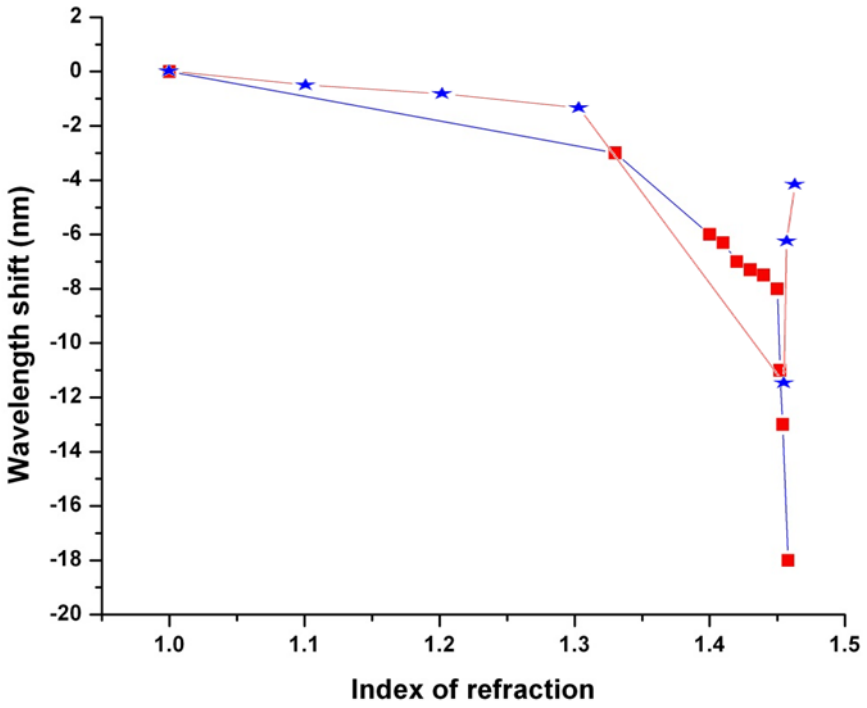

Figure 3.9 Simulated (square) and Experimental (star) results of RI responses

The plot shows that the resonant wavelength decreases from 1.00 to 1.40 before falling sharply to a minimum around 1.45, at which point, it jumps back up to a wavelength near its original position. LPG is most sensitive to changes in the ambient index when the indices are close to the material index of the cladding (n_2), which is approximately 1.45. The points beyond 1.45, at the cladding threshold, the peak nearly disappears when cladding mode converted to radiation mode losses and then slowly begins to increase in depth with the ambient index .This is the case when surrounding refractive index is higher than the cladding refractive index. At that point, no significant shift of wavelength will occur [177].

The experiment is repeated several times. The repeatability of sensor comes out to be 99%. The effect of change in temperature on LPG was also observed as shown in the Figure 3.10 and the thermal sensitivity comes out to be 0.38 nm/°C, and 0.043 RI units change for per degree rise in temperature which can be overcome by using temperature compensation techniques. The approach similar to temperature insensitive refractometer based on two concatenated dual-resonance long-period gratings with an appropriate inter-grating space (IGS) in between can be explored [178].

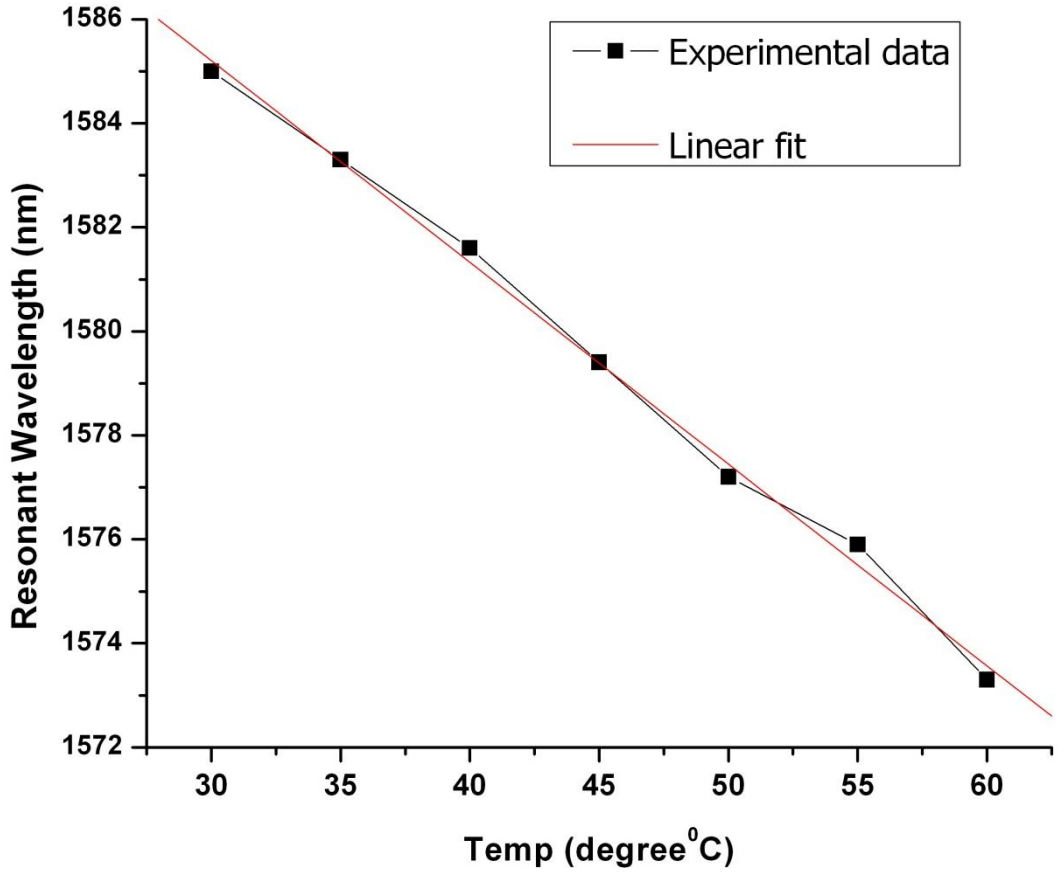

Figure 3.10 Thermal response of LPG

The thermal response of LPG was determined by placing the LPG inside the water bath and increasing its temperature by using hot plate. Expected red shift is obtained when the temperature increases. To the water, LPG showed approximately linear thermal behavior; therefore linear regression was used to determine the sensitivity.

Temperature cross sensitivity is also an important issue checking thermal response of LPG. It can be compensated by using dummy LPG in parallel having same parameters written on same fiber. The Other method is to provide thermal packaging. This packaging will make no effect of temperature on LPG. One point should be taken in account that all the experiments should be performed at maintained room temperature.

The drive current fluctuations effect contributes a refractive index measurement error of 0.01 RI units for 10% change in it. The sensor gives 0.004 RI units change of refractive index for bend curvature of 40 cm^{-1}. The light source has output stability of ±0.05 dB at 25 ^{0}C, therefore we assume negligible effect of light source drift on sensor performance.

3.6 Coupling Coefficient

It is observed that the coupling between two modes propagating in the same direction is a strong function of the detuning ratio δ/κ, where δ is the detuning parameter and κ is the coupling coefficient of the grating as described earlier. The detuning parameter is dependent on the proximity of the operating wavelength to the phase-matching wavelength for the grating. Conversely, the coupling coefficient is a function of index change and the modal overlap between the guided and cladding modes over the region of perturbation. For maximum power transfer, it is required for the value of the detuning ratio to be as small as possible, which means that the coupling coefficient should be optimized to improve the grating performance. Additionally, there is a dependence of the coupling coefficient on the order of the cladding mode and the operating wavelength as well as the peak index change.

To derive an expression for the coefficient, the following approach should be used. A function $\delta n(x)$ is used to describe the periodic refractive index modulation in the fiber core such that the modified profile n(x) is given by [179].

$$n(x) = n_1 + \delta n(x) \tag{3.49}$$

where n_1 is the unperturbed core index of refraction. The periodic variation in the index can be expressed in terms of its Fourier series, which is given by [179]:

$$\delta n(x) = \Delta n \left[A_0 + \sum_{N=1}^{\infty} A_N \cos\left(\frac{2\pi N}{\Lambda} x\right)\right] \tag{3.50}$$

where A_N are the Fourier coefficients. It is normally limited to first order interactions (N=1) for coupling to all cladding modes. The coupling coefficient κ is given by the square root of the product of the two cross-coupling coefficients κ_{12} and κ_{21}, given by

$$\kappa = \sqrt{\kappa_{12}\kappa_{21}} \tag{3.51}$$

where 1 and 2 are guided and cladding mode respectively. The cross-coupling coefficients are functions of the order of the mode m and expressed as:

$$(\kappa)^{(m)} = k\frac{|A_N|}{2}\frac{\left|\int_0^a \Delta n E_{01}(r) E_{cl}^m(r) dr\right|}{\sqrt{\int_0^\infty (E_{01}(r))^2 r dr \int_0^\infty (E_{cl}^m(r))^2 r dr}} \tag{3.52}$$

where $E_{01}(r)$ and $E_{cl}^m(r)$ are electric field distributions of the fundamental guided mode and the circularly-symmetric cladding mode of order m respectively. The integration in the numerator is over core only since the refractive index perturbation for grating is confined in fiber core. It is presumed that the index modulation is small compared to the unperturbed core index and hence from equation (3.49), $n^2(x) - n_1^2 = 2n_1\delta n(x)$. In defining the overlap integral which is given by [179]

$$\eta^m = \frac{\left|\int_0^a \Delta n E_{01}(r) E_{cl}^m(r) dr\right|}{\sqrt{\int_0^\infty (E_{01}(r))^2 r dr \int_0^\infty (E_{cl}^m(r))^2 r dr}} \tag{3.53}$$

The coupling coefficient can be rewritten by:

$$(\kappa)^{(m)} = \frac{\pi |A_N| \eta^m}{\lambda^m} \tag{3.54}$$

where it has been assumed that the coupling coefficient is constant across the spectral width of a resonance band of order m and centered at $\lambda^{(m)}$.

Therefore, the coupling coefficient for a LPG has the same form as that for a FBG. Since the coupling coefficient is directly proportional to the overlap integral, the modal distribution of the cladding mode will have a strong impact on its magnitude. Additionally, since the index modulation has no azimuthal variation, the coupling of the guided mode can occur only to circularly-symmetric cladding modes, and for all other cladding modes, overlap integral is zero.

3.7 Transmission Spectrum of LPG

Detailed analysis of LPG in cylindrical fiber has been given in various papers and books [22, 71, 77, 90, 91, 103, 105]. In this thesis we consider LPGs which involve interaction between core mode and a single cladding mode for a given wavelength range of interest. Knowing the β values of the modes, for a given wavelength one can find the required grating period which would satisfy the phase matching condition for interaction between any two modes. The grating strength κ depends upon the overlap of the fields of the two interacting modes. Solving the four Equations (3.31-3.34), we can calculate the propagation constants for the cladding modes and the field profiles are shown in Figure 3.11.

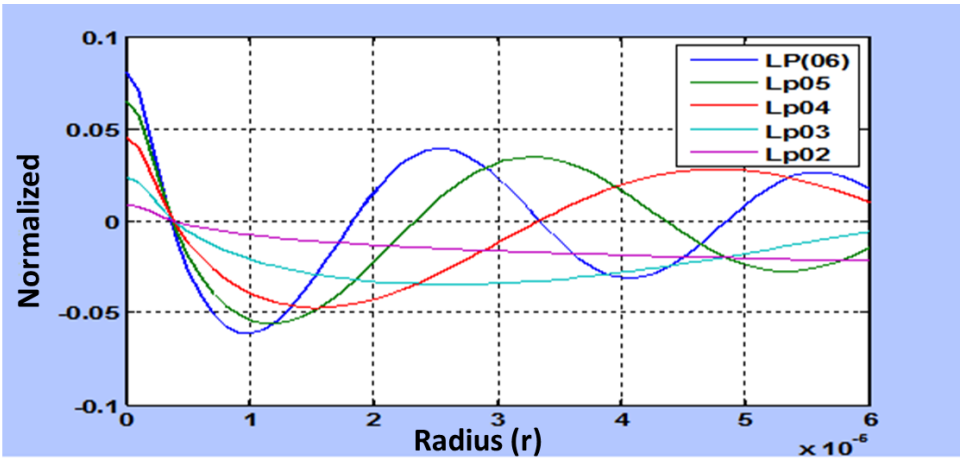

Figure 3.11 Field profile of various cladding modes

Similarly, the resonance wavelength changes with grating period for different cladding modes as described in Figure 3.12.

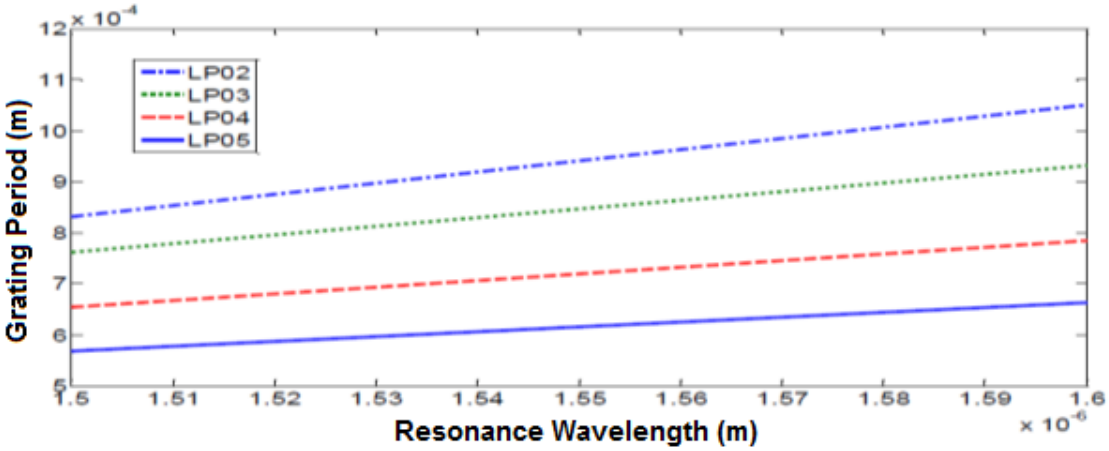

Figure 3.12 Variation of resonance wavelength with change in grating period for different cladding modes

Simulated transmission spectrum of an LPG with period 625 μm, Δn= 0.0003, length 2 cm and resonance wavelength 1.55 μm is shown in Figure 3.13 using Matlab.

The grating period enables coupling of 4th cladding mode[5]. The value of effective refractive index for $LP_{0,1}$=1.4516052, $LP_{0,2}$=1.4499505, $LP_{0,3}$=1.4497861, $LP_{0,4}$=1.4495110, $LP_{0,5}$=1.4491284.

.

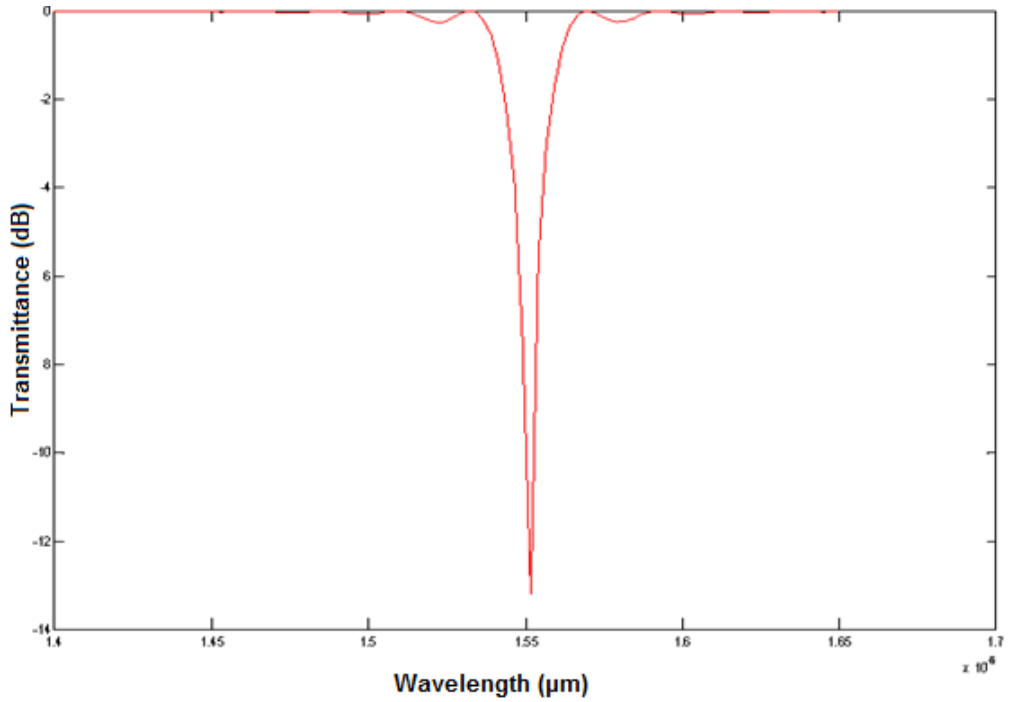

Figure 3.13 Transmission spectrum of an LPG with period 600 μm, Δn= 0.0003, λ =1.55 μm

Similarly, the transmission spectrum of LPG is calculated using software Optigrating 4.2.2 with period 600μm, grating length 10 mm, Δn= 0.0001, λ =1.52 μm as shown in Figure 3.14. The grating period enables coupling of 5th cladding mode. The value of effective refractive index for $LP_{0,1}$=1.4515200, $LP_{0,2}$=1.4499478, $LP_{0,3}$=1.4497752, $LP_{0,4}$=1.4494869, $LP_{0,5}$=1.4490864, $LP_{0,6}$=1.4485763

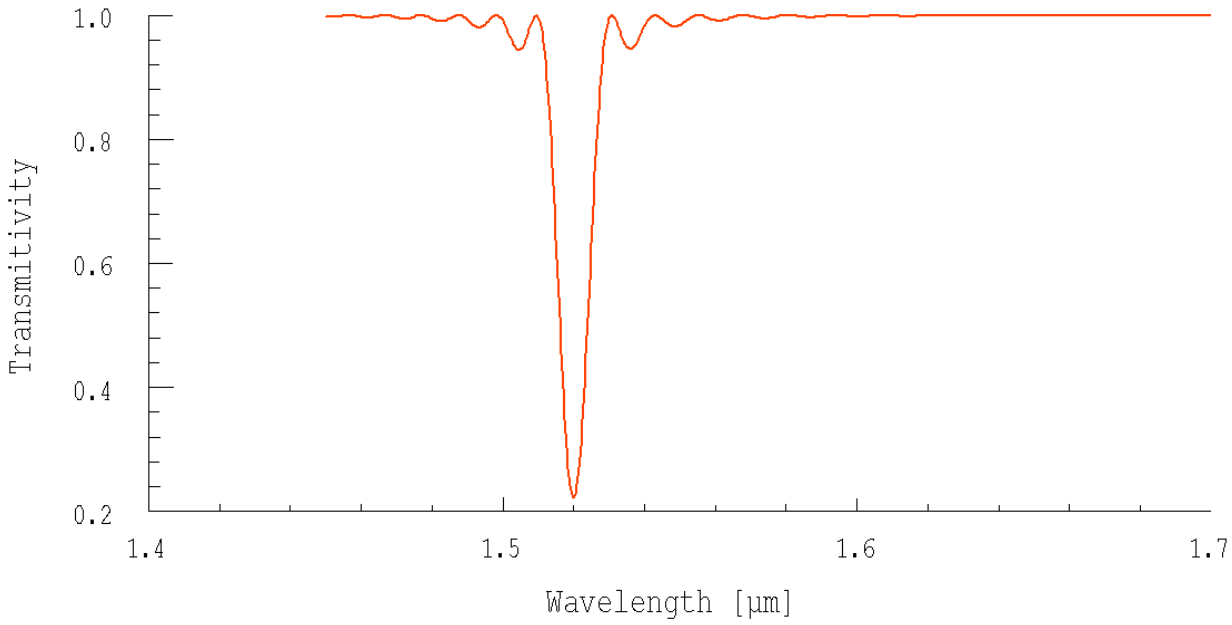

Figure 3.14 Transmission spectrum of an LPG with period 600 μm, Δn=0.0001, λ =1.52 μm

3.8 Summary

This chapter outlined the coupled mode theory which is used to analyze mode interactions in LPG. Two layer and three layer models are discussed for cladding mode calculation. Typical transmission curves for uniform LPGs are shown using Matlab and Optigrating 4.2.2. Experimental validation of the simulated refractive index response of LPG is covered.

CHAPTER 4. FABRICATION AND CHARACTERIZATION OF LONG PERIOD GRATING

4.1 Introduction

Photosensitivity in optical fiber refers to a permanent change in the index of refraction of the fiber core when exposed to light with characteristic wavelength and intensity that depends upon core material. Photosensitivity also known as photo refractivity was discovered by Hill [180]. This is commonly used to modulate the refractive index of materials spatially and fabricate devices such as gratings. A refractive index grating is an optical device that performs to modulate the amplitude or phase of an incident wave periodically. Initially, photosensitivity has been thought to be phenomenon only associated with optical fibers having large concentration of Germania in the core and photo excited with 240-250 nm UV light. However, photosensitivity has been observed with excitation at different UV wavelengths (e.g. 157 nm, 193 nm, 325 nm, 351 nm) [181-183] in a wide variety of different fibers, many of which have other dopants (e.g. boron, erbium, tin, phosphorous) [184-187] in addition to Germania and some of which contain no germanium at all (e.g. rare earth doped fibers, aluminosilicate fiber, flurozirconate fiber doped with cerium:erbium) [188-190]. There have been efforts to enhance the photosensitivity in fibers by introducing techniques such as hydrogen loading [191], flame brushing [192] and co-doping.

In Hill's experiment, he used the interference pattern of two counter-propagating beams of blue green light (488 or 514 nm) inside a germanium-doped single mode fiber to form a refractive index grating internal to the fiber core. Such gratings couple light from the forward-propagating LP_{01} fundamental mode to the reverse-propagating LP_{01} mode at a wavelength for which the phase-matching condition for mode coupling is obeyed. For the grating fabricated by Hill *et al.*, the reflection

wavelength, which is known as Bragg wavelength, was equal to the writing UV wavelength as the grating was written by launching light in the fiber core. Since these gratings in the visible spectrum were not useful for optical communication applications at 1.31 mm. Telecommunication devices had limited applications for fiber Bragg gratings till 1989 when the transverse holographic method for grating fabrication was proposed by Meltz *et al* [57]. The side-writing technique enabled mass production of in-line fiber gratings at the desired wavelength using the interference pattern between two spatially and temporally coherent UV beams. Photosensitivity has also been utilized to modify the mode field diameter of the fundamental guided mode to assist in mode conversion. Numerous models have been proposed such as color centre model [193], the stress relief model (SRM) [194], dipole model [195], the compaction-densification model (CDM) [196], etc. for understating the mechanism of photo induced refractive index change in fibers. The electronics defect oriented changes and structural changes are involved in photosensitivity. The structural model associated the photosensitivity with the local structural changes in glass which occur during illumination. Stress-Relief Model and Compaction-Densification Model can be grouped under this category.

4.1.1 Stress Relief Model (SRM)

This model explains the change in refractive index as a direct result of the relaxation of built-in thermo-elastic stresses in the core of the fiber during Ultra Violet(UV) irradiation, brought about by the rapture of wrong bonds [197]. The model takes into account the intrinsic relaxation of the stressed glassy network and the external interfacial stresses. The residual stress arises from the difference in the thermal expansion between core (α_{core}) and cladding material (α_{clad}) and due to the difference in glass transition temperature (T_g).

During fiber drawing, as glass is cooled below the fictive temperature, the difference in thermal expansion of the core and cladding ($\alpha_{core} > \alpha_{clad}$) manifests as a frozen-in thermal stresses in the fiber core. The refractive index changes as a consequence of

stress relief in the core fiber, initiated by breakage of the wrong bonds by UV light. Refractive index change due to stress relaxation in a highly stressed fiber is of order of 10^{-3} [198]. Fonjallaz *et al* [199] has reported the measurement of axial stress modification in FBG and it was shown that the tension in the core of single mode germanosilicate fibers is greatly increased during Bragg grating formation. A strong increase in tension has been observed in [200], which contradicts SRM [194]. Finally, the thermal reversibility of grating cannot be explained by this model [201].

4.1.2 Compaction–Densification Model (CDM)

The compaction model is based on laser irradiation –induced density changes that leads to refractive index changes. A differential form of the Lorentz-Lorenz relation for glass of molar refractivity R_f is given by [202, 203]

$$\frac{\Delta n}{n} = \frac{(n^2+2)(n^2-1)}{6n}\left\{\frac{V}{\Delta V}\frac{\Delta R}{R} - 1\right\}\frac{\Delta V}{V} \tag{4.1}$$

Equation (4.1) shows that the fractional change in the refractive index n can be the result of photo-induced changes in the glass volume V and/or in the refractivity R_f. Here R_f is given as

$$R_f = \frac{(n^2-1)}{\varrho(n^2+2)} \tag{4.2}$$

where ϱ being the specific gravity. The Eq. (4.1) may be expressed as [204]

$$\Delta n \propto \left({}^{\Delta V}/_{V} - {}^{\Delta R_f}/_{R_f}\right) \tag{4.3}$$

This clearly shows that there is a competition between these two terms, which affect the refractive index. Irradiation by laser light at 248 nm at intensities well below the breakdown threshold has been shown to induce thermally reversible, linear compaction in amorphous silica, resulting in refractive index changes [205] for the first time by Fiori and Devine. Although the density change model for fiber photosensitivity was recommended, as a possible mechanism among others, as early

as 1991 [206], it was only in 1998 that direct evidence for its existence was demonstrated in the cores of germanosilicate preform slices through transmission electron microscopy (TEM) [207], interferometric microscopy (IM), and atomic force microscopy (AFM) [208]. The density change model is relatively new and it has not been examined comprehensively. Even though there is some literature available on density change in germanosilicate fibers, this area is not explored much.

4.2 Techniques for Improving Optical Fiber Photosensitivity

The photosensitivity can be determined by measuring the amount of change in refractive index produced in a fiber core following a specific exposure to UV light on it. Therefore, the discovery of photosensitivity and the first demonstration of grating formation in germanosilica fibers play a major role in understanding and increasing the photosensitivity in optical fibers. Optical fibers that were fabricated initially, with high germanium dopant levels or under reduced oxidizing conditions were confirmed to be highly photosensitive. Since then, many methods and techniques have been developed for improving and enhancing the photosensitivity in optical fibers. Those methods include thermal-induced refractive index change, the hydrogen-loading technique, photosensitivity increase by strain, and the co-doping technique [192].

4.2.1 Hydrogen-loading of germanosilicate fibers

In 1985, Tomita and Lemaire [209] were the first to show that hydrogen results in defect formations in germanosilicate glass. Later Salik *et al.*[210] suggested that optical fibers treated with hot hydrogen show increased photosensitivity in applications involving second harmonic generation. It was revealed that this observable fact could be used for grating formation in fibers along with achieving permanent index changes in germania-silica planar waveguides [191, 211] . The chemical bonding of hot hydrogen enables permanent increase in the photosensitivity of germanium-doped fibers.

High-pressure loading of germanosilicate fibers with molecular hydrogen has also been demonstrated to increase the photoinduced refractive index changes due to ultraviolet radiation. The addition of hydrogen to Ge-doped glass leads to the breakdown of the Si-O-Ge bonds, resulting in the formation of Si-OH bonds and germanium oxygen deficiency centers (GODCs), both of which lead to an increase in the index of refraction (Figure 4.1). The absence of any refractive index modulation in hydrogen-loaded non-germanosilicate fibers lend credence to the belief that hydrogen attacks the germanium sites to produce index changes [212].

The Si-OH bond has an absorption band centered at 1390 nm, and can be detrimental to the performance of communication as well as sensing systems operating in that spectral region. This constrain can be conquer by substituting molecular hydrogen with deuterium, that results in the formation of corresponding Ge-OD bonds with absorption peaks outside the telecommunication spectral window [191].

With hydrogen or deuterium loading, refractive index changes as large as 10^{-2} have been reported by Lemaire *et al* [191]and this value is at least two orders of magnitude larger than the index modulation previously achieved in fibers not loaded with hydrogen . In hydrogen-loaded fibers, the loss at 1390 nm can also be measured to estimate the OH concentration in the fibers. It has observed experimentally that the OH concentration in a photo-exposed fiber is slightly lower than the GeO_2 content of the fiber which reveals that hydrogen loading forces a majority of the germania sites in the glass network to participate in the photosensitivity process [211].

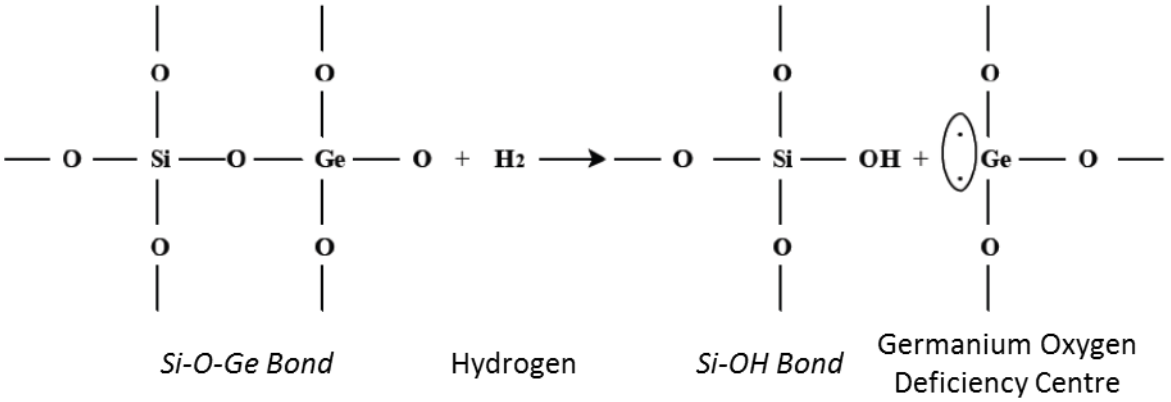

Figure 4.1 Thermal reaction at the Si-O-Ge bonds leading to the formation of GODC sites and Si-OH bonds [213]

The process of hydrogen loading involves exposure of the fiber to gaseous hydrogen at high pressure (100–700 atm) and temperatures ranging from 20 to 100 ºC [191]. As the acrylate provides negligible resistance to hydrogen diffusion, the fiber coating for this process need not be removed. Adding up hydrogen to optical fibers produces first overtone absorption at 1240 nm and this loss is related to the magnitude of hydrogen present in the fiber. Hydrogen loading at room temperature requires one to two weeks to obtain a concentration of 1 – 2% (1% is defined as 1 mole of H_2 per 100 moles of SiO_2) in case of standard fibers. The out diffusion of the hydrogen-sensitized fiber is prevented by storing the fiber at low temperature or high pressure. To guarantee that all germania sites contribute in the formation of defects, the content of hydrogen is made higher than that of GeO_2 doping level in the fiber. Therefore on completion of the UV irradiation process, some excess hydrogen still remains in the fiber. Since the diminution of hydrogen occurs only in the regions that undergo refractive index modulation, it raises differential hydrogen concentration along and across the fiber. The existence of hydrogen enhances the index of refraction locally and its diffusion to maintain equilibrium results short-term instability in the characteristics of the photo induced fiber. Hence, it becomes essential to remove this excess hydrogen from the fiber. A simple way to do this is to anneal the fiber at high temperature for a short period of time. The annealing process also serves to remove the unstable germanium defects (at the expense of reduction in

refractive index) and provides long-term stability at lower operating temperatures [214, 215].

4.2.2 Co-doping technique

Enhanced photosensitivity is found in two kinds of co-doped germanosilicate optical fibers, which include B-and Tin-co-doped optical fibers. A comparison of the relative photosensitivity of four different types of fiber including boron co-doping is given in Table 4.1. The fibers were irradiated with modest power intensities of 1 W/cm^2 from a frequency-doubled Continuous Wave (CW) argon ion laser until the grating reflectivity was saturated [192]. The results showed that the fiber containing boron had an enhanced photosensitivity. This fiber resulted in much more higher photosensitivity than the fiber with higher germanium concentration and with boron. Moreover, the saturated index changes were higher and achieved faster than for any of the other fibers. This means that there is an additional mechanism operating in the boron-co-doped fiber, which enhances the photo induced refractive index changes.

Table 4.1 Photosensitivity assessment of four different fibers [192]

Fiber design to saturate	**Fiber Δn**	**Standard index modulation**	**Maximum reflectivity for 2 mm grating**	**Time for reflectivity to saturate**
Standard low loss fiber ~ 4 mol% Germania	0.005	0.000034	1.2%	~2 hours
High index fiber ~ 20 mol% germania	0.03	0.00025	45%	~ 2 hours
Reduced fiber ~ 10 mol% germania	0.01	0.0005	78%	~ 1 hour
Boron co-doped fiber ~ 15 mol% germania	0.003	0.0007	95%	~ 10 minutes

The germanium-boron-co-doped fiber was fabricated with a germanium composition of 15 mol%. In the absence of boron, this fiber could possess core and cladding index of refraction difference 0.025. The additions of boron lessen the core index of refraction. It is believed that boron co-doping increases the photosensitivity of the fiber by allowing photo induced stress relaxation to occur [192].

Dong *et al*. also reported on enhanced photosensitivity in Tin-co-doped germanosilicate fibers. A factor of ~3 photo induced index changes was demonstrated. The gratings in the Tin-doped fibers have a much improved high temperature stability compared to B-co-doped fibers. Unlike B-co-doping, Tin-co-doping does not introduce significant loss at the important telecommunication window of 1.55 μm.Tin can also be easily introduced in the vapor phase as $SnCl_4$ using vapor-phase deposition. Alternatively, tin can be incorporated by using the solution-doping technique.

4.3 Fabrication Process of Long-Period Gratings

A number of novel and interesting techniques have been reported for the fabrication of long-period gratings since the first long-period gratings was realized by Vengsarkar *et al* [11, 216] by using the amplitude-mask writing method. Hydrogen loaded germanosilicate fibers were exposed to a KrF laser (λ=248nm) through an amplitude mask made of chrome-plated silica through this technique. The weakness of this technique is that change of grating periodicities could be realized only by using different periodicities of amplitude-mask which results in increasing the cost.

Zhang *et al*. [89] fabricated long-period gratings by using the point-by-point UV direct writing method which is the same technique used for fabrication of fiber Bragg gratings. Depending on the requirements of period and spectral profile, the periodic exposure could be provided by a computer-controlled shutter program in this point-by-point writing process. The major advantage of this technique is the great flexibility because a grating of arbitrary periodicity and length can readily be

written by appropriately programming the shutter and translational stage. The main disadvantage of using the point-by-point writing method is that it takes a long time to write a single long-period grating and the technical requirements are very strict.

So far, most long-period gratings are made by using the UV exposure of optical fiber, but Davis *et al.* [87] and Karpov *et al* [217] have shown that it is possible to use CO_2 lasers. Their experimental configuration consisted of a computer-controlled translational stage that positioned the fiber in an alignment fixture. Computer controlled, single laser pulses (~0.5 W, 300 ms) were focused onto a 140 μm diameter spot (~ 7.7 J/mm2) at the desired positions along axes of the fiber. An optical imaging system, which was mounted above the fiber aided in the alignment and enabled verification that no physical deformation was occurring. A spectrum analyzer and a broadband source with a free-space wavelength in the range 1.4 - 1.6 μm were used to monitor the fiber transmission spectrum as the grating was written. The major advantage of this technique are that CO_2 lasers are rather inexpensive, neither hydrogen loading nor UV exposure of optical fiber is required, and the optical fiber is not physically deformed.

LPG should be easy to fabricate and suitable for mass production due to their wider uses and expanded applications in optical communications and sensing systems. Liu [218] reported a novel manufacturing technique suitable for industrialization. It used commercial UV-grade fibers to construct a micro-lens array. The array can withstand in excess of 1 J/cm^2 per 20 ns pulses of 248 nm laser light. In terms of growth rate, the long-period gratings fabricated by using the array is four times faster than by using a metal mask.

In short, there are number of methods, which belong to either UV exposure or non-UV exposure for fabricating LPG. Point-by-point direct writing method or amplitude mask technique falls in category of UV exposure technique. Point by Point method is flexible for fabricating long-period gratings with different spectral characteristics but not

suitable for the mass production. The later techniques could be used for the mass production of LPGs. There are three main types of amplitude masks: chrome mask, dielectric mask and the metal mask. In the non-UV exposure, the facilities of CO_2 laser are inexpensive, whereas the cladding etching method and ion implantation technique are still in the experimental stage. In this section, we will discuss the methods of by which LPGs used in the experiments are fabricated.

4.3.1 Point-by-point UV exposure [89]

The point-by-point UV direct writing method is among the most used method due to its inexpensive facilities and ease of operation. Figure 4.2 is a schematic diagram of the experimental set-up for fabricating long periods by using a UV-beam-scanning system.

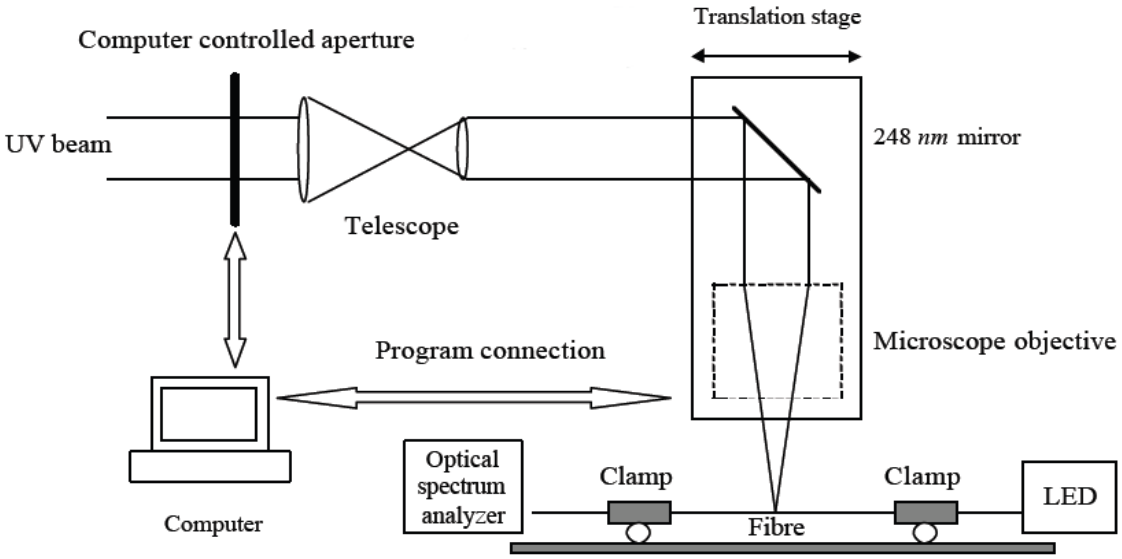

Figure 4.2 Experimental set-up for long-period grating fabrication by using the point-by-point technique [89]

In order to reduce beam size microscope objective lens configuration and a telescope is used in the setup. The system is equipped with computer controllable translation stage and shutter. LPGs of single as well as cascaded structures can be realized by using this method.

In the point-by-point technique, UV light is generated by a cavity resonator KrF excimer laser. Then it is passed through a slit. A lens images the slit on the core of the optical fiber with the long dimension of the image oriented perpendicular to the axis of the optical fiber. The image size is estimated as 500x1.5 μm^2in the image plane. A single 248 nm UV-light pulse produces fluence level of about 5 J/cm^2. A computer-controlled aperture can be finely adjusted to achieve desired duty cycle of gratings. Long-period gratings can then be fabricated by translating fiber between each irradiation step with the aid of an interferometrically controlled translation stage. The whole point-by-point writing process has been automated so that the triggering of the excimer laser and the precision stepping of the fiber are carried out under computer control.

LPG with a period of 500 μm and a total length of 1.1 cm in conventional B/Ge co-doped photosensitive fiber was fabricated using point by point technique [89]. This grating achieved ~18 dB coupling loss to the LP_{05} cladding mode in the 1550 nm region. Arbitrary duty cycle long-period grating can be using the point-by-point UV direct writing method. Thus, this technique is very flexible, thereby permitting the fabrication of long-period gratings with a variety of different spectral responses lengths and grating periods.

4.3.2 Amplitude mask method

The most popular method used to fabricate long-period gratings is by employing a pulsed excimer laser and is illustrated in Figure 4.3. Excimer laser method is popular as Amplitude mask UV exposure method. Amplitude masks with a rectangular transmittance function are imprinted on chrome-plated glass and have a 100 mJ/cm^2/pulse optical threshold damage level [11]. Several masks with different periods could be produced on the surface of a glass plate resulting in economical mask fabrication and providing easier access to different periodicities. The duty-cycle of the rectangular function is normally 50% and the length of the mask varies from 1 to 3 cm. The KrF excimer laser (manufactured by Lumonics Corporation)

produced a pulsed beam of energy 250-300 mJ/pulse, area 2.6x1.1 cm^2, repetition frequency 20 pulses/sec, and pulse duration of 10 ns at a wavelength of 248 nm. To avoid blazing of grating it was ensured that the fiber was exactly parallel to the axis of the mask. The grating transmission spectrum was monitored in real time as the bare fiber was exposed to UV radiation and resonance bands coupling to different cladding modes were observed.

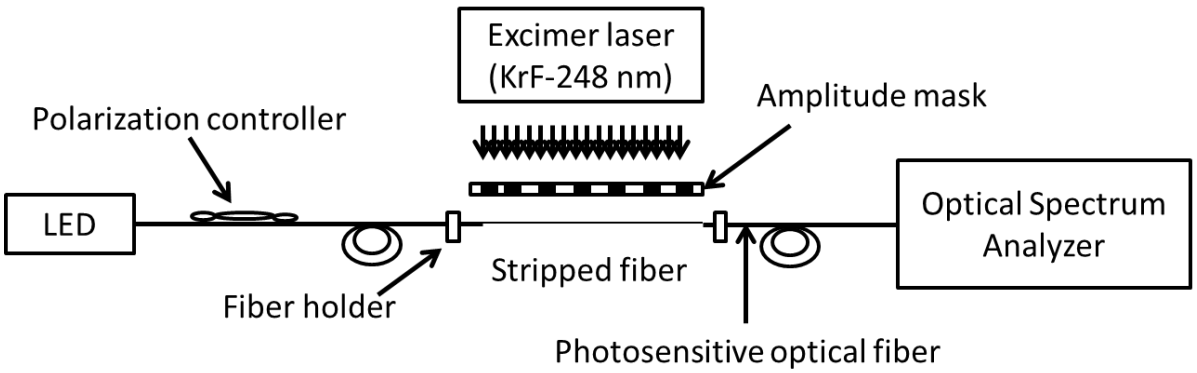

Figure 4.3 Configuration of an experimental set-up for long-period grating fabrication using the amplitude mask

The acrylate jacket was removed from about 3 to 4 cm length in the middle of the photosensitive optical fiber and the fiber was aligned behind the amplitude mask of appropriate period. To prevent bends from influencing the coupling to cladding modes fiber was supported on both sides of the bare region. Light from a broadband source such as an LED was launched from one end of the fiber while the normalized transmission spectrum was obtained on the optical spectrum analyzer display.

The grating transmission spectrum is monitored in real time as the bare fiber is exposed to UV radiation and resonance bands corresponding to coupling to different cladding modes could be observed. The resonance band shifts to longer wavelengths and the peak loss increases as the UV irradiation is continued. The spectral shift can be attributed to the increase in the guided mode effective index whereas isolation growth is related to the enhancement in the coupling coefficient. The shift in a resonance band during the writing process is a function of the order of the corresponding cladding mode. The band at the highest wavelength typically shifts

from 40 to 100 nm during the fabrication process. The wavelength shift can be related to the magnitude of the index modulation during the writing process.

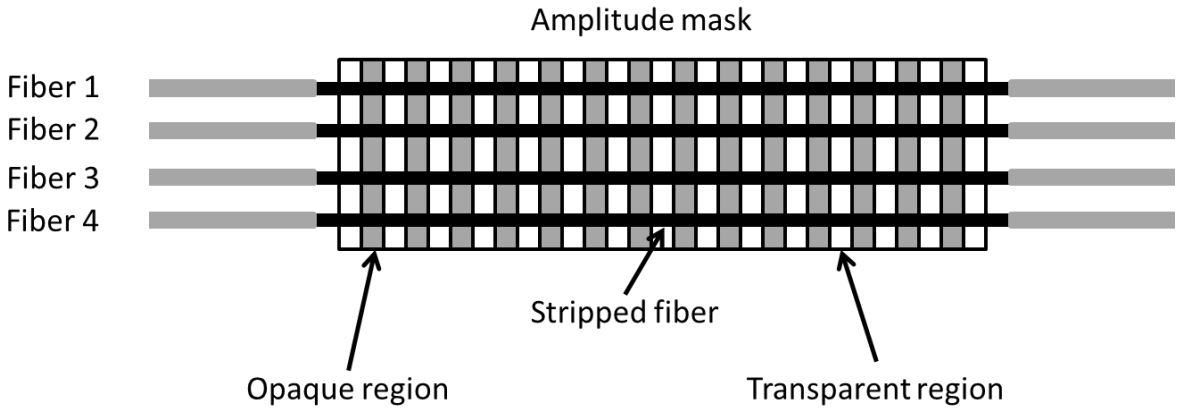

Figure 4.4 Procedure to fabricate multiple long-period gratings using the broad dimensions of an excimer laser beam.

The exposure to UV is stopped when the complete power transfer condition is satisfied for the resonance wavelength with the longest coupling wavelength in the OSA. The time required to produce a grating varies from 5 to 15 minutes for fibers with 3-10% GeO_2 and 2-3% hydrogen in this condition. The coupling to different cladding modes is clearly evident in the grating transmission spectrum. Each resonance band has a different peak loss or isolation due to the distinct coupling [110] coefficients for the corresponding cladding modes.

The major advantage of using the amplitude mask and the excimer laser-based fabrication method is that a number of gratings with the same period may be easily batch produced. For the purpose of mass production, more than a single fiber can be placed behind the amplitude mask as shown in Figure 4.4. Although only one grating is monitored during the writing process, if the transverse profile of the UV radiation is supposed to be invariant, then it is anticipated to have similar transmission spectra for all the gratings.

The amplitude mask can be replaced with a variable size slit that can be translated across the UV beam and the fiber in above said method. The aperture width is set to half of the value of desired periodicity. The fiber is irradiated for a fixed interval of

time. Then the aperture is translated a distance equal to the grating period and the fiber is exposed again. The procedure of exposing alternate half periods is continued until the desired coupling wavelength or isolation is achieved. By selecting appropriate aperture widths and translation distances, gratings with different periods and/or duty cycle in index modulation can be acquired using the same slit in aperture method. Furthermore, making the aperture size and the exposure duration a function of grating length the grating can also easily be chirped in period or in index change along the fiber axis. The above method can also be executed by translating the fiber even as keeping the aperture stationary [22, 216, 219].

Both in amplitude mask and phase mask writing process for a fiber Bragg grating, refractive index modulation in a fiber is produced by the UV beam through the mask. However, there is a fundamental difference subsist. The amplitude mask produces index modulation which is direct reproduction of the mask pattern, e.g. the periodicity of a LPG is the same as the mask itself. Whereas, the periodicity of a FBG is half of that of the phase mask since the fringe pattern results from the interference between the ± 1 diffraction orders of the phase mask. In spite of the restriction of one mask for one grating, the amplitude mask technique presents more precision in the spectral response as compared with the point-by-point method.

4.4 In-House Grating Writing Station

LPGs used in the experiments are fabricated using the TeraXion Grating Writing Station at CSIO. The system, shown in the Figure 4.5, is based around an excimer laser. The system has four grating writing options:

- Static mode (in which the laser beam is fixed),
- Scanning mode (in which the laser beam is scanned across the length of the phase mask)
- Interferometric mode

- Step mode (in which the system can be moved from one point to another and exposed).

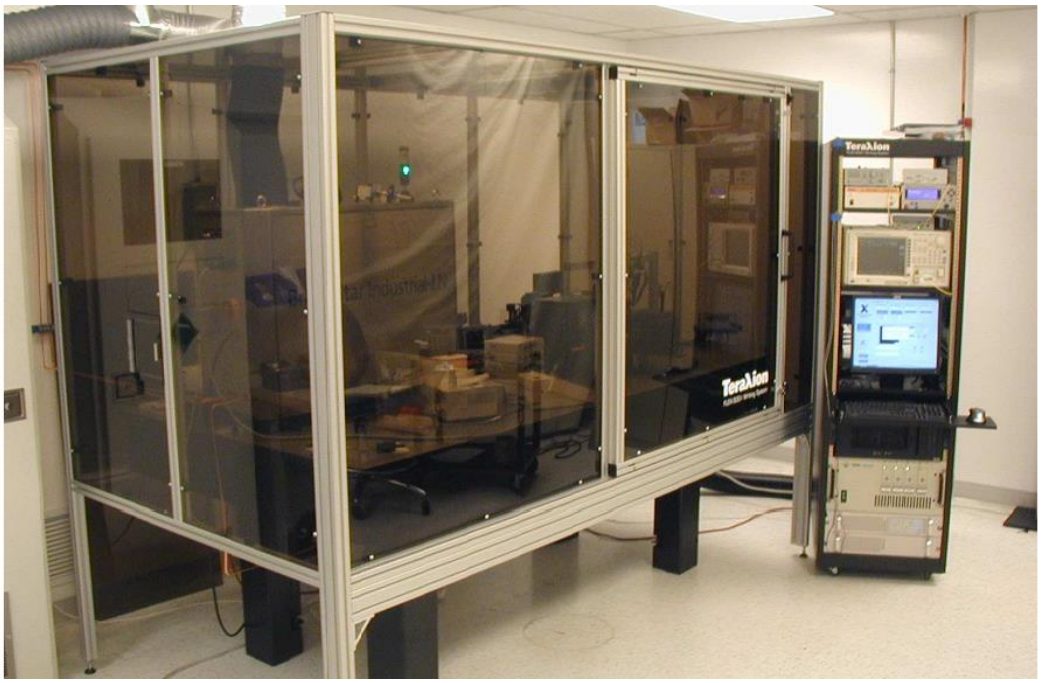

Figure 4.5 TeraXion Grating Writing Station at CSIO

The simple schematic of the optical system is illustrated in Figure 4.6

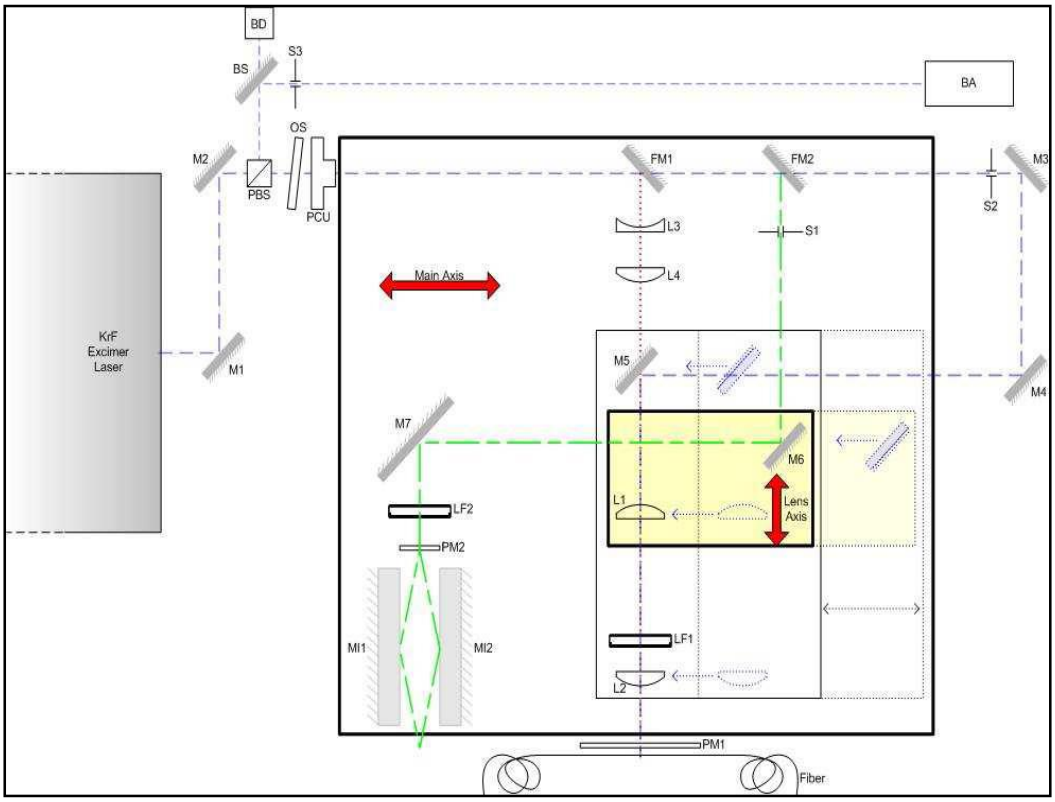

Figure 4.6 Simple schematic of writing station optical system

4.5 Different Modes of Grating Writing

4.5.1 Static mode

In static mode the laser beam is reflected on (M1) than on (M2), pass thru (PBS) (OS) (PCU) before to be reflected with (FM1) in the beam expander composed with (L3) and (L4) and then focus in the fiber with (LF1). The FBG are written in static mode. The period of FBG is half of the period of the phase mask. The distance between the fiber and phase mask is approximately 110 microns. The best way to manufacture FBG in static mode is to keep the optical fiber directly in contact with phase mask at desired tension, but without losing axial tension.

4.5.2 Scanning and stepping mode

In Scanning and Stepping modes the laser beam is reflected on (M1) then on (M2), pass through (PBS) (OS) (PCU) and (S2) before to be reflected with (M3) and (M4) on the scanning mirror (M5). From there the beam is formatted in the fringe control telescope comprising of (L1) and (L2) and the focusing lens (LF1). Then the laser beam passes through the phase mask (PM1) before exposing the fiber. LPGs are written in step mode using a slit and a blank silica plate to replace the phase mask. The silica plate is necessary to allow the system to do all of the fiber alignment procedures; otherwise it is not a critical element. The operator determines the step size and laser intensity. The grating is monitored in transmission.

4.5.3 Interferometric mode

In the interferometric mode a phase mask (PM2) is used to split the laser beam in two parts. Each of these two beams is reflected on a mirror (MI1) and (MI2) mounted on a goniometer. This setup gives the flexibility to change the angle between the superposed beams in the fiber. The phase mask (PM2) is mounted on a linear stage to compensate for the beam path length change. In interferometric mode the laser beam is reflected on (M1) then on (M2), pass thru (PBS) (OS) (PCU) before to be reflected with (FM2) in the adjustable aperture (S1). The modified beam is reflected

on the scanning mirror (M6) to be reflected at 90° on (M7). The scanning laser beam passing thru (LF2) is split with (PM2) and then recombined at the fiber position with (MI1) and (MI2). The module is also used for the fabrication of FBG.

4.6 Fabrication Steps

Here is the brief description of fabrication steps, which are common in all modes. Firstly the coating of fiber where writing has to be done is removed using thermo mechanical stripper as shown in Figure 4.7. The length of stripped part should be greater than that of phase mask.

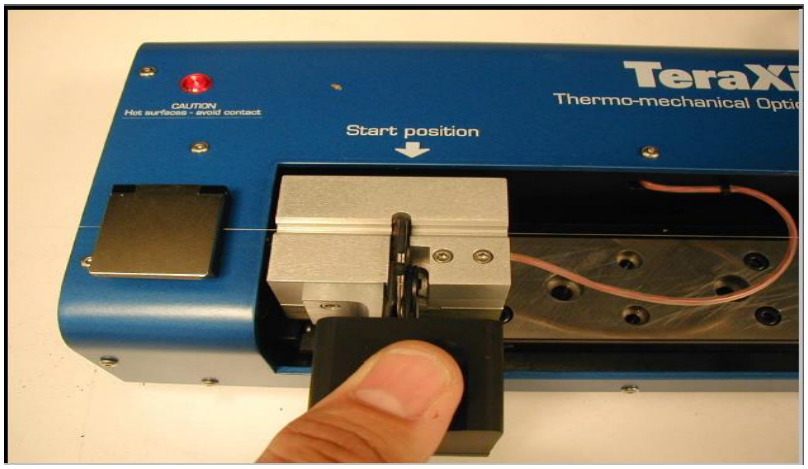

Figure 4.7 Removal of coating of fiber with Thermo mechanical optical fiber stripper

After removal of fiber coating, Laser beam alignment is done. Ensuring that the Laser beam profile is cleaned using the Beam Analyzer as well it should be always parallel to edge of the working table.

This is followed by Fringe Control/Scanning mode alignment. The laser beam launch is shown in the Figure 4.8. Then the selection of mode of operation for lens axis stage, Laser power stage and amplitude mask stage is done. After alignment, Laser beam is launched with desired repetition rate and energy so that writing can be completed.

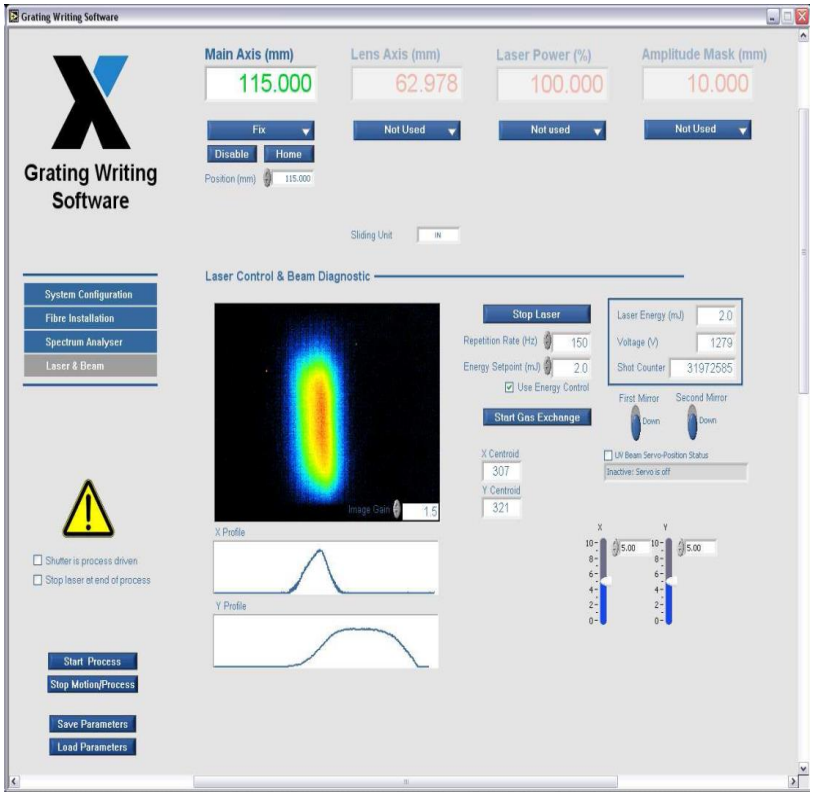

Figure 4.8 Laser beam launch view during writing

Third step involves the fiber Installation, that includes adjustment of the tension in the fiber before approaching it near the phase mask or silica slit/plate.

In fiber approaching stage the fiber moves towards and away from the phase mask or silica slit/plate. Once tension value is adjusted, vertical/horizontal Alignment is performed. This allows the user to align the fiber vertically/horizontally with respect to the phase mask or silica slit/plate.

The horizontal and vertical alignment windows are shown in the Figure 4.9 and Figure 4.10 respectively. The red coloured lines are the reference for the alignment process. The fiber has to be in between and exactly parallel to these red lines. Position of the fiber can be adjusted by approach and retract fibers buttons.

The writing is done according to the mode selected using phase mask or point by point method. Upon selecting the spectrum analyzer tab the user can control the supplied optical spectrum analyzer directly from the program. There are two menus

available within this tab: Setup, Cursor & Analysis. The setup menu allows the user to configure the OSA as required. The Cursor & Analysis menu permits the user to perform analyses on gratings. The Figure 4.11 shows the run time growth of grating during writing process observed on OSA

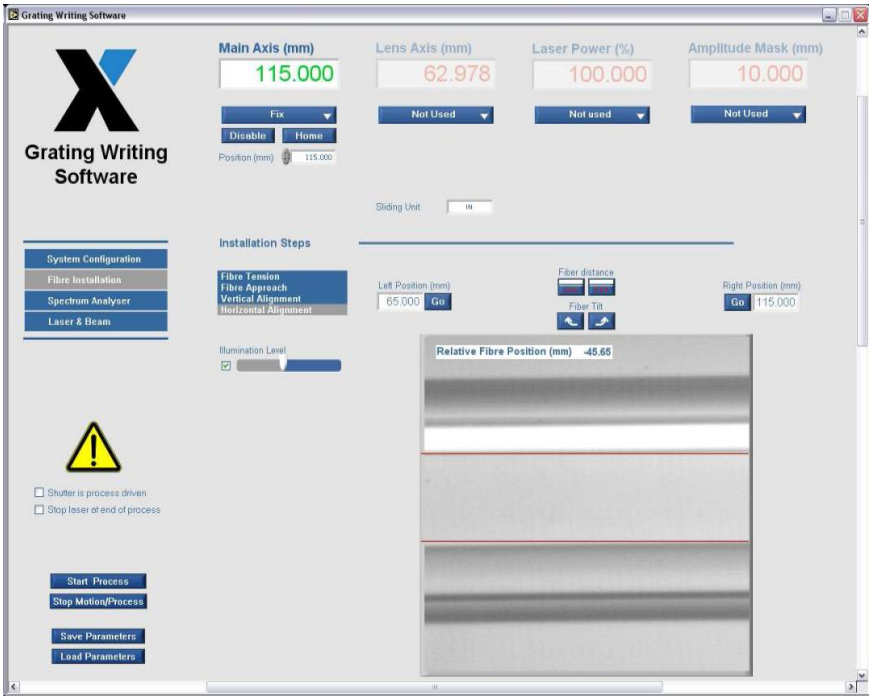

Figure 4.9 Image during horizontal alignment process.

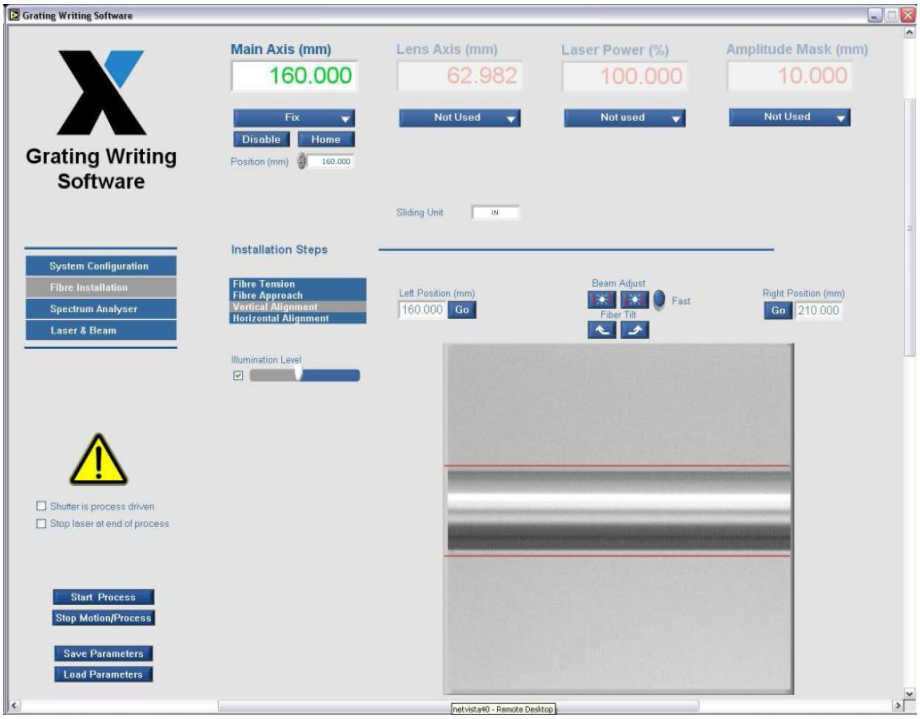

Figure 4.10 Image during vertical alignment process

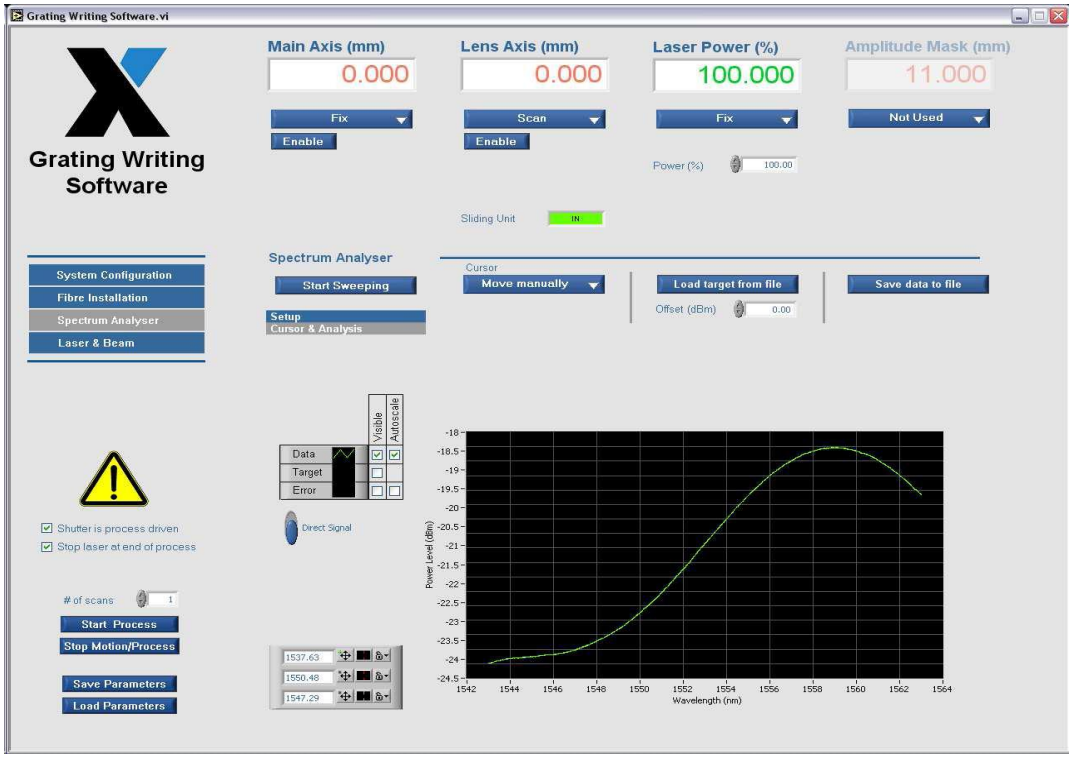

Figure 4.11 Growth of grating shown in OSA during writing process

4.7 Characterization of Fabricated LPG

The LPGs are written in step mode and the phase mask is replaced by a blank silica plate. The periodicity is of the order of hundreds of microns. No phase mask is required; instead one relies on point-by-point writing. A boron co-doped fiber was subjected to the excimer KrF UV laser having pulse repetition rate of 200 Hz and pulse duration of ~15 ns. The peak pulse energy of the UV laser beam was ~3 mJ. The gratings are written over different length with different periodicities and resonant wavelengths. The fabricated LPGs are then annealed at 150 °C for 24 hours for thermal stabilization.The Figure 4.12 shows the spectrum of simulated and fabricated LPF with resonance wavelength 1584.6 and period 575 μm.

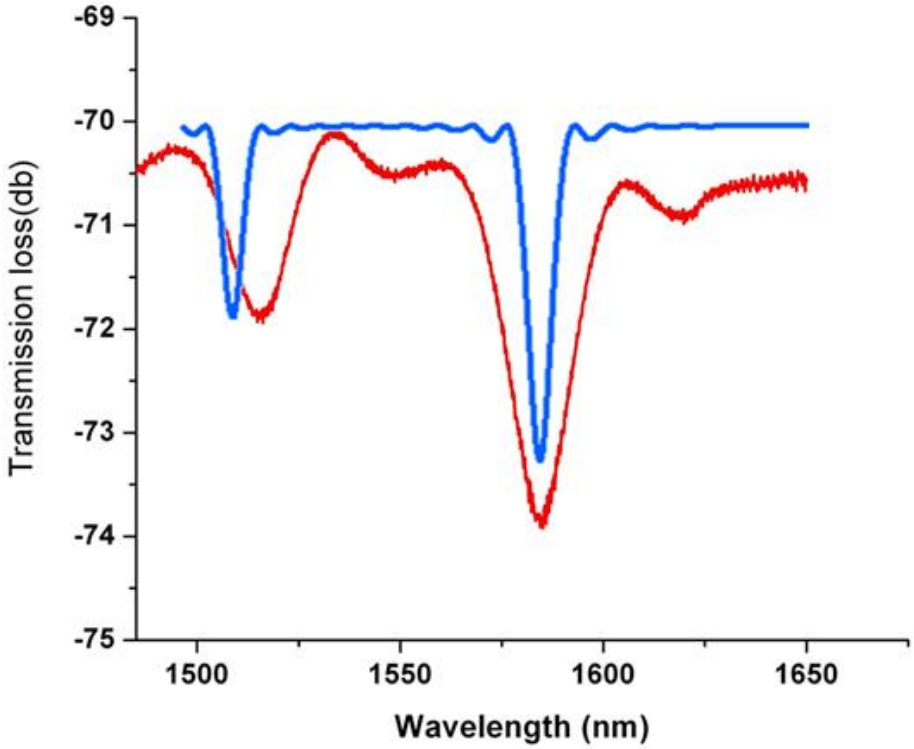

Figure 4.12 Spectrum of fabricated(red) and simulated(blue) LPG with resonance wavelength 1584.6 nm, period 575 μm

We have fabricated all the LPGs used in our experiments by above mentioned methods written in Boron co-doped fibers. To characterize the fabricated LPGs, a common method is used as described in Section 3.5. To gain information on the performance of LPG, it is exposed to standard RI liquids and its wavelength response is monitored on the OSA. The experimental set-up for calibrating the LPG against the standard RI solutions is shown in Figure 3.7.

Unlike FBG, LPGs couple power from the core mode towards the cladding modes through a periodic perturbation of refractive index. The effective indices of the cladding modes in an LPG are strong functions of the index of refraction (n_3) of the medium surrounding the cladding. Any change in this ambient index serves to modulate the effective index of the cladding modes ($n_{cl}^{(m)}$) with higher order modes undergoing larger variations. Since the coupling wavelength to a particular cladding mode (resonant wavelength λ_{res}) is dependent on $n_{cl}^{(m)}$ through the phase matching condition, a change in n_3 will effectively vary the value of λ_{res}. The standard RI

liquids used for LPG calibration have the following RI values at 1550 nm: 1.4358, 1.4398, 1.4439, 1.4479, 1.4496, 1.5 and 1.5018. The procedure includes launching of broadband light into the fiber core and receiving the transmission spectrum on the OSA.

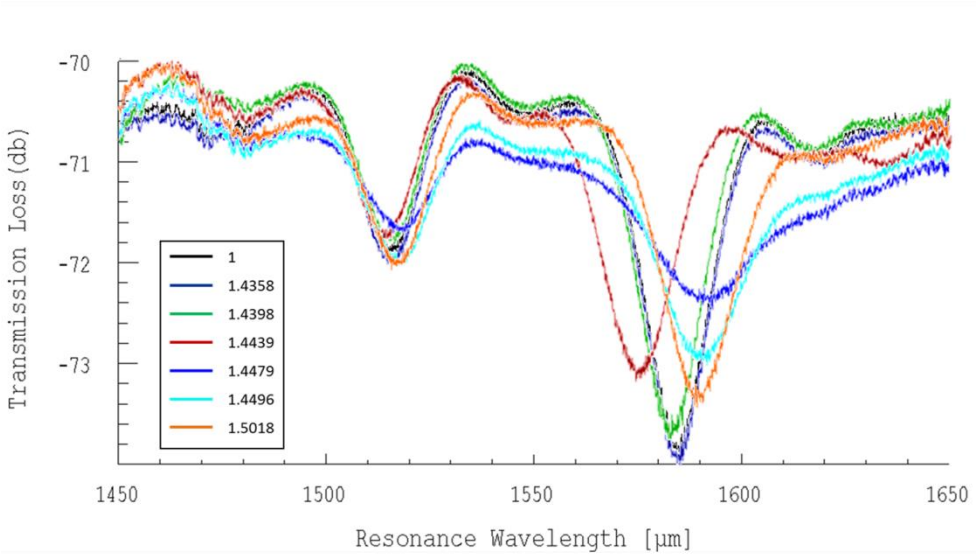

Figure 4.13 Simulated LPG spectrum for different RI values

The simulated and experimentally obtained LPG transmission spectra corresponding to all the above RI values are shown in Figure 4.13 & Figure 4.14.

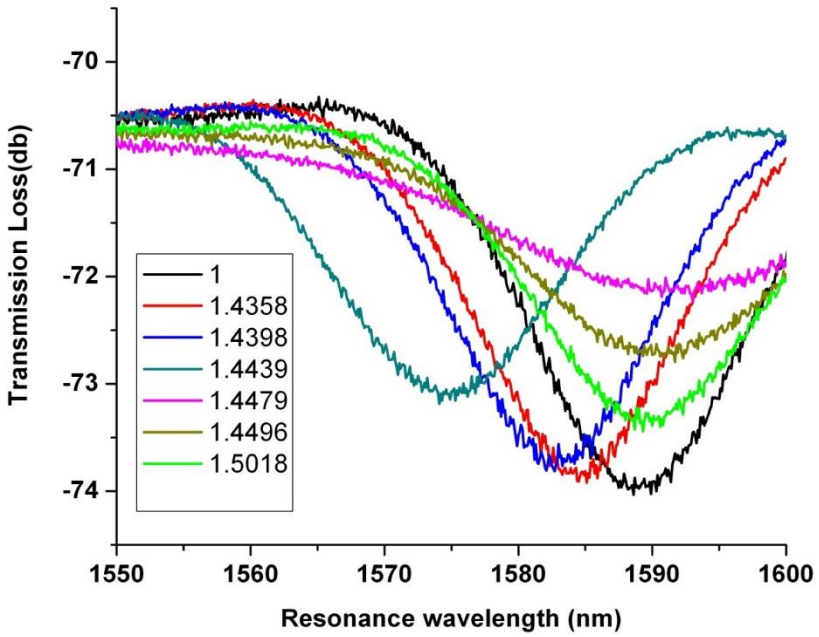

Figure 4.14 The LPG transmission spectrum for different RI values recorded on OSA during characterization

4.8 Wavelength Dependency of Long Period Grating on Temperature

The phase matching condition of long-period gratings as a function of the mode index of the core and the cladding can be expressed by Equation 1.19. Two factors affecting the temperature sensitivity of wavelength are produced by:

- The change in the effective indices due to the temperature dependence of the refractive index of the material
- The change in the grating periodicity due to the thermal expansion of the fiber.

This is given by [22]:

$$\frac{d\lambda_{pm}}{dT} = \frac{d\left(n_{eff}^{core} - n_{eff}^{clad}\right)}{dT}\Lambda_L + \left(n_{eff}^{core} - n_{eff}^{clad}\right)\frac{d\Lambda_L}{dT} \tag{4.4}$$

where L is the length of the grating. The sensitivity of a grating to the temperature strongly depends upon change in the effective indices of the guided and cladding modes.

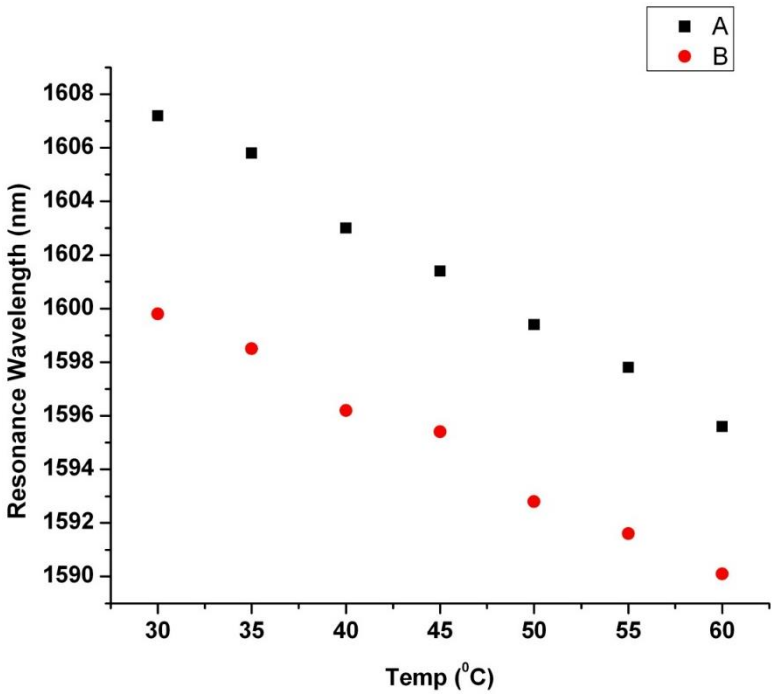

Figure 4.15 Variation of resonance wavelength with temperature for LPG written in boron co-doped SMF. 'A' represents grating with resonance wavelength 1607.2 nm and B with resonance wavelength 1599.8 nm

As we know that effective indices are the function of the core and cladding indices and radii, the effect of variation in the core and cladding radii has very small contribution to the temperature sensitivity in the comparison to core and cladding index variations. In general $\frac{dn_{eff}}{dT}$ is larger for germanium co-doped core than pure silica. The temperature dependence of the loss peak wavelength in the transmission spectrum for a long-period grating written in a standard single-mode optical fiber is shown in Figure 4.15.

4.9 Wavelength Dependency of Long Period Grating on Strain

The effect of strain on the wavelength shift of a long-period grating is different from that of a fiber Bragg grating. Qualitatively, the fiber Bragg grating and long-period grating responses are different because although the fiber Bragg grating wavelength is linearly proportional to the grating period multiplied by the effective index of refraction of the core, the long-period grating wavelength is proportional to the grating period multiplied by the difference in index of refraction between the core and the cladding. Furthermore, the effect of strain on the long-period grating is more dependent on the type of fiber. The most common method of approximating the index n(λ), as a function of wavelength λ, for a particular material uses the Sellmeier equation given by [220]:

$$n^2(\lambda) = 1 + \sum_{i=1}^{m} \frac{A_i \lambda^2}{\lambda^2 - \lambda_i^2} \tag{4.5}$$

where A_i and λ_i are material dependent parameters. For most practical applications only the first three terms are necessary to obtain an accuracy of about 10^{-5} in refractive index calculations. The typical shift of the center wavelength of a long-period grating is about 0.8 pm/micro strain [221].

4.10 Summary

The chapter described the methods for fabricating long-period gratings. The fibers that are used in our experiments are photosensitive optical fibers (Boron co-doped).

Long-period gratings can be written directly into these fibers without hydrogenation. We have fabricated LPGs using TeraXion grating writing station available in the lab. Various optical and non-optical components along with different modes of grating writing are discussed. Additionally, the simulation as well as experimental transmission spectrum of these gratings is presented. The characterization of fabricated LPG with available standard RI solutions is done experimentally. Wavelength dependency of LPG on strain and temperature is also discussed.

CHAPTER 5. ITO COATED LONG PERIOD GRATING REFRACTIVE INDEX SENSOR

5.1 Introduction

This chapter includes the designing and demonstration of Indium tin oxide (ITO) coated RI sensor. The approach is divided into two parts that include metal oxide coating development and characterization, and application of coatings to the LPG surface and evaluation. As we know that the cylindrical structure of optical fiber makes it challenging to achieve uniformity in coating. The other important considerations include coating refractive index and adhesion coating robustness. Many work have been reported on the material ITO [72, 119, 120, 222-224] on fiber for different applications. Recently [178], ITO has been used as a transparent contact in advanced optoelectronic devices leading towards becoming an integral part of modern electronic technology. Moreover it has also shown the potential for improving refractive index sensitivity of LPG.

5.2 Cladding Mode Transitions

Mode coupling in LPG has been discussed in Chapter 3. Nonetheless modes couple in a different way, which improves the characteristics of sensors in a great manner. Regarding numerical methods for analysis of LPGs, two cases have been considered so far in literature. In the first one, the LPG is surrounded by an infinite medium of lower refractive index than the cladding, which causes that the core mode couples to cladding modes [77, 225]. As the ambient refractive index approaches that of the cladding, the sensitivity of the resonance wavelength to variations of the ambient refractive index is higher.

The second case starts when the LPG is surrounded by an infinite medium of higher refractive index than the cladding. The core mode couples to radiation modes [112, 226-229], and the dependence of the resonance wavelength on the ambient refractive

index is not so important. Instead, the resonance depth is more dependent on this parameter for values close to the refractive index of the cladding [230]. In both cases, the region of highest sensitivity is located around the refractive index of fiber.

The third probability is when the LPG is no longer surrounded by an infinite medium. Now a thin overlay of higher refractive index than the cladding is deposited between the cladding and the surrounding media. One of the cladding modes will be guided by the overlay if this is thick enough [231]. This causes a reorganization of the effective indices of the modes of the cladding. As a result, there are important variations of resonance wavelength if we work around the thickness value where there is a transition to guidance of a cladding mode in the overlay for a specific ambient refractive index and thickness of the overlay. In this way, it increases the sensitivity of the effective index of the cladding modes for a specific application. Figure 5.1 shows the transversal view of coated fiber.

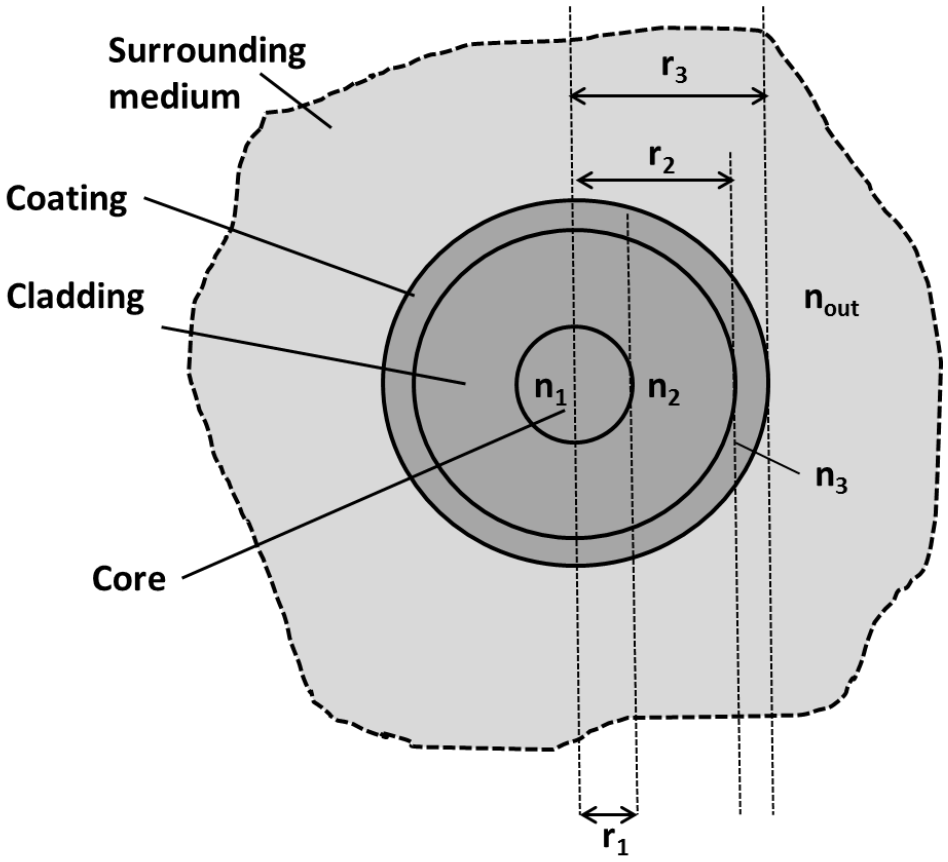

Figure 5.1 Transversal view of coated fiber [222]

Here n_1, n_2 and n_3 are the core, cladding and overlay refractive indices, respectively, while n_{out} is the surrounding refractive index and n_{eff} is the effective refractive index, r_1 and r_2 are the core and cladding radii and r_3-r_2 is the overlay thickness. Due to the presence of coating, the transition from cladding to overlay mode occurs and the lowest order cladding modes becomes guided into overlay. The higher modes move to recover the original field configuration leading to improvement in surrounding refractive index (SRI) sensitivity. This concept is also investigated theoretically. The transverse electrical field component, with azimuthal order ν, propagating along the z axis, is given by [222]:

$$R_v(r) = A_0\, Z_{V,1}\left\{u_1 \frac{r}{r_1}\right\} \qquad for\ r \le r_1 \tag{5.1}$$

$$= A_1 Z_{V,2}\left\{u_2 \frac{r}{r_2}\right\} + A_2 T_{V,2}\left\{u_2 \frac{r}{r_2}\right\} for \quad r_1 < r \le r_2 \tag{5.2}$$

$$= A_3 Z_{V,3}\left\{u_3 \frac{r}{r_3}\right\} + A_4 T_{V,3}\left\{u_3 \frac{r}{r_3}\right\} for \quad r_2 < r \le r_3 \tag{5.3}$$

$$= A_5 K_V\left\{v \frac{r}{r_3}\right\} \qquad for \quad r > r_3 \tag{5.4}$$

where $Z_{V,i}(x) = J_V(x)\ if\ n_{eff} < n_i$

$= I_V(x)\ if\ n_{eff} > n_i$

$T_{V,i}(x) = Y_V(x) \qquad if\ n_{eff} < n_i \qquad = K_V(x)\ \ if\ n_{eff} < n_i$

$$u_i = r_i k_0 \sqrt{\left|n_i^2 - n_{eff}^2\right|} \qquad for\ i = 1,2,3$$

$$v = r_3 k_0 \sqrt{\left(n_{eff}^2 - n_{out}^2\right)}$$

where r is the radius, J_V and I_V are the ordinary Bessel functions of first and second kind of order ν and Y_V and K_V are the modified Bessel functions of first and second kind of order v, respectively. The set of equations from (5.1) to (5.4) represent the approximation required for obtaining transmission, if the ambient refractive index is

higher than that of cladding. On applying the boundary condition, field must be continuous along the interface between the each two cylindrical layer as well as the continuity of derivatives of field should be satisfied at radius r = r_i (i=1, 2, 3). In addition, A_1, A_2, A_3, A_4 and A_5 can be obtained, as function of A_0, by imposing the continuity of the fields at the interface between core and cladding, cladding and overlay and overlay and surrounding medium while A_0 is related to the optical power of the mode. In the Figure 5.2, the cladding modes LP_{02} to LP_{11} are shown without any overlay. The core and cladding radii are 4.2 μm and 62.5 μm, refractive indices of 1.5362 & 1.5306 respectively, length of grating 25 mm, period 276 μm and operating wavelength 1200 nm (These are the same parameters chosen in [72]). The LP modes are calculated using coupled mode theory. Let us consider LP_{01} to LP_{05} modes with calculated associated n_{eff} values LP_{01}=1.5341034, LP_{02} = 1.5305748, LP_{03}=1.5304895, LP_{04}=1.5303452, LP_{05}=1.5301430 without any overlay. On deposition of overlay of RI value 1.67 and thickness 3.5 μm, the cladding mode LP_{02} is shifted to value near 1.663 and accordingly rest of the cladding modes. Therefore the new modified values of n_{eff} calculated by Optigrating 4.2.2 are LP_{03}=1.644, LP_{04}=1.612, LP_{05}= 1.568, which are in accordance with the results reported by Villar [72].

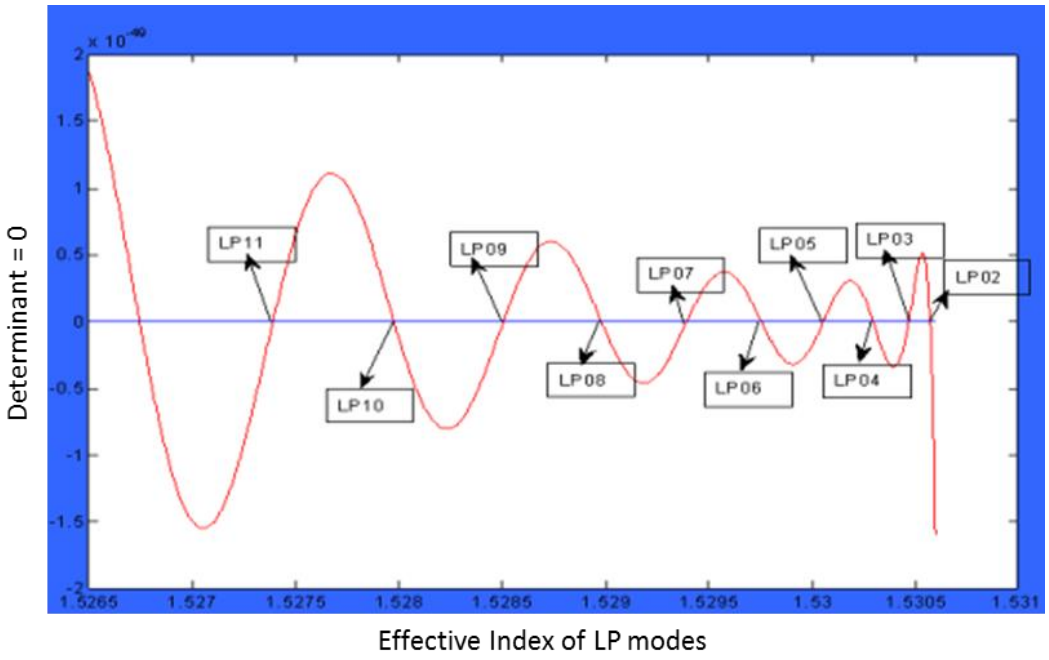

Figure 5.2 Cladding modes LP_{02} to LP_{11} without overlay

As the overlay of higher refractive index is deposited on an LPG, the cladding modes shift their effective index to higher values. When the overlay is thick enough, one of the cladding modes is guided by the overlay. It is exactly the lowest order cladding mode (highest effective index cladding mode) that jumps to the overlay. This causes a reorganization of the effective index of rest of modes. Higher order cladding mode than that is guided by the overlay which will shift their effective index value towards the effective index of the immediate lower order cladding mode. The immediate consequence of the shift in effective index is that it leads to a displacement in all attenuation bands. In order to compare the resonance wavelength shift of several resonances with overlay thickness, graph is generated by using application software designed and provided by Villar [232]. Figure 5.3 and Figure 5.4 depicts the general representation of evolution of modes for a fixed wavelength range caused as a function of the overlay thickness and overlay RI which is fixed 1.8 for surrounding refractive index n_s=1 and n_s =1.338 respectively.

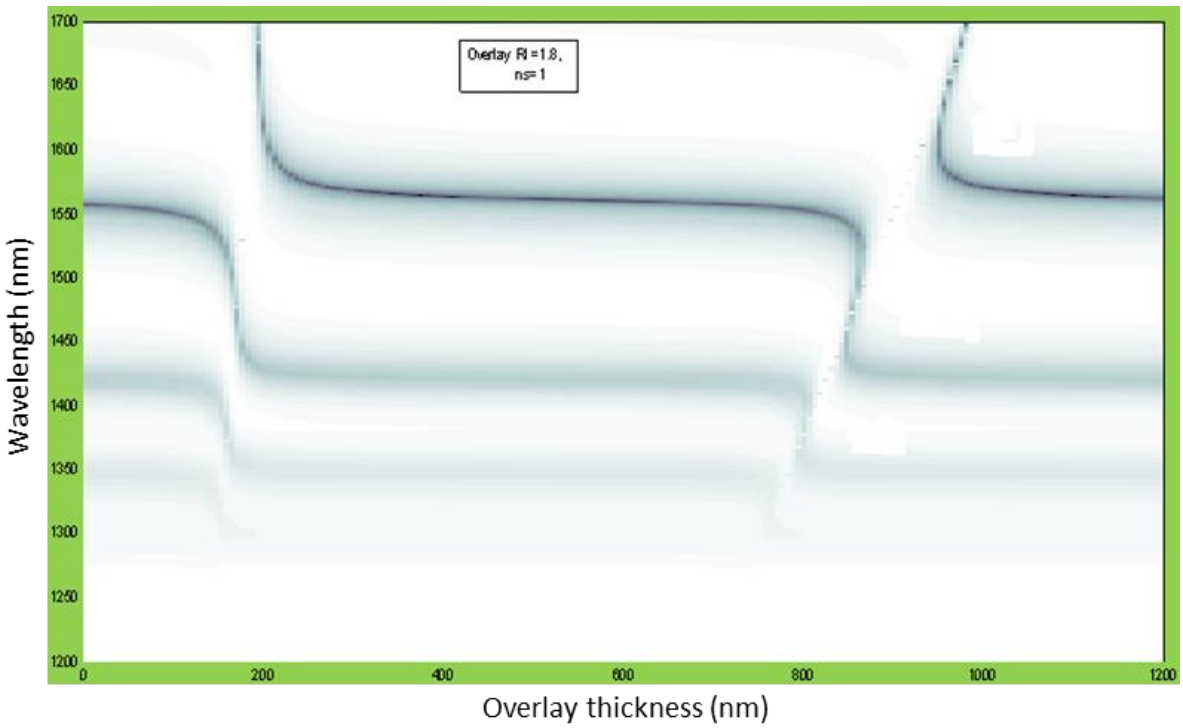

Figure 5.3 Growth of various cladding mode resonances as a function of overlay thickness (1.8) and refractive index n_s=1

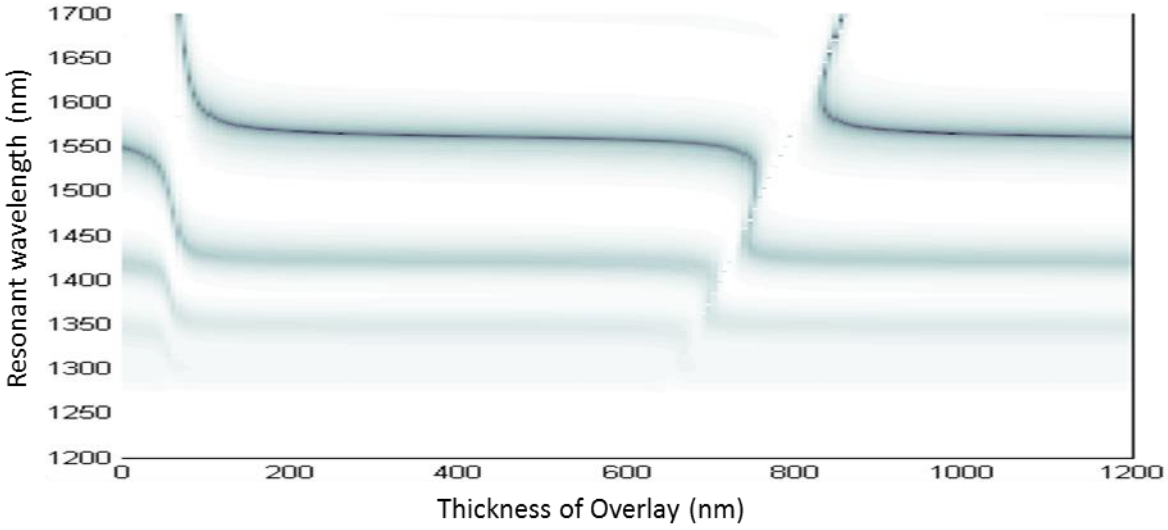

Figure 5.4 Growth of various cladding mode resonances as a function of overlay thickness (1.8) and refractive index n_s=1.338

If the results of Figure 5.3 are compared with those of Figure 5.4, a variation can be appreciated in the optimum thickness as the ambient refractive index. From slab waveguide theory, a slab between two different media starts guiding for a lower thickness as both media refractive indices are more similar [233]. When both media are the same, the slab always guides at least one mode. This theory can be extra poled to cylindrical waveguides. There is an influence of the mode order in the optimum overlay thickness, and the range of displacement is higher for higher-order modes. This four layer analysis is in primary stage, more rigorous analysis need to be done for optimizing the value of coating thickness for a particular application. The immediate consequence of the shift in effective index is that it leads to a displacement in all the attenuation bands. E.g the attenuation band corresponding with the eighth mode shifts the wavelength to that of the seventh mode; the same is true for the seventh mode that shifts the wavelength to the attenuation band of the sixth mode, and so forth. Furthermore, there is an optimal deposition thickness where the central wavelength shift as a function of the ambient refractive index is highest. This value depends mainly on two variables: the refractive index of the overlay, and the ambient refractive index. Consequently, a good choice for a high sensitive device to the ambient or the overlay refractive index is to stop the

deposition when the effective index value of a mode is located between the effective index of the mode itself before deposition, and that of the next lower cladding mode before deposition. Therefore in above figures, the general representation of evolution of modes for a fixed wavelength range, overlay thickness, but varying surrounding RI.

5.3 ITO Film Preparation and Characterization

ITO is essentially formed by substitutional doping of In_2O_3 with Sn which replaces the In^{3+} atoms from the cubic bixbyte structure of indium oxide. Sn thus forms an interstitial bond with oxygen and exists either as SnO or SnO_2 accordingly it has a valency of +2 or +4 respectively. This valence state has a direct bearing on the ultimate conductivity of ITO.

To develop metal oxide coating the solution is prepared with Indium chloride ($InCl_3$) (Fisher Scientific) and Tin chloride $SnCl_2.2H_2O$ (Spectrochem Pvt. Ltd) in the ratio 1:0.2 in 25 ml of ethanol in the ultrasonic cleaner. Surfactant Tween 80 0.01% by volume (Merck Specialities Pvt. Ltd) is also added to the prepared solution. The dip coating method is done to form the over lay on LPG surface. The Apex dip coater with special attachment for holding the fiber shown in the Figure 5.5 is used in the experiment. The parameters like dipping and lifting speed, deposition cycles, dry and wet time are optimized after performing number of trails.

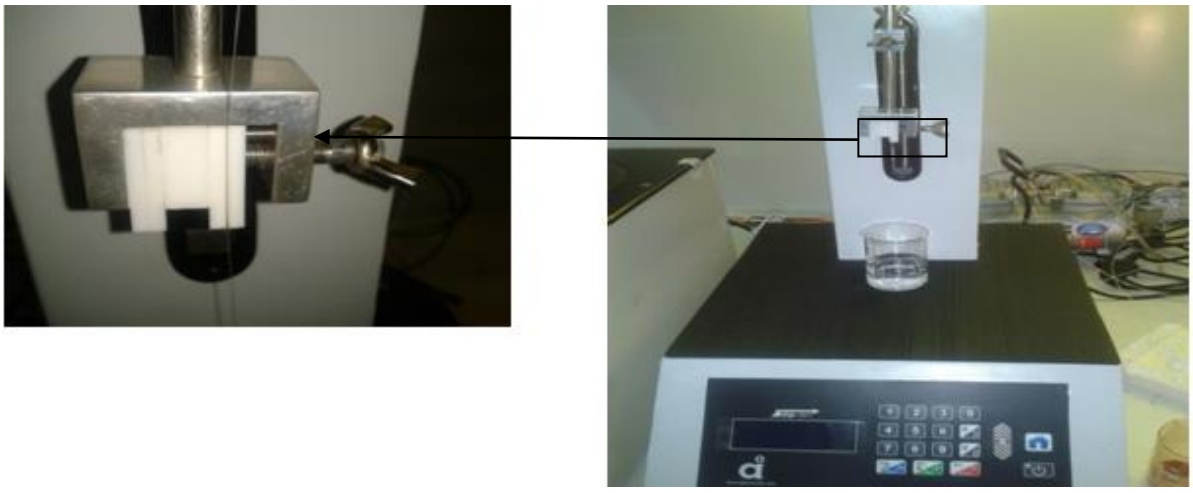

Figure 5.5 Dip coater with special attachment for holding fibers

After dip coating, heat treatment is given to the samples and then air dried. An optimized, reproducible and reliable approach to the coating process is generated with a number of trial experiments to allow a smooth and thin coating on the LPG. Consistency in the coating of ITO solution on the optical fibers is investigated by Field Scanning Electron Microscope (FESEM) (Hitachi S4300 SE/N). The Figure 5.6(a) & (b) showed the FESEM micrographs where surface modification is evident. The coating thickness ~1μm was observed.

5.3.1 Fourier transform infra-red spectroscopy (FTIR)

FTIR transmission spectrum is acquired from Nicolet iS10 and the results are shown in Figure 5.7 (a) and (b). The optical transmittance is closely related to the free electrons in ITO film. The relative intensity change of the FTIR vibrational peaks shows that there may be some predominant structure orientation change. The spectrum reveals several peaks, which can be ascribed to vibration modes of different bonds in the ITO film. The peak variation situated at 419 cm^{-1} and 561 cm^{-1} confirms the existence of In-O-In bonding. Also, the Sn-O-Sn bonds are evidenced by the peak situated at 618 cm^{-1} and the large peak variation at 1100 cm^{-1} is given by the Si-O-Si vibration at the interface of fiber and film [234].

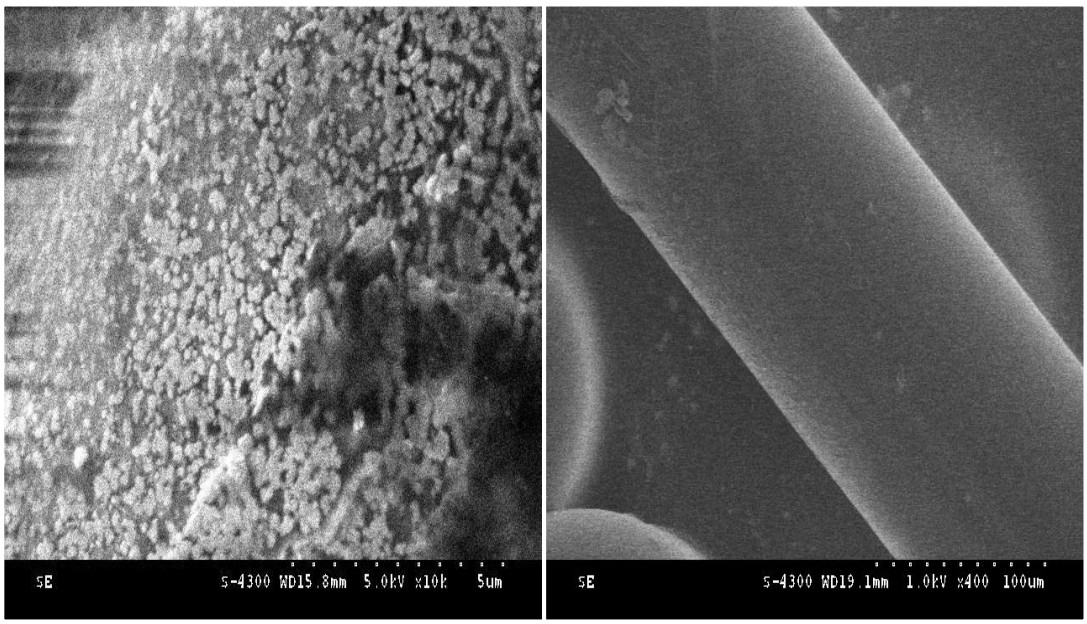

(a) (b)

Figure 5.6(a) FESEM micrograph of ITO coating (b) ITO coated fiber

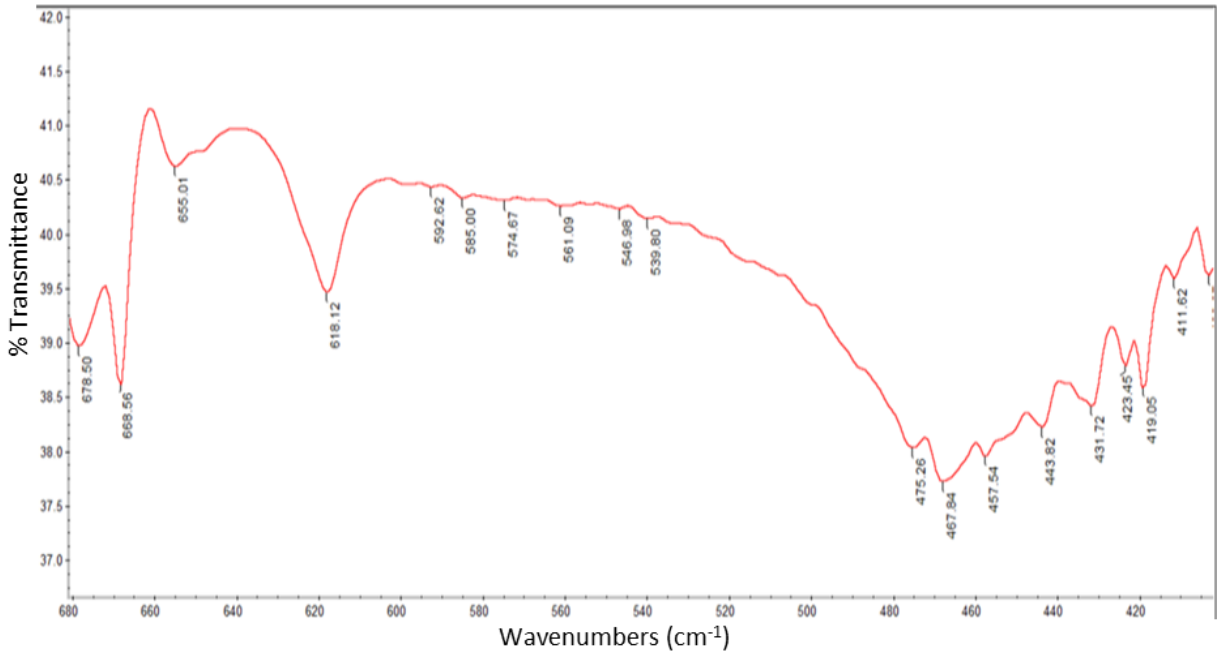

(a)

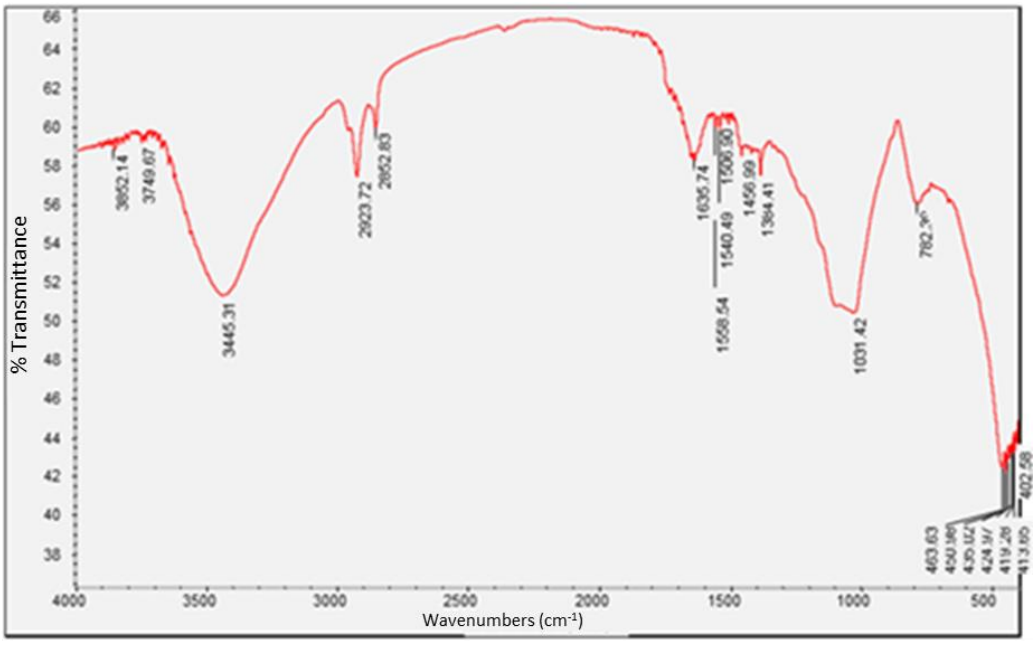

(b)

Figure 5.7 (a) & (b) FTIR spectrums of ITO coated LPG

5.3.2 RAMAN spectroscopy

The Raman spectroscopy deals with the structural changes related to the strain. The laser light interacts with molecular vibrations, phonons or other excitations in the system, resulting in the energy of the laser photons being shifted up or down. The sample is analyzed by using Invia Raman, (Renishaw) and results are shown in Figure 5.8.

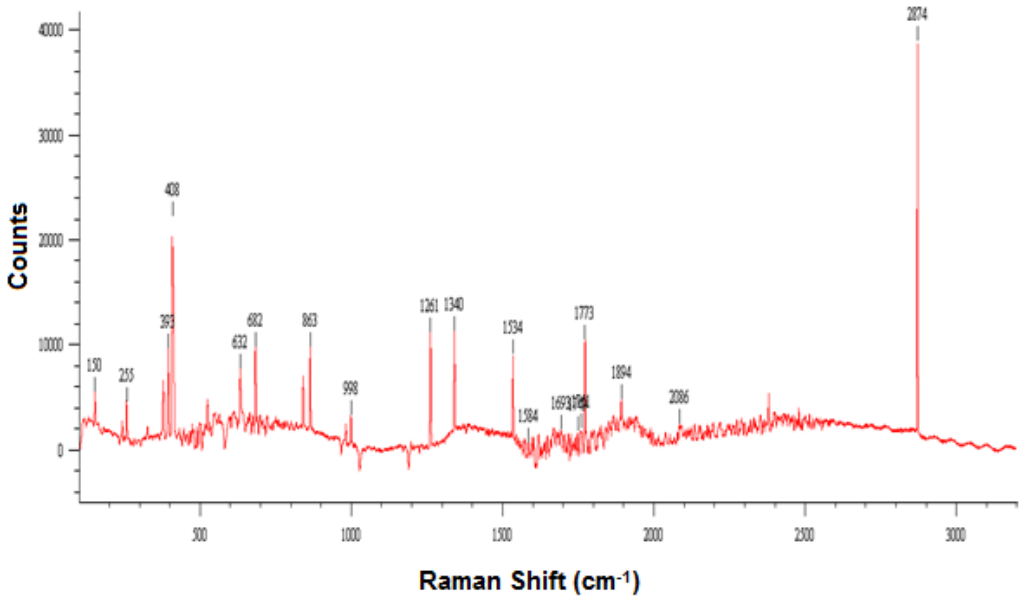

Figure 5.8 Raman Spectroscopy results of ITO coated LPG

The Raman results shows the peak at 863 cm^{-1} and 1261.7 cm^{-1} and 1773 cm^{-1} shown in Figure 5.8 in accordance with the signature intensity pattern of ITO due to band gap of ITO and two phonon process respectively [235].

5.4 Sensitivity Analysis of Uncoated & ITO coated LPG Refractive Index Sensor

The spectral sensitivity of LPG is given by [114]

$$\frac{d\lambda}{dn_s} = \left(\frac{d\lambda}{dn_{cl,m}^{eff}}\right)\left(\frac{dn_{cl,m}^{eff}}{dn_s}\right) \tag{5.1}$$

The spectral sensitivity depends upon the effective refractive index of the coupled cladding mode of $n_{cl,m}^{eff}$ order m, which is further dependent on the refractive index of surrounding material n_s. The RI sensitivity is experimentally analyzed. The experiment is performed by LPG with a resonant wavelength of 1591 nm and period of 670 μm written over a 2.0 cm length of boron co-doped fiber by point-by-point writing method using an excimer KrF UV laser having a pulse repetition rate of 200 Hz, pulse duration of ~ 15 ns and peak pulse energy of ~ 3 mJ. The fabricated LPG is then annealed at 150^0C for 24 hours for thermal stabilization. To gain an understanding of the LPG performance for measuring refractive index change, both the uncoated and

coated LPG are characterized with various standard RI liquids 1, 1.45, 1.454 and 1.458 from (Cargille Labs). From this data, LPG sensitivity, operation range, and expected response curves can be obtained. A broadband light source (AQ4305, Ando Electric Co. Ltd) connected to one end of the LPG and an optical spectrum analyser (OSA) to the otherwith level resolution 0.01 dBm and wavelength resolution of 0.1nm (Yokogawa, AQ6319, Ando electric Co. Ltd) as shown in the Figure 5.9. The LPG is fixed between two micro-positioners for keeping it straight throughout the experiment .LPG is fixed inside the sample cell.

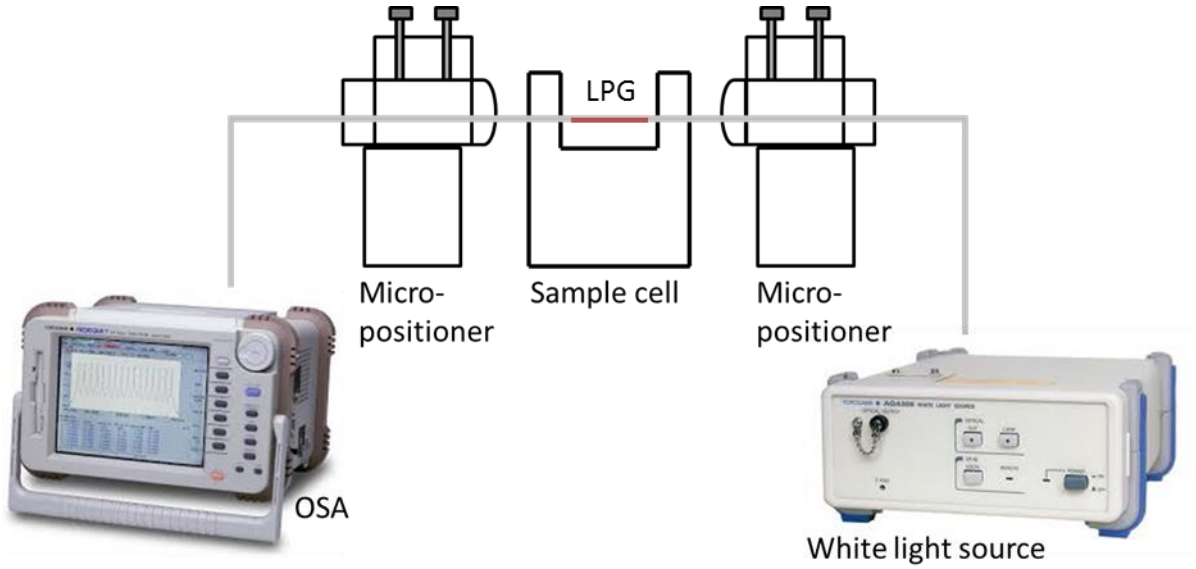

Figure 5.9 Schematic view of Experimental set up

The glycerol solution of different concentrations (20-80%) is filled in the sample glass cell, where the LPG is already kept straight with the help of two micro positioners. The RI values of different concentration of glycerol solution are measured by using BS-RFM 840 Refractometer giving sensing region with refractive indices from 1.3490 to 1.4198. Figure 5.10 (a) and (b) shows the spectral signature of both uncoated and ITO coated LPG with different concentration of glycerol.

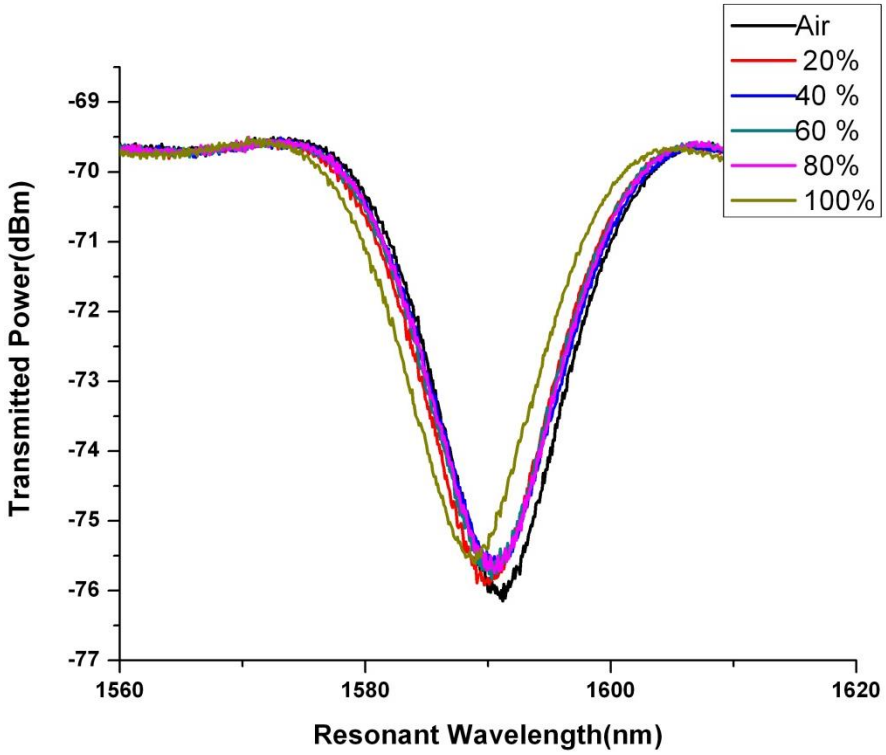

(a)

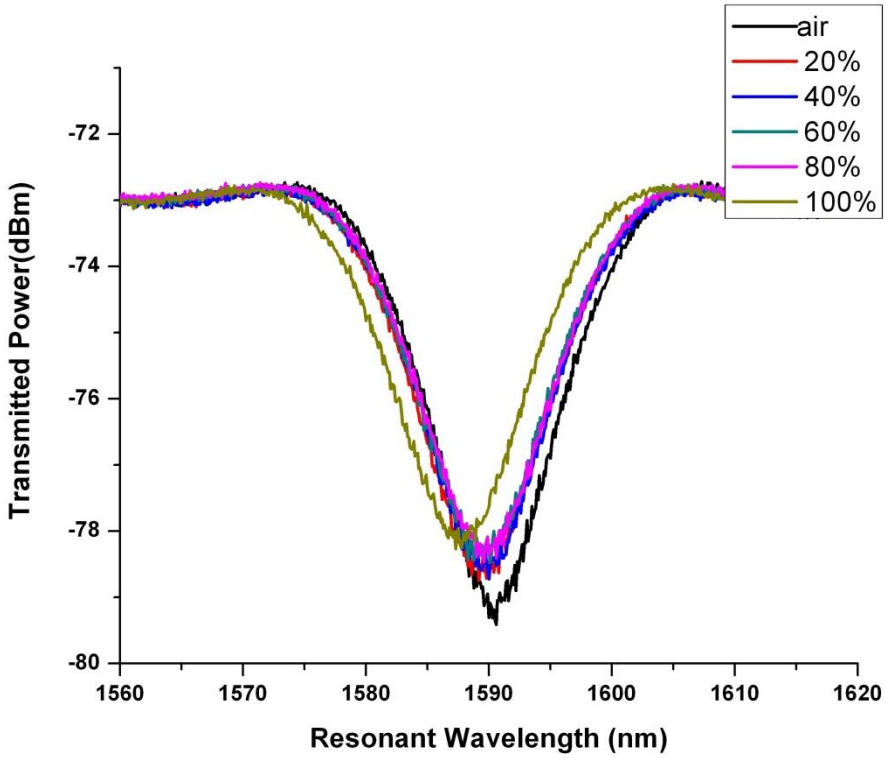

(b)

Figure 5.10 Spectral response of (a) uncoated LPG (b) ITO coated LPG with different concentrations of glycerol

The sensitivities for both the uncoated and the ITO coated LPG have been tabulated in Table 5.1.

Table 5.1 The sensitivities of both uncoated and ITO coated LPG for glycerol solution with varying concentration (20-100%)

Glycerol Solution (%)	Sensitivity of Simple LPG (nm/RIU)	Sensitivity of Coated LPG (nm/RIU)	Enhancement Factor
1(air)			
20-40	156	322	2
40-60	114	302	2.5
60-80	145	500	3
80-100	49	91	2

Villar *et al* [121] reported wavelength shift of 100 nm with overlay $PDDA^{+}$/PolyR-478 with thickness 128nm for five concentrations of sucrose in water: 30%, 40%, 50%,60% and 70% for very high order mode. If the ambient refractive indices lower than the cladding of the LPG, the wavelength shift of the attenuation bands for materials with a refractive index close to that of the LPFG is good, whereas this quality decreases as we move to lower refractive indices. The deposition of an overlay solves this limitation. It was theoretically proved in literature that the highest variation of the resonance wavelength depends on three parameters: the ambient and overlay refractive indices and the overlay thickness. If the overlay refractive index is fixed, the implementation of a refractometer for a specific refractive index range depends on the overlay thickness. For each specific ambient refractive index range and overlay refractive index there is an optimum overlay thickness. The selection is clearer for high-order mode resonances. We observed that the coated LPG is 2-3 times more sensitive than uncoated LPG in our case. This factor can be higher for lesser value of grating period and around highly optimized overlay thickness [72]. We have done the experiment for comparatively high value of grating period due to writing limitations. The limitation of grating writing system is actually associated

with available LASER options. The excimer laser is by far the most powerful source of UV laser light. However it is not a panacea for grating writing because of its large size, high power consumption and relatively high cost of ownership. LASER power in our grating station can vary from 3.5 to 4 MJ. Length of grating cannot be more the 5-10 cm. LPG can be written on specialized fiber i.e. photosensitive fiber as UV beam is used. Its primary drawback is low power. This leads to long exposure, thus requiring careful elimination of ambient vibration, thermal cycling and air currents. Furthermore, the long exposure of the fiber can cause it to become heated itself; this changes its dimensions and can alter grating characteristics.

5.5 Summary

The properties of long period grating has been investigated with conducting metal oxides (ITO) coating. We discussed the concept of rearrangement of modes due to deposition of higher refractive index value overlay on it. The utilization of ITO as coating material allows the fabrication of sensitive and easy to implement refractive index sensors. A very simple, dip coating method has been used for thin film deposition of ITO. The coating structure and its properties had been investigated using SEM, FTIR and Raman spectroscopy analysis. The RI sensitivities of the uncoated as well as ITO coated LPG was monitored with glycerol solutions of different RI. A comparison of both demonstrated that the sensitivity was enhanced by 2-3 times because of coating in our case. This factor can be improved by further optimizing the coating methods. This approach has given a better understanding about the coated LPG behavior.

CHAPTER 6. LONG PERIOD GRATING HUMIDITY SENSOR

6.1 Fiber-Optic Techniques for Humidity Detection

With the advent of optical fiber technology, a considerable level of research has been focused on fiber-optic-based techniques for humidity sensing. In a similar way to their electronic or mechanical counterparts, fiber-optic humidity sensors are secondary devices but show additional features like small size, immunity to electromagnetic interference, multiplexing and remote sensing capabilities, of which the counterpart electronic sensors lack. However, the limitations of the operating and accuracy of the fiber-optic-based humidity sensors are some of the drawbacks which researchers are striving to continue to address. Nevertheless, these sensors have found useful applications in various areas where electronic sensors were found to be inappropriate, thereby showing the real potential of fiber-optic-based sensors. Generally, fiber-optic based humidity sensing techniques include direct spectroscopic, evanescent wave, in-fiber grating and interferometric methods, as discussed in sections below.

6.2 Choice of Material for LPG Out-cladding Overlay

One of the most important design aspects of the LPG-based RH sensor is that it should allow interaction of the guided light with a hygrosensitive overlaid material for sensing the ambient humidity without endangering the fibre. Gelatine films with cobalt chloride ($CoCl_2$) as hygroscopic agents have been reported earlier with simple optical fiber based humidity sensors [40] but their response as out-cladding overlays of LPG has not yet been investigated.

6.2.1 The Cobalt Chloride – Gelatine composite

Cobalt Chloride ($CoCl_2$), a complex compound formed by the transition metal Cobalt (Co), varies its coordination number from 1 to 6 when exposed to water, forming a

hexa-hydrated compound $CoCl_2.6H_2O$. The colorimetric interaction of cobalt(II) chloride with water vapour has been studied and utilized extensively for the detection of water. The anhydrous form is bright blue in colour and as it becomes subjected to moisture, it absorbs molecules of water till the blue colour turns pink.

The use of cobalt chloride on the surface of optical fibers requires that it should be suspended in an optically transparent binding medium because by itself cobalt chloride forms salts of crystals which adhere poorly to the fiber surface. Further, it is necessary to avoid formation of discrete crystals on the surface of LPG because this would inhibit the proper interaction of cladding modes with the ambient. Gelatine is found to be satisfactory material because cobalt chloride dissolves readily in gelatine solution at 65^0C and dries to a transparent crystal free film on the fiber.

Gelatine comes under the class of a fibrous protein produced by partial hydrolysis of collagen extracted from the skin, boiled crushed bones, connective tissues and organs of cattle chicken and pigs. It exhibits strong mechanical and at the same time elastic behaviour. The long amino acid sequences dissociate into separate strands on heating and get entangled when they are cooled. The open and fluctuating structure leaves room for things to diffuse within the water matrix. However, once the water is removed via evaporation, the whole structure collapses into a 3D web.

The water adsorbing properties of both cobalt chloride and gelatine allow the refractive index of the combination to change according to the water content. The property of thin film formation, water binding capacity and refractive index variation on water adsorption of $CoCl_2$-Gelatine matrix makes them a suitable choice of material to be overlaid on the cladding of LPG for the purpose of RH sensing. Moreover, gelatine films do not deteriorate over a period of four months [40] at room humidity thus supporting our choice for the same.

6.2.2 The process of humidity sensing

The solution of $CoCl_2$-Gelatine prepared according to pre-determined sequence of steps is to be applied as an LPG out-cladding material by the process of dip coating. The refractive index of the mixture in which gelatine and cobalt chloride are mixed in 2:1 proportion is calculated to be 1.342 according to Equation 6.3 given in [9].

$$\frac{P_1}{100} = \frac{n_m - n_2}{n_1 - n_2} \tag{6.3}$$

Here, P_1 is the volume percent of gelatine, n_1 is the RI of gelatine, n_2 is the RI of $CoCl_2$ and n_m is the RI of mixture. Thus, the abovementioned case represents a model of low refractive index coating on the surface of LPG cladding that is sensitive to moisture. As RH levels increase, more water vapour diffuses into the overlay coating and brings about a reduction in the refractive index. Moreover, the addition of water content in the coating induces the gelatine to swell. The simultaneous effect of both these factors firstly, reduction in RI of film with absorption of water vapours and secondly, the swelling of gelatine present in the film have to be taken into account for a cumulative response to a particular RH level. Any LPG is characterised by its signature wavelength, called resonant wavelength, which are represented as loss dips in the transmission spectrum. The magnitude and position of these loss dips are a function of various parameters, some of which are intrinsic i.e. they depend solely on the fabrication parameters of LPG for example, the laser power, duration of irradiation, length of LPG, and some parameters like grating period, coupling coefficient, number of cladding modes, their effective indices etc. depend on extrinsic factors such as strain, temperature, RI of external medium. The underlying principle for LPG-based sensors rests upon the shift in resonant wavelength of the LPG caused by a combination of one or more of these factors.

6.2.3 Change of RI of overlay with RH

A combination of $CoCl_2$ and gelatine is applied as an out-cladding overlay over the LPG. Being hygrosensitive in nature, the coating absorbs water vapour as the coated LPG is subjected to increasing levels of RH. As water vapour diffuses into the

coating matrix, the density of the coating reduces which causes a reduction in the refractive index. The effect of reduction in RI of the overlay reduces the effective index of the cladding modes and thus the resonant wavelength of the LPG shifts to the red side of the spectrum according to the phase matching condition described in Equation 1.9.

6.2.4 Effect of RH on morphology of overlay

The presence of gelatine material in the overlay offers more interesting consequences of being subjected to moisture. Due to its elastic behaviour, swelling of the overlay takes place. These morphological changes induce tension in the LPG thus arousing effects due to both material as well as waveguide contributions [51]. This results in change of grating period as well as the differential effective index between core and cladding so much that these changes dominate the RI induced change in the LPG. Also, the swelling of the overlay reduces the interaction of the evanescent wave of LPG cladding modes with the surrounding medium.

Hence, taking consideration of all these effects, a net decrease in the resonant wavelength of the LPG is expected to occur with increasing levels of Relative humidity. A reverse trend is expected to be followed when RH levels fall down and tension of the grating is reduced.

6.2.5 Refractive index calibration of long period grating sensor

The effective indices of the cladding modes in an LPG are strong functions of the index of refraction (n_3) of the medium surrounding the cladding. Any change in this ambient index serves to modulate the effective index of the cladding modes ($n_{cl}^{(m)}$) with higher order modes undergoing larger variations [10]. Since the coupling wavelength to a particular cladding mode (resonant wavelength λ_{res}) is dependent on $n_{cl}^{(m)}$ through the phase matching condition, a change in n_3 will effectively vary the value of λ_{res}.

To gain information on the performance of LPG, it is exposed to standard RI liquids and its wavelength response is monitored on the OSA. The experimental set-up for calibrating the LPG against the standard RI solutions has been shown in Figure 3.7. In brief, the procedure includes launching of broadband light into the fiber core and receiving the transmission spectrum on the OSA. The portion of the fiber with grating inscribed in it is fixed at both ends. Micro-positioning stages with a glass slide attached on its surface are placed beneath the grating. The stages can be positioned in such a way that the LPG gets submerged with the RI liquid completely. The RI response is then monitored. Prior to the next RI liquid, the previous liquid is rinsed off the slide, the slide is cleaned and the LPG is washed thoroughly with isopropyl alcohol several times so that the LPG spectrum returns to its original position. Similar steps are followed for subsequent RI liquids. The standard RI liquids used for LPG calibration have the following RI values at 1550 nm: 1.4358, 1.4398, 1.4439, 1.4479, 1.4496, 1.5 and 1.5018. The LPG transmission spectra for all the above RI values were recorded.

6.2.6 Preparation of $CoCl_2$/Gelatine mixture

Chemicals i.e. cobalt (II) chloride and gelatine powder were procured from CDH chemicals. A number of samples with a concentration of 2% to 10% weight by volume were prepared in 40 ml de-ionized (DI) water. In all the samples, gelatine and $CoCl_2$ were added in the ratio of 2:1. Firstly, the measured volume of distilled water placed in an Ultrasonic water bath was allowed to attain a temperature of 65°C. The temperature was monitored by means of a thermocouple immersed in the water bath. The weighed quantity of gelatine using digital weighing balance was added to the hot water and after a gentle stir it the solution was subjected to ultrasonic mixing for about 20 minutes to facilitate homogeneous mixing of gelatine in water and avoiding the formation of crystals of gelatine that could turn into gel form when cooled. After a clear solution of gelatine in DI water was formed, measured amount of $CoCl_2$ powder was added to the same and allowed to

ultrasonicate for aduration of 10 minutes. The prepared solution was allowed to cool to room temperature before it could be used for coating on the fiber.

6.3 Characterization of $CoCl_2$/Gelatine coated LPG

From the batch of the prepared samples, the 6% by volume one was chosen to be coated on the fiber surface as it had the optimum viscosity and refractive index much lower than that of cladding. The fiber was coated with the material by dip coating technique using Apex dip coater as shown in Figure 5.5 in previous chapter. The coated fiber was dried at room temperature for about 12 hours and fragmented into small parts for FESEM and Near-Field Surface Optical Microscopy (NSOM) imaging. Topographic details about the overlay coating were obtained through FESEM measurements and knowledge about the thickness of the coating was gained through NSOM analysis. The vacuum level required for the samples in the specimen chamber of SEM was 1kV.

The LPG was coated with the $CoCl_2$/gelatine mixture by dip coating technique using Apex dip coater with special attachment for fiber. The parameters like dipping and lifting speed, deposition cycles, dry and wet time are optimized after performing number of trails. We optimized dipping speed 2 mm/min, lifting speed 2mm/min, wet time 0.5 min, dry time 0.5 min and number of cycles 2. Confirmatory information about the deposition of coatings was obtained by performing SEM analysis of the coated fiber samples. FE-SEM gave convincing proofs of deposition of overlay material on the LPG cladding surface. Figure 6.1 shows some FE-SEM micrographs where $CoCl_2$/gelatine coatings are evident.

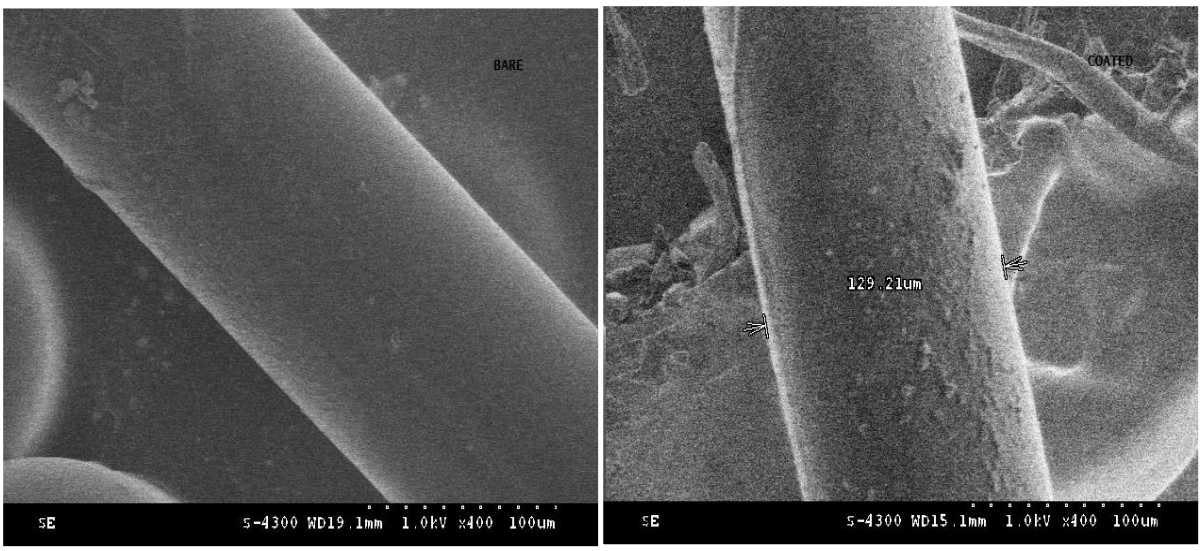

(a)

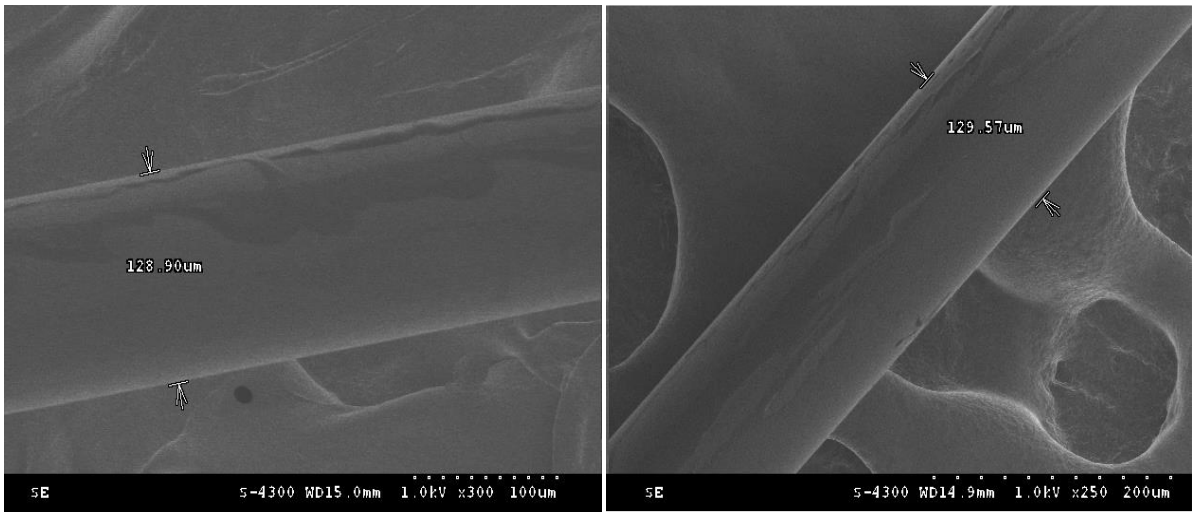

(b)

Figure 6.1 (a) & (b) FE-SEM micrographs showing bare (top-left) and coated LPGFs

FE-SEM images confirm the deposition of $CoCl_2$/gelatine coating. Modifications in the surface morphology of the fiber surface are observed on comparison with the image of bare fiber. The thickness of the coating was roughly estimated to lie between 1to 1.5 microns.

However, Near-Field Surface Optical Microscopy was performed to check the thickness of the overlay coating for the sake of exactness. The images obtained by NSOM, shown in Figure 6.2 reveal clear boundaries of the coated fiber. NSOM images reveal that coating thickness up to 1.5 micron level was achieved. It must be

stated here that several samples were prepared with differing dipping duration and drawing speed before such small coating thickness was obtained. Further experiments for relative humidity testing were conducted on 1.5 micron $CoCl_2$/gelatine coated LPG.

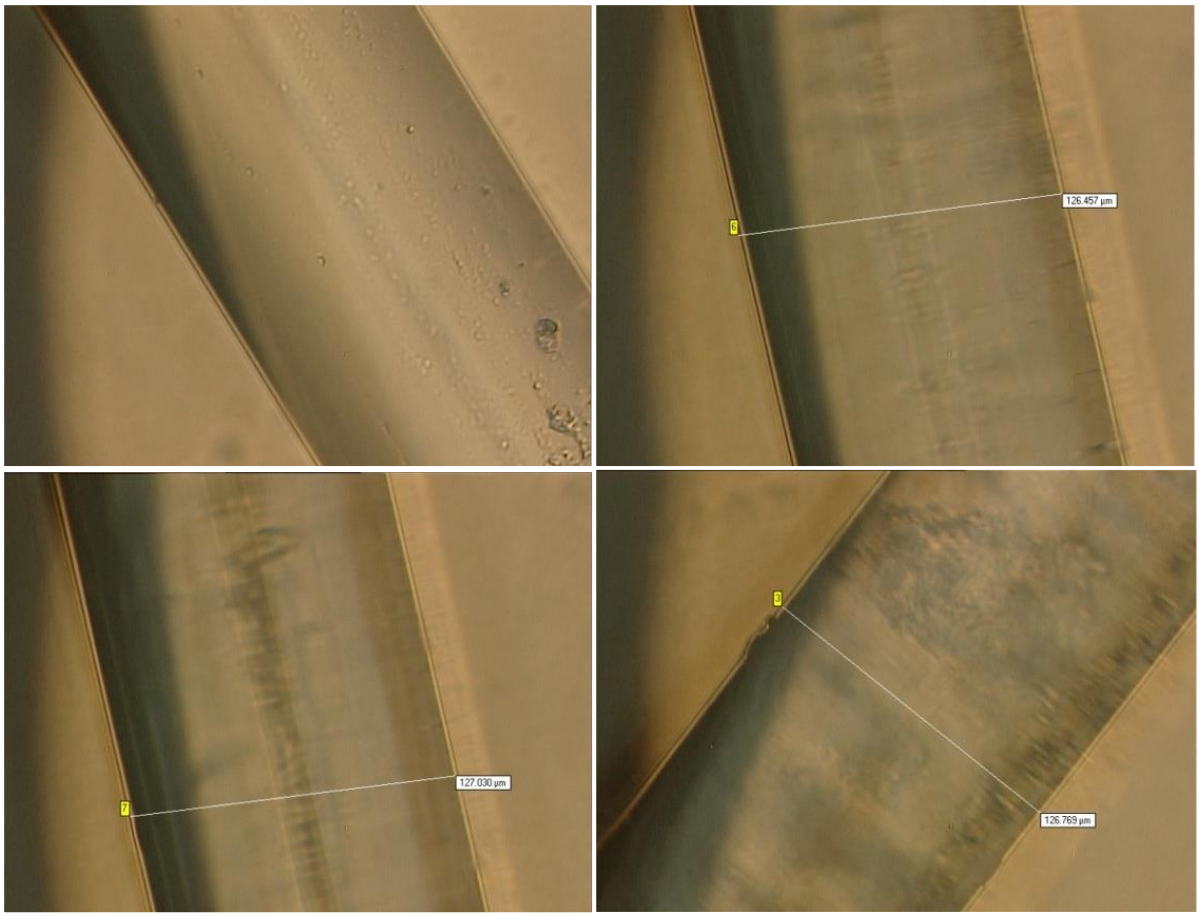

Figure 6.2 Characterization of coating thickness by NSOM imaging

6.3.1 Humidity measurementtest on $Cocl_2$/Gelatine coated LPG

The $CoCl_2$/gelatine coated LPG of 525 µm grating period was arranged by means of fixtures in a humidity control chamber supplied by NSW. One end of the fiber was spliced with the YOKOGAWA AQ4305 White Light Source and the other end was spliced to YOKOGAWA AQ6319 Optical Spectrum Analyzer. The humidity chamber had digital humidity level controller that varied humidity according to tables of wet and dry bulb thermometer reading as shown in Figure 6.3.

Figure 6.3 The humidity control chamber

A Broadband light from 1450 nm to 1650 nm was launched into LPG and the relative humidity level was varied from the ambient level to 90% RH in steps of five. The relative humidity levels were compared with an analog hygrometer and the % error was calculated. The corresponding transmission spectra of LPG for each of these RH levels were recorded in the OSA. All the measurements were performed at 33°C with an accuracy of ±1°C. A schematic of such an arrangement is shown in Figure 6.4.

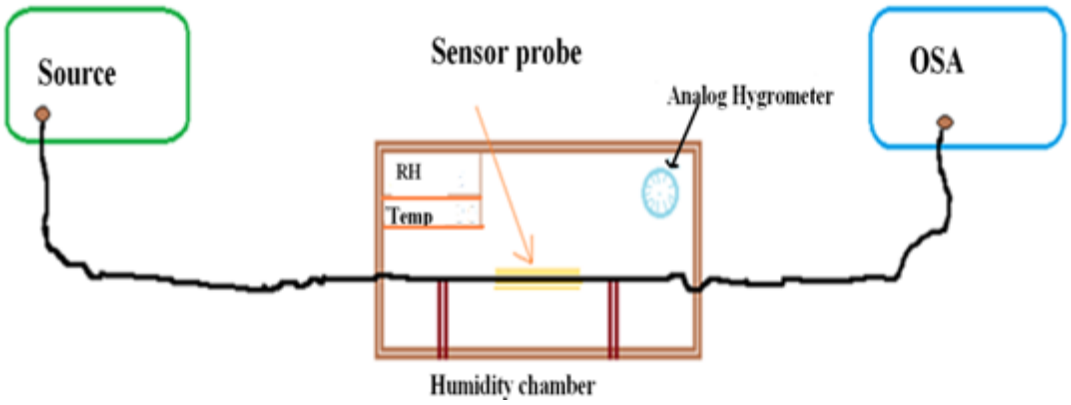

Figure 6.4 Schematic of relative humidity measurement set-up

After the highest RH level was reached, the reverse process was carried out. LPG transmission response for decreasing values of RH levels was obtained to get information about the hysteresis loss of the sensor. The entire process was repeated with another LPG having 575 μm grating period to evaluate the effect of grating period on the response of LPG based humidity sensor. All parameters were same as in the previous experiment except that the former LPG was replaced with a new one.

6.4 Humidity Response

All experiments as described in the previous session were performed with the stated parameters chronologically. The outcomes of every stage were carefully recorded for further analysis and reference. Following sections are the comprehensive notes of the results obtained and the inferences that derive from them. It may be stated here that these deductions are not mere speculations but supported by theoretical proofs.

Long Period Fiber Gratings of periodicities 525 and 575 μm were fabricated by point by point method described in Chapter 4 using grating writing station in step mode. The resonant wavelengths of the two LPGs were 1540.8 nm for 525 μm pitch and 1588.6 nm for 575 μm pitch. The LPG with period 525 μm is denoted as LPG_1 and grating with period 575μm as LPG_2. The transmission responses of both the fabricated LPGs are shown in Figure 6.5 (a) and (b).

LPG dip depends upon grating length in other words length of interaction, because the two LPGs used in the experiment are of different lengths, therefore dip comes out to be different. The LPG with dip 3db relative refractive index difference is less and for 5 dB dip the same is more. It also depends upon the term coupling coefficient. Moreover the period of both the gratings is also different.

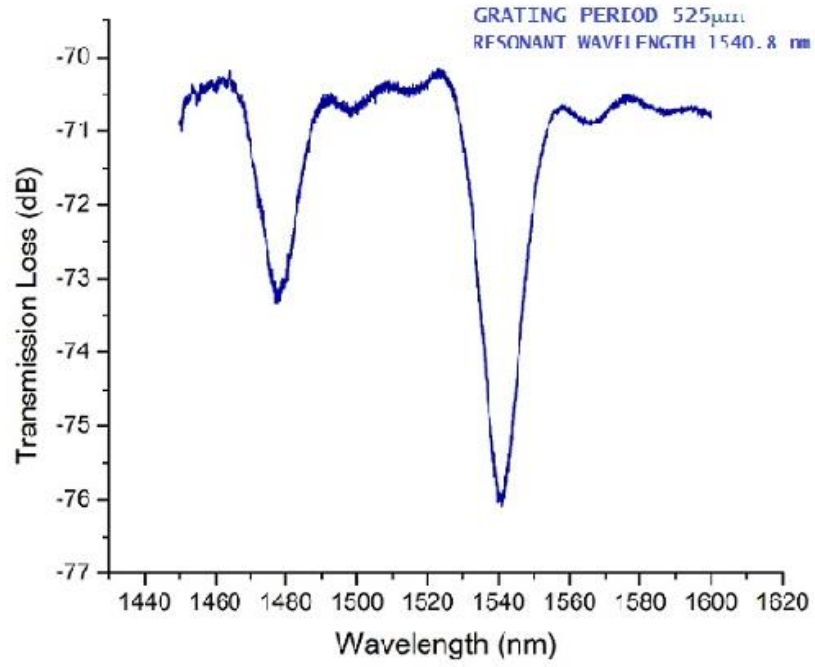

(a)

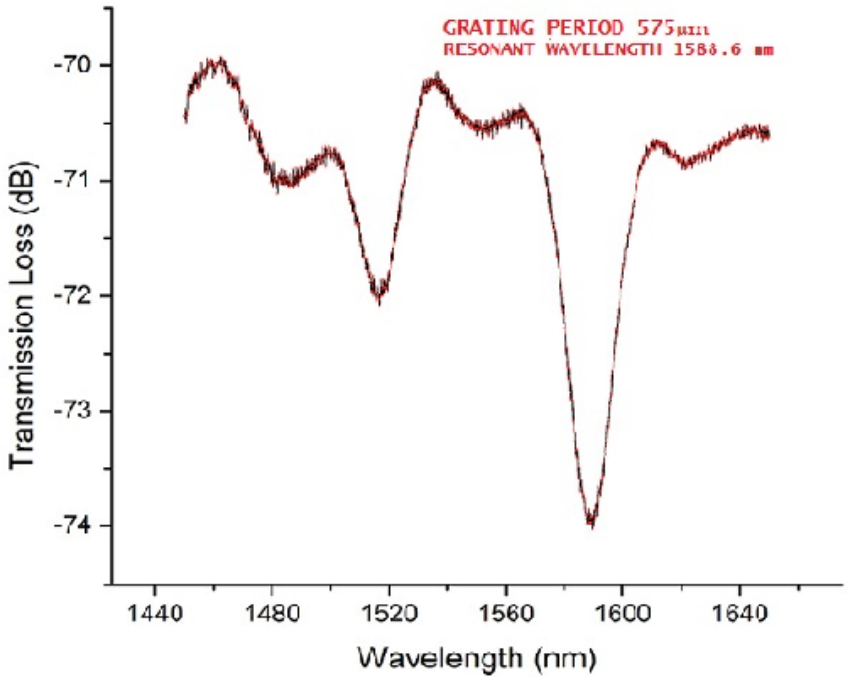

(b)

Figure 6.5 (a) & (b) Transmission spectra of the two fabricated LPGs

It can be observed from the transmission spectra of both the gratings that more light is coupled to the cladding modes in the grating with a shorter period. Thus, one can witness more dip in the loss bands in case of 525 μm LPG.

6.4.1 RI calibration of LPGs

For calibration of LPGs against RI of surrounding medium, both the gratings were subjected to standard RI solutions ranging from 1.4358 to 1.5018. Figure 6.6 is a plot of resonant wavelength response of both the LPGs.

From the pattern of both the curves it can be easily stated that for RI values less than the cladding mode i.e. 1.455 for LPG_1 and 1.445 for LPG_2, a blue shift is observed for increasing ambient RI till the ambient index value matches with that of the cladding. Beyond that red shift occurs. These curves form the basis for behavior prediction of LPGs when coated with an overlay material.

The sensitivity of LPG towards external refractive index change can be significantly enhanced if they are designed to operate near Turnaround point (TAP). This added functionality is due to resonant coupling of higher order cladding modes and significant change in the slope of phase matching curve at TAP. However, the inscription of TAP LPGs necessarily requires short grating periods (less than 250 μm) with precision better than 0.5 μm. Here the fabricated LPGs have grating period towards higher values i.e more than 500 μm. The TAP in our experiment comes out to be around1.454, where maximum wavelength shift is recorded. One can also write near TAP gratings which require the exact control of grating period (better than 1 μm) while the period is relatively low (< 250μm). Order of the cladding modes and reaches its maximum close to the so-called turning points. In these regions the slope of the phase matching curves changes from positive to negative and beyond this turning point, and for each grating period, there are two resonance wavelengths for each cladding mode. The sensitivity increases as the refractive index of the surrounding approaches that of the cladding. In this case the evanescent field

extends further into the surrounding medium leading to a higher interaction. However, when the surrounding refractive index equals that of the cladding (it becomes an infinite medium), the resonances disappear. For refractive indices above that of the In this case, the modes are guided by Fresnel reflection and not by total internal reflection and loose part of the energy at each reflection at the interface being called lossy modes. As the refractive index increases the modes become more confined and the dips more pronounced. However, the resonance wavelengths are insensitive to changes in the surrounding refractive index because the phase of the partially reflected field at the surrounding-cladding interface does not change with the external index. In general, grating periods shorter than 200 μm are required in order to have access to this sensitive region (around the turning points),

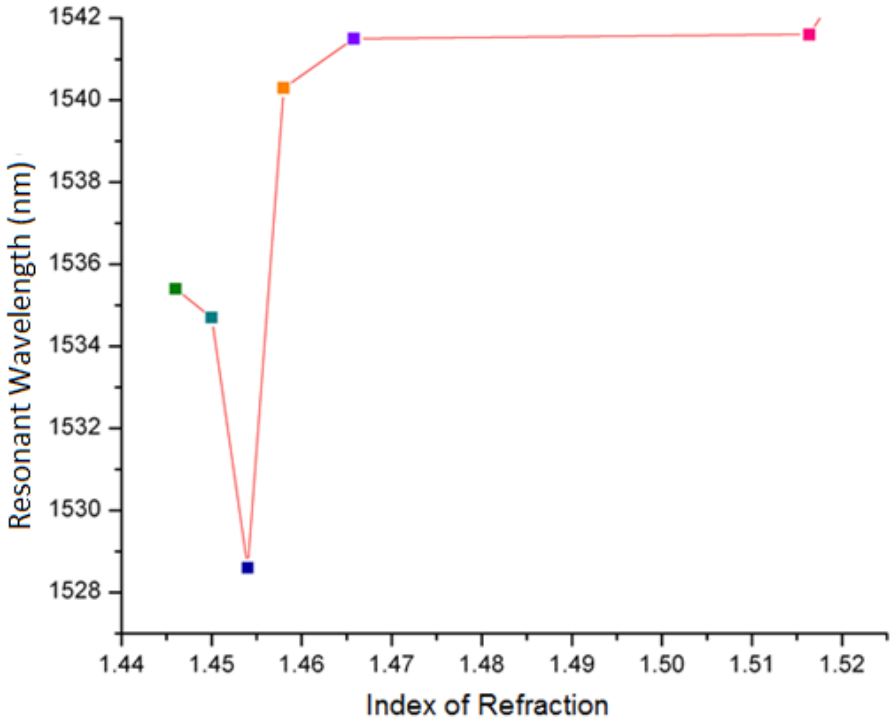

(a)

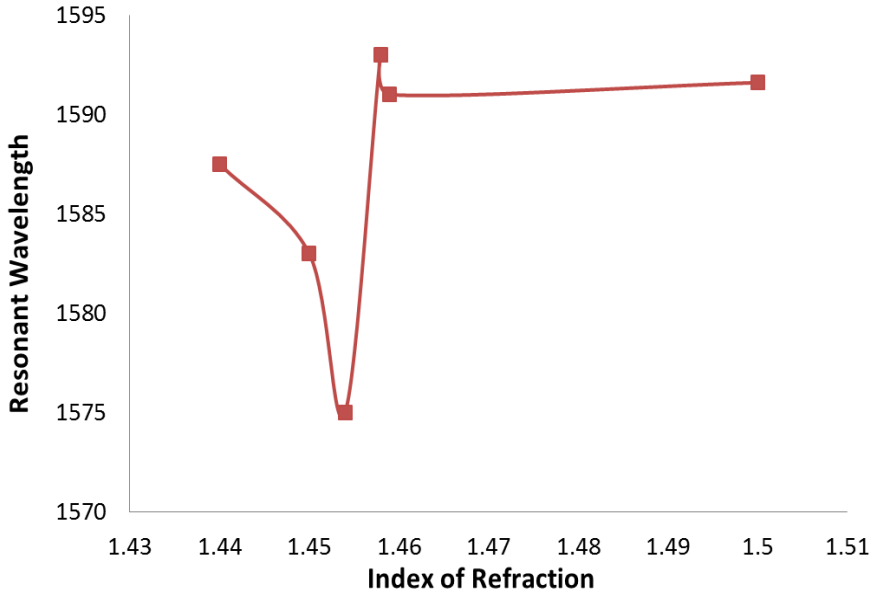

(b)

Figure 6.6 (a) and (b) RI calibration curves for both the LPG_1 (525 μm) and LPG_2 (575 μm) respectively

6.4.2 Characterization of $Cocl_2$/Gelatine mixture

Many samples of $CoCl_2$/gelatine mixture of varying concentrations by % volume were prepared keeping gelatine:$CoCl_2$ in the ratio of 2:1 as described in the Table 6.1. The samples were tested for viscosity since viscosity plays a major role in the thin film formation process. Ostwald viscometer was used to determine the viscosity of the samples. The densities of the prepared samples were determined using specific gravity bottle by following the method discussed in literature. Other mechanical properties like viscosity of the prepared samples were also studied using Ostwald viscometer in order to determine the relation between viscosity and concentration. Ostwald viscometer consists of a U-shaped glass tube held vertically in a controlled temperature bath [236]. In one arm of the U is a vertical section of a narrow capillary. Above this is a bulb, and another one is present lower down on the other arm. Two marks (one above and one below the upper bulb) indicate a known volume. The fluid was sucked up to the upper mark of the bulb and allowed to pass through the capillary. The time taken by the fluid to cross the lower mark was recorded and the

viscosity of the samples was determined relative to that of water at 40°C using Equation 6.4 [237] :

$$\eta = \frac{\pi r^4 pt}{8Vl} \tag{6.4}$$

Here, p is the hydrostatic pressure on the liquid (proportional to the density ϱ), t is the time of flow in seconds, r is the radius of the tube, l is the length of the capillary in cm, and V is the volume of the liquid in cm^3.By recording the time taken by the samples to cross the two marks on the upper bulb of viscometer and density, viscosity was calculated as stated earlier.

All the solutions were prepared in 40 mL DI water. It can be clearly seen from table 6.3 that as the solutions become more concentrated, the time elapsed to cross the lower mark on the bulb increases and so does the viscosity.

Table 6.1 Estimation of Viscosity of Samples

Sample	**Concentration % by vol.**	**Density kg/m³**	**Time Taken sec**	**Viscosity mPa.s**
A	2	1015.94	60.84	0.9387
B	4	1034.89	94.2	1.478
C	6	1069.4	151.7	2.538
D	8	1095.22	228.7	3.9187
E	10	1155.42	271.72	4.752

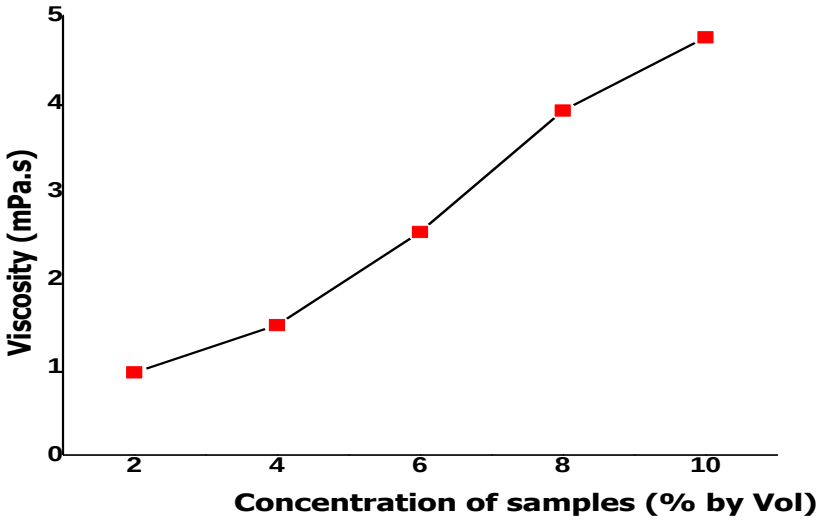

Figure 6.7 Viscosity profile of the $CoCl_2$/gelatine mixture

All the experiments for measurement of viscosity were held at 40°C. Figure 6.7 shows that the viscosity of $CoCl_2$/gelatine mixture follows an almost linear relationship with concentration. Hence, it may be classified under the category of Newtonian fluids.

For further characterization and coating the LPGs with $CoCl_2$/gelatine mixture, Sample "C" was used as it offered optimum working conditions for experimentation. The refractive index of the above sample which had to be deposited as an overlay material on LPG was calculated both theoretically and experimentally. Putting the values for RI of gelatine and $CoCl_2$ as 1.54 and 1.336 respectively in Equation 6.3, the RI of the mixture was found to be 1.3418. The same sample was tested for RI in RFM990-AUS32 Refractometer which read the value for RI as 1.34146. Both the results were in good agreement with each other.

Thus case presented here of "low RI" coating over LPG cladding because the RI of the cladding modes for both the LPGs did not exceed 1.455. From the calibration data of LPG, it is expected that as water is absorbed by the coating, a blue shift will occur.

6.4.3 Relative humiditymeasurement by $CoCl_2$/Gelatine coated LPG

The $CoCl_2$/gelatine coated LPG_1 (525 μm) was spliced to the White Light Source at one end and Optical Spectrum Analyzer at the other. The LPG part of the arrangement was fixed at both ends to micropositioners to avoid any bending loss. Patch cords from ends were brought outside through outlets provided in the humidity control chamber. The %RH was set at ambient value i.e. 35% and the temperature at 30^0C. The humidity could be varied with 1% RH resolution and temperature with 0.1^0C resolution in the humidity control chamber. WLS supplied broadband light in the C-band region i.e. from 1520 to 1650 nm. OSA used for the experiment exhibited a resolution of 0.1 nm.

So, the output response of the LPG for the ambient RH level was first checked on the OSA. Likewise, the response was noted for every 5% rise in RH level. After the maximum %RH value was attained, another set of output was obtained by decreasing the %RH values from the maximum to the ambient. In this way, the humidity response of the coated LPG along with its hysteresis loss was obtained. The resonant wavelengths for increasing and decreasing values of %RH are listed in Table 6.2

Table 6.2 LPG_1 Wavelength response for increasing and decreasing values of RH

Relative Humidity (%)	Wavelength (increasing) (nm)	Wavelength (decreasing) (nm)
35	1543.7	1543.6
40	1543.7	1543.3
45	1542.8	1542.4
50	1542	1541.8
55	1539.7	1539.4
60	1538.2	1538.3
65	1537.2	1537.3

70	1537	1537
75	1536.9	1536.7
80	1536	1536.3
85	1535.5	1535.8

By having a look at Table 6.2 , one can easily observe that the humidity response of LPG_1 upto 50% RH level is feeble, beyond which a considerable shift in resonant wavelength is seen. It can be inferred that the overlay material does not behave actively at low RH values; therefore no major changes occur in the overlay structure and RI. As observed by Russell and Fletcher [40], there is little or no water absorbed by $CoCl_2$/gelatine material when the relative humidity is less than 57.6%, hence the sensor shows negligible response in terms of shift in resonant wavelength.

$CoCl_2$/gelatine coated LPG based humidity sensor shows a negative shift in resonant wavelength as the humidity level is raised i.e. the wavelength shift towards the left side of the base value of the resonant wavelength. This decrease in resonant wavelength toward the negative direction is termed as "blue shift". The phenomenon is clearly evident in Figure 6.8.

It has been theoretically and experimentally demonstrated that [238] a blue shift in the resonant wavelength of the LPG takes place when it is coated with a low RI overlay than that of cladding. The RI of the overlay in our case is measured to be 1.34146 which is less than the cladding mode RI of LPG (which is 1.445 for LPG_1). As the RH level increases, the overlay material being hygroscopic in nature, absorbs more water molecules, become less dense and hence exhibit even lower RI. But in addition to this factor, there is another contributing element that adds to the observed red shift.

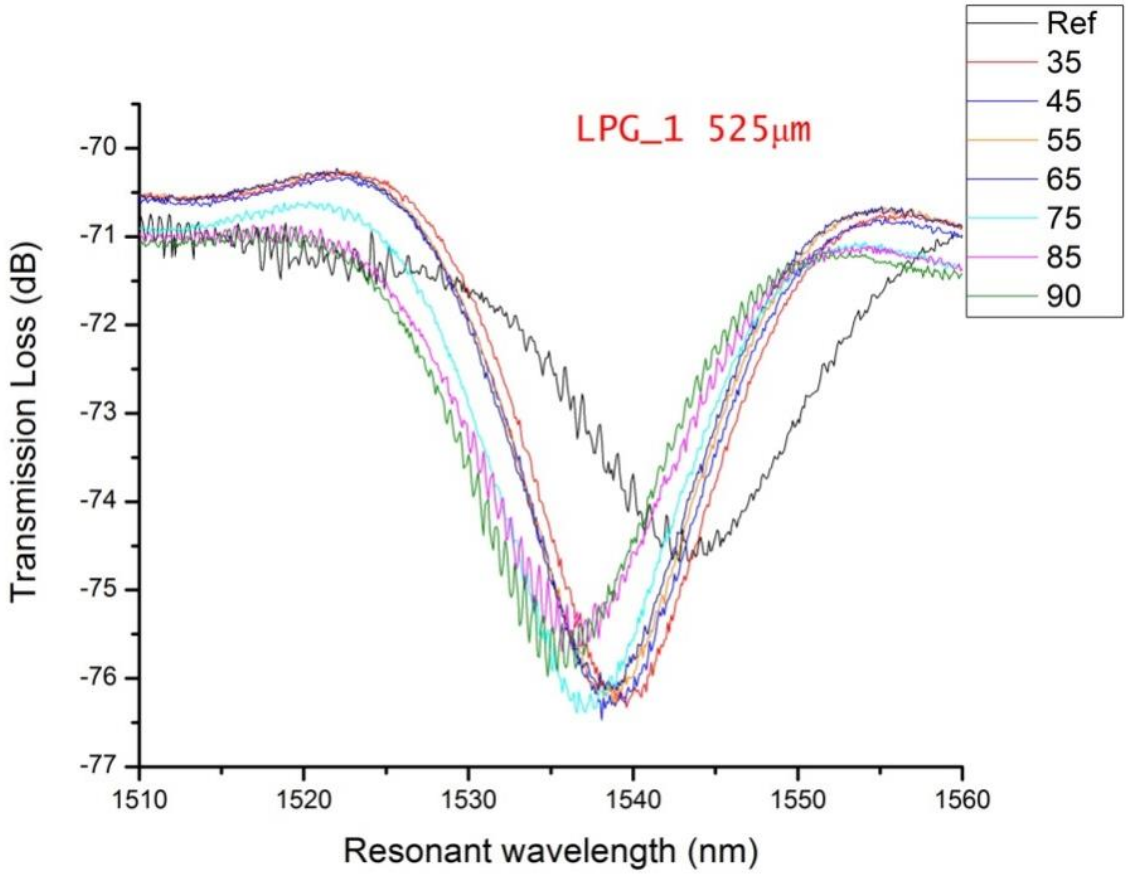

Figure 6.8 Plot of LPG_1 when subjected to 35% to 90% RH depicting blue shift

The presence of gelatine plays a major role in blue shift. As RH values increase, swelling of the gelatine material occurs which bring about morphological changes in the grating structure. This induces tension on the LPG, reducing the grating period and effecting the coupling strength. Hence the resonant wavelength further experiences a shift in the negative direction. In effect, both reduction in RI and swelling of the overlay coating are responsible for the observed blue shift in the transmission of LPG when it is subjected to rising levels of RH. A reverse phenomenon is seen during the downward shift of RH level. The open and fluctuating structure of gelatine matrix enables the coating to lose the adsorbed water molecules gradually. The LPG-based sensor shows slight changes in output when subjected to reverse cycle of RH. This can be attributed to the hysteresis loss of the sensor. Similar experiments were conducted with LPG_2 (575 μm) to confirm the pattern of wavelength shift and study the effect of grating period on the sensitivity

of the sensor. Table 6.3 shows the humidity response of the LPG_2 with overlay coating, both in the upward and downward directions.

Table 6.3 Wavelength response for increasing and decreasing values of RH

Relative Humidity (%)	Wavelength (increasing) (nm)	Wavelength (decreasing) (nm)
50	1588	1588.8
55	1587.2	1588.1
60	1587	1587.6
65	1587	1587.1
70	1586.2	1586.4
75	1585.7	1585.6
80	1585.1	1585.2
85	1584.7	1584.1

6.5 Sensor Performance

Experimental demonstration has given enough evidence on the performance of coated LPG based humidity sensor. Every sensor is characterized by its sensitivity, accuracy, repeatability, hysteresis and stability. In Figure 6.9 are shown the plots of differential wavelength shift versus RH level for LPG_1 and LPG_2 respectively. Both the curves are fitted with their best fit line through the least squares fit method.Interesting results were obtained during sensitivity analysis of both the LPGs. While the LPG_1 showed a sensitivity of 0.18 nm/%RH with an error of ±1.45%, LPG_2 gave a sensitivity of 0.09 nm/%RH along with an error of just ±0.54%. The error is the percentage error that is calculated by using the statistical features of software OriginPro 7.5.The error bars are the deviation of obtained experimental reading from the linear fit values. In Figure 6.9 (a) & (b) at humidity value 70%RH no error bar is present as the experimental value is same as expected from the linear

fit. The above discussion presents a clear case of trade-off between sensitivity and accuracy. Also, it can be interpreted that LPGs with a lower grating period have better dynamic response as compared with higher ones. It even turned out that the hysteresis response of LPG_1 was better than the other one.

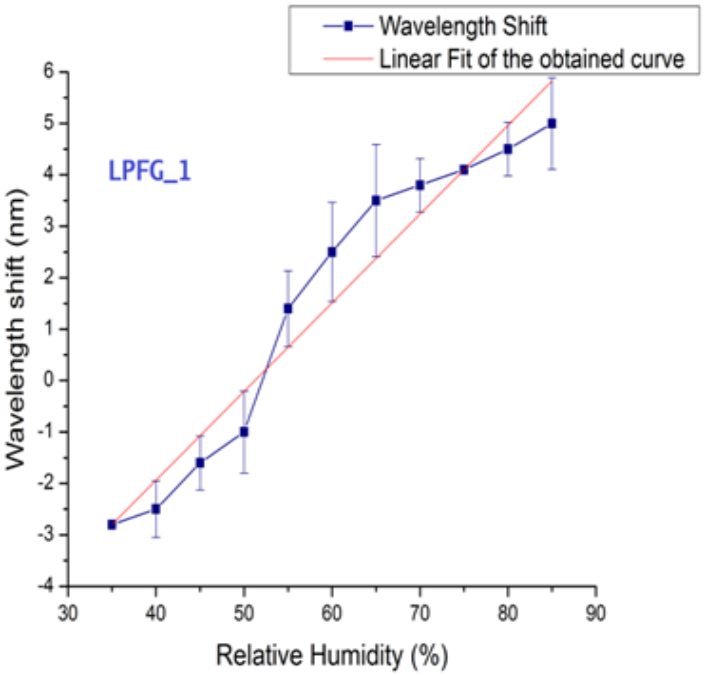

(a)

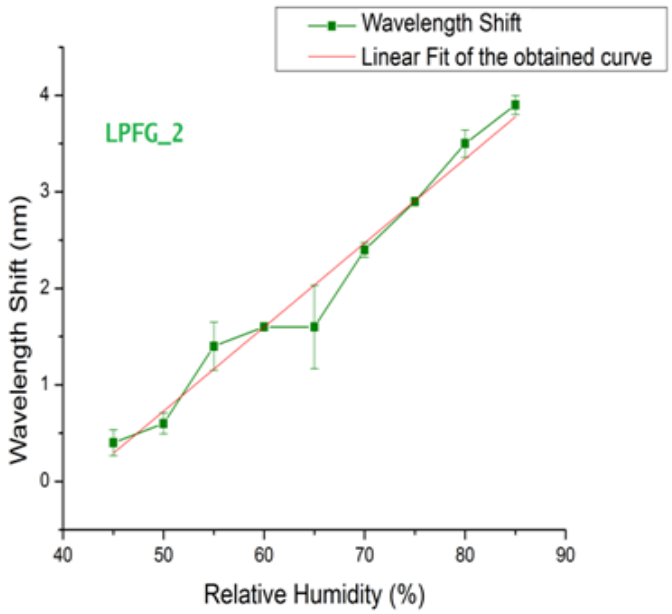

(b)

Figure 6.9 (a) & (b) Actual and linear fits of humidity response of both the LPGs

The hysteresis loss of the LPG_1 based sensor was evaluated by comparing the values of the increasing cycle of RH with the corresponding values of the decreasing cycle. Figure 6.10 shows the hysteresis curve of LPG_1.

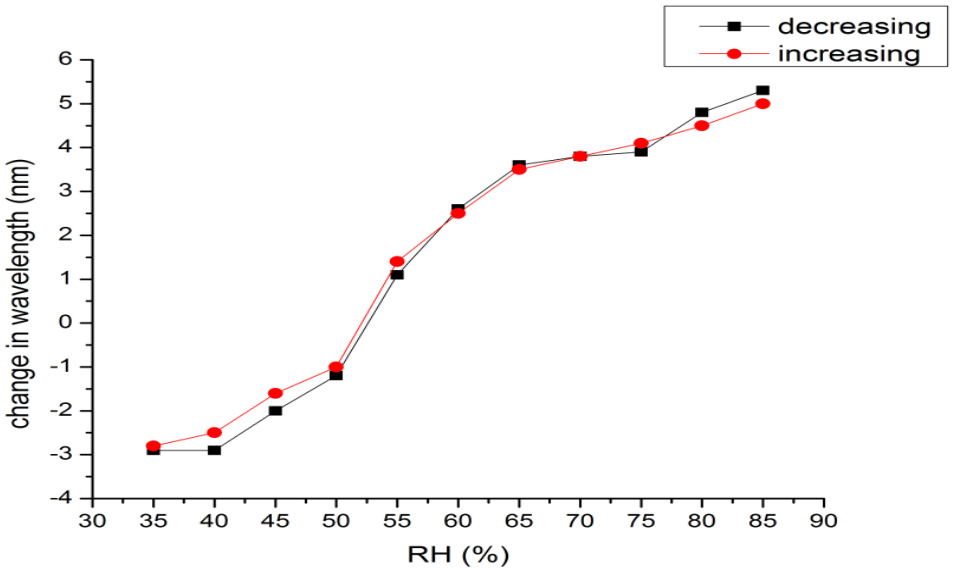

Figure 6.10 Hysteresis response of LPG_1

The sensor hysteresis loss was calculated to be ±0.18%. This value can be obtained by measuring the slope of the graph shown in Figure 6.10. The accuracy is determined by calculating coefficient of regression from linear fit of the same graph. If we see the variation pattern, from 35 to 50% RH little water is taken by the coating beyond 50% RH there is considerable shift in the resonant wavelength .The Figure 6.10 shows a decrease in resonant wavelength as RH level is increased from 35% to 90%. This "blue shift" is explained as follows.The overlay material being hygroscopic in nature absorbs more water molecules as RH levels are increased thereby resulting in decrease of the coating RI. The sensitivity of LPG sensor to external index of refraction is governed by [114]:

$$\frac{d\lambda_{res}}{dn_{sur}} = \lambda_{res}.\gamma.\Gamma_{sur} \qquad (6.5)$$

where γ is the waveguide dispersion and Γ_{sur} is the surrounding RI dependency of the waveguide dispersion. The value of γ for cladding modes m<8 remains positive [94]. This condition was satisfied for our fabricated LPG which was calculated by

OptiGrating 4.2.2 software. The value of Γ_{sur} in Equation 6.5 always remains negative for $n_{sur}<n_{cl}$ [8]. This is true in our case as the RI of the overlay solution was found to be 1.34146 using refractometry and it keeps on decreasing as RH levels increase further. This confirms the obtained blue shift. The nature of graph reported by [137] highlighted that there was little or no water taken up from 30-50% RH, while about 6 mol of water is taken up beyond 50% RH by same combination. The nonlinearly mentioned in Figure 6.10, is primarily due to light source fluctuations and over a large humidity change this can be avoided. Dual source techniques can be used to overcome this non linearity.

Sensitivity will increase with decrease in period as reported by Tan et al. We have also verified the fact in this work by using LPGs of two different periods 525μm and 575μm. Experimental results show that LPGs having lower period have high sensitivity for RI. The reason for such a trend is that each of the cladding modes of LPG can be characterized by rays whose angle with the fiber normal decreases with increase in cladding mode number (*m*). For the same index of refraction of external medium, lower order cladding modes save well confined modal power. Thus, they have less interaction with the external medium. As the order of the cladding mode increases, a larger portion of the modal field interacts with the external medium. This leads to the LPG spectrum being more sensitive to change in index of refraction of the external medium. Our LPF fabrication system allowed writing LPGs with a minimum period of 500 μm. Hence experiments have been performed on 525μm and 575μm period gratings.

For stability check both the LPGs were kept in the humidity control chamber one at a time at 70% RH level for 300 minutes and the transmission spectrum of LPG was monitored after every 10 minutes. The response of the sensor subject to the same humidity level for an elongated duration is shown in Figure 6.11.

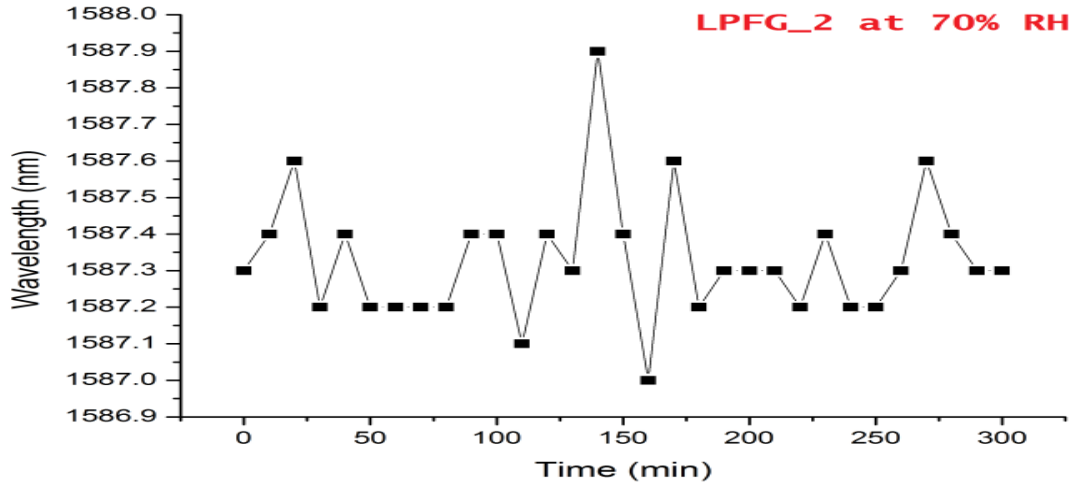

Figure 6.11 Plot depicting wavelength response of LPG_2 at 70% RH for a duration of 300 minutes

It follows from the above experiment that the stability error of the sensor is about 0.056%. The stability error is calculated by linear fit of graph between wavelength shift and time. The other method used, is the ratio of the difference between maximum and minimum obtained values divided by original value. Thus the designed sensor shows appreciable stability.

6.6 Humidity Sensing using Gelatin & Cobalt Chloride Coating on ITO coated LPG

Humidity sensor using gelatin & cobalt chloride on ITO coated LPG was also proposed and demonstrated. LPG firstly coated with ITO, then with a combination of gelatin-cobalt chloride. This sensor expands range up to 95% RH with better stability. LPG is fabricated with a resonant wavelength of 1602.5 nm and period of 720 μm over a 2.0 cm length of boron co-doped single mode photosensitive fiber by the point-by-point writing method using an excimer KrF UV laser having a pulse repetition rate of 200 Hz, pulse duration of ~ 15 ns and peak pulse energy of ~ 3 mJ.

To develop metal oxide coating a combination of Indium chloride ($InCl_3$) and tin chloride ($SnCl_2.2H_2O$) in the ratio 1:0.2 was prepared in 25 ml of ethanol in ultrasonic cleaner and applied on LPG surface. The solution was stirred for five hours

continuously at room temperature. 0.01% by volume of surfactant Tween 80 was added to the prepared solution. The hygroscopic layer was prepared with a combination of gelatin-$CoCl_2$ solution in the ratio of 2:1. Dip coating method was adapted to form both of the overlays on LPG. The later solution was prepared using 1.5 gm powdered gelatin dissolved in 40 ml DI (de-ionized) water and heated up to 60℃ for 10 minutes in ultrasonic cleaner and mixed with 0.75 gm of cobalt chloride. An optimized, reproducible and reliable approach to the coating process was generated with a number of trial experiments to allow a smooth and thin coating on the LPG. The FESEM graph is shown in Figure 6.12. As described in the previous session similarly the LPG RH sensor was placed in the humidity chamber, and the fiber is held straight by use of two fiber holding stage to eliminate bend losses to the LPG. The humidity was varied from 40% to 95% in the chamber to test the performance of the proposed LPG humidity sensor. The chamber temperature was maintained at 25 °C throughout the experiments. The chamber's temperature accuracy and humidity resolution was $\pm 1^0$C and 1% RH respectively. A commercial hygrometer was placed inside the chamber for comparison, and to enhance the accuracy in the measurements.

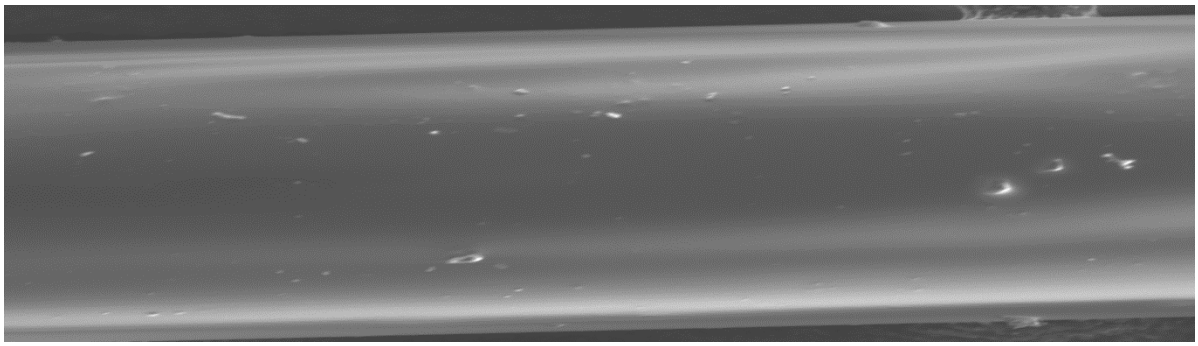

Figure 6.12 SEM graph of ITO & gelatin -$CoCl_2$ coated LPG

The humidity response of the sensor for both increasing and decreasing values of RH is shown in the Figure 6.13.

Similarly Stability test was also carried out with sensor kept in the humidity control chamber at 65% RH level for 300 minutes and monitoring its transmission spectrum after every 10 minutes as shown in Figure 6.14.

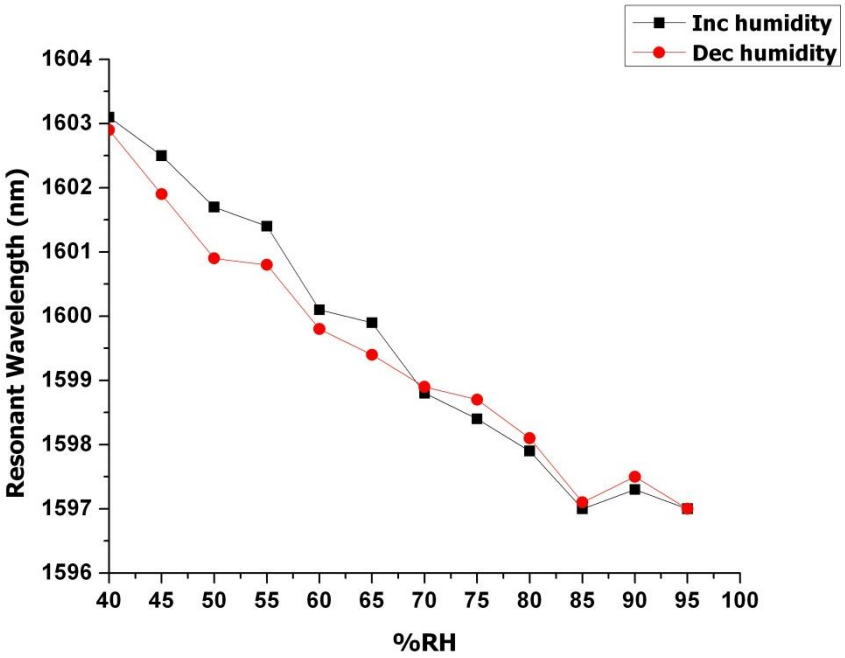

Figure 6.13 Sensor response exposed to 40% to 95%RH (For both increasing and decreasing values of RH)

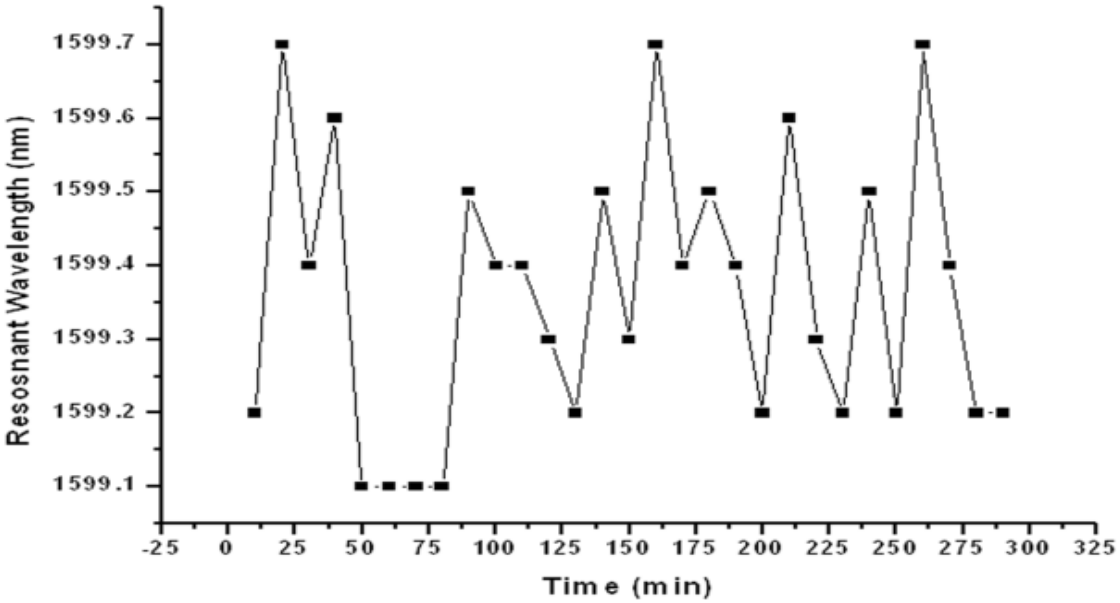

Figure 6.14 Plot depicting wavelength response of LPG at 65% RH for duration of 300 minutes

The stability error of the sensor found to be 0.031%. Thus the designed sensor showed appreciable stability. The designed sensor shows a sensitivity of 0.12

nm/%RH with an accuracy of 98.45%, thermal sensitivity 0.34 nm/ºC and hysteresis loss of ±0.12%.

6.7 Summary

It may thus be summarized that long period grating is not just a highly sensitive refractometer but by applying a hygroscopic coating it can be used to determine the RH level of the ambient medium. The presented data supports the promising performance of LPGs as humidity sensors on a commercial platform. Along with the inherent advantages of optical fibers, LPGs can offer the flexibility of distributed sensing system. The LPG coated with mixture demonstrated a sensitivity response of 0.18 nm/ %RH with an error of ±1.45%. The design offers minimal hysteresis loss of ±0.18% and a stability error of 0.056% and repeatability of 99.7%. In addition to this, the effect of grating period on the performance of sensor has also been studied. It is seen that LPGs with a lower grating period have higher sensitivity of RH level changes. The ITO and $CoCl_2$/gelatine coated LPG as humidity sensor is demonstrated. The sensor can be used to measure the RH variation efficiently in the range of 40% to 95% RH with sensitivity of 0.12 nm/%RH, accuracy of 98.45%, stability error 0.031%, hysteresis error of ±0.12% RH and repeatability of 98.7%.

CHAPTER 7. INVESTIGATIVE STUDY OF FIBER BRAGG GRATING IN MULTI MODE FIBER

7.1 Introduction

In its simplest form, a fiber Bragg grating consists of a periodic modulation of the index of refraction in the core of an optical fiber. The basic structure of FBG is shown in Figure 7.1. These kind of uniform fiber gratings, where the phase fronts are perpendicular to the fiber longitudinal axis and the grating planes are of a constant period, are regarded as the elementary building blocks for most Bragg grating structures. Light guided along the core of an optical fiber will be scattered by each grating plane. If the Bragg condition is not satisfied which is given by Equation 7.1, the reflected light from each of the subsequent planes becomes progressively out of phase and will ultimately cancel out [239]. Where the Bragg condition is fulfilled, the involvement of reflected light from each grating plane adds constructively in the backward direction to form a back-reflected peak with a center wavelength defined by the grating parameters.

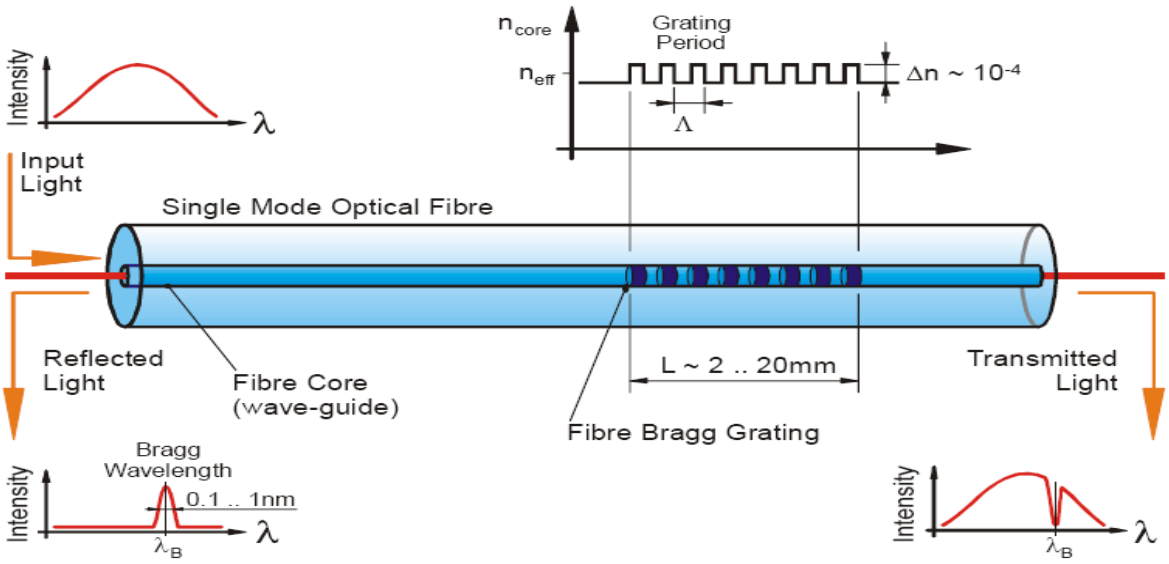

Figure 7.1 Structure of fiber Bragg grating [240]

The simplified first-order Bragg condition is given by:

$$\lambda_B = 2n_{eff}\,\Lambda \tag{7.1}$$

where the Bragg grating wavelength, λ_B is the free-space center wavelength of the input light that will be back reflected from the Bragg grating, n_{eff} is the effective refractive index of the fiber core at the free-space-center wavelength and Λ is the grating period.

7.2 Uniform Bragg Grating Reflectivity

Consider a uniform Bragg grating formed within the core of an optical fiber with an average refractive index n_0. The index of refractive profile can be expressed as [239] :

$$n(x) = n_0 + \Delta n \cos\left(\frac{2\pi x}{\Lambda}\right) \tag{7.2}$$

where Δn is the amplitude of the induced refractive-index perturbation typically10^{-5} to 10^{-2} and x is the distance along the fiber longitudinal axis. Using the coupled-mode theory analytical description of the reflection properties of Bragg gratings may be obtained. The reflectivity of a grating with constant modulation amplitude and period is given by the following expression [1]:

$$R = \frac{k^2 sinh^2(sl)}{\Gamma^2 sinh^2(sl) + s^2 cosh^2(sl)} \tag{7.3}$$

where *R(l ,λ)* is the reflectivity, which is a function of the grating length *l*, and wavelength λ. *k* is the coupling coefficient, Γ is the detuning wave vector, k= $\frac{2\pi n_0}{\lambda}$ is the propagation constant as described in Chapter 2.

7.2.1 Coupling coefficient for contra directional coupling

As described in Chapter 3, for contra directional coupling between two LP_{01} modes propagating in opposite directions, φ_1=φ_2 and coupling coefficient becomes [73]:

$$k = \frac{\omega\varepsilon 0}{8} \iint \Delta n^2(x,y)|\varphi|^2 \tag{7.4}$$

If we use the Gaussian approximation for φ, then

$$\varphi = \frac{2}{\omega_0}\sqrt{\frac{\omega\mu_0}{\pi\beta}}e^{-r^2/\omega_0^2} \tag{7.5}$$

where the multiplying constant will satisfy equation (7.4)

For Fiber Bragg Grating, we may assume that the periodic refractive index perturbation is uniform inside the core and zero outside, that is:

$$\Delta n^2(x,y) = \Delta n^2; x^2{+}y^2 < a^2$$

$$= 0; \qquad otherwise \tag{7.6}$$

And equation (7.4) becomes

$$k = \frac{\omega\varepsilon_0}{8}\Delta n^2 \frac{4}{\omega_0}\frac{\omega\mu_0}{\pi\beta}\int_0^a rdr\int_0^{2\pi} d\emptyset e^{-2r^2/w_0^2} = \frac{k_0\Delta n^2}{4n_{eff}}\left(1 - e^{-2a^2/w_0^2}\right)$$

If we write $\Delta n^2 \cong 2n\Delta n$and assume n$\cong n_{eff}$, we obtain

$$k = \frac{\pi\Delta n}{\lambda_0}\left(1 - e^{-2a^2/w_0^2}\right) \tag{7.7}$$

One can, in general, evaluate Equation (7.4) for any given perturbation $\Delta n^2(x,y)$ and modal field profiles $\varphi_1(x,y)$and$\varphi_2(x,y)$.

For the sinusoidal variation of index, perturbation along the fiber axis is given by:

$$k = \frac{\pi\Delta nI}{\lambda} \tag{7.8}$$

where *I* is given by $\left(1 - e^{-2a^2/w_0^2}\right)$ under the Gaussian approximation and *is*called as integral overlap. For sinusoidal variation it is given by:

$$I = 1 - \frac{1}{V^2} \tag{7.9}$$

a function of the fiber parameter V that represents the fraction of the integrated fundamental-mode intensity contained in the core. At the Bragg grating center wavelength, there is no wave-vector detuning and becomes ($\delta = 0$) zero, therefore, the expression for the reflectivity becomes [77, 103]

$$R(l,\lambda) = tanh^2(kl) \tag{7.10}$$

The reflectivity increases as the induced index of refraction change increases. Similarly, as the length of the grating increases so does the resultant reflectivity. A calculated reflection spectrum as a function of the wavelength detuning is shown in

Figure 7.2. The side lobes of the resonance are due to multiple reflections to and from opposite ends of the grating regionand due to the non-uniform laser intensity profile. The spectrum of experimentally fabricated FBG is shown in Figure 7.3. Simulation of reflected spectrum has shown good agreement with the observed spectrum.

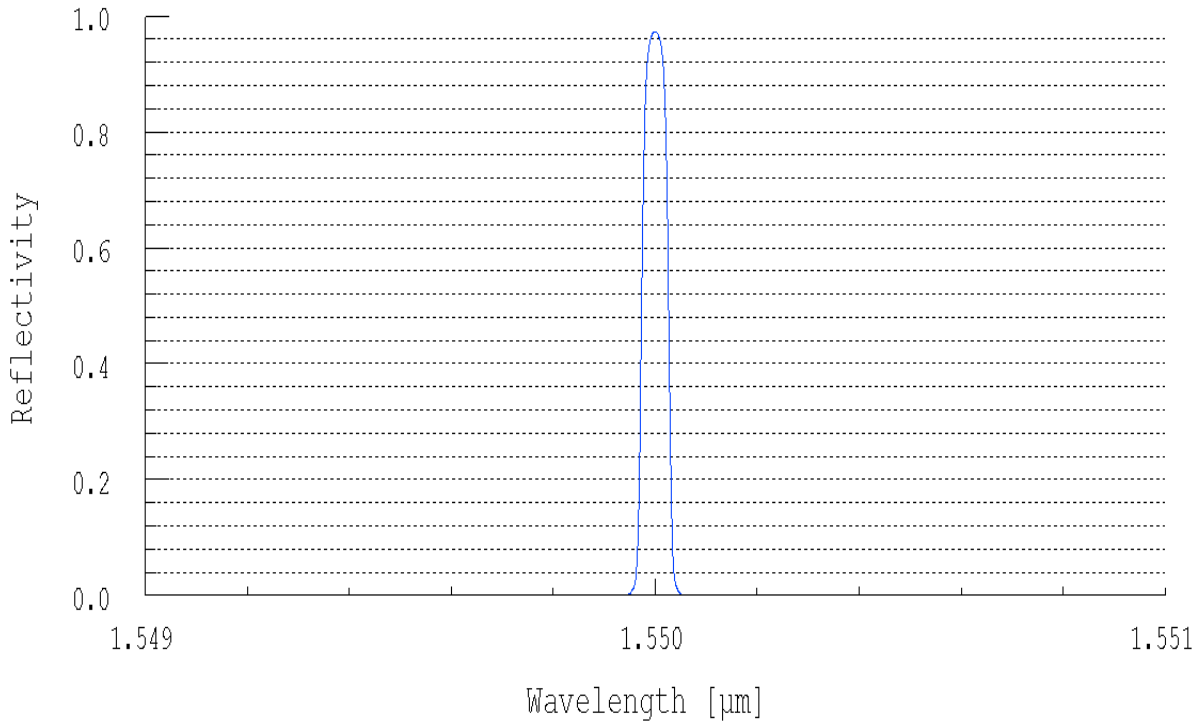

Figure 7.2 Calculated reflected FBG spectrum

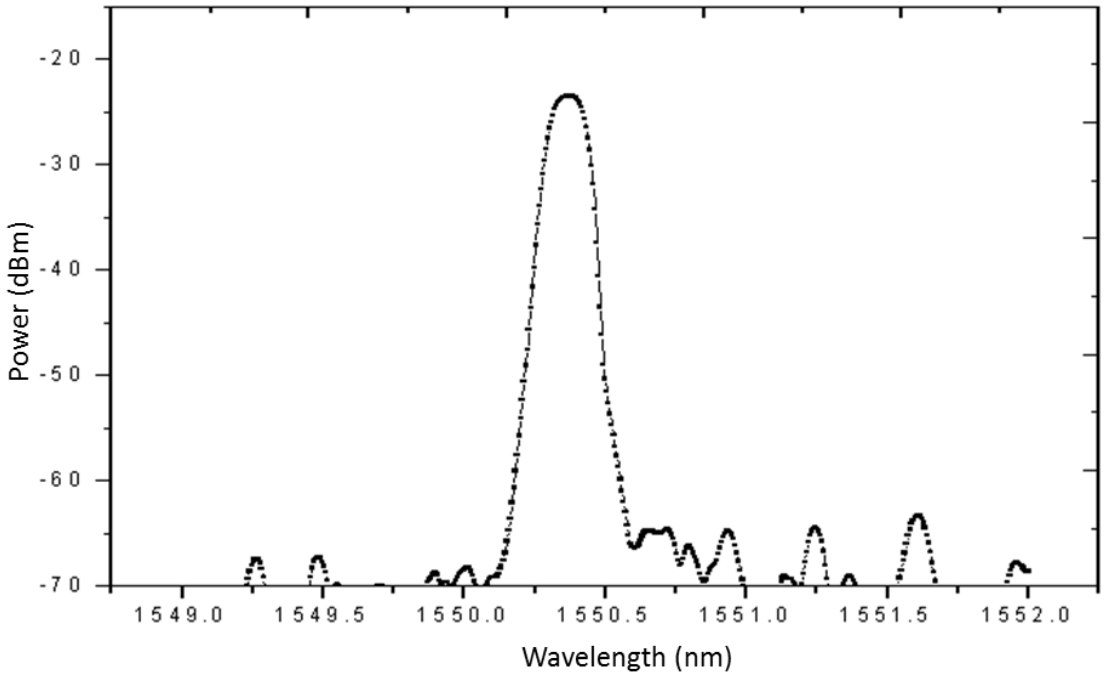

Figure 7.3 Experimental spectrum of FBG

7.3 Fabrication of FBG

There are only a few externally written fabrication techniques, namely, the interferometric technique and the phase mask technique. In house grating system provides the advantage to write gratings in both modes. Next section will describe the phase mask technique for FBG writing.

7.3.1 Phase mask technique

One of the most effective methods for inscribing Bragg gratings in photosensitive fiber is the phase mask technique. KrF excimer lasers are the most common UV sources used to fabricate Bragg gratings with a phase mask. This method employs a diffractive optical element phase mask to spatially modulate the UV writing beam. Phase masks may be produced holographically or by electron-beam lithography [241]. Holographically induced phase masks have no stitch error, which is normally present in the electron-beam phase masks. In spite of this, complicated patterns can be written into the electron beams fabricated masks quadratic chirps, Moire patterns, etc. The phase-mask grating has a one-dimension surface-relief structure fabricated in a high-quality fused silica flat transparent to the UV writing beam. The profile of

the periodic gratings is selected such that when an UV beam is incident on the phase mask, the zero-order diffracted beam is suppressed to less than a few percent typically, less than 5% of the transmitted power as described in Figure 7.4. In addition, the diffracted plus and minus first orders are maximized; each containing, typically, more than 35% of the transmitted power [242].

A near-field fringe pattern is produced by the interference of the plus and minus first-order diffracted beams. Experimental setup is of an excimer pump dye laser with a frequency doubled BBO crystal for generating UV light at 245 nm for inscribing Bragg gratings in an interferometer minus first-order diffracted beams. The period of the fringes is one-half that of the mask. The interference pattern photoimprints a refractive-index modulation in the core of a photosensitive optical fiber placed in contact with or in close proximity immediately behind the phase mask. A cylindrical lens may be used to focus the fringe pattern along the fiber core. The phase mask greatly reduces the complexity of the fiber grating fabrication system. The simplicity of using only one optical element provides a robust and an inherently stable method for reproducing Fiber Bragg Gratings. Since the fiber is usually placed directly behind the phase mask in the near field of the diffracting UV beams, sensitivity to mechanical vibrations and, therefore, stability problems are reduced. Low temporal coherence does not affect the writing capability as opposed to the interferometric technique due to the geometry of the problem. KrF excimer lasers are the most common UV sources used to fabricate Bragg gratings with a phase mask as they have low spatial and temporal coherence. The low spatial coherence requires the fiber to be placed in near contact to the grating corrugations on the phase mask in order to induce maximum modulation in the index of refraction. The separation of the fiber from the phase mask is a critical parameter in producing quality gratings. Conversely, placing the fiber in contact with the fine grating corrugations is not desirable due to possible damage to the phase mask. Improving the spatial coherence of the UV writing beam not only get better the

strength and quality of the gratings inscribed by the phase-mask technique, it also relaxes the requirement that the fiber has to be in contact with the phase mask.

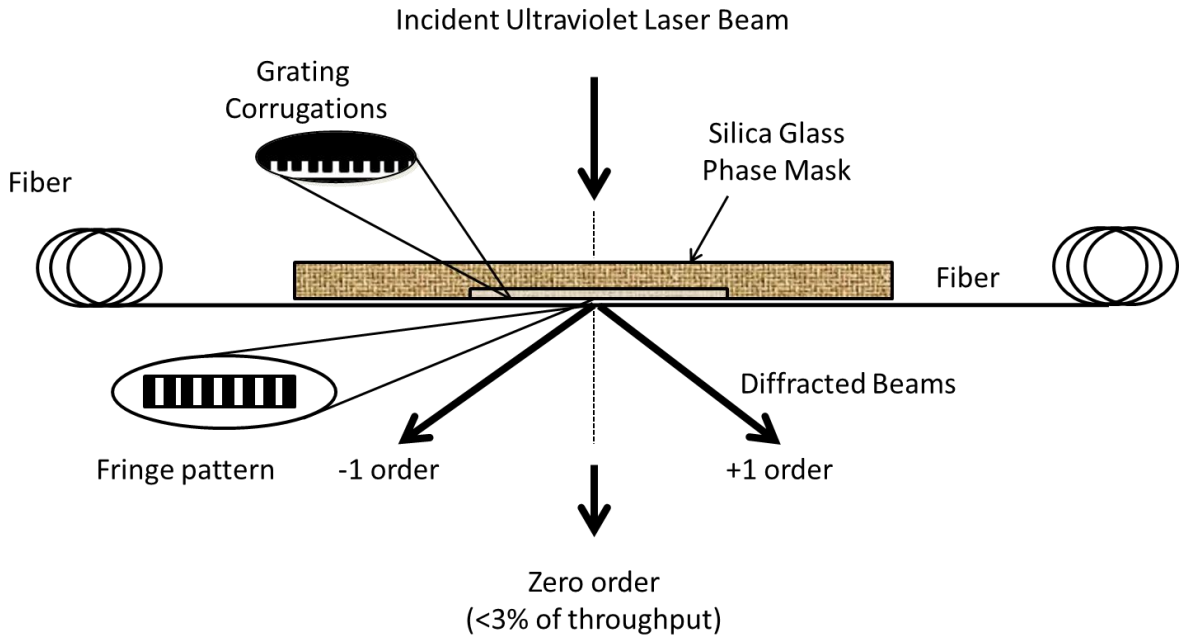

Figure 7.4 Phase Mask fiber Bragg grating inscribing method

For writing FBG static mode of operation in TeraXion grating station is used. This method of fabrication is based upon the phase mask technique, which is described in above section.

7.4 Investigative Study of FBG in Multimode Fibers

When a multimode fiber (MMF) is subject to axial periodic index modulation with a spatial period of Λ, the phase matching or Bragg reflection condition for a specific spatial mode is [161]

$$\beta_1 - \beta_2 = {}^{2\pi}/_{\Lambda} \tag{7.11}$$

where β_1 and $\beta_2$are the propagation constants of the forward and backward mode. The standard multimode fiber can guide hundreds of modes for the wavelengths around 1310 or 1550 nm. While some of them have almost identical propagation constants, they manifest themselves as a number of degenerated principal modes [165], corresponding to a series of different Bragg reflection wavelengths. In

multimode fiber, the propagation constant for the Nth principal mode, β_N can be described by [161]:

$$\beta_N = \frac{2\pi n_1}{\lambda}\sqrt{1-\frac{4\Delta(N+1)}{V}} \tag{7.12}$$

where n_1 is the core refractive index, Δ the maximum relative index difference, $V=2\pi aNA/\lambda$ normalized frequency, a core radius, and NA numerical aperture.

The phase matching conditions can be satisfied for both i.e between reflection of the same modes as well as the neighboring modes. For the reflection between the same Nth principal mode, the Bragg wavelength is determined by:

$$\lambda = 2n_1\Lambda\sqrt{1-\frac{4\Delta(N+1)}{V}} \tag{7.13}$$

For the matching conditions between the Nth and the (N+1)th reflection modes, the Bragg wavelength is determined by the average value of the two neighboring propagation constants.

$$\beta = \beta_N + \beta_{N+1} \tag{7.14}$$

Hence the peak reflection will fall between the Nth and (N+1)th reflection modes.

The number of principal modes or Bragg wavelengths depends on the how many modes have been excited in the fiber. Light from broadband white light sources can excite all the fiber modes hence all the principal modes. More than 20 Bragg wavelengths can be observed for multimode excitation. From the Figure 7.5 it is clear that multiple small peaks are coming along with main peaks, because of large value of diameter carrying more number of modes.

The simulated spectrum for MMF FBG with Bragg wavelength 1586 nm, core and cladding radii 25 & 62.5 μm and refractive indices 1.46, 1.45 and grating period 0.543 μm is shown in the Figure 7.5. The simulation is done by software package Optigrating 4.2.2.

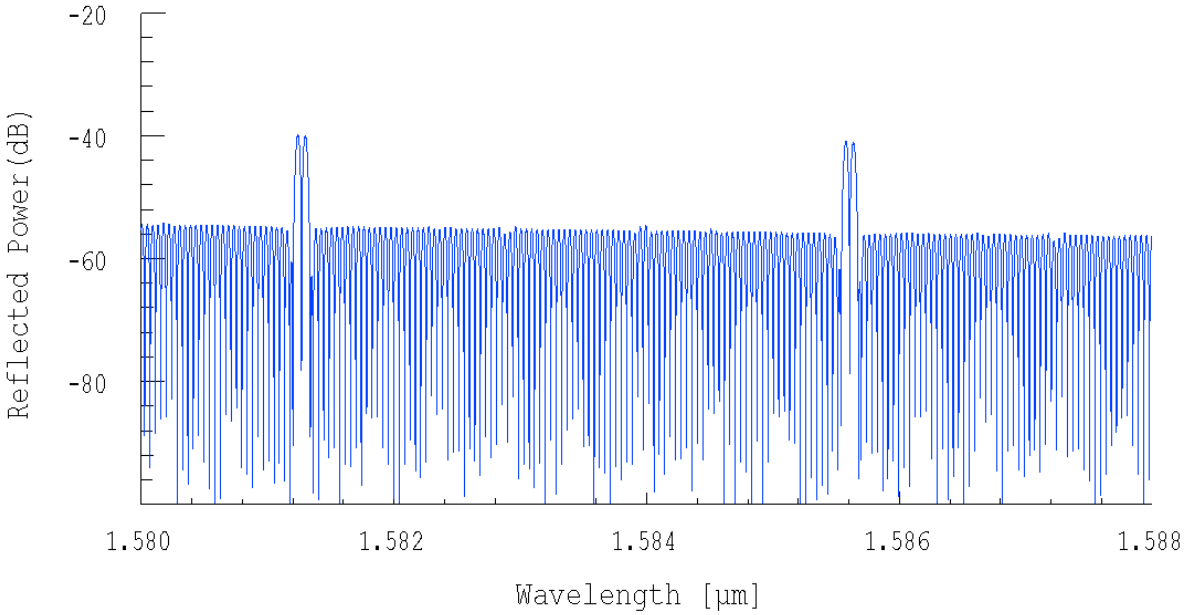

Figure 7.5 Simulated spectrum of MMF FBG with Bragg wavelength 1586 nm

Experimentally observed spectrum on OSA is shown in Figure 7.6. The spectrum contains two major peaks as expected from the simulated spectrum.

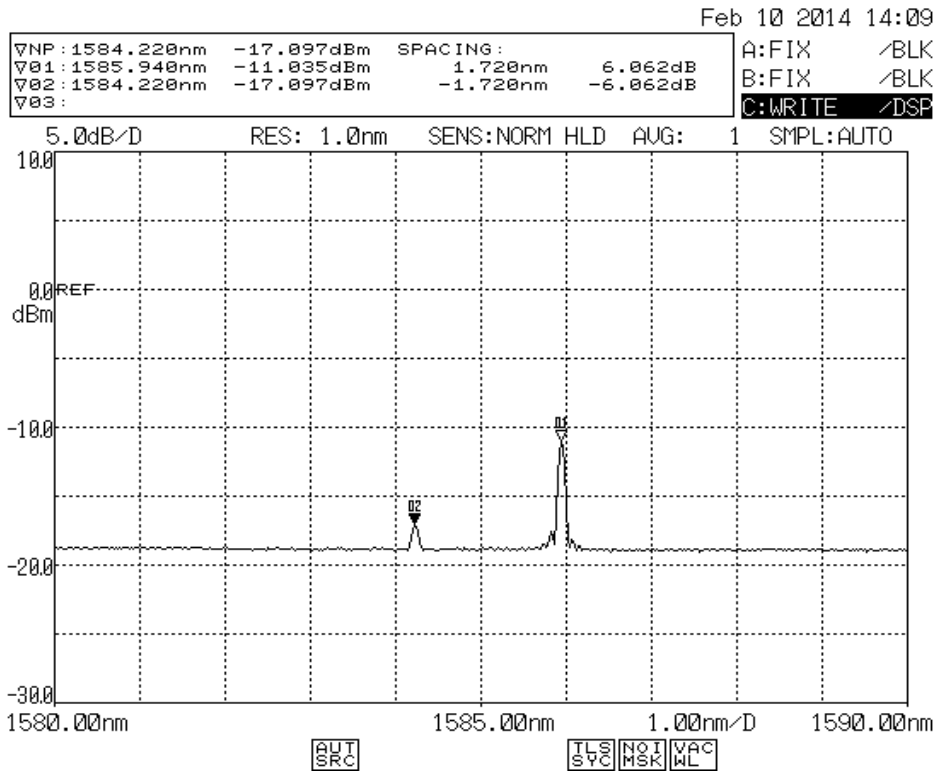

Figure 7.6 Spectrum of fabricated FBG in multimode fiber at wavelength 1586 nm

7.4.1 Characterization of FBG

To characterize the RI sensitivity of MM FBG, glycerol solutions of different concentration are used as an external media. The Figure 7.7 shows its response to

different concentration of glycerol solutions varying from (0 to 100%). The experiment is performed by MM FBG with major peak at 1550 nm. The theoretical result obtained by Optigrating 4.2.2 showed more variation than that of experimentally observed results. In order to increase the sensitivity chemical etching can be performed. Xinzhu Sang [170] reported the chemical sensitivity enhancement by chemical etching the FBG written in MMF.

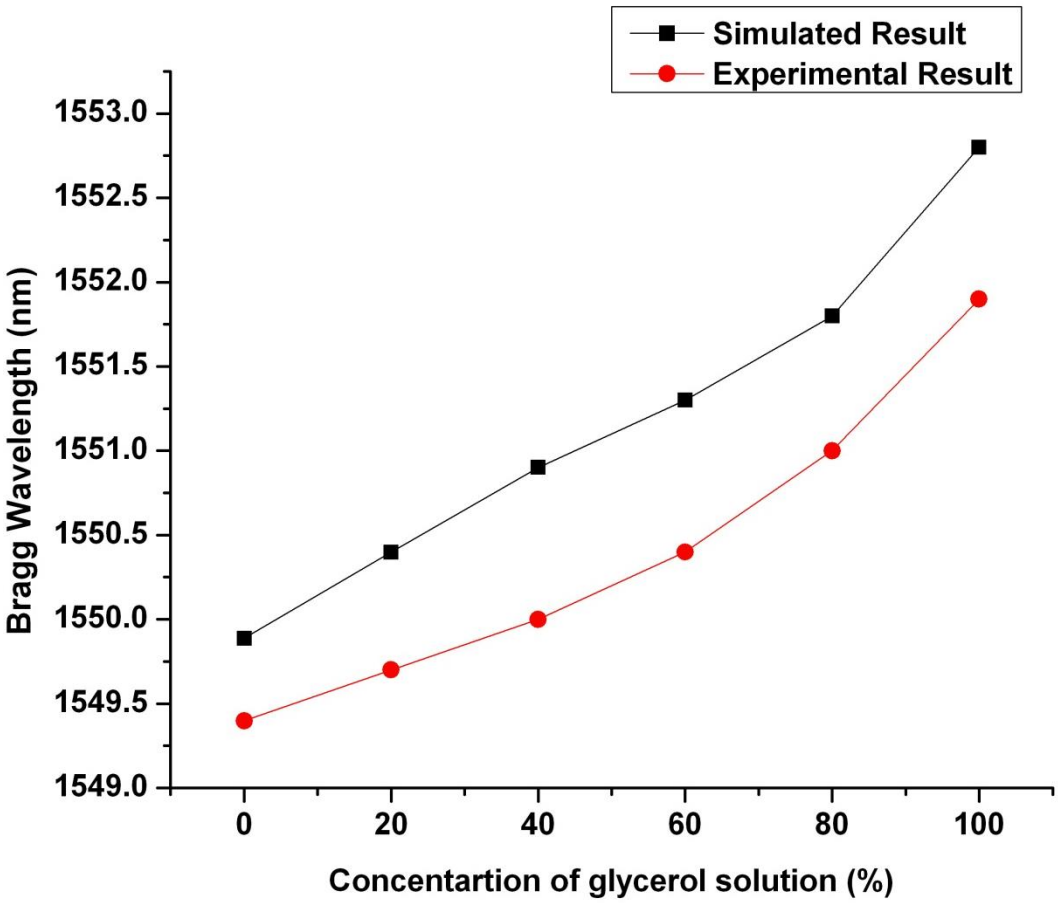

Figure 7.7 MM FBG response to different concentration of glycerol solution

7.4.2 Strain and temperature effect on Fiber Bragg Grating in MMF

Similar to single mode fiber FBGs, the reflection wavelengths of the multimode FBGs can be modulated by both the ambient temperature and axial strain. The core effective index of refraction and the periodicity of the grating determine its center wavelength so that the change of fiber with strain and temperature will affect its core refractive index. The shift in the Bragg grating center wavelength due to strain and temperature changes is given by [243]

$$\Delta\lambda_B = 2\left(\Lambda\frac{\partial \mathrm{n_{eff}}}{\partial \mathrm{l}} + n_{eff}\frac{\partial\Lambda}{\partial l}\right)\Delta l + 2(\Lambda\frac{\partial \mathrm{n_{eff}}}{\partial \mathrm{T}} + n_{eff}\frac{\partial\Lambda}{\partial T})\Delta T \quad (7.15)$$

where T is temperature. The first term in Equation (7.15) represents the strain effect on an optical fiber. The change of grating length Δl, which is caused by a strain on the fiber, will also affect the period of grating and the strain-optic induced refractive index.

The strain effect term could also be defined as:

$$\Delta\lambda_{B(s)} = \lambda_B(1 - p_e)\varepsilon_z \quad (7.16)$$

where ε_z is the applied strain on the fiber grating longitudinal axis, and p_e is an effective strain optic constant defined by:

$$p_e = \frac{n_{eff}^2}{2}(p_{12} - v(p_{11} + p_{12})) \quad (7.17)$$

where $p_{11}$and p_{12} are components of the strain-optic tensor, n_{eff} is the index of the core, and v is Poisson's ratio. The second term in Equation (7.15) represents the temperature effect on an optical fiber. There is a shift in the fiber Bragg grating center wavelength because the thermal expansion changes the grating period and the index of refraction. This fractional wavelength shift for a temperature change (ΔT) could be written as:

$$\Delta\lambda_{B(t)} = \lambda_B(\alpha + \zeta)\Delta T \quad (7.16)$$

where $= \left(\frac{1}{\Lambda}\right)\left(\frac{\partial\Lambda}{\partial T}\right)$, is the thermal expansion coefficient for the fiber and $\zeta = \left(\frac{1}{n_{eff}}\right)\left(\frac{\partial \mathrm{n_{eff}}}{\partial \mathrm{T}}\right)$ represents the thermo-optic coefficient. For a typical MMF p_{11}= 0.121, p_{12} = 0.27, v=0.17 and n_{eff} = 1.4532, length of grating 5 cm, index modulation 0.0001, thermal expansion coefficient = 5.5 e-007 $^{o}C^{-1}$ and thermo optic coefficient = 8.3e-006 $^{o}C^{-1}$. By using these parameters and the above equations, the sensitivity of the fiber

Bragg grating at 1550 nm is about 1 pm of the wavelength shift for 1 μm applied to the grating and temperature sensitivity approximately 13.7 pm/^{0}C.

The effects of strain and temperature on FBG written in multi-mode fiber have been theoretically analyzed and investigated using Optigrating 4.2.2. FBG is taken with parameter Bragg wavelength 1550 nm, core and cladding radii 50 & 125 μm and core refractive indices 1.46, 1.45 respectively and period 0.5308 μm. The Figure 7.8 shows the simulated results of Bragg wavelength variation with temperature vary from 25 to 90^{o}C with zero strain applied on it. Similarly Figure 7.9 depicts the simulated results of stain effect on Bragg wavelength on varying value from 0 to 1200 με keeping temperature constant at 25^{0}C.

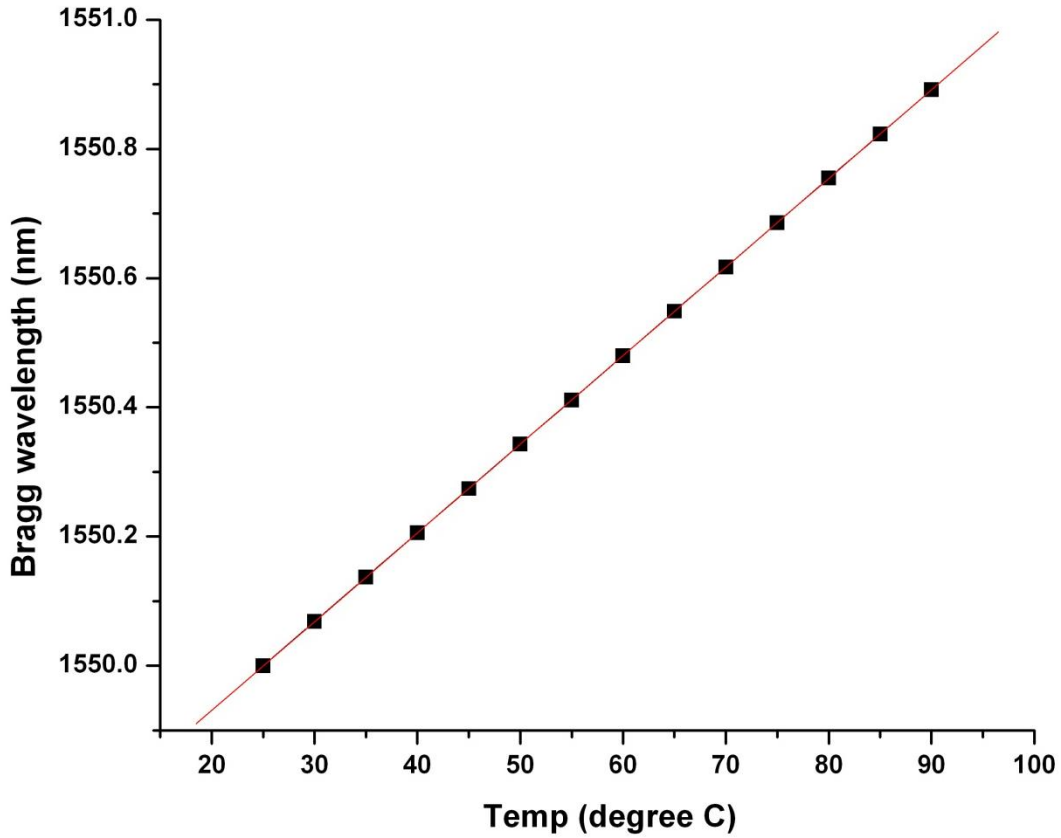

Figure 7.8 The simulated results of Bragg wavelength variation with temperature vary from 25 to 90 ^{0}C with zero strain applied on it

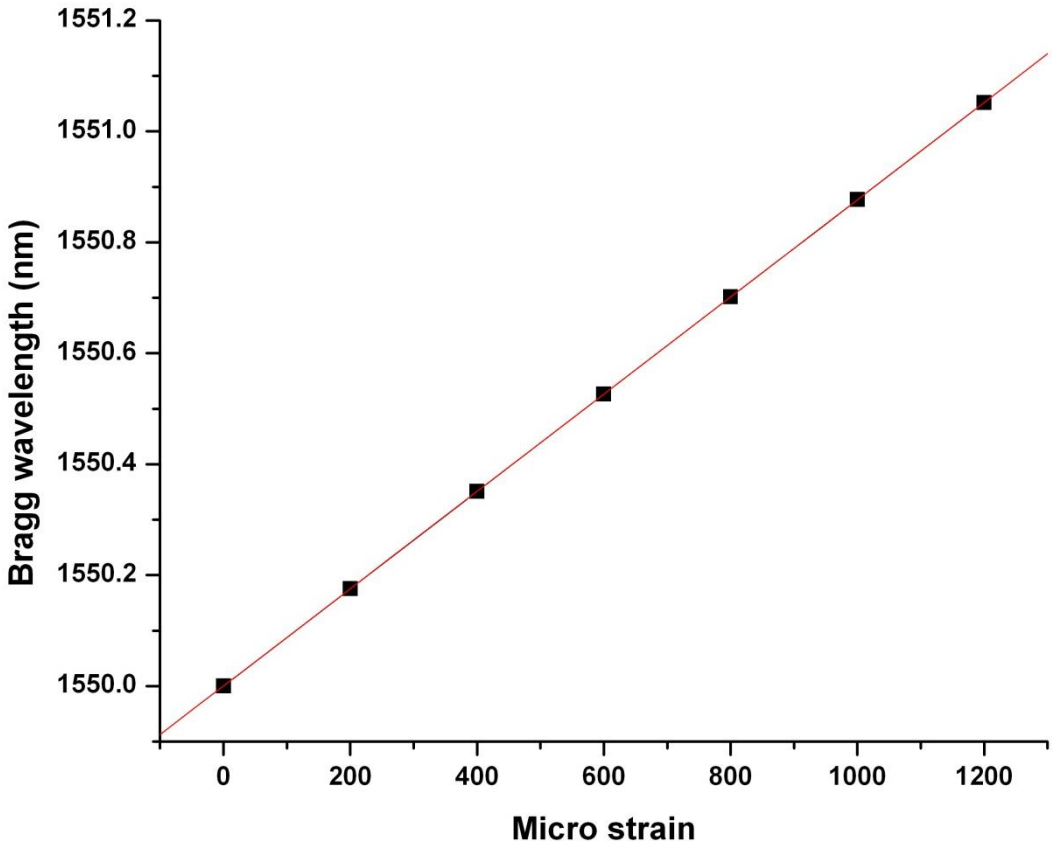

Figure 7.9 The simulated results of stain effect on Bragg wavelength on varying value from 0 to 1200 με keeping constant temperature 25 ºC

7.5 FBG as Current Sensor

Conventional optical fiber sensors for electric current measurement are based upon Faraday effect that uses magnetostrictive alloy and metal coatings [244]. Recently optical fiber based sensors are being investigated as an alternative to conventional current sensors because of their advantages such as freedom from Electromagnetic interference(EMI), wide bandwidth, compactness, geometric versatility, and cost effectiveness. Optical fibers based on birefringence characteristics have been utilized to measure current in which the polarization state of the light that propagates along the fiber is detected by polarimetric or interferometric system [245-247]. In another approach, Fiber Fabry–Perot interferometer (FFPI) has also been reported where a metal (Au and Ni-Cr) is plated onto the optical fiber as a heater to measure the AC electrical current. Amongst various FO (Fiber Optic) techniques, fiber Bragg grating technology has generated much interest as a sensor for strain, temperature, and

other physical parameters. Moreover recently [248] the study revealing the relationship between relative displacement of interference pattern with surface temperature has also been successfully demonstrated. Chin-Hsing Cheng *et al*. [249] also measured wavelength as a function of the applied current from 0 Amp to 2 Amp resulting Bragg wavelength increased from 1547.837 to 1547.912 nm utilizing the Faraday Effect.

Here a current sensor was designed and studied using temperature sensitivity of FBG. In our case, current changes from 0.05 Amp to 1 Amp results Bragg wavelength shift from 151.009 to 1553.461 nm (without housing setup). And with the housing setup, change of 1 Amp to 4 Amp current shifts Bragg wavelength from 1547.99 nm to 1550.682 nm. It is known that when FBG is subjected to change in temperature or strain shows shift in the Bragg wavelength. Thus by monitoring the change in the Bragg wavelength, we can calculate the temperature of the surroundings when no strain is applied to the FBG. The design of the sensor was inspired by this idea. Nichrome coil was used as the heating element with strain-free FBG kept at its center in the experiment. This coil is also used in various heating appliances such as hair dryer etc. FBG was strain free because it was not surface mounted, it is just passed through the current carrying coil. So there was no mechanical or any residual stain/stress present. When Alternating current (AC) current was passed through this coil, it heated up, thus shifting the Bragg wavelength. This kind of sensing technique is simple in structure and low in cost.

7.5.1 Theory and experimental details

In an FBG light is coupled between forward propagating mode to backward propagating mode and the reflected Bragg wavelength is given by Equation 7.1. The heat produced in the Nichrome coil is proportional to the current supplied [236]:

$$H = I^2 * R_{coil} \tag{7.17}$$

where H is the heat produced, I the value of current and R_{coil} is the resistance of the coil. When the coil is heated there is a shift in the Bragg wavelength of the FBG kept inside because the thermal expansion changes the grating period and the index of refraction.

In the first step, the nichrome coil was calibrated with respect to the current and temperature using available thermometer. Coil was subjected to known value of current through a current source and corresponding temperature was noted for each value with normal thermometer. The calibration curve is as shown in Figure 7.10

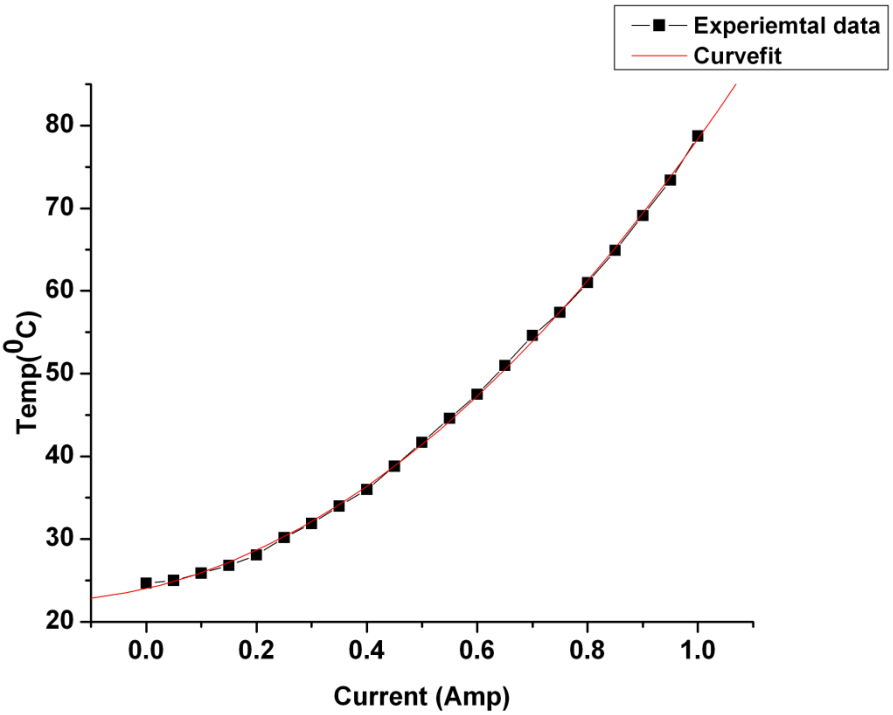

Figure 7.10 The curve fit of the experimental values of current versus temperature.

Two FBGs were fabricated by using phase mask method as mentioned in Section 7.3 with resonance wavelengths of 1550.85 nm and 1547.95 nm. The calibration curve for Bragg wavelength and temperature variation was observed. For this, FBG fiber was inserted inside the coiled nichrome wire. The temperature was varied from 20 to 80 ^{0}C. For each value of current, corresponding Bragg wavelength was recorded using

Micron Optics Si425 interrogator (Micron Optics Inc. Atlanta, GA). The Bragg wavelength and temperature variation is shown in the Figure 7.11.

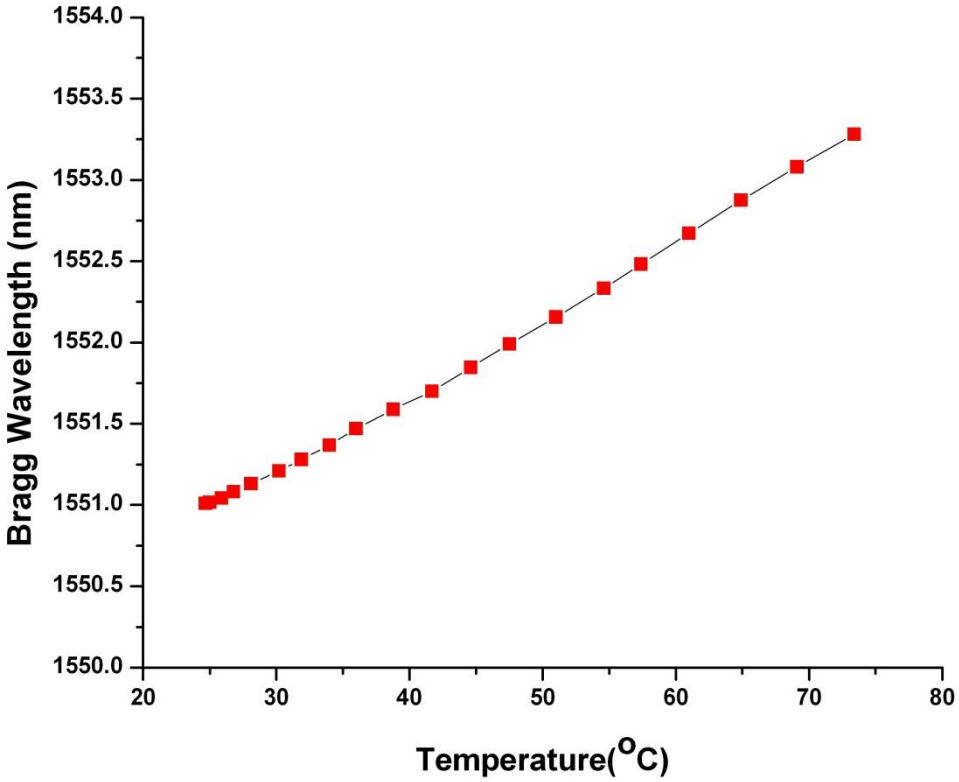

Figure 7.11 Experimental value of variation of Bragg wavelength with increasing value of temperature

7.5.2 Housing and without housing

To perform the current sensing an electric current from AC current source was passed through this coil, generating heat and there was a temperature rise in the surroundings of sensing FBG resulting in a shift in its Bragg wavelength. This arrangement was without housing setup. The variation of Bragg wavelength with increasing and decreasing values of applied current is tabulated in Table 7.1 and shown in Figure 7.12. In this setup there were fluctuations in the Bragg wavelength for constant value of current observed in the readings. The cause of these fluctuations was air currents produced due to temperature variation. FBGs used in our experiment were of very high reflectivity and very narrow bandwidth. Therefore second setup is used in which housing has been provided to get more accurate readings.

Table 7.1 Bragg Wavelength vs. Current (without housing setup)

Current in Amperes	Wavelength in nm
0	1551.009
0.05	1551.015
0.1	1551.041
0.15	1551.082
0.2	1551.132
0.25	1551.211
0.3	1551.281
0.35	1551.368
0.4	1551.47
0.45	1551.588
0.5	1551.699
0.55	1551.847
0.6	1551.99
0.65	1552.156
0.7	1552.334
0.75	1552.482
0.8	1552.671
0.85	1552.876
0.9	1553.081
0.95	1553.282
1	1553.461
0.95	1553.231
0.9	1553.016

0.85	1552.813
0.8	1552.64
0.75	1552.463
0.7	1552.26
0.65	1552.095
0.6	1551.95
0.55	1551.801
0.5	1551.661
0.45	1551.536
0.4	1551.419
0.35	1551.315
0.3	1551.213
0.2	1551.062
0.1	1550.947
0	1550.925

To overcome the above mentioned limitations setup was modified with providing housing. Housing was basically used to put the setup inside a metallic chamber and cover whole setup with thick thermocol sheets. The need of housing was to make the system isothermal and to avoid the cross-sensitivity with ambient temperature, moreover to make heat concentrated near the vicinity of the fiber. The experiment was repeated with increasing as well as decreasing values of current. The schematic of housing setup is shown in Figure 7.13.

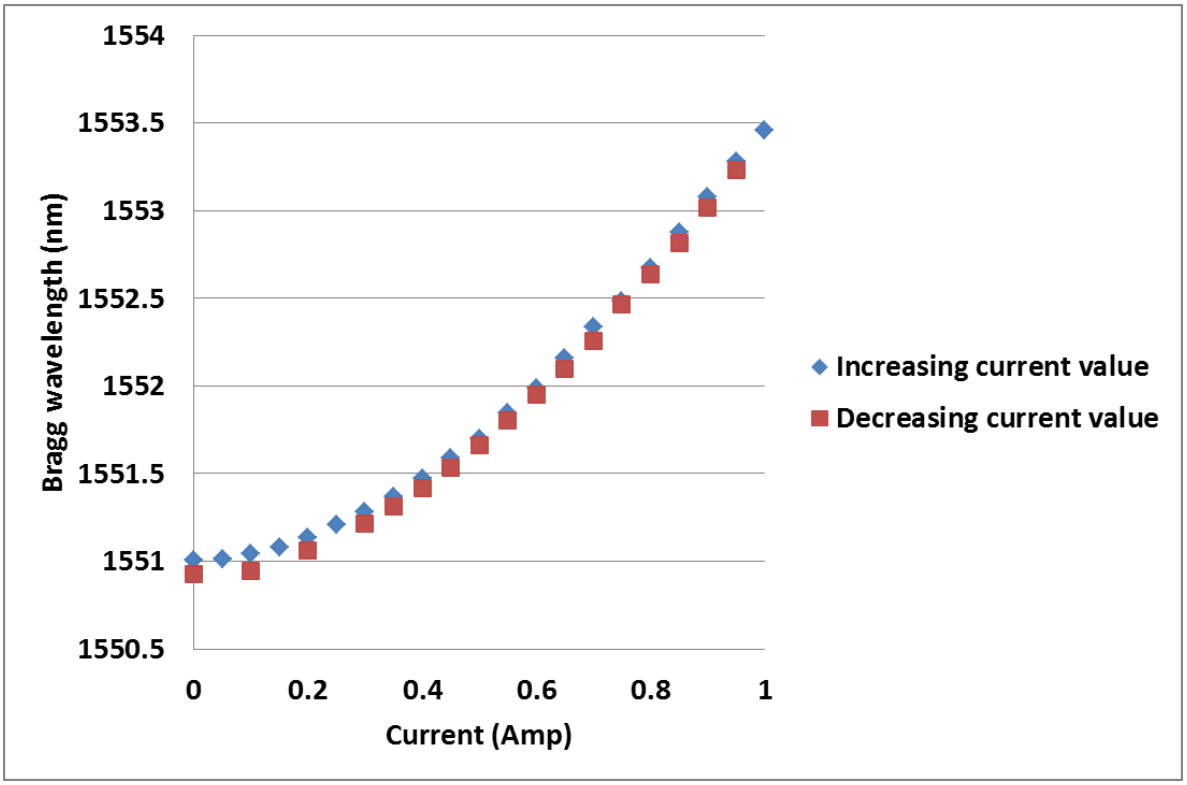

Figure 7.12 Graph showing the variation of resonant wavelength with the increasing and decreasing value of applied current (without housing)

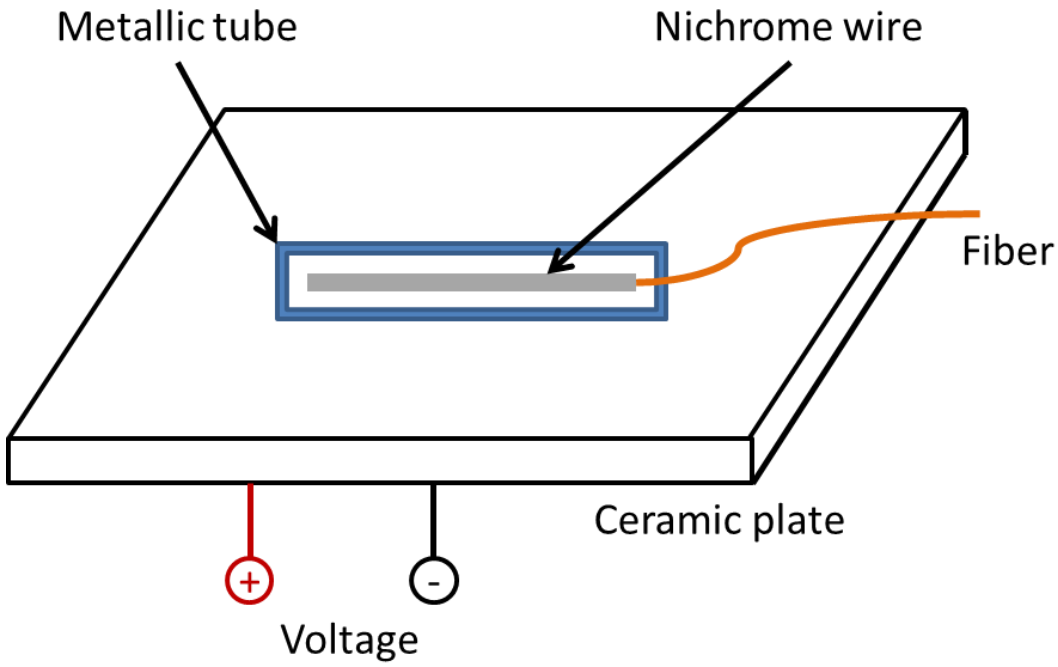

Figure 7.13 Schematic of the experimental setup (with housing)

The Figure 7.14 shows the experimental setup, where the interrogator, FBG and current source were shown in with housing configuration. The whole experimental

setup was covered with hard thermocol sheets so that there should be minimum effect of surrounding fluctuations.

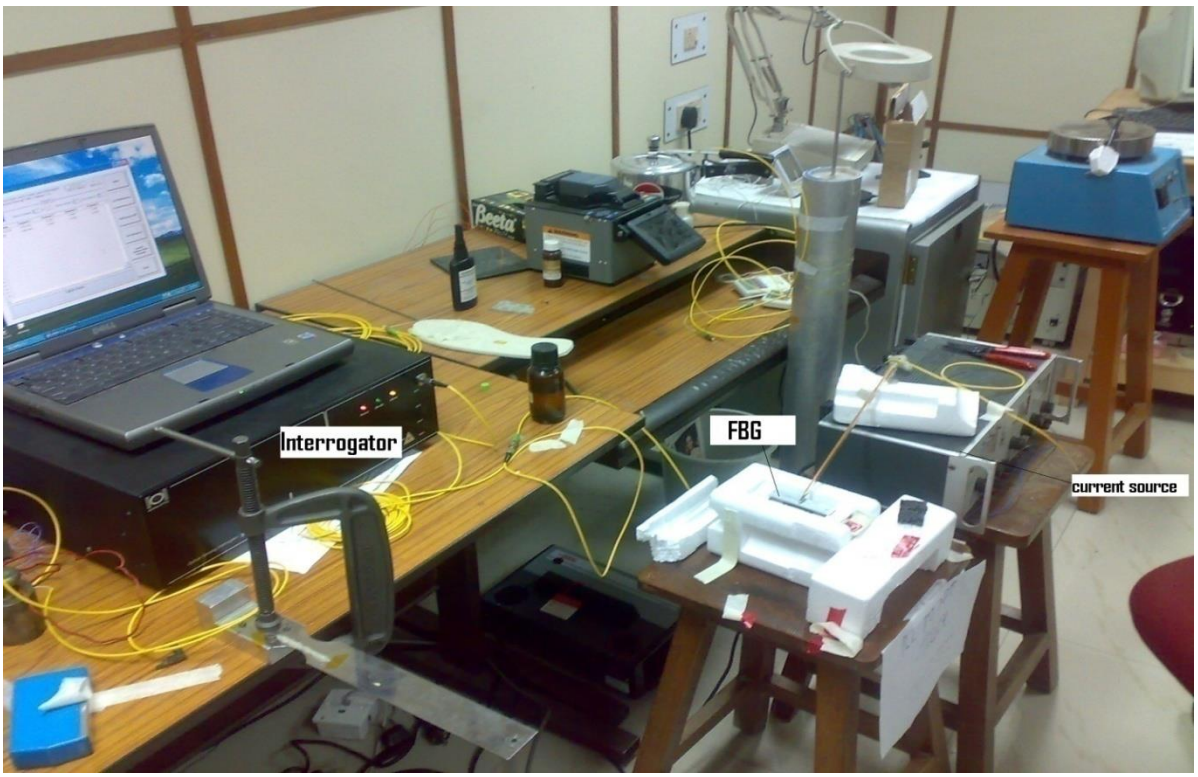

Figure 7.14 Experimental set up of with housing configuration

Figure 7.15 shows the hysteresis curve for with housing setup i.e. the variation of Bragg wavelength w.r.t increasing and deceasing value of applied current. To reduce the surrounding effect and to make heat concentrated near the fiber, nichrome wire with less diameter and closed metallic chamber was used in the setup. The metallic housing did result in improved performance. It resulted in decreasing the hysteresis as temperature variation in surrounding was comparatively lesser as shown in Figure 7.15 and values are summed up in the Table 7.2. The peak wavelength varies in accordance with temperature change. Further resonant wavelength increases and decreases consistently as current varies in the same manner.

Table 7.2 Bragg Wavelength vs. Current (with housing setup)

Current (amperes)	Center Wavelength (nm)
0	1547.99
1	1548.196
2	1548.718
3	1549.63
4	1550.682
3	1549.702
2	1548.79
1	1548.227
0	1547.99

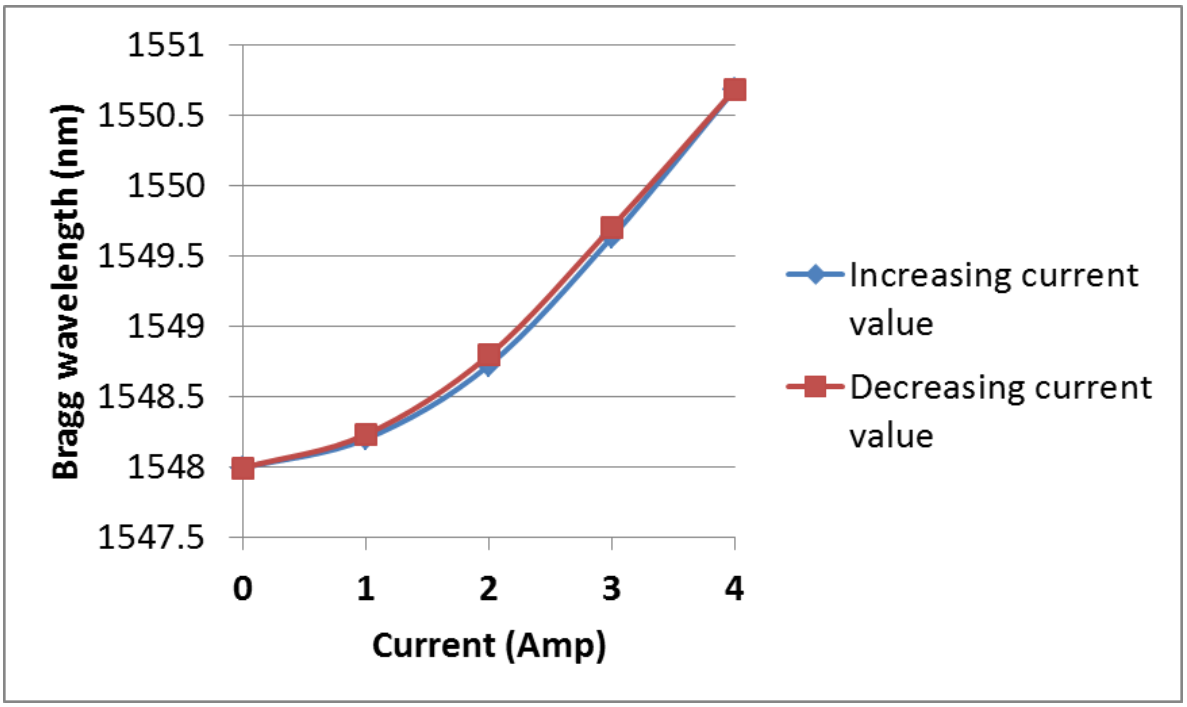

Figure 7.15 Graph showing the variation of resonant wavelength with the increasing and decreasing value of applied current (with housing).

The design of the sensor is very simple. The experiment was repeated three times and the results were found consistent. The minimum and maximum values of current measured without housing is 0.05 Amp and 1 Amp and with the housing

setup it is 1 Amp and 4 Amp. A current sensor based on FBG has been designed, developed, and investigated.

7.6 Summary

The chapter investigated and analyzed study of FBG written in multi-mode fibers. The fabrication and characterization was covered. The effect of temperature and strain was studied theoretically. FBG as a current sensor was demonstrated successfully. The designed sensor has accuracy 0.05 Amp and repeatability 95%. As the current sensor is in initial stages, it is far from being a commercial product. This sensor is different from available current sensors in terms of its new and simple design, low cost and ability to withstand harsh environment. This type of sensor has a great scope in electrical industries and labs.

CHAPTER 8. CONCLUSIONS, RECOMMENDATION AND FUTURE SCOPE

8.1 Conclusions

This thesis presented the investigation on long period grating for Fiber Optic sensing systems. The motivation and objective of this thesis is to do an in-depth analysis of the properties-characteristics, fabrication, characterization and experimental demonstration of LPG in sensing. The work presented in this thesis deals with two major areas: refractive index sensitivity enhancement and relative humidity sensing. The simulation of long period grating has been carried out and the results presented have been validated using theoretical and experimental work. The development of long-period gratings, the state-of-the-art for applications and associated fabrication technology are reviewed. The concept of mode coupling is extended to investigation of the fundamental characteristics of long-period gratings. An analytical model is presented to explain the spectral modulation offered by these devices. It is shown that the multiple loss bands in a long-period grating result from coupling to discrete forward-propagating cladding modes. The periodicity of the refractive index modulation characterizes the spectral properties of long-period gratings through phase-matching condition. Characteristic curves that predict the resonant wavelengths for different grating periods are obtained. It is observed that locations of bands are strong functions of properties of the host fiber, grating period, and effective refractive indices.

In this work, coupled mode theory is employed to investigate the coupling between modes in a perturbed system. This method assumes that modal fields of waveguide remain unchanged in the presence of weak perturbation. The phenomenon of photosensitivity is reviewed. Theoretical models are discussed for the concept of photosensitivity in optical fibers. There are many different methods of fabricating

long-period gratings, which have been discussed. The experiments for fabricating long-period gratings include: experimental set-up, experimental procedure and measurements of transmission spectra of the gratings fabricated. The various components and modes for writing of grating writing station are discussed in length. Finally, the simulation results are also shown for the above mentioned. The work includes experimental characterization of fabricated LPG with available standard RI solutions. Wavelength dependency of LPG on strain and temperature is also discussed.

The properties of long period grating have been investigated with conducting metal oxide coating, followed by the investigative study on rearrangement of modes due to deposition of higher refractive index value overlay on it. The utilization of ITO as coatings material allows the fabrication of sensitive, highly reproducible and easy to implement refractive index sensors. For the purpose dip coating method has been used for thin film deposition of ITO. The coating structure and its properties had been investigated using SEM, FTIR and Raman spectroscopy analysis. The RI sensitivities of the uncoated as well as ITO coated LPG are monitored with glycerol solutions of varying concentration with different RI. A comparison of both uncoated and ITO coated LPGs demonstrated that the sensitivity has been enhanced by 2-3 times because of coating. This factor can be improved by further optimizing the coating methods. This approach has given a better understanding about the coated LPG behavior. If the thickness and refractive index of the overlay are fixed, the sensitivity to specific ambient refractive index ranges can be optimized by adequate selection of the other two variables that are fixed. One example has been shown for the RI sensor.

It is demonstrated that long period grating is not just a highly sensitive refractometer but it can also be used to determine RH level of the ambient medium, by applying a hygroscopic coating over it. We designed and experimentally demonstrated for the very first time, a sensor probe based on LPG coated with gelatin-Cobalt Chloride

($CoCl_2$) that covers a reasonably large range of RH from 35 to 90%. The presented data supports the promising performance of LPGs as humidity sensors on a commercial platform. Along with the inherent advantages of optical fibers, LPGs can offer the flexibility of distributed sensing system. The LPG coated with mixture gelatin-Cobalt Chloride ($CoCl_2$) demonstrated a sensitivity response of 0.18 nm/ %RH with an error of ±1.45%. The designed sensor offers minimal hysteresis loss of ±0.18%, stability error of 0.056%, repeatability of 99.7% and response time of 24 seconds. The overlay coating is found to be durable for a period of 3 months. In addition to this, the effect of grating period on the performance of sensor has also been studied. It is seen that LPGs with a lower grating period have higher sensitivity of RH level changes.

The ITO and $CoCl_2$/gelatine coated LPG as humidity sensor is demonstrated very first time. The sensor can be used to measure RH variation efficiently in the range of 40% to 95% RH with sensitivity of 0.12 nm/%RH, accuracy of 98.45%, stability error 0.031%, hysteresis error of ±0.12% RH and repeatability of 98.7%

Also, investigated and analyzed FBG written in multi-mode fibers. The fabrication and characterization by taking different concentration of glycerol solutions has also been discussed. The effect of temperature and strain is studied theoretically. Bragg gratings in multimode or few-mode fibers can be used for bending or displacement sensors.

FBG as a current sensor is demonstrated successfully. The designed sensor has resolution 0.05 Amp, accuracy 95%, and repeatability 5 pm. The sensor will work for both alternating current and direct current. The design of the sensor is very simple. The experiment was repeated three times and results were found consistent. The minimum and maximum value of current measured without housing is 0.05 Amp and 1 Amp and with the housing setup it is 1 Amp and 4 Amp. This sensor is different from available current sensors in terms of its new and simple design, low

cost and ability to withstand harsh environment. The study of this type of sensor has a great scope in electrical industries and labs.

8.2 Recommendations

- It is recommended to implement humidity sensors for moisture measurement in food storage systems. As the light does not leave the fiber and light modulation takes place inside the fiber, this kind of sensor presents the major benefit to have the ability to reach otherwise inaccessible places and without the need of electrical energy at the sensing location.
- LPG sensors are passive and require no electrical power. Because of this, they are totally immune to interference from electrostatic or radio frequency sources. Furthermore, they are intrinsically safe and can be used to instrument the most hazardous explosive environments. For monitoring and controlling corrosion in structures, this study can be beneficial for exploring LPG as pH sensor.
- The two Long Period grating sensors are presented in this thesis work i.e. refractive index and moisture sensors. In chemical industries, where bulk of chemical solutions are used every day, fiber based refractive index sensing can be very beneficial in performing fast purity & quality checks. Nevertheless, both the sensors can contribute in the fields like agriculture, food processing, medicines, bio sensing and structure health monitoring.
- FBG based current sensor presented here is different from available current sensors in terms of its new and simple design, low cost and ability to withstand harsh environment. This type of sensor has a great scope in electrical industries and labs.

8.3 Future Scope

- Towards future scope, rigorous simulation studies have to be carried out on the coated long period gratings. It is clear that higher-order resonances permit

to obtain wider wavelength shifts as function of the different ambient refractive indices. Other applications like detection of gases and detection of oils can also be explored.

- The RH sensor coated with gelatin-Cobalt Chloride ($CoCl_2$) is experimentally demonstrated with sensitivity 0.18 nm/%RH and covers a reasonably large range of RH from 35 to 90%. More sensitive sensor can be designed by etching the cladding of the LPG. The gelatin-Cobalt Chloride ($CoCl_2$) amalgamation on etched LPG will surely give much more sensitive RH sensor.
- Simulation studies can be further carried out on the LPG directly inscribed into the Erbium doped fiber (EDF) and Photonic Crystal Fiber (PCF), this is currently being investigated by many research groups and characteristics can be further worked out for some novel applications [250—251].
- The new combination of hygroscopic materials should be explored for covering much wider range of humidity.
- This study of humidity sensing can also be helpful for exploring for the possibility of pH sensors particularly in applications of corrosion monitoring and early corrosion detection.

REFERENCES

[1] A. Ghatak and K. Thyagarajan, *Introduction to Fiber Optics*: Cambridge University press India Pvt.Ltd.

[2] D. A. Pinnow, T. C. Rich, F. W. Ostermayer, and M. DiDomenico, "Fundamental optical attenuation limits in the liquid and glassy state with application to fiber optical waveguide materials," *Applied Physics Letters,* vol. 22, pp. 527-529 1973.

[3] R. Yun-Jiang, D. J. Webb, D. A. Jackson, Z. Lin, and I. Bennion, "In-fiber Bragg-grating temperature sensor system for medical applications," *Journal of Lightwave Technology,* vol. 15, pp. 779-785, 1997.

[4] K. A. M. V.Bhatia, M.J.de Vries and M.B.Sen, *A Comparative evaluation of the types and applications of various sensors*, 1995.

[5] J. P. Dakin and B. Culshaw, *Optical Fiber Sensors: Principles and Components*: Artech House, 1988.

[6] K. A. Murphy, M. F. Gunther, A. M. Vengsarkar, and R. O. Claus, "Quadrature phase-shifted, extrinsic Fabry-Perot optical fiber sensors," *Optics Letters,* vol. 16, pp. 273-275,1991.

[7] F. J. Arregui, Y. Liu, I. R. Matias, and R. O. Claus, "Optical fiber humidity sensor using a nano Fabry–Perot cavity formed by the ionic self-assembly method," *Sensors and Actuators B: Chemical,* vol. 59, pp. 54-59, 1999.

[8] H.H.Yu, L. Yao, L.X.Wang, W.B.Hu, and D.S.Jiang, "Fiber optic humidity sensor based on self-assembled polyelectrolyte multilayers " *Journal Wuhan University of Technology, Materials Science Edition,* vol. 16, pp. 65-69, 2001.

[9] H. I. Bjelkhagen, *Silver-Halide Recording Materials: for Holography and Their Processing*, 2 ed. USA: Springer-Verlag, 1995.

[10] V. Bhatia, "Properties and Sensing Applications of Long-Period Gratings," Ph.D, Electrical Engineering, Virginia Polytechnic Institute and State University, 1996.

[11] A. M. Vengsarkar, P. J. Lemaire, J. B. Judkins, V. Bhatia, T. Erdogan, and J. E. Sipe, "Long-period fiber gratings as band-rejection filters," *Journal of Lightwave Technology,* vol. 14, pp. 58-65, 1996.

[12] M. Harurnoto, M. Shigehara, and H. Suganurna, "Gain-flattening filter using long-period fiber gratings," *Lightwave Technology, Journal of,* vol. 20, pp. 1027-1033, 2002.

[13] N.-K. Chen and G.-L. Cheng, "High sensitivity micro Sagnac loop interferometer based on tightly twisted micro fiber tapers," in *Optical Fiber Communication Conference/National Fiber Optic Engineers Conference 2013*, Anaheim, California, 2013, p. JW2A.28.

[14] M. Sumetsky, "Optimization of optical ring resonator devices for sensing applications," *Optics Letters,* vol. 32, pp. 2577-2579,2007.

[15] E. M. Dianov, S. A. Vasiliev, A. S. Kurkov, O. I. Medvedkov, and V. N. Protopopov, "In-fiber Mach-Zehnder interferometer based on a pair of long-period gratings," in *Optical Communication, 1996. ECOC '96. 22nd European Conference on*, 1996, pp. 65-68 vol.1.

[16] C. Gräf, A. Thüring, H. Vahlbruch, K. Danzmann, and R. Schnabel, "Length sensing and control of a Michelson interferometer with power recycling and twin signal recycling cavities," *Optics Express,* vol. 21, pp. 5287-5299, 2013/03/11 2013.

[17] Y. H. K. Byeong Ha Lee , Kwan Seob Park, Joo Beom Eom , Myoung Jin Kim , Byung Sup Rho and Hae Young Choi, "Review :Interferometric Fiber Optic Sensors," *Sensors,* vol. 12, pp. 2467-2486, 2012.

[18] T. Woo-Hu and L. Chun-Jung, "A novel structure for the intrinsic Fabry-Perot fiber-optic temperature sensor," *Journal of Lightwave Technology,* vol. 19, pp. 682-686, 2001.

[19] K. Sang-Hoon, L. Jung-Ju, L. Dong-Chun, and K. Il-Bum, "A study on the development of transmission-type extrinsic Fabry-Perot interferometric optical fiber sensor," *Lightwave Technology, Journal of,* vol. 17, pp. 1869-1874, 1999.

[20] Y. Verbandt, B. Verwilghen, P. Cloetens, L. Kempen, H. Thienpont, I. Veretennicoff, G. Vinckenroy, W. P. Wilde, and M. H. Voet, "Polarimetric optical fiber sensors: aspects of sensitivity and practical implementation," *Optical Review,* vol. 4, pp. A75-A79,1997.

[21] J. Zhang, X. Tang, J. Dong, T. Wei, and H. Xiao, "Zeolite thin film-coated long period fiber grating sensor for measuring trace chemical," *Optics Express,* vol. 16, pp. 8317-8323, 2008.

[22] V. Bhatia, "Applications of long-period gratings to single andmulti-parameter sensing," *Optics Express,* vol. 4, pp. 457-466, 1999.

[23] A. Iadicicco, A. Cusano, G. V. Persiano, A. Cutolo, R. Bernini, and M. Giordano, "Refractive index measurements by fiber Bragg grating sensor," in *Proceedings of IEEE of Sensors* 2003, pp. 101-105.

[24] M. Kheiri, M. I. Zibaii, J. Sadeghi, and H. Latifi, "Refractive index measurement by fat long period grating sensor on a single mode optical fiber," in *Communications and Photonics Conference and Exhibition, 2011. ACP. Asia*, 2011, pp. 1-6.

[25] F. Baldini, M. Brenci, F. Chiavaioli, A. Giannetti, and C. Trono, "Optical fibre gratings as tools for chemical and biochemical sensing," *Analytical and Bioanalytical Chemistry,* vol. 402, pp. 109-116, 2012.

[26] L. Xu, J. C. Fanguy, K. Soni, and S. Tao, "Optical fiber humidity sensor based on evanescent-wavescattering," *Optics Letters,* vol. 29, pp. 1191-1193, 2004.

[27] L. Alwis, T. Sun, and K. T. V. Grattan, "Optical fibre-based sensor technology for humidity and moisture measurement: Review of recent progress," *Measurement,* vol. 46, pp. 4052-4074, 2013.

[28] P. R. Wiederhold, *Water Vapor Measurements*: CRC Press, 1997.

[29] T. L. Yeo, T. Sun, and K. T. V. Grattan, "Fibre-optic sensor technologies for humidity and moisture measurement," *Sensors and Actuators A: Physical,* vol. 144, pp. 280-295, 2008.

[30] D. K. Roveti. (2001, Choosing a Humidity Sensor: A Review of Three Technologies.

[31] D. J. Beaubien, "The Chilled Mirror hygrometer: How It Works, Where It Works-and Where It Doesn't," in *Sensors*, ed: E-News Letters, 2005.

[32] L. W. Foskett, N. B. Foster, W. R. Thickstun, and R. C. Wood. (1953) Infrared Absorption Hygrometer. *Monthly Weather Review*.

[33] Z. Chen and C. Lu, "Humidity Sensors: A Review of Materials and Mechanisms," *Sensor Letters,* vol. 3, pp. 274-295, 2005.

[34] C.-Y. Lee and G.-B. Lee, "Humidity Sensors: A Review," *Sensor Letters,* vol. 3, pp. 1-15, 2005.

[35] S. Otsuki, K. Adachi, and T. Taguchi, "A novel fiber-optic gas-sensing configuration using extremely curved optical fibers and an attempt for optical humidity detection," *Sensors and Actuators B: Chemical,* vol. 53, pp. 91-96, 1998.

[36] G.Gauglitz, "Opto-Chemical and Opto-Immuno Sensors," *Sensors Update,* vol. 1, pp. 1-48, 1996.

[37] B. T. Meggitt and K. T. V. Grattan, "Optical Fiber Sensor Technology," in *Chemical and Environmental Sensing,Vol 4*, ed: Academic Publisher, 1999.

[38] G.Steward, "Fiber optic sensors in environmental monitoring," presented at the Optical Fiber Sensor Technology:chemical and Environmental sensing, 1999.

[39] J.C.Palais, *Fiber Optic Communications*: Prentice Hall, 2005.

[40] A.P.Russell and K.S.Fletcher, "Optical Sensor for the Determination of Moisture," *Analytica Chimica Acta,* vol. 170, pp. 209-216, 1985.

[41] A. Kharaz and B. Jones, "A distributed fibre optic sensing system for humidity measurement," *Measurement and Control,* vol. 28, pp. 101-103, 1995.

[42] R. Jindal, S. Tao, J. P. Singh, and P. Gaikwad, "High dynamic range fiber optic relative humidity sensor," *Optical Engineering,* vol. 41, pp. 1093-1096, 2002.

[43] B. E. J. A. Kharaz, K.F. Hale, L. Roche, K. Bromley, , "Optical fibre relative humidity sensor using a spectrally absorptive material," *SPIE Proceedings of International Conference on Optical Fiber Sensors,* vol. 4185, pp. 370-373, 2000.

[44] S. K. Khijwania, K. L. Srinivasan, and J. P. Singh, "Performance optimized optical fiber sensor for humidity measurement," *Optical Engineering,* vol. 44, pp. 034401-034407, 2005.

[45] H. Limberger, P. Giaccari, and P. Kronenberg, "Influence of humidity and temperature on polyimide-coated fiber Bragg gratings," presented at the Bragg Gratings Photosensitivity and Poling in Glass Waveguides, Stresa, Italy, 2001.

[46] P. Kronenberg, P. K. Rastogi, P. Giaccari, and H. G. Limberger, "Relative humidity sensor with optical fiber Bragg gratings," *Optics Letters,* vol. 27, pp. 1385-1387, 2002/08/15 2002.

[47] H. M. Laylor, S. Calvert, T. Taylor, W. L. Schulz, R. W. Lumsden, and E. Udd, "Fiber optic grating moisture and humidity sensors," presented at the The Smart Structures and Materials: Smart Sensor Technology and Measurement Systems, San Diego, CA, USA, 2002.

[48] W. Kunzler, S. Calvert, and M. Laylor, "Measuring humidity & moisture with fiber optic sensors," presented at the Sixth Pacific Northwest Fiber Optic Sensor Workshop, Oregon, USA, 2003.

[49] T. L. Yeo, M. A. C. Cox, L. F. Boswell, T. Sun, and K. T. V. Grattan, "Optical fiber sensors for monitoring ingress of moisture in structural concrete," *Review of Scientific Instruments,* vol. 77, pp. 055108-055108-7, 2006.

[50] S. Luo, Y. Liu, A. Sucheta, K. M. Evans, and R. V. Tassell, "Applications of LPG fiber optical sensors for relative humidity and chemical-warfare-agents monitoring," *Advanced Sensor Systems and Applications,* pp. 193-204, 2002.

[51] K. M. Tan, C. M. Tay, S. C. Tjin, C. C. Chan, and H. Rahardjo, "High relative humidity measurements using gelatin coated long-period grating sensors," *Sensors and Actuators B: Chemical*, vol. 110, pp. 335-341, 2005.

[52] M. Konstantaki, S. Pissadakis, S. Pispas, N. Madamopoulos, and N. A. Vainos, "Optical fiber long-period grating humidity sensor with poly(ethylene oxide)/cobalt chloride coating," *Applied Optics,* vol. 45, pp. 4567-4571, 2006.

[53] T. Venugopalan, T. L. Yeo, S. Tong, and K. T. V. Grattan, "LPG-Based PVA Coated Sensor for Relative Humidity Measurement," *IEEE Sensors Journal,* vol. 8, pp. 1093-1098, 2008.

[54] E.Udd, "Fiber optic sensor based on the Sagnac interferometer and Passive Ring resonator," *Fiber optic Sensors,* pp. 199-230, 2011.

[55] G.L.Mitchell, *Intensity based and Fabry-Perot Interferometer Sensors*: John Wiley and Sons, 2011.

[56] F. Mitschke, "Fiber-optic sensor for humidity," *Optics Letters,* vol. 14, pp. 967-969, 1989.

[57] G. Meltz, W. W. Morey, and W. H. Glenn, "Formation of Bragg gratings in optical fibers by a transverse holographic method," *Optics Letters,* vol. 14, pp. 823-825, 1989/08/01 1989.

[58] A. D. Kersey and T. A. Berkoff, "Fiber-optic Bragg-grating differential-temperature sensor," *IEEE Photonics Technology Letters,* vol. 4, pp. 1183-1185, 1992.

[59] W. Johnstone, G. Stewart, T. Hart, and B. Culshaw, "Surface plasmon polaritons in thin metal films and their role in fiber optic polarizing devices," *Journal of Lightwave Technology,* vol. 8, pp. 538-544, 1990.

[60] W.Johstone, G.Thursby, B.Culshaw, S.Murray, M.Gill, A. McDonavh, D.Moodie, G.Fawcett, G.Stewart, and K.Mccallion, "A Mutimode approch to optical fiber componebts and sensors," *Proc. SPIE conference on Micro-optics II,* vol. 1506, p. 145, 1991.

[61] M. G. Xu, L. Dong, L. Reekie, J. A. Tucknott, and J. L. Cruz, "Temperature-independent strain sensor using a chirped Bragg grating in a tapered optical fibre," *Electronics Letters,* vol. 31, pp. 823-825, 1995.

[62] R. Aashia, K. V. Madhav, B. Srinivasan, and S. Asokan, "Strain-Temperature Discrimination Using a Single Fiber Bragg Grating," *IEEE Photonics Technology Letters,* vol. 22, pp. 778-780, 2010.

[63] S. W. James, R. P. Tatam, and "Optical fibre long-period grating sensors: characteristics and application,"" *Meas.Sci. Technol,* vol. 14, pp. R49-61, 2003.

[64] V. Rastogi and K. S. Chiang, "Long-period gratings in planar optical waveguides," *Appl. Opt,* vol. 41, pp. 6351-6355, 2002.

[65] H. Kogelnik and C. V. Shank, "Coupled Wave Theory of Distributed Feedback Lasers," *Journal of Applied Physics,* vol. 43, pp. 2327-2335, 1972.

[66] B. G. Kim and E. Garmire, "Comparison between the matrix method and the coupled-wave method in the analysis of Bragg reflector structures," *Journal of the Optical Society of America A,* vol. 9, pp. 132-136, 1992.

[67] M. Yamada and K. Sakuda, "Analysis of almost-periodic distributed feedback slab waveguides via a fundamental matrix approach," *Applied Optics,* vol. 26, pp. 3474-3478, 1987.

[68] P. S. J. Russell, "Bloch Wave Analysis of Dispersion and Pulse Propagation in Pure Distributed Feedback Structures," *Journal of Modern Optics,* vol. 38, pp. 1599-1619, 1991.

[69] J. E. Sipe, L. Poladian, and C. M. d. Sterke, "Propagation through nonuniform grating structures," *Journal of the Optical Society of America A,* vol. 11, pp. 1307-1320, 1994.

[70] H. Kogelnik, "Theory of Optical Waveguides," in *Guided-Wave Optoelectronics*. vol. 26, T. Tamir, Ed., ed: Springer Berlin Heidelberg, 1988, pp. 7-88.

[71] T. Erdogan, "Fiber grating spectra," *Journal of Lightwave Technology,* vol. 15, pp. 1277-1294, 1997.

[72] I. D. Villar, I. R. Matías, F. J. Arregui, and P. Lalanne, "Optimization of sensitivity in Long Period Fiber Gratings with overlay deposition," *Optics Express,* vol. 13, pp. 56-69, 2005.

[73] A. Yariv, "Coupled-mode theory for guided-wave optics," *IEEE Journal of Quantum Electronics,* vol. 9, pp. 919-933, 1973.

[74] D. K. Mynbaev, L. L. Scheiner, and S. Helba, *Fiber-Optic Communications Technology*: Prentice-Hall, Inc Upper Saddle River, New Jersey.

[75] G. P. Agrawal, *Fiber-Optic Communication Systems*: K. Chang, Ed &John Wiley & Sons, Inc., New York, NY, 1997.

[76] E. Hecht, *Optics*: Addison-Wesley, 1998.

[77] T. Erdogan, "Cladding-mode resonances in short- and long-period fiber grating filters," *Journal of the Optical Society of America A,* vol. 14, pp. 1760-1773, 1997.

[78] J. E. Lee, "A Quantitative Analysis of Tunable Long Period Grating Technology and its Application," Ph.D, Electrical Engineering, The Pennsylvania State University, 2007.

[79] C. Caucheteur, F. Lhommé, K. Chah, M. Blondel, and P. Mégret, "Simultaneous strain and temperature sensor based on the numerical reconstruction of polarization maintaining fiber Bragg gratings," *Optics and Lasers in Engineering,* vol. 44, pp. 411-422, 2006.

[80] H.-y. Ling, K.-t. Lau, L. Cheng, and W. Jin, "Viability of using an embedded FBG sensor in a composite structure for dynamic strain measurement," *Measurement,* vol. 39, pp. 328-334, 2006.

[81] H. Tsuda, "Ultrasound and damage detection in CFRP using fiber Bragg grating sensors," *Composites Science and Technology,* vol. 66, pp. 676-683, 2006.

[82] F. Xie, X. Chen, L. Zhang, and M. Song, "Realisation of an effective dual-parameter sensor employing a single fibre Bragg grating structure," *Optics and Lasers in Engineering,* vol. 44, pp. 1088-1095, 2006.

[83] A. V. Koulaxouzidis, M. J. Holmes, C. V. Roberts, and V. A. Handerek, "A shear and vertical stress sensor for physiological measurements using fibre Bragg gratings," in *Proceedings of the IEEE 22nd Annual International Conference of Engineering in Medicine and Biology Society*, 2000, pp. 55-58.

[84] V. Mishra, N. Singh, D. V. Rai, U. Tiwari, G. C. Poddar, S. C. Jain, S. K. Mondal, and P. Kapur, "Fiber Bragg grating sensor for monitoring bone decalcification," *Orthopaedics & Traumatology: Surgery & Research,* vol. 96, pp. 646-651, 2010.

[85] L. Mohanty, S. C. Tjin, D. T. T. Lie, S. E. C. Panganiban, and P. K. H. Chow, "Fiber grating sensor for pressure mapping during total knee arthroplasty," *Sensors and Actuators A: Physical,* vol. 135, pp. 323-328, 2007.

[86] X. Li and F. Prinz, "Embedded Fiber Bragg Grating Sensors in Polymer Structures Fabricated by Layered Manufacturing," *Journal of Manufacturing Processes*, vol. 5, pp. 78-86, 2003.

[87] D. D. Davis, T. K. Gaylord, E. N. Glytsis, and S. C. Mettler, "CO_2 laser-induced long-period fibre gratings: spectral characteristics, cladding modes and polarisation independence," *Electronics Letters,* vol. 34, pp. 1416-1417, 1998.

[88] P. F. Wysocki, J. B. Judkins, R. P. Espindola, M. Andrejco, and A. M. Vengsarkar, "Broad-band erbium-doped fiber amplifier flattened beyond 40 nm using long-period grating filter," *Photonics Technology Letters, IEEE,* vol. 9, pp. 1343-1345, 1997.

[89] L. Zhang, Y. Liu, L. Everall, J. A. R. Williams, and I. Bennion, "Design and realization of long-period grating devices in conventional and high birefringence fibers and their novel applications as fiber-optic load sensors," *IEEE Journal of Selected Topics in Quantum Electronics,* vol. 5, pp. 1373-1378, 1999.

[90] O. Duhem, A. DaCosta, J. F. Henninot, and M. Douay, "Long period copper-coated grating as an electrically tunable wavelength-selective filter," *Electronics Letters,* vol. 35, pp. 1014-1016, 1999.

[91] A. S. Kurkov, M. Douay, O. Duhem, B. Leleu, J. F. Henninot, J. F. Bayon, and L. Rivoallan, "Long-period fibre grating as a wavelength selective polarisation element," *Electronics Letters,* vol. 33, pp. 616-617, 1997.

[92] W. T. Chen and L. A. Wang, "Laser-to-fiber coupling scheme by utilizing a lensed fiber integrated with a long-period fiber grating," *Photonics Technology Letters, IEEE,* vol. 12, pp. 501-503, 2000.

[93] X. J. Gu, "Wavelength-division multiplexing isolation fiber filter and light source using cascaded long-period fiber gratings," *Optics Letters,* vol. 23, pp. 509-510, 1998.

[94] S. Xuewen, T. Allsop, B. Gwandu, Z. Lin, and I. Bennion, "Room-temperature operation of widely tunable loss filter," *Electronics Letters,* vol. 37, pp. 216-218, 2001.

[95] J. N. Kutz, B. J. Eggleton, J. B. Stark, and R. E. Slusher, "Nonlinear pulse propagation in long-period fiber gratings: theory and experiment," *IEEE Journal of Selected Topics in Quantum Electronics,* vol. 3, pp. 1232-1245, 1997.

[96] O. Duhem and M. Douay, "Effect of UV-induced birefringence on long-period-grating coupling characteristics," *Electronics Letters,* vol. 36, pp. 416-417, 2000.

[97] M. de Vries, V. Bhatia, T. D'Alberto, V. Arya, and R. O. Claus, "Photoinduced grating-based optical fiber sensors for structural analysis and control," *Engineering Structures,* vol. 20, pp. 205-210, 1998.

[98] D. M. Costantini, C. A. P. Muller, S. A. Vasiliev, H. G. Limberger, and R. P. SalathÃ©, "Tunable loss filter based on metal-coated long-period fiber grating," *IEEE Photonics Technology Letters,* vol. 11, pp. 1458-1460, 1999.

[99] L. Byeong Ha and J. Nishii, "Notch filters based on cascaded multiple long-period fibre gratings," *Electronics Letters,* vol. 34, pp. 1872-1873, 1998.

[100] Y. Liu, J. A. R. Williams, and I. Bennion, "Optical bend sensor based on measurement of resonance mode splitting of long-period fiber grating," *IEEE Photonics Technology Letters,* vol. 12, pp. 531-533, 2000.

[101] H. J. Patrick, C. Chang, and S. T. Vohra, "Long period fibre gratings for structural bend sensing," *Electronics Letters,* vol. 34, pp. 1773-1775, 1998.

[102] C. Kin Seng, L. Yunqi, N. Mei Nar, and L. Shenping, "Coupling between two parallel long-period fibre gratings," *Electronics Letters,* vol. 36, pp. 1408-1409, 2000.

[103] R. Kashyap, *Fibre Bragg Gratings*: Harcourt Brace & Company, New York, 1999.

[104] V. Grubsky, D. S. Starodubov, and J. Feinberg, "Wavelength-selective coupler and add-drop multiplexer using long-period fiber gratings," in *Optical Fiber Communication Conference*, 2000, pp. 28-30.

[105] D. S. Starodubov, V. Grubsky, and J. Feinberg, "All-fiber bandpass filter with adjustable transmission using cladding-mode coupling," *Photonics Technology Letters, IEEE,* vol. 10, pp. 1590-1592, 1998.

[106] H. J. Patrick, A. D. Kersey, F. Bucholtz, K. J. Ewing, J. B. Judkins, and A. M. Vengsarkar, "Chemical sensor based on long-period fiber grating response to index of refraction," in *Lasers and Electro-Optics*, 1997, pp. 420-421.

[107] C. Trono, F. Baldini, M. Brenci, F. Chiavaioli, and M. Mugnaini, "Flow cell for strain- and temperature-compensated refractive index measurements by means of cascaded optical fibre long period and Bragg gratings," *Measurement Science and Technology,* vol. 22, p. 075204, 2011.

[108] J. Joo-Nyung, K. Se Yoon, K. Sun-Wook, and K. Min-Sung, "Temperature insensitive long-period fibre gratings," *Electronics Letters,* vol. 35, pp. 2134-2136, 1999.

[109] Y. Han, C. S. Kim, and U. C. Paek, "Performance enhancement of long period fibre gratings for strain and temperature sensing," *IEICE Trans. Electron,* vol. E83-C, pp. 263-286, 2000.

[110] K. O. Hill and G. Meltz, "Fiber Bragg grating technology fundamentals and overview," *Journal of Lightwave Technology,* vol. 15, pp. 1263-1276, 1997.

[111] V. Bhatia, D. Campbell, R. O. Claus, and A. M. Vengsarkar, "Simultaneous strain and temperature measurement with long-period gratings,," *Optics Letters,* vol. 22, pp. 648-650, 1997.

[112] Y. Koyamada, "Numerical analysis of core-mode to radiation-mode coupling in long-period fiber gratings," *IEEE Photonics Technology Letters,* vol. 13, pp. 308-310, 2001.

[113] R. Hou, Z. Ghassemlooy, A. Hassan, C. Lu, and K. P. Dowker, "Modelling of long-period fibre grating response to refractive index higher than that of cladding," *Meas. Sci. Technol,* vol. 12, 2001.

[114] S. Xuewen, Z. Lin, and I. Bennion, "Sensitivity characteristics of long-period fiber gratings," *Journal of Lightwave Technology,* vol. 20, pp. 255-266, 2002.

[115] J. A. Besley, T. Wang, and L. Reekie, "Fiber cladding mode sensitivity characterization for long-period gratings," *Journal of Lightwave Technology,* vol. 21, pp. 848-853, 2003.

[116] K.-W. Chung and S. Yin, "Analysis of a widely tunable long-period grating by use of an ultrathincladding layer and higher-ordercladding mode coupling," *Optics Letters,* vol. 29, pp. 812-814, 2004.

[117] X. Daxhelet and M. Kulishov, "Theory and practice of long-period gratings: when a loss becomes a gain," *Optics Letters,* vol. 28, pp. 686-688, 2003.

[118] R. Singh, H. Kumar, and E. K. Sharma, "Design of long-period gratings: Necessity of a three-layer fiber geometry for cladding mode characteristics," *Microwave and Optical Technology Letters,* vol. 37, pp. 45-49, 2003.

[119] I. M. Ishaq, A. Quintela, S. W. James, G. J. Ashwell, J. M. Lopez-Higuera, and R. P. Tatam, "Modification of the refractive index response of long period gratings using thin film overlays," *Sensors and Actuators B: Chemical,* vol. 107, pp. 738-741, 2005.

[120] Z. Wang, J. Heflin, R. Stolen, and S. Ramachandran, "Analysis of optical response of long period fiber gratings to nm-thick thin-film coating," *Optics Express,* vol. 13, pp. 2808-2813, 2005.

[121] I. Del Villar, I. R. Matias, and F. J. Arregui, "Influence on cladding mode distribution of overlay deposition on long-period fiber gratings," *Journal of the Optical Society of America A,* vol. 23, pp. 651-658, 2006.

[122] Q. Chen, J. Lee, M. Lin, Y. Wang, S. Yin, Q. Zhang, and K. M. Reichard, "Investigation of Tuning Characteristics of Electrically Tunable Long-Period Gratings With a Precise Four-Layer Model," *Journal of Lightwave Technology,* vol. 24, p. 2954, 2006/07/01 2006.

[123] Y. Jian, Y. Li, X. Chang-Qing, and L. Yingfu, "Optimization of Cladding-Structure-Modified Long-Period-Grating Refractive-Index Sensors," *Journal of Lightwave Technology,* vol. 25, pp. 372-380, 2007.

[124] H. Hochreiner, M. Cada, and P. D. Wentzell, "Modeling the Response of a Long-Period Fiber Grating to Ambient Refractive Index Change in Chemical Sensing Applications," *Journal of Lightwave Technology,* vol. 26, pp. 1986-1992, 2008.

[125] D. Edward, V. Reeta, S. Mikko, A. Sami, Z. Lin, and B. Ian, "Sol–gel derived coating applied to long-period gratings for enhanced refractive index sensing properties," *Journal of Optics A: Pure and Applied Optics,* vol. 11, p. 015501, 2009.

[126] J. Mu and W.-P. Huang, "Analytical Expressions for Radiation Effects on Guided Mode Propagation in Long Period Gratings," *Journal of Lightwave Technology,* vol. 29, pp. 997-1002, 2011.

[127] D. C. Bownass, J. S. Barton, and J. D. C. Jones, "Detection of high humidity by optical fibre sensing at telecommunications wavelengths," *Optics Communications,* vol. 146, pp. 90-94, 1998.

[128] C. Bariáin, I. R. Matías, F. J. Arregui, and M. López-Amo, "Optical fiber humidity sensor based on a tapered fiber coated with agarose gel," *Sensors and Actuators B: Chemical,* vol. 69, pp. 127-131, 2000.

[129] T. Venugopalan, T. Sun, and K. T. V. Grattan, "Long period grating-based humidity sensor for potential structural health monitoring," *Sensors and Actuators A: Physical,* vol. 148, pp. 57-62, 2008.

[130] D. Fuxin, W. Lutang, F. Nian, and H. Zhaoming, "Experimental study on humidity sensing using a FBG sensor with polyimide coating," in *Communications and Photonics Conference and Exhibition*, 2010, pp. 280-281.

[131] R. Aneesh and S. K. Khijwania, "Titanium dioxide nanoparticle based optical fiber humidity sensor with linear response and enhanced sensitivity," *Applied Optics,* vol. 51, pp. 2164-2171,2012.

[132] D. Viegas, M. Hernae, J. Goicoechea, J. L. Santos, F. M. Araujo, F. Arregui, and I. R. Matias, "Simultaneous Measurement of Humidity and Temperature Based on an SiO_2 Nanospheres Film Deposited on a Long-Period Grating In-Line With a Fiber Bragg Grating," *Sensors Journal, IEEE,* vol. 11, pp. 162-166, 2011.

[133] M.-Y. Fu, G.-R. Lin, W.-F. Liu, and C. Wu, "Fiber-optic humidity sensor based on an air-gap long period fiber grating," *Optical Review,* vol. 18, pp. 93-95, 2011/01/01 2011.

[134] W. Zhang, D. J. Webb, and G. Peng, "Investigation Into Time Response of Polymer Fiber Bragg Grating Based Humidity Sensors," *Journal of Lightwave Technology,* vol. 30, pp. 1090-1096, 2012.

[135] S. Zheng, Y. Zhu, and S. Krishnaswamy, "Fiber humidity sensors with high sensitivity and selectivity based on interior nanofilm-coated photonic crystal fiber long-period gratings," *Sensors and Actuators B: Chemical,* vol. 176, pp. 264-274, 2013.

[136] L. Alwis, T. Sun, and K. V. Grattan, "Analysis of Polyimide-Coated Optical Fiber Long-Period Grating-Based Relative Humidity Sensor," *IEEE Sensors Journal,* vol. 13, pp. 767-771, 2013.

[137] A. P. Russell and K. S. Fletcher, "Optical sensor for the determination of moisture," *Analytica Chimica Acta,* vol. 170, pp. 209-216, 1985.

[138] K. Ogawa, S. Tsuchiya, H. Kawakami, and T. Tsutsui, "Humidity-sensing effects of optical fibres with microporous SiO_2 cladding," *Electronics Letters,* vol. 24, pp. 42-43, 1988.

[139] Q. Zhou, M. R. Shahriari, D. Kritz, and G. H. Sigel, "Porous fiber-optic sensor for high-sensitivity humidity measurements," *Analytical Chemistry,* vol. 60, pp. 2317-2320, 1988.

[140] A. Kharaz and B. E. Jones, "A Distributed Fibre Optic Sensing System for Humidity Measurement," in *Applications of Photonic Technology*, G. Lampropoulos, J. Chrostowski, and R. Measures, Eds., ed: Springer US, 1995, pp. 335-338.

[141] B. D. Gupta and Ratnanjali, "A novel probe for a fiber optic humidity sensor," *Sensors and Actuators B: Chemical,* vol. 80, pp. 132-135, 2001.

[142] R. Jindal, S. Tao, J. P. Singh, and P. S. Gaikwad, "High dynamic range fiber optic relative humidity sensor," *Optical Engineering,* vol. 41, pp. 1093-1096, 2002.

[143] S. Muto, O. Suzuki, T. Amano, and M. Morisawa, "A plastic optical fibre sensor for real-time humidity monitoring," *Meas. Sci. Technol.* , vol. 14, pp. 746-750, 2003.

[144] A. Gaston, I. Lozano, F. Perez, F. Auza, and J. Sevilla, "Evanescent wave optical-fiber sensing (temperature, relative humidity, and pH sensors)," *IEEE Sensors Journal,* vol. 3, pp. 806-811, 2003.

[145] A. Alvarez-Herrero, H. Guerrero, and D. Levy, "High-sensitivity sensor of low relative humidity based on overlay on side-polished fibers," *IEEE Sensors Journal,* vol. 4, pp. 52-56, 2004.

[146] J. M. Corres, J. Bravo, I. R. Matias, and F. J. Arregui, "Nonadiabatic tapered single-mode fiber coated with humidity sensitive nanofilms," *IEEE Photonics Technology Letters,* vol. 18, pp. 935-937, 2006.

[147] L. Zhang, F. Gu, J. Lou, X. Yin, and L. Tong, "Fast detection of humidity with a subwavelength-diameter fiber taper coated with gelatin film," *Optics Express,* vol. 16, pp. 13349-13353, 2008.

[148] A. Vijayan, M. Fuke, R. Hawaldar, M. Kulkarni, D. Amalnerkar, and R. C. Aiyer, "Optical fibre based humidity sensor using Co-polyaniline clad," *Sensors and Actuators B: Chemical,* vol. 129, pp. 106-112, 2008.

[149] S. K. Shukla, A. Tiwari, G. K. Parashar, A. P. Mishra, and G. C. Dubey, "Exploring fiber optic approach to sense humid environment over nano-crystalline zinc oxide film," *Talanta,* vol. 80, pp. 565-571, 2009.

[150] M. V. Fuke, P. Kanitkar, M. Kulkarni, B. B. Kale, and R. C. Aiyer, "Effect of particle size variation of Ag nanoparticles in Polyaniline composite on humidity sensing," *Talanta,* vol. 81, pp. 320-326, 2010.

[151] Z. Yu, J. Yongxing, L. Houhui, D. Xinyong, and W. Jianfeng, "All-fiber-optic sensor for relative humidity measurement," in *International Conference on Electronics and Optoelectronics*, 2011, pp. V2-83-V2-86.

[152] Y. Liu, Y. Zhang, H. Lei, J. Song, H. Chen, and B. Li, "Growth of well-arrayed ZnO nanorods on thinned silica fiber and application for humidity sensing," *Optics Express,* vol. 20, pp. 19404-19411, 2012.

[153] L. Xia, L. Li, W. Li, T. Kou, and D. Liu, "Novel optical fiber humidity sensor based on a no-core fiber structure," *Sensors and Actuators A: Physical,* vol. 190, pp. 1-5, 2013.

[154] S. Tao, C. B. Winstead, R. Jindal, and J. P. Singh, "Optical-fiber sensor using tailored porous sol-gel fiber core," *IEEE Sensors Journal,* vol. 4, pp. 322-328, 2004.

[155] M. Hernáez, C. R. Zamarreño, I. R. Matías, and F. J. Arregui, "Optical fiber humidity sensor based on surface plasmon resonance in the infrared region," *Journal of Physics: Conference Series* vol. 178, 2009.

[156] J. Estella, P. de Vicente, J. C. Echeverría, and J. J. Garrido, "A fibre-optic humidity sensor based on a porous silica xerogel film as the sensing element," *Sensors and Actuators B: Chemical,* vol. 149, pp. 122-128, 2010.

[157] P. J. Rivero, A. Urrutia, J. Goicoechea, and F. J. Arregui, "Optical fiber humidity sensors based on Localized Surface Plasmon Resonance (LSPR) and Lossy-mode resonance (LMR) in overlays loaded with silver nanoparticles," *Sensors and Actuators B: Chemical,* vol. 173, pp. 244-249, 2012.

[158] M. Y. Noor, N. Khalili, I. Skinner, and G. D. Peng, "Optical relative humidity sensor based on a hollow core-photonic band gap fiber," *Measurement Science and Technology* vol. 23, pp. 085103-085110, 2012.

[159] L. Alwis, T.Sun, and K.T.V.Grattan, "Optical Fiber based sensor technology for humidity and moisture measurement:Review of recent progress," vol. 46, pp. 4052-4074, 2013.

[160] K. H. Wanser, K. F. Voss, and A. D. Kersey, "Novel fiber devices and sensors based on multimode fiber Gragg gratings," *Proc SPIE-Int Soc Opt Eng,* vol. 2360, pp. 265-268., 1994.

[161] T. Mizunami, T. V. Djambova, T. Niiho, and S. Gupta, "Bragg gratings in multimode and few-mode optical fibers," *Journal of Lightwave Technology,* vol. 18, pp. 230-235, 2000.

[162] W. Zhao and R. O. Claus, "Optical fiber grating sensors in multimode fibers," *Smart Materials and Structures,* vol. 9, p. 212, 2000.

[163] T. Szkopek, V. Pasupathy, J. E. Sipe, and P. W. E. Smith, "Novel multimode fiber for narrow-band Bragg gratings," *IEEE Journal of Selected Topics in Quantum Electronics,* vol. 7, pp. 425-433, 2001.

[164] Y. Sun, T. Szkopek, and P. W. E. Smith, "Demonstration of narrowband high-reflectivity Bragg gratings in a novel multimode fiber," *Optics Communications,* vol. 223, pp. 91-95, 2003.

[165] T. Liu, D. Wang, R. Raenaei, X. Chen, L. Zhang, and I. Bennion, "A low-cost multimode fiber Bragg grating sensor system," 2005, pp. 54-61.

[166] L. Changgui and Y. Cui, "Fiber Bragg grating spectra in multimode optical fibers," *Journal of Lightwave Technology,* vol. 24, pp. 598-604, 2006.

[167] J. Lim, Y. Qingping, B. E. Jones, and P. R. Jackson, "Strain and temperature sensors using multimode optical fiber Bragg gratings and correlation signal processing," *IEEE Transactions on Instrumentation and Measurement,* vol. 51, pp. 622-627, 2002.

[168] X. Sang, P. L. Chu, C. Yu, and R. Lai, "Novel growth phenomena in fibre Bragg gratings under low irradiation power," *Optics Communications,* vol. 251, pp. 94-99, 2005.

[169] X. Sang, P. L. Chu, C. Yu, and R. Lai, "Growth dynamics of Bragg gratings in multimode optical fibre," *Optics Communications,* vol. 260, pp. 131-135, 2006.

[170] X. Sang, C. Yu, B. Yan, T. Mayteevarunyoo, K. Wang, and N. Lu, "Experimental investigation on chemical sensor based on a multimode fiber Bragg grating," *Microwave and Optical Technology Letters,* vol. 48, pp. 1739-1741, 2006.

[171] J. Albert, L.-Y. Shao, and C. Caucheteur, "Tilted fiber Bragg grating sensors," *Laser & Photonics Reviews,* vol. 7, pp. 83-108, 2013.

[172] A. Singh and D. Engles, "Calculation of cladding modes using both two layer and three layer geometry in LPFG," *Optik - International Journal for Light and Electron Optics,* vol. 124, pp. 5042-5045, 2013.

[173] G.-D. Wang and Y. Wang, "Refractive index sensitivity analysis of long period fiber grating by new transfer matrix method," *Optik - International Journal for Light and Electron Optics,* vol. 124, pp. 1767-1769, 2013.

[174] R. Sing, Sunanda, and E. K. Sharma, "Propagation characteristics of single-mode optical fibers with arbitrary complex index profiles: a direct numerical approach," *IEEE Journal of Quantum Electronics,* vol. 37, pp. 635-640, 2001.

[175] S. S. Wang and R. Magnusson, "Theory and applications of guided-mode resonance filters," *Applied Optics,* vol. 32, pp. 2606-2613, 1993.

[176] M. Das, "Study on synthesis and applications of long period grating," PhD, Department of physics, IIT delhi, 2003.

[177] S. Chaubey, S. Kher, and S. M. Oak, "Radiation and taper tuning of Long Period Grating for high sensitivity strain measurement," in *Fibre and Optical Passive Components (WFOPC), 2011 7th Workshop on*, 2011, pp. 1-4.

[178] S. M. Tripathi, W. J. Bock, A. Kumar, and P. Mikulic, "Temperature insensitive high-precision refractive-index sensor using two concatenated dual-resonance long-period gratings," *Optics Letters,* vol. 38, pp. 1666-1668, 2013.

[179] A.W.Synder and J. D. Love:. *Optical waveguide theory*: Chapman and Hall, London,, 1984.

[180] K. O. Hill, Y. Fujii, D. C. Johnson, and B. S. Kawasaki, "Photosensitivity in optical fiber waveguides: Application to reflection filter fabrication," *Applied Physics Letters,* vol. 32, pp. 647-649, 1978.

[181] S. Ness and P. R. Herman, "157-nm photosensitivity in germanosilicate planar waveguides," in *Lasers and Electro-Optics, 1999. CLEO '99. Summaries of Papers Presented at the Conference on*, 1999, pp. 76-77.

[182] J. Albert, Y. Hibino, M. Kawachi, B. Malo, F. Bilodeau, D. C. Johnson, and K. O. Hill, "Photosensitivity in Ge-doped silica optical waveguides and fibers with 193-nm light from an ArF excimer laser," *Optics Letters,* vol. 19, pp. 387-389, 1994.

[183] R. M. Atkins and R. P. Espindola, "Photosensitivity and grating writing in hydrogen loaded germanosilicate core optical fibers at 325 and 351 nm," *Applied Physics Letters,* vol. 70, pp. 1068-1069, 1997.

[184] F. Bilodeau, T. F. Morse, A. Kilian, D. C. Johnson, B. Malo, L. Reinhart, K. A. Vineberg, and K. O. Hill, "Ultraviolet-light photosensitivity in Er^{3+} Ge-doped optical fiber," *Optics Letters,* vol. 15, pp. 1138-1140,1990.

[185] D. L. Williams, B. J. Ainslie, J. R. Armitage, R. Kashyap, and R. Campbell, "Enhanced UV photosensitivity in boron codoped germanosilicate fibres," *Electronics Letters,* vol. 29, p. 45, 1993.

[186] L. Dong, J. L. Cruz, L. Reekie, M. G. Xu, and D. N. Payne, "Enhanced photosensitivity in tin-codoped germanosilicate optical fibers," *Photonics Technology Letters, IEEE,* vol. 7, pp. 1048-1050, 1995.

[187] L. Dong, L. Reekie, J. L. Cruz, and D. N. Payne, "Grating formation in a phosphorus-doped germanosilicate fiber," in *Optical Fiber Communication Conference*, San Jose, California, 1996, p. TuO2.

[188] M. M. Broer, A. J. Bruce, and W. H. Grodkiewicz, "Photoinduced refractive-index changes in several Eu3+-, Pr3+-, and Er3+-doped oxide glasses " *Physical Review B,* vol. 45, pp. 7077-7083, 1992.

[189] K.O.Hill, B.Malo, F. Bilodeau, D. C. Johnson, and T. F. Morse, "Photosensitivity in Eu3+: Al2O3 doped core fiber: preliminary results and applications to mode converters," *Conference on Optical fiber Communication, Technical digest Series (OSA, Washington, DC),* vol. 14, p. 14, 1991.

[190] G. M. Williams, T. Tsai, C. I. Merzbacher, and E. J. Friebele, "Photosensitivity of rare-earth-doped ZBLAN fluoride glasses," *Journal of Lightwave Technology,* vol. 15, pp. 1357-1362, 1997.

[191] P. J. Lemaire, R. M. Atkins, V. Mizrahi, and W. A. Reed, "High pressure H2 loading as a technique for achieving ultrahigh UV photosensitivity and thermal sensitivity in GeO2 doped optical fibres," *Electronics Letters,* vol. 29, pp. 1191-1193, 1993.

[192] F. Bilodeau, Y. Hibino, M. Abe, B. Malo, J. Albert, M. Kawachi, D. C. Johnson, and K. O. Hill, "Photosensitization of optical fiber and silica-on-silicon/silica waveguides," *Optics Letters,* vol. 18, pp. 953-955, 1993/06/15 1993.

[193] D. P. Hand and P. S. J. Russell, "Photoinduced refractive-index changes in germanosilicate fibers," *Optics Letters,* vol. 15, pp. 102-104, 1990/01/15 1990.

[194] M. G. Sceats, G. R. Atkins, and S. B. Poole, "Photolytic Index Changes in Optical Fibers," *Annual Review of Materials Science,* vol. 23, pp. 381-410, 1993.

[195] D. L. Williams, B. J. Ainslie, R. Kashyap, G. D. Maxwell, J. R. Armitage, R. J. Campbell, and R. R. Wyatt, "Photosensitive index changes in germania-doped silica glass fibers and waveguides," 1993, pp. 55-68.

[196] J. P. Bernardin and N. M. Lawandy, "Dynamics of the formation of Bragg gratings in germanosilicate optical fibers," *Optics Communications,* vol. 79, pp. 194-199, 1990.

[197] M. G. Sceats and S. B. Poole, "Stress-relief-The mechanism of photorefractive index control in fiber cores," *Aust.Conf. Opt. Fiber Technol.,* pp. 302-305, 1991.

[198] M. G. Sceats and P. A. Krug, "Photoviscous annealing: dynamics and stability of photorefractivity in optical fiber," in *Proc. SPIE*, 1993, pp. 113-120.

[199] P. Y. Fonjallaz, F. Cochet, B. Leuenberger, H. G. Limberger, and R. P. Salathé, "Tension increase correlated to refractive-index change in fibers containing UV-written Bragg gratings," *Optics Letters,* vol. 20, pp. 1346-1348,1995.

[200] H. G. Limberger, P. Y. Fonjallaz, R. P. Salathé, and F. Cochet, "Compaction- and photoelastic-induced index changes in fiber Bragg gratings," *Applied Physics Letters,* vol. 68, pp. 3069-3071, 1996.

[201] R. M. Atkins and V. Mizrahi, "Observations of changes in UV absorption bands of singlemode germanosilicate core optical fibres on writing and thermally erasing refractive index gratings," *Electronics Letters,* vol. 28, pp. 1743-1744, 1992.

[202] K. O. Hill, B. Malo, F. Bilodeau, and D. C. Johnson, "Photosensitivity in Optical Fibers," *Annual Review of Materials Science,* vol. 23, pp. 125-157, 1993.

[203] D.Williams, *Molecular Physics*: Academic Press, 1961.

[204] M. V. Bazylenko, D. Moss, and J. Canning, "Complex photosensitivity observed in germanosilica planar waveguides," *Optics Letters,* vol. 23, pp. 697-699,1998.

[205] C. Fiori and R. A. B. Devine, "Ultraviolet irradiation induced compaction and photo etching in amorphous, thermal SiO2," *Proc. Mater. Res. Soc. Symp.* , vol. 61, pp. 187-195, 1986.

[206] M. Rochette, M. Guy, S. LaRochelle, J. Lauzon, and F. Trepanier, "Gain equalization of EDFA's with Bragg gratings," *Photonics Technology Letters, IEEE,* vol. 11, pp. 536-538, 1999.

[207] K. Hyo Sang, Y. Seok Hyun, K. Hyang-Kyun, P. Namkyoo, and K. Byoung-Yoon, "Actively gain-flattened erbium-doped fiber amplifier over 35 nm by using all-fiber acoustooptic tunable filters," *IEEE Photonics Technology Letters,* vol. 10, pp. 790-792, 1998.

[208] D. Krcmarik, R. Slavik, M. Karasek, and M. Kulishov, "Theoretical and Experimental Analysis of Long-Period Fiber Gratings Made Directly Into Er-Doped Active Fibers," *Journal of Lightwave Technology,* vol. 27, pp. 2335-2342, 2009.

[209] A. Tomita and P. J. Lemaire, "Hydrogen-induced loss increases in germanium-doped single-mode optical fibres: long-term predictions," *Electronics Letters,* vol. 21, pp. 71-72, 1985.

[210] E. Salik, D. S. Starodubov, V.Grubsky, and J.Feinberg, " Increase of photosensitivity in germania doped silica fiber for future optical networks," *Optical fiber Communication Conference,* p. TuH5, 2000.

[211] G. D. Maxwell, R. Kashyap, B. J. Ainslie, D. L. Williams, and J. R. Armitage, "UV written 1.5 mu m reflection filters in single mode planar silica guides " *Electronics Letters,* vol. 28, pp. 2106-2107, 1992.

[212] P. J. Lemaire, A. M. Vengsarkar, W. A. Reed, V. Mizrahi, and K. S. Kranz, "Refractive-index changes in optical fibers sensitized with molecular hydrogen," in *Conference on Optical Fiber Communication*, San Jose, California, 1994, p. TuL1.

[213] V. M. T.Erdogan, P.J.Lemaire and D.Monroe, "Decay of ultraviolet induced fiber bragg grating," *Journal of Applied Physics,* pp. 73-80, 1994.

[214] P. J. Lemaire, V. Mizrahi, R. M. Atkins, and K. S. Kranz, "High-temperature stability of phase gratings in GeO2-doped optical fibers," in *Conference on Optical Fiber Communication/International Conference on Integrated Optics and Optical Fiber Communication*, San Jose, California, 1993, p. FA7.

[215] P. J. Lemaire and T. Ergodan, "Hydrogen–enhanced UV photosensitivity of optical fibers: mechanisms and reliability," *Proc.OSA Topical Meeting on*

photosensitivity and Quadratic Nonlinearity in glass waveguides, vol. SuA4, p. 78, 1995.

[216] A. A. Abramov, A. Hale, R. S. Windeler, and T. A. Strasser, "Widely tunable long-period fibre gratings," *Electronics Letters,* vol. 35, pp. 81-82, 1999.

[217] V. I. Karpov, M. V. Grekov, E. M. Dianov, K. M. Golant, S. A. Vasiliev, O. I. Medvedkov, and R. R. Khrapko, "Mode-field converters and long-period gratings fabricated by thermo-diffusion in nitrogen-doped silica-core fibers," in *Optical Fiber Communication Conference and Exhibit, Technical Digest*, 1998, pp. 279-280.

[218] S. Y. Liu, H. Y. Tam, and M. S. Demokan, "Low-cost microlens array for long-period grating fabrication," *Electronics Letters,* vol. 35, pp. 79-81, 1999.

[219] L. Huang and A. Asundi, "Improvement of least-squares integration method with iterative compensations in fringe reflectometry," *Applied Optics,* vol. 51, pp. 7459-7465, 2012.

[220] J. W. Fleming, "Material dispersion in lightguide glasses," *Electronics Letters,* vol. 14, pp. 326-328, 1978.

[221] Y. Zhu, "Realization of Chirped Fiber Bragg Gratings by Strain Gradients and their Applications for Fiber Dispersion Compensation and Sensors," M.Phil, Rand Afrikaans University, South Africa, 1998.

[222] A. Cusano, A. Iadicicco, P. Pilla, L. Contessa, S. Campopiano, A. Cutolo, and M. Giordano, "Mode transition in high refractive index coated long period gratings," *Optics Express,* vol. 14, pp. 19-34, 2006.

[223] A. Cusano, A. Iadicicco, P. Pilla, L. Contessa, S. Campopiano, A. Cutolo, and M. Giordano, "Cladding mode reorganization in high-refractive-index-coated long-period gratings: effects on the refractive-index sensitivity," *Optics Letters,* vol. 30, pp. 2536-2538, 2005.

[224] I. Del Villar, M. Achaerandio, I. R. Matías, and F. J. Arregui, "Deposition of overlays by electrostatic self-assembly in long-period fiber gratings," *Optics Letters,* vol. 30, pp. 720-722, 2005.

[225] E. Anemogiannis, E. N. Glytsis, and T. K. Gaylord, "Transmission Characteristics of Long-Period Fiber Gratings Having Arbitrary Azimuthal/Radial Refractive Index Variations," *Journal of Lightwave Technology,* vol. 21, p. 218, 2003.

[226] D. B. Stegall and T. Erdogan, "Leaky cladding mode propagation in long-period fiber grating devices," *IEEE Photonics Technology Letters,* vol. 11, pp. 343-345, 1999.

[227] J. Yoonchan, L. Byoungho, J. Nilsson, and D. J. Richardson, "A quasi-mode interpretation of radiation modes in long-period fiber gratings," *IEEE Journal of Quantum Electronics,* vol. 39, pp. 1135-1142, 2003.

[228] S. Barai and A. Sharma, "Inverse Algorithm With Built-In Spatial Filter to Obtain the 2-D Refractive Index Profile of Optical Waveguides From the Propagating Mode Near-Field Profile," *Journal of Lightwave Technology,* vol. 27, pp. 1514-1521, 2009.

[229] A. Kumar, V. Rastogi, A. Agrawal, and B. M. A. Rahman, "Birefringence analysis of segmented cladding fiber," *Applied Optics,* vol. 51, pp. 3104-3108, 2012.

[230] H. J. Patrick, A. Kersey, and F. Bucholtz, "Analysis of the response of long period fiber gratings to external index of refraction," *Journal of Lightwave Technology,* vol. 16, pp. 1606-1612, 1998.

[231] I. Del Villar, I. Matias, F. Arregui, and R. Claus, "Analysis of one-dimensional photonic band gap structures with a liquid crystal defect towards development of fiber-optic tunable wavelength filters," *Optics Express,* vol. 11, pp. 430-436, 2003.

[232] I. D. V. Fernández, "Doctorate thesis on Theoretical analysis and fabrication of nanostructures with Electrostatic Self-Assembly Monolayer process," *Universidad Pública de Navarra, Pamplona, Navarra, Spain,* 2006.

[233] P. Yeh, *Optical Waves in Layered media*: Wiley,New York, 1988.

[234] T. A. S. T. F. Stoica, M. Zaharescu, M. Popescu, F. Sava, N. Popescu-Pogrion, L. Frunza, "Characterization of ito thin films prepared by spinning deposition starting from a sol-gel process," *Journal of Optoelectronics and Advanced Materials,* vol. 2, pp. 684-688, 2000.

[235] M.K.M Ali, O. S. H. K. Ibrahim, M.H. Eisa, M.G. Faraj, and F. Azhari, "Deposited Indium Tin Oxide (ITO) Thin Films ByDc- Magnetron Sputtering On Polyethylene Terephthalate Substrate (Pet)," *Rom.Jouranl of Physics, Bucharest,* vol. 56, pp. 730-741, 2011.

[236] [Online]. Available: en.wikipedia.org/wiki/Electrical resistance and conductance

[237] T. K. G. Dabir S Viswanath, Dasika H.L.Parsad, Nidamarty V.K Dutt,Kalipatnapu Y Rani, *Viscosity of Liquids:Theory,Estimation,Experiment and Data*: Springer, 2007.

[238] H. J. Patrick, A. D. Kersey, and F. Bucholtz, "Analysis of the response of long period fiber gratings to external index of refraction," *Lightwave Technology, Journal of,* vol. 16, pp. 1606-1612, 1998.

[239] R. Kashyap, *Fiber Bragg Gratings*: Academic Press, 1999.

[240] *Fiber Bragg Grating*. Available: en.wikipedia.org/wiki/Fiber_Bragg_grating

[241] Nahar Singh, S. C. Jain, and A. K. Aggarwal, "Fabrication of In-Fiber Bragg Gratings using phase mask technique," presented at the National conference on Advances in contemporary physics and energy, 2002.

[242] O. V. Ivanov, "Near-field effects in fabrication of fiber Bragg gratings using phase masks," *Optics Communications,* vol. 229, pp. 167-172, 2004.

[243] A. Kersey, M. A. Davis, H. J. Patrick, M. Leblanc, K. P. Koo, C. G. Askins, M. A. Putnam, and E. J. Friebele, "Fiber grating sensors," *Lightwave Technology, Journal of,* vol. 15, pp. 1442-1463, 1997.

[244] J. A. Ferrari, E. Garbusi, E. M. Frins, and C. s. D. Perciante, "Optical current sensor using a self-induced light source," *Optical Engineering,* vol. 43, pp. 2120-2123, 2004.

[245] Y. W. Lee, I. Yoon, and B. Lee, "A simple fiber-optic current sensor using a long-period fiber grating inscribed on a polarization-maintaining fiber as a sensor demodulator," *Sensors and Actuators A: Physical,* vol. 112, pp. 308-312, 2004.

[246] G. Frosio and R. Dändliker, "Reciprocal reflection interferometer for a fiber-optic Faraday current sensor," *Applied Optics,* vol. 33, pp. 6111-6122,1994.

[247] Y. Zhao, Q.-y. Meng, and K. Chen, "Novel current measurement method based on fiber Bragg grating sensor technology," *Sensors and Actuators A: Physical,* vol. 126, pp. 112-116, 2006.

[248] R. Castillo-Rincón, J. J. Flores-Prieto, M. E. Baltazar-Lopez, and E. F. Zenteno-Cardozo, "Temperature Sensor Using Fiber Optic Fizeau Homodyne Interferometer," *Experimental Techniques,* vol. 36, pp. 50-59, 2012.

[249] C.-H. Cheng, M.-H. Chen, and W.-F. Liu, "Measurement of AC current using a superstructure fiber grating," *Microwave and Optical Technology Letters,* vol. 50, pp. 1168-1171, 2008.

[250] K.S.Bhatia, R S Kaler, T.S Kamal, "Simulative analysis of intergrated DWDM and MIMO-OFDM system with OADM", *OPTIK-International journal for Light and electron Optics,* 124(2), 117-121

[251] R.Randhawa, S.Singh, J.S Sohal, R.S Kaler, "Wavelength converter using semicondutor optical amplifier Mach-Zehnder interferometer based on XPM at 40 Gb/s for future transport networks", *Fiber and Intergarted Optics,* 28(2), 154-168

APPENDIX-I

The simple schematic of the optical system is illustrated in Figure 4.6.The main components are identified and discussed in further detail in the following section.

Optical components

1. Laser

The laser used in the system is an excimer set with a krypton fluorine transition for a central lasing wavelength of 248 nm (Excimer laser).

2. PDL Unit

The PDL control unit consists of a high power polarizing beam splitter cube (PBS) which serves to split the S & P polarizations. P polarization is used to ensure low PDL gratings.

3. Beam Tap

The beam tap (BS) is used to tap a small portion of the UV unwanted S polarization beam in order to provide a feedback loop for preservation of the laser beam position.

4. Beam Feedback Control

(M1) also serves as an actively controlled redirecting mirror and thus is mounted on a double axis tilting mount which can be controlled by the feedback received from the UV beam analyzer (BA). The feedback loop is controlled entirely by the software.

5. Beam Dump

The beam dump (BD) captures all the unwanted S radiation from the PDL unit and disposes of it safely.

6. Optical Shutter

The computer controlled optical shutter (OS) allows for the rapid triggering of the UV laser beam for grating writing.

7. Power control unit

The power control unit (PCU) allows for precise control of the power of the laser beam incident on the fiber during the grating writing process. The power control unit utilizes a high power laser polarizing cube beam splitter which is mounted in a computer controlled rotation stage. The laser beam power can be varied anywhere from 0 to 100% simply by turning the cube over a 90°range.

8. 450 mm Translation Stage (Main Axis)

The 450 mm translation stage allows for long gratings to be written using the scanning or stepping modes. The stage is set to fix when static or interferometer mode is deployed.

9. First Flipper Mirror

The state mode of the first flipper mirror (FM1) defines whether the grating writing station is in static or not. If the mirror is in the optical path, then the system is in static mode. This flipper is activated when the 'Lens axis' module is moved in OUT position.

10. Beam Expander Lens Arrangement

If static writing mode is chosen, then the laser beam passes through a 5X beam expander which is essential in ensuring that the beam is large and uniform enough for writing good wideband filters. The beam expander lens arrangement consists of a Plano-concave lens (L3) with a focal length of 25 mm in series with a Plano-convex lens (L4) with a focal length of 125 mm.

11. Cylindrical Focusing Lens

The cylindrical focusing lens focuses the UV laser beam into the plane of the fiber and permits efficient grating writing. In this system two focusing lenses are needed. In interferometric mode the cylindrical lens (LF2) has a focal length of 200 mm. In static, scanning and stepping mode the cylindrical lens (LF1) has a focal length of 100 mm.

12. Amplitude Mask

The amplitude masks permits the user to reproduce a variable index change as a function of physical position in the fiber. The position of the amplitude mask can be controlled by software using amplitude mask axis.

13. Phase Mask

The phase mask (PM1) generates the interference pattern which is necessary to produce fiber gratings. In interferometric mode a phase mask (PM2) is used to split the beam in two parts.

14. Second Flipper Mirror

The state of the second mirror (FM2) defines whether the system is in interferometric mode or scanning/stepping (LPG) mode. If this mirror is in the ON position then the system is in interferometric mode. If the mirror is in the OFF position then the system is in scanning mode or stepping mode.

15. Aperture

The aperture (S1) is used to remove any unwanted portions of the UV beam prior to grating writing using the interferometric mode.

16. UV Beam Analyzer

The beam analyzer (BA) is used to monitor the quality and absolute position of the UV laser beam both before and during grating writing.

17. Variable Slit/Aperture

The aperture (S2) encountered in the optical path serves to further reduce the beam width down to values of 1.0 mm prior to incidence on the fringe control unit.

18. Fringe Control Unit

The fringe control unit consists of a Plano-convex lens (L1) with a focal length of 100 mm in series with a Plano-convex lens (L2) with a focal length of 25 mm. The fringe control unit also includes an automated 100 mm translation stage which allows for

modification of the 100 mm lens position and thus wavelength modification. The Fringe Control Unit must be in 'IN' position for Scanning, Interferometric and LPG mode and 'OUT' position for Static Mode.

Non optical components

There are also a number of complementary features which are not shown in the optical schematic. The main non optical components are listed as follows:

1. Phase Mask Mount

The phase mask mount is fabricated from titanium. It has three degrees of freedom and can accept phase masks up to 150 mm in length.

2. Fiber Mount

The fiber mount has been specifically designed for the writing station and consists of a mount fabricated from aluminum. The approach of the fiber to the phase mask is motor powered, as is the alignment in all other axes.

3. Vision System

The vision system consists of two cameras and high intensity LEDs. This module is an essential tool for motorized alignment of the fiber optic with respect to the phase mask and laser beam.

4. Tension System

The tension system is separate from the fiber mount. The fiber is first clamped on the right side of the fiber mount and then on the tension system. The load cell thus directly measures the tension on the fiber. The load cell tension level is read by an indicator and fed directly to the grating writing software. Once the tension is adjusted, the left clamp on the fiber mount is closed and the tension clamp is opened.

5. Light Sources

TeraXion system is equipped with three light sources.

- A broadband C+L Light Source (FL-7002) from Thorlabs which has a wavelength range of 1530 nm to 1610 nm.
- A broadband source at 1480 nm (BLS1480) from Electro Photonics Corporation.
- A broadband source at 980 nm (FLS-2200) from EXFO

6. Optical Spectrum Analyzer

The main functions of the OSA have also been incorporated into the software for the writing station thus allowing the user to operate the OSA directly from the provided PC with loaded software.

7. Piezo and Controller

The piezo and controller arrangement permits the user to produce fiber gratings with a variety of apodization profiles. Two distinct system are used, one for the Interferometric Mode and the other for Scanning/Static mode. Dynamic dithering of the phase mask is the mechanism used to achieve apodization.

8. Housing

The housing is fabricated from aluminum with Perspex panels. The front panel is mounted on sliding rails.

PUBLICATIONS

SCI Journal

- **Nidhi**, Umesh Tiwari, Nishtha Panwar, R.S. Kaler, Randhir Bhatnagar and Pawan Kapur, "Long Period Fiber Grating Humidity Sensor with Gelatin/Cobalt Chloride coating Gelatin/Cobalt Chloride coating" IEEE Sensors Journal, ISSN: 1530-437X, VOL. 13, NO. 11, 4139-4140, 2013
- **Nidhi**, Umesh Tiwari, Vandana Mishra, R.S. Kaler, Nahar Singh and Pawan Kapur, "Fiber Bragg Grating Based Technique for Sensing current " Journal Experimental Techniques, Wiley-Blackwell, ISSN: 0732-8818 (*online available)*
- **Nidhi**, R.S. Kaler and Pawan Kapur, "Enhancement of sensitivity of the refractive index using ITO coating on LPG**",** Journal of optoelectronics & advanced materials, ISSN:1454-4164,Vol 8, No.1-2, pp 45-48, 2014
- **Nidhi**, R.S. Kaler and Pawan Kapur, "Humidity sensing using Gelatin & Cobalt chloride coating on ITO coated LPG", Fiber and Integrated Optics, Taylor & Francis, ISSN:0146-8030, 33:120–125, 2014
- **Nidhi**, R.S. Kaler and Pawan Kapur, "Theoretical and Experimental study of Long Period Grating refractive index sensor" Fiber and Integrated Optics, Taylor & Francis, ISSN:0146-8030, 33:37–46, 2014

Conference Papers

- **Nidhi**, Umesh Tiwari, Vandana Mishra, Atesh kumar, Yashudeep Singh, Bharat kumar, S.C. Jain, Nahar Singh and Pawan Kapur, "A current sensing technique based upon fiber bragg grating", pp-266, Photonics 2010- IIT Gawahati.
- **Nidhi**, Umesh Tiwari, Vandana Mishra, R.S. Kaler, S C Jain, Nahar Singh and Pawan Kapur, " ITO coated Long Period Fiber Grating Sensor with enhanced

RI sensitivity", pp 220, OSI SYMPOSIUM on Frontiers in Optics and Photonics (FOP11),IIT Delhi

- Nishtha Panwar, Umesh Tiwari, **Nidhi**, Mohd Mansoor Khan, Subhash C. Jain, Rajeev Garg and Pawan Kapur, "Long Period Fiber Grating Humidity Sensor with Gelatin/Cobalt Chloride coating", is presented in International Conference on Fiber Optics and Photonics, , pp-W2B.4,OSA 2012,IIT Chennai